University of Washington
Department of Civil and Environmental Engineering

APPLICATIONS OF SCIENTIFIC MODELING OF HYDROLOGIC RESPONSES FROM HYPOTHETICAL SMALL CATCHMENTS TO ASSESS A COMPLEX CONCEPTUAL RAINFALL-RUNOFF MODEL

Thian Yew Gan

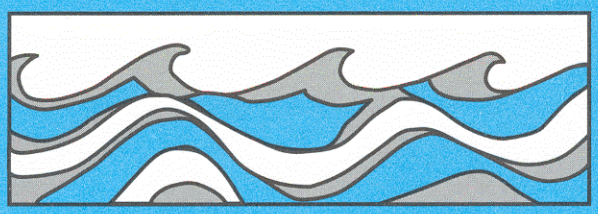

Water Resources Series
Technical Report No.111
June 1988

Seattle, Washington
98195

Department of Civil Engineering
University of Washington
Seattle, Washington 98195

APPLICATIONS OF SCIENTIFIC MODELING OF HYDROLOGIC RESPONSES FROM HYPOTHETICAL SMALL CATCHMENTS TO ASSESS A COMPLEX CONCEPTUAL RAINFALL-RUNOFF MODEL

Thian Yew Gan

Water Resources Series
Technical Report No. 111

June 1988

Department of Civil Engineering
University of Washington
Seattle, Washington, 98195

Applications of Scientific Modeling of Hydrologic Responses From Hypothetical Small Catchments to Assess a Complex Conceptual Rainfall-Runoff Model

by

Thian Yew Gan

Water Resources Series
Technical Report No. 111

June, 1988

Project Completion Report: An Assessment of a Complex Conceptual Rainfall-Runoff Model and Aspects of Catchment Response to Extreme Rainfall

Prepared For: U.S. National Science Foundation

NSF Grant Number: CES 8515250

Principal Investigator: Stephen J. Burges
Professor of Civil Engineering
University of Washington
Seattle, WA 98195

Abstract

Conceptual rainfall-runoff (r-r) models, which have been used extensively for simulating catchment streamflow, have limitations when operated beyond the range of calibration or validation experience; there is no guarantee that they will predict runoff accurately. This potential shortcoming is investigated by evaluating objectively, in prediction and forecasting modes, the performance of an explicit soil moisture-accounting model, the Sacramento model (SMA) of the U.S. National Weather Service. The evaluation process uses streamflow data generated by a hillslope r-r causal model (S-H) (Smith and Hebbert, 1983) which can simulate interdependent surface and subsurface hydrologic processes precisely for hypothetical small catchments; its output can be regarded as "error-free". To model infiltration, S-H replaces the 1-dimensional Richards' equation with a computationally efficient, kinematic model which was demonstrated to be reliable by Smith (1983) for soils with saturated hydraulic conductivities $\geq$ 0.02 m/hr. S-H's effectiveness was demonstrated further here by its accurate comparisons of steady-state aquifer profiles with those from an analytical model (Yates et al., 1985).

Eighteen numerical experiments, comprising combinations of three sets of input data (hourly precipitation and evapotranspiration data) and five hypothetical two-layered small catchments (areas $\leq$ 0.5 km^2; saturated hydraulic conductivity from 0.02 to 0.2 m/hr; soil depth from 0.8 to 1.6 m; hillslope length from 100 to 250 m, and slope from 0.04 to 0.10), representing a wide range of flow mechanisms, were conducted. A manual and automatic (Nelder and Mead (NMS), 1965 pattern search

algorithm) approach was adopted to calibrate SMA which was assessed in terms of graphical plots and summary statistics. The calibrated SMA could simulate fundamental flow mechanisms but generally performed poorly during dry to wet catchment transitions. Difficulties in calibration and model structure limitations of SMA are the main causes of inaccurate SMA predictions. SMA was found to be unreliable in forecasting extreme flood events, especially under dry antecedent moisture conditions and for calibration data that were comprised primarily of baseflow. For each case, the sum of the SMA conceptual storages differed from the physical catchment storage.

ACKNOWLEDGEMENT

Numerous people contributed in various ways to my education and to this report which was first prepared as my doctoral dissertation. First and foremost, I am grateful to my mother and teacher, whose years of dedication to education inspired me to pursue further knowledge in the United States. Her tender words of encouragement and intercessory prayer support, together with those from other members of my family, have sustained me when time was bleak.

I am greatly indebted to Stephen J. Burges, my adviser, committee chairman, and friend, for his invaluable advice throughout my tenure in the research environment of the University of Washington. It was Steve who first stimulated my interest to explore the viability of conceptual rainfall-runoff models for describing the phenomena of hydrologic processes at hillslope scale. Dennis Lettenmaier provided constant help and guidance and introduced me to the advantages of the pattern search optimization algorithm by Nelder and Mead. Thomas Dunne, whose candid yet immensely wise suggestions, helped in steering this work productively. Terry Cundy provided many insights into my work, particularly in kinematic surface and subsurface representations of flow processes.

This work could not have been carried out without the hillslope model (S-H) provided by Roger Smith and Bob Hebbert. Their kindness in sharing their expertise on their model, built in 1983, has been very helpful. It was a welcome opportunity to work with Roger on this model at the USDA-ARS office in Fort Collins, Colorado during the summer of 1986. I was able to function effectively in that office environment with much appreciated help from Virginia Ferreira. The MCP3 version of the Sacramento model was

provided by Larry Brazil of the National Weather Service. Some of the hourly precipitation data were provided by Bob Dickinson of the University of Florida, Gainsville. I wish to extend my appreciation to all these people who kindly helped me.

Financial support for this work was provided by grant CES-85 15250, from the U.S. National Science Foundation. Computing resources were provided through the University of Washington's Academic Computing Services. The help of ACS staff and Jim Mock of the college of engineering during the conduct of this work are appreciated.

Among special friends who provided me indispensable assistance, I especially wish to thank the following: Ryan Tran and Philip Ng who sacrificed long hours straining their eyes on my horrible hand writing to type large portions of the several drafts of this manuscript, parts of which were proof read by Karen Law, Malcolm Leytham and Carrie Ellen who generously shared their writing skills. Also, my endurance and strength would have failed if without the prayer support and encouragement of Johnny Lau, Sam Law, Jonathan Seopardjo, SoiCam, Ling May, Bernie Han and his prayer group.

Finally, I am thankful to the Creator of this universe whose handiworks are so intricate and profound that man can never hope to unlock fully the mystery of just one of His countless creations, the hydrologic cycle of nature.

TABLE OF CONTENTS

LIST OF FIGURES

LIST OF TABLES

CHAPTER 1

INTRODUCTION

He searches the sources of the rivers
  and brings hidden things to light.
But where can wisdom be found ?
  Where does understanding dwell ?
Man does not comprehend its worth;
  it cannot be found in the land of the living.

Job 28:11-13

Numerous large water resource projects have been implemented during the past five decades and others will be implemented in the future. In other words, major decisions have been made and continue to be made under sets of uncertain hydrologic, economic, and environmental conditions. Possible irreversible long term impacts resulting from unwise water resource development include diseconomy of resource utilization, land erosion, upset of the ecological balance, and even the risk of project failure leading to catastrophic loss of human life and property such as the flood losses due to the breaching of an earthfill dam in Rapid City, South Dakota (Rahn, 1975) and other similar examples (Viessman et al., 1977).

One aspect of water resource project failure is related to unreliable flood predictions in designing the project. Because the scale of the impact involved in case of project failure can be enormous, much research has been conducted by hydrologists and engineers with the aim of improving such prediction skill. Since the advent of digital computers, the trend has been towards developing and

using mathematical rainfall-runoff models to provide appropriate hydrologic information.

Because of the present incomplete state of scientific knowledge in hydrology, the lack of field data, limitations in computing power, and difficulties in putting causal elements together in a meaningful way, it is difficult to model hydrologic processes causally. Hydrologists are often driven to use models that are simplified representations of hydrologic systems because of the complexity of hydrologic processes, which often involve both interrelated known and unknown physical variables. Clarke (1973) classified mathematical models used in hydrology as empirical and conceptual. Both groups of models can be further classified either as stochastic or deterministic. The former refers to models with variables that are random, having probability distributions, while in the latter, variables are free from random variations.

Since Thomas and Fiering (1963) introduced the Markov lag-one hydrologic model, stochastic-empirical models have become popular. Empirical relationships of hydrologic processes can be derived through statistical analysis of collected data, without much understanding of the phenomena modeled. Such relationships, coupled with a noise component, have been used widely in simulating the response of water resource systems for engineering purposes. Hence, applied statistical methods have been used to produce simplified representations of nature. This modeling approach has, however, probably come to a stage where

further refinement will not yield significant improvements in its effectiveness as a tool in applied hydrology (Klemes, 1982; Fiering, 1982; Leopold, 1982).

Conceptual modeling is another useful approach to describe hydrologic processes. Models allocated to this class of modeling may be further classified as lumped, probability-distributed, and geometrically-distributed. In lumped-parameter conceptual models, the various phases of water movement in the hydrologic cycle of a drainage basin are conceptualized by a network of interacting, lumped parameter submodels (or conceptual reservoirs) that ignore any spatial variability. They are moisture-accounting models that conceptualize the catchment response physics, rather than representing physical mechanisms. This approach has been improved to a stage where simulation of continuous streamflow hydrograph response to input sequences of short interval rainfall data (hours or minutes) is common. The Stanford Watershed model (SWM) (Linsley and Crawford, 1960; Crawford and Linsley, 1962; Crawford and Linsley, 1966) marks the beginning of such a refinement in conceptual modeling. From there, many offsprings of the SWM came into being, including the Hydrocomp Simulation Program (HSP), Kentucky Watershed model (Liou, 1970), Texas Watershed model (Claborn and More, 1970), Ohio State University Version of SWM (Ricca, 1972) and independently the Sacramento model (Burnash et al., 1973), which became the U. S. National Weather Service basic catchment-response model for operational forecasting (NWSRFS).

Conceptual models are used widely to augment short stream flow records and to make operational forecasts. For example, with the current soil moisture, snow, river and reservoir conditions, the Extended Streamflow Prediction program (ESP) of the Sacramento Model uses historical climatic data to produce probabilistic forecasts for future streamflow, e.g., spring flood outlooks (Day, 1985). Based on long precipitation records, conceptual models produce synthetic streamflows to augment short historical runoff records for design purposes, such as using HSP to study the hydrologic effects of physical changes to watersheds by Onstad and Jamieson (1970) and in simulation of the effects of the channel systems designed for urban drainage (Huang and Keenan,1987). Despite relatively wide acceptance and apparently successful applications reported by various users, there have been criticisms concerning the validity and limitations of conceptual models (Gregory and Walling, 1973; Betson and Ardis, 1978; Fiering and Kuczera, 1982; Klemes, 1982).

Synthetic runoff hydrographs (of apparently high fidelity) produced by a calibrated conceptual rainfall-runoff (r-r) model do not necessarily guarantee that the model's structure is not faulty or that the model has not incorporated false premises during its calibration process which includes subjective input. Some researchers have hypothesized such possibilities. Betson and Ardis (1978) argued that consistent parameter values could not be obtained through calibration of a conceptual model because many combinations of the highly-interrelated parameter values could achieve similar results. This is

unfortunate because the parameters of a calibrated conceptual r-r model should represent the physical characteristics of the catchment modeled, otherwise it would be just another set of values resulting from curve fitting, as used in stochastic models. Klemes (1982) cautioned that models with many optimized parameters may give good results because wrong assumptions may be compensated by some parameters with physically unrealistic values.

Gregory and Walling (1973), among others, indicated that the SWM can be faulted in that it does not make full allowance for the partial area and variable source area concepts of runoff production. Pilgrim (1983), through extensive study of storm runoff processes in Australia, gathered enough evidence to conclude that a wide range of runoff forms can occur rather unpredictably, even in a basin of apparent uniform soil and topography. Such findings indicate the need for enquiries into the validity of conceptual model structures - a network of lumped-parameter, interacting, conceptual linear reservoirs that are used to represent natural hydrologic dynamics.

Another shortcoming of conceptual models is that they are interpolative. This means there is no guarantee that they will predict accurately once they are used to extrapolate beyond the range of calibration or verification experience. This is restrictive because a major concern of many water resource decisions involve extreme hydrologic events, e.g., calculation of flood hazards. Klemes (1982) pointed out that a conceptual model should be tested for its

credibility under varied and diverse hydrologic conditions. Sorooshian (1983) suggested that a rigorous model validation process should test the model's forecasting ability during a time period of hydrologic response that is remotely different from the calibration period.

Apart from the above two modeling approaches, there is a relatively new class of mathematical models in hydrology, known as causal models. By using known scientific theories, causal models attempt to describe the physics of hydrologic processes. Unlike the previous two approaches, causal modeling is only at an infant stage of development. This is attributed to limited scientific knowledge and the great difficulties involved in modeling any natural physical process causally because it is complex. A more detailed discussion on causal modeling is given in Chapter 2. Hence, hydrologists face the problem of selecting the right type of hydrologic model which at present may not exist.

The hydrologist's quandary is apparent. Hence, there is an urgent need to test the validity of conceptual models. Also, a major objective of hydrology is to develop understanding of the cause-effect relationships that exist between hydrologic variables such as precipitation and streamflow (Beard, 1981). The present work builds on the spirit of these concerns.

The subsequent chapters are arranged to be as independent as possible. As outlined in Chapter 2, a major concern of this work is to determine the ability of conceptual models to represent each of the

several fundamental hillslope flow mechanisms which physically-based models attempt to capture. Chapter 3 summarizes the relevant literature for these flow mechanisms. Pertinent aspects of past research in causal runoff models are also discussed. For reasons to be discussed later, the causal hillslope runoff model built by Smith and Hebbert (1983) (S-H) is selected to assess the reliability of a conceptual model chosen for this study, the Sacramento model (SMA). Chapter 4 contains summaries of two conceptual models (SMA, and the Stanford Watershed Model), of S-H, and the verification of its model structure to authenticate its credibility, and modifications made to S-H and SMA.

Chapter 5 gives the research design of this work which includes the selection of climatic data, the assumptions and procedures involved in setting up hypothetical catchments, and general methods for testing conceptual models. Chapter 6 gives a detailed account of the procedure used in calibrating the conceptual model, the problems encountered, and the rules of thumb for calibration developed during the experiments. Evaluations of the performance of SMA and related discussions are given in Chapter 7 and results are presented in the form of summary statistics and graphical plots. Concluding remarks are delivered in Chapter 8 and future work recommended in Chapter 9. Theories, derivation of some pertinent formulae, tables of hypothetical catchment design criteria and results are included in the appendices.

CHAPTER 2

STATEMENT OF THE PROBLEM

"Have you comprehended the vast expanses of the earth ?
Tell me, if you know all this."
Job 38:18

Any attempt to verify conceptual model structures explicitly is futile because many of the model parameters used to replace the unmeasurable, spatially-varied, hydrologic and soil-water processes of nature are not observable directly. Such models can only be validated implicitly, such as through testing of model performance.

Physical experiments using simple laboratory scale catchments may be possible but the cost incurred even to test a basin of the simplest geometry would be very high. Moreover, there are great difficulties in any attempt to model the catchment geometry, soil and hydrologic properties, and soil moisture states accurately of any physical basin of much smaller scale than the prototype. An alternative is to replace a physical laboratory by a mathematical one, which means that causal rainfall-runoff (r-r) models of certain kinds are necessary. Have causal r-r models been developed to a sufficient state to permit such use?

Causal modeling has been the subject of interest of many researchers who wish to arrive at precise, scientific descriptions of mechanisms of the hydrologic cycle. Bohm (1957) defines causal laws as " the necessary relationships between objects, events, conditions or

other things at a given time and those at later times. ". In general, causal models are sets of differential equations that describe the physical principles governing the systems modeled. Ideally, for a given set of physical states, a causal model can represent the behavior of a hydrologic process, without having to go through model calibrations by data fitting, as conceptual models do. Therefore, causal modeling is a deeper level of enquiry over conceptual modeling, by one or two orders. The differential equations of causal models are necessary simplifications of the real causal chains of nature. They will undoubtedly fail at the molecular level and so they are far from being ultimate. Klemes (1978) and Vigier (1957) pointed out that causality cannot be identified with determinism because any phenomenon is a combination of causal and random properties interwoven together.

The causal modeling approach is not without difficulty, because the dynamic mechanisms of nature are complex. Until now, the most complicated causal models (Freeze 1972a, 1972b), which integrate some of the presently known dynamic mechanisms of catchment response to precipitation require enormous amounts of input data, and place huge demands on computer storage and execution time, are impractical for routine application. Consequently, causal modeling should be approached such that the physical interactions of dynamic mechanisms are simplified, either lumped together or ignored in the process of model building, to make the computations manageable and the input requirements feasible. Such simplifications must be done carefully to

ensure that they do not rob the causal model of a credible, physical basis.

Examination of the literature reveals that many of the causal r-r models built so far are, with a few exceptions, more for learning than for application (Chapter 3). The causal hillslope r-r model developed by Smith and Hebbert (S-H) (1983) is one of the few exceptions. A detailed discussion of the selection process used to choose a causal model for the present work is given in Section 3.2. S-H contains the essential dynamic features of the hillslope hydrologic cycle, yet is computationally efficient. With specified climatic input, and given soil and topographic characteristics, its output, in the context of idealized catchments, can be taken as "precise". (A description of the model is given in Section 4.1). Because of its structure, S-H is computationally much more demanding than comparable conceptual r-r models (on the order of fifty fold or more) and requires more detailed soil and basin topographic data for input.

Given the unresolved question of the reliability of conceptual models and the availability of a robust and scientifically sound hillslope catchment model, two broad objectives are investigated.

(1) To determine the relative sensitivity of the flow mechanisms to changes in hillslope topographic parameters, to climatic data variability (from wet to dry conditions), and to spatial distributions of rainfall data, and

(2) To assess the fidelity of SMA in both prediction and extreme forecasting modes under a wide range of hydrologic and climatic conditions.

The conceptual r-r model explored was the Sacramento model because of its present wide use in the United States. Moreover, many research works on conceptual r-r model development and application are based on the Sacramento model (Brazil et al. 1986; Hendrickson et al., 1986; Curtis and Colton, 1986; Gupta and Sorooshian, 1985; Sorooshian and Gupta, 1983). Because of the limitations of S-H and in computing power, only small hypothetical catchments (0.1 to 0.5 km^2) with uniform topographic geometry and homogeneous soil properties were tested.

Though conceptual models are generally applied to catchments of larger scale, there are reports on their applications on small scale catchments, e.g., Crawford and Linsley (1966) demonstrated that SWM successfully modeled a small turfed watershed near Stanford with a total area of 0.26 square miles. For large catchments, the effects of spatial variations may cancel each other so that lumped-parameter conceptual models such as SMA might be applicable. For small catchments, such as those used in the experiments, such cancellation effects are less likely to occur. Therefore, idealized catchments which ignore any spatial variation were designed to concentrate on exploring the validity of the explicit soil moisture accounting approach of SMA. Even though the scale of these catchments is much smaller than those commonly modeled, the results are still significant.

If the selected conceptual model does produce adequate storm hydrographs, then the logical follow-up step is to test its performance with catchments of heterogeneous soil properties. Soil heterogeneities give rise to complications that significantly affect hydrologic processes such as infiltration and runoff rates (Smith and Hebbert, 1979; Freeze, 1980). Based on real data and synthetic data generated by Freeze's (1980) model, which includes spatial catchment heterogeneities generated by sampling from random fields, Loague and Freeze (1985) tested the predictive and forecast capabilities of a regression model, a unit-hydrograph model and a quasi-physically based model . They found that in general the models performed better in predictive than in forecasting modes, and with synthetic rather than with real catchment data (Loague, 1986). The term "prediction" refers to long term streamflow simulations used for design purposes while the term "forecast" refers to specific real time (future) streamflow events simulated for operational decisions. Hence, extensions of the current work should be focused on catchment heterogeneities, a more realistic representation of nature, and the study of the effects of spatial variability of precipitation on runoff.

CHAPTER 3

LITERATURE REVIEW

The review given herein focuses on the primary elements related to observed runoff processes on a hillslope, and past work that quantifies the physics of such water movement. The respective merits, successes, and limitations of these works are discussed.

3.1 Types of Runoff Processes

Dunne (1978,1982) summarized succinctly (Fig. 3.1) the current knowledge of various runoff processes and the governing climatic and environmental factors that affect their respective occurrences.

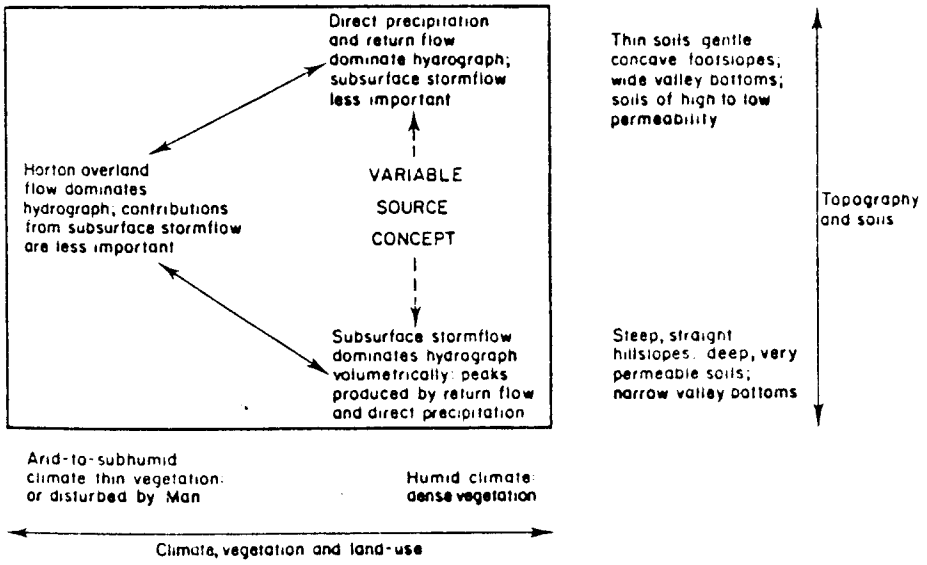

Figure 3.1 Schematic illustration of runoff processes and their occurrences in relation to various controlling factors (from Dunne, 1978)

The Smith and Hebbert (S-H) model represents each of these processes for homogeneous hillslopes. How well a conceptual r-r model represents these distinct processes has not been addressed fully previously. Each

of these basic runoff-producing mechanisms and methods for modeling them are described here briefly for completeness.

3.1.1 Horton Overland Flow

When rainfall intensity exceeds the rate of infiltration, which decreases with time due to the filling of soil pores with water and rainsplash effects, excess water will accumulate on surface depressions and eventually spill over, running down the hillslope (no matter how slight the slope) as a thin sheet (or in rills). This is now known as Horton overland flow, named after Robert Horton (Dunne, 1982). Overland flows generally are assumed to be turbulent and subcritical, and can be described by the classic shallow water equations, often approximated by the kinematic description which Woolhiser and Ligget (1967) found to be valid on almost all overland flow planes. Kinematic wave equations can be applied also to convexo-concave hillslope surfaces by using a kinematic cascade, introduced by Brakensiek(1967).

The Hortonian runoff process usually dominates runoff hydrographs of arid or semi-arid regions where infiltration is low because vegetation is sparse, but it is uncommon in humid, heavily vegetated basins. Horton overland flow typically moves at velocities of 0.003 to 0.15 m/sec (Dunne, 1982). Betson (1964) and others have observed that certain portions of a drainage basin regularly contribute Horton overland flow to streamflow, whereas others seldom do. They coined the term "partial source areas" to describe this. Faithful representation of partial source areas is important in hydrologic

modeling. In the limit, of course, some entire catchments (typically pasture) contribute overland flow.

3.1.2 Saturation Overland Flow

As water continues to percolate into soil layers during persistent precipitation, the water table rises upward until it meets the ground surface, usually at the lower portion of a concave hillslope and near the stream channel. Any further direct precipitation onto this saturated area of the hillslope runs over the surface as saturation overland flow, since it cannot infiltrate into the soil, at least not for a while. Some of the water that previously infiltrated into the topsoil may now return to the surface as overland flow, known as return flow (Dunne and Black, 1970). The occurrence of saturation overland flow, which may or may not include return flows, can be integrated into the variable source concept (Hewlett and Hibbert, 1967). The saturated area expands and contracts dynamically during a storm. Field experiments show that concave hillslope profiles are more favorable for such expansions of the saturation area because there the water table is closer to the ground surface than beneath straight or convex slopes.

Hillslopes that have gentle slopes and soils of low vertical and high horizontal hydraulic conductivities also cause rapid spreading of the saturated areas. In humid, densely vegetated regions, most runoff production is attributed either to shallow subsurface stormflow, saturation overland flow, or a combination of the two (Fig. 3.1).

Though saturation overland flow occurs under different conditions, the same shallow water equations used for Hortonian overland flow are applicable. Saturation overland flow velocities typically are slower than Horton overland flow velocities because in the former case, water travels through dense vegetation on mild slopes. Velocities of saturated overland flows are between 0.00008 and 0.03 m/sec (Dunne, 1982). The response time and peak discharge from the land are intermediate between those of Horton overland flow and subsurface flow.

3.1.3 Subsurface Flow

Subsurface flow is another source of runoff production and is prevalent in humid climates where vegetation is dense, and soils are thick and well drained. Whipkey (1969, 1965) reported subsurface flows with peak velocities up to 0.0099 m/hr from a 0.44 m deep silt loam and up to 0.0054 m/hr from a 0.90 m deep sandy loam. Dunne (1970) reported occurrence of such flows in the well drained soils at the Sleepers River Experimental Watershed in Vermont, and showed that such flow is not always quantitatively an important contributor to storm runoff. Through extensive investigations of stormflows over hillslopes by computer simulations, Freeze (1974) concluded that only on convex slopes that feed deeply incised channels with soils of high saturated hydraulic conductivities (greater than 0.036 m/hr) would such a flow mechanism dominate, but his results were limited to hillslopes with gentle gradients (up to 7.5 %).

Typical velocities of subsurface flow are several orders of magnitude slower than those of overland flow. Subsurface flows can be described by the continuity equation and Darcy's law for transient, saturated-unsaturated flow in a porous medium (Freeze, 1972a, 1972b; Beven, 1975). By applying Dupuit's Theory and approximating a hillslope element as homogeneous and anisotropic, Smith and Hebbert (1983) have modeled this phenomenon effectively. With the Dupuit assumption, the differential equation has been greatly simplified but numerical methods are still necessary except for some steady-state situations (Chapter 4 describes an analytical method for steady-state situations).

3.2 Physically Based (Causal) Models and Related Research

Much work has been done on modeling the physical aspects of rainfall-runoff processes causally, but progress has been slow. Upon examination, many causal models appear to possess certain attractive features but most suffer from some shortcomings which make them unsuitable for the work reported here. For example, Kibler and Woolhiser (1970) modeled Horton overland flow on hillslopes represented by a sequence of discrete planes of different slopes and roughness parameters. Kinematic wave equations were used independently to describe unsteady flows on the planes with matching boundary conditions, according to the "kinematic cascade" concept. Kibler and

Woolhiser assumed the planes to be impervious, thus ignoring infiltration into the soils.

Kibler and Woolhiser's method was extended by Smith and Woolhiser (1971) to couple both Horton overland flow and infiltration for a hillslope. Once again, the hillslope was represented by a sequence of discrete planes but in this case, they were permeable and have soil layers below. The one-dimensional Richard's equation (Richards, 1931) was used to describe infiltration, and the effect of soil swelling was incorporated to account for the change in stored moisture. Smith and Woolhiser successfully modeled runoff from a natural hillslope plot, but only after laborious hydraulic parameter estimations and fitting of boundary conditions between the overland flow and infiltration components were carried out. Additionally, Smith and Woolhiser's model does not account for all three fundamental hillslope flow mechanisms mentioned earlier.

A more complete model was developed by Freeze (1972a, 1972b) who coupled a detailed, mathematical two-dimensional subsurface stormflow model with a one-dimensional channel flow model that received the subsurface flows as lateral input. Hydraulic properties of soils and geometry of the subsurface flow region were needed in detail to satisfy the necessary boundary conditions for solving the 2-D parabolic differential equation that described time-dependent, unsaturated-saturated flow in a heterogeneous, anisotropic porous medium. Iterative implicit finite-difference methods were used for solutions. In the

coupled model, Freeze found that 98 percent of the computer time was taken up by subsurface computations; only 2 percent was needed for the overland flows.

Several simple, computationally efficient models are available but from the perspective of hillslope hydrodynamics, they are incomplete. Engman and Rogowski's (1974) infiltration and overland flow model is one of several such examples. The model uses Philip's two-parameter infiltration equation (Philip, 1957a, 1969) to compute the time-dependent infiltration capacity and rainfall excess. By following the partial area concept and taking soil variability as the guiding index, it accounts for the expansion of the watershed area contributing to Horton overland flow. This quasi-physically based model is appealing because of its simplicity. Unfortunately, Philip's equation is appropriate only for ponded fluxes which certainly will not always take place, especially when the soils are well-drained and the rain intensity is low. On two of three natural catchments and on most synthetic data tested, Loague (1986) found that this model gave surprisingly poor performance.

Another physically-based yet simple model was built by Beven and Kirkby (1978) for medium sized basins, with the intent of combining the essential elements of causality and the advantages of simplified lumped parameter representation. This model avoids enormous data and computing requirements by integrating the distributed effects of the basin into simple, lumped storage components for subbasins linked

together by a channel network. The subbasins are divided according to soil types and topography. In each subbasin, any of the three basic flow mechanisms may be generated using simple storage and dynamic contributing area relationships.

Beven and Kirkby's model was applied to an 8-Km^2 drainage basin in England and produced satisfactory results. Despite some attractive features, the model attempts to combine the distributed effects of channel network and dynamic contributing areas by simple lumped parameters that lack physical basis. However, Beven and Kirby's model has one important characteristic adopted here. That is, the basin modeled was divided into subbasins according to soil types and topography, and the subbasins are joined together by a channel network. The hypothetical basins used for the thrust of this work were constructed in similar fashion.

Several other related works include a hillslope hydrograph model by Reeves and Duguid (1975), who used the Galerkin finite element method for solution. It has a sound physical basis but unfortunately its computational requirements are excessive. Another finite element model for hillslope runoff simulations was built by Beven (1977), who assumed a hillslope soil mantle that is homogeneous, isotropic and single-layered. This is a considerable simplification of nature. His more recent hillslope model (Beven, 1982) which uses an analytical approach is only applicable to some highly simplified subsurface stormflow cases.

Table 3.1 summarizes the essential characteristics of causal models that have been reviewed for this work. A brief comment on each model is also given. Though it is by no means a comprehensive list of causal models, it reflects the general capabilities of models that are currently available. Apparently, only three models listed in the table, Nos. 3, 6 and 9 account for all the three basic flow mechanisms. Beven and Kirkby's model (No. 6) is not adequate because it uses analytical relationships that necessitate highly simplified assumptions. Freeze's model (No. 3) is impractical computationally (16.5 minutes of IBM 360/91 CPU time for 13.5 days of simulation).

All but the S-H model are inadequate for the research undertaken here because they either demand excessive computation efforts or are "incomplete" from the standpoint of hydrodynamics. S-H is an attractive choice because it is efficient computationally and despite some limitations (Chapter 4), it retains all the key elements of hillslope processes. Instead of using the full Richard's equation, S-H approximates the vertical water movement in the unsaturated zone by a kinematic method which depends on the rainfall intensity and the saturated hydraulic conductivity of the topsoil. While S-H is relatively simple, it accounts for infiltration under both ponded and non-ponded situations. A detailed description of S-H and two conceptual r-r models are given in Chapter 4.

Table 3.1 Comparisons of causal rainfall-runoff models

Model	Hydrologic Mechanisms: Horton Overland Flow	Saturation Overland Flow	Infiltration	Subsurface Flow	Comments
1. Kibler and Woolhiser (1970)	Yes	No	No	No	It simulates Horton flow (2-D Lax Wendroff finite difference scheme) according to kinematic theory.
2. Smith and Woolhiser (1971)	Yes	No	Yes	No	It simulates Horton flow (2-D Lax Wendroff); & infiltration (Implicit Crank Nicholson) by Richards' Equation.
3. Freeze (1972a, 1972b)	Yes	Yes	Yes	Yes	It solves full shallow water equation (Lax Wendroff) and infiltration (line successive over-relaxation) by Jacob-Richards diffusion equation.
4. Engman and Rogowski (1974)	Yes	Yes	Yes	No	It uses partial area concept to account for overland flow and Philip's equation for ponded infiltration.
5. Reeves and Duguid (1975)	No	No	Yes	Yes	A 2-D Galerkin finite element model that describes saturated-unsaturated flow in porous media.
6. Beven and Kirkby (1978)	Yes	Yes	Yes	Yes	A variable contributing area model that uses analytical, lumped-parameter equations to compute flows.
7. Beven (1977)	No	No	Yes	Yes	A 2-D Galerkin finite element model for a single-layer, isotropic, homogeneous hillslope soil.
8. Beven (1982)	No	No	Yes	Yes	It uses a analytical, kinematic model to solve simplified subsurface flow.
9. Smith and Hebbert (1983)	Yes	Yes	Yes	Yes	It uses kinematic models for overland flow (Newton-Raphson scheme) and infiltration (Richards' & Philip's Eqs.); & Dupuit's equation for subsurface flow.

CHAPTER 4

CAUSAL AND CONCEPTUAL RAINFALL-RUNOFF MODELS

4.1 Smith-Hebbert Hillslope Model (S-H)

Smith and Hebbert(1983) built a physically based model (S-H) (Figure 4.3) that simulates interdependent surface and subsurface hydrologic processes on a two-dimentional (2-D) hillslope segment made up of two uniform, homogeneous soil layers, the subsoil being less permeable than the top layer. The model approximates two-dimensional subsurface flow phenomena with a vertical, one-dimensional (1-D) representation of partially saturated flow; lateral flow occurs from the saturated flow domain. Lateral partially saturated flow is not modeled. Consequently, the model is inappropriate for steep hillsides where lateral partially saturated flow occurs preferentially to vertical flow. Even though S-H is a quasi 2-D model, it can be extended to a specific kind of three dimensionality such that the hillslope segment to be simulated is either linearly converging or linearly diverging, with angle BC (Figure 4.1).

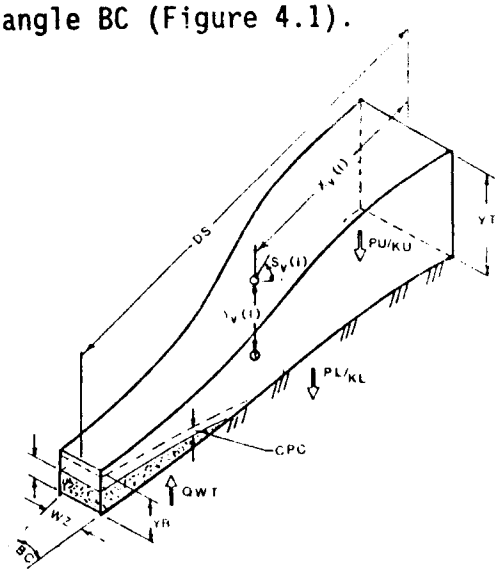

Figure 4.1 An elementary hillslope segment (from Smith and Hebbert, 1984)

While it can simulate all the key hydrologic response mechanisms, the S-H model avoids the dilemma of excessive computer storage and run time requirements. This is achieved by incorporating certain physically sound, simplifying assumptions to approximate vertical water movements in the unsaturated soil zone. This significant feature is discussed below.

The general unsaturated flow mechanism is described by Richards' 1-D equation (Richards, 1931). By expressing this equation in the Fokker-Planck nonlinear form, the unsaturated soil water flow can be treated as a diffusion-convection wave process (Smith, 1983). Hence Richards' equation is written as

$$\frac{d\theta}{dt} = \frac{d}{dz}\left[D(\theta)\frac{d\theta}{dz} - K(\theta)\right] \tag{4.1}$$

where

$D(\theta)\frac{d\theta}{dz}$ = diffusive wave component (LT^{-1}),

$K(\theta)$ = gravitational wave component (hydraulic conductivity, LT^{-1}),

θ = volumetric soil water content (L^3L^{-3}),

t = time (T),

z = vertical distance below soil surface (L),

$D(\theta)$ = soil water diffusivity (L^2T^{-1}),

$q(\theta)$ = water flux (LT^{-1}),

$$= -D(\theta)\frac{d\theta}{dz} + K(\theta)$$

Equation 4.1 can be approximated in two ways, the type of simplification applied being dependent on the relative magnitude of the rainfall rate r and the topsoil saturated hydraulic conductivity K_s, as shown below.

Case I: Rainfall intensity less than saturated hydraulic conductivity

$$r < K_s$$

The diffusive wave component is neglected so water flux $q(\theta)$ becomes

$$q(\theta) = K(\theta) \tag{4.2}$$

By assuming $d\theta/dz$ to be a function of θ only, i.e., independent of time, Eq. 4.1 can be approximated kinematically by

$$\frac{d\theta}{dt} + \frac{dq(\theta)}{d\theta}\frac{d\theta}{dz} = 0 \tag{4.3}$$

so that θ is translated according to the characteristic wave velocity

$$V_c(\theta) = dq(\theta)/d\theta \tag{4.4}$$

For advancing waves (θ decreases from θ_2 to θ_1 with z), the average wave velocity $V_s(\theta_1,\theta_2)$ is

$$V_s(\theta_1,\theta_2) = \frac{(K(\theta_2) - K(\theta_1))}{\theta_2 - \theta_1} \tag{4.5}$$

For trailing waves (θ increases with z), the wave velocity is

$$V_c(\theta) = K'(\theta) \tag{4.6}$$

where $K'(\theta)$ is given by Brooks and Corey's (1964) relationship, written

as

$$K'(\theta) = K_s\left[\frac{\theta - \theta_r}{\theta_s - \theta_r}\right]^{\epsilon} \tag{4.7}$$

in which

θ_r = residual value of θ, below which water cannot be extracted by capillary forces,

θ_s = saturated water content,

ϵ = a parameter, typically 3 to 4.

Neglecting the diffusive part of unsaturated flow is not acceptable when K_s is very low in comparison to the gradients and flux available. Therefore, approximations of the Richards' equation given here are accurate for more permeable soils. Smith (1983) showed that for a soil of K_s = .02m/hr soil water routing by the kinematic wave approximation compares well with that of the complete solution to Richards' equation (Fig. 4.2). Since the approximation is more accurate for more permeable soils, only soils with saturated hydraulic conductivities greater than .02m/hr were used in this research (Tables 5.4 and E.3).

Case II: Rainfall intensity exceeds saturated hydraulic conductivity

$r > K_s$

From the instant rainfall begins, until the time of surface ponding (t_p), the surface flux is equal to r. After ponding begins, and as long as $r > g(f)$ (Eq. 4.8), a supply of water is available at the surface. Hence, infiltration becomes surface controlled and is dominated by diffusivity.

When $t > t_p$, the surface flux f (LT^{-1}) and infiltrated depth F (L) can be obtained either from Green and Ampt 's (1911) equation or Philip's (1957) equation given by

$$f = g(f)$$

$$f = K_s + .5St^{-.5} \tag{4.8}$$

or $$F = K_s t + St^{.5} \tag{4.9}$$

The time to surface ponding t_p is estimated from Equations 4.8 and 4.9 with f = r, giving

$$t_p = \frac{A_p(\theta_i)}{2r}\left[\frac{r}{r - K_s}\right]^2 - 1 \tag{4.10}$$

Where

θ_i = initial volumetric soil moisture content,

$A_p(\theta_i) = S^2/2K_s$,

S = sorptivity ($LT^{-0.5}$), a θ_i dependent parameter (The derivation of S is given in Appendix D).

In S-H, a perched water table may result on the surface of the lower soil layer (Figures 4.1 and 5.7) when the rate of vertical water movement in the upper layer exceeds $K_L(\theta)$, the hydraulic conductivity of the lower layer, which is always assumed to be less than $K_U(\theta)$, the hydraulic conductivity of the upper layer. By assuming the transient subsurface flow of the perched aquifer to be closely parallel to the soil layer interface, the Dupuit Theory for unconfined saturated flow can be applied to describe flow movement. A more detailed description is given in Section 4.4.1.

Likewise, when r exceeds f or when the total depth of the perched aquifer $h(X_v)$ and capillary fringe CPC exceeds the soil profile depth Y_v (see Fig. 4.1), rainfall excess takes place at that point on the slope, and free surface flow, describable by differential equations of momentum and continuity (mass conservation), is generated. These equations, expressed in terms of kinematic wave approximations, are solved by a finite difference scheme. All the runoff produced (surface and subsurface) enters the channnel as lateral inflow and is routed downstream to the catchment outlet as the runoff hydrograph.

The discussion of the model structure of S-H given above indicates that accurate simplifications of flow dynamics have been incorporated to achieve computational efficiency, while maintaining a sound physical basis. To specify a catchment uniquely, as represented by Fig. 4.1, boundary conditions are necessary. First of all, for the 2-D or pseudo 3-D hillslope segment to qualify as a closed system, a no-flow condition is specified at the upper boundary. At the lower vertical boundary, an initial fixed control depth HOUT is specified. At the User's option, (HOUT) can be allowed to "float" upwards when the hydraulic gradient at the boundary becomes steep. The remaining boundary condition is the net flux in or out of the subsurface flow along X_v. It is equal to the net difference between the vertical unsaturated flow into the perched aquifer on top, and leakage (downwards) or groundwater seepage (upwards) (QWT) at the soil layer interface.

Lastly, being a simplified representation of natural catchments, S-H has limitations as listed below:-

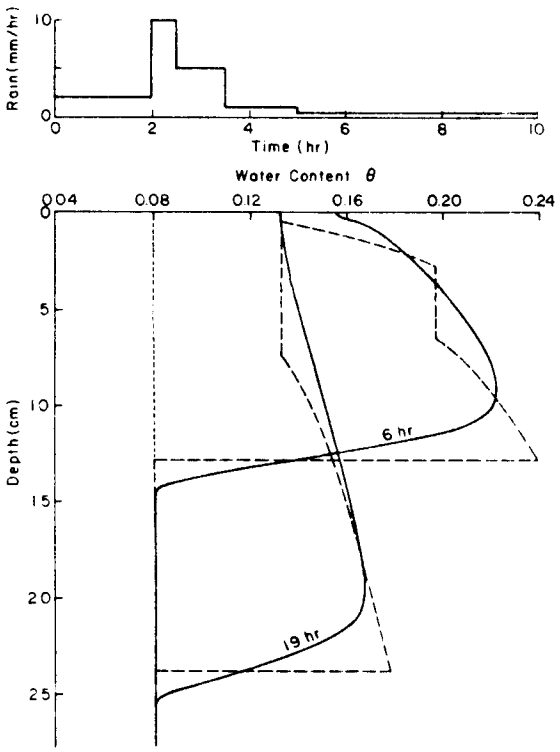

Figure 4.2 Demonstration of the relative accuracy of the kinematic wave approximation for routing soil water, by comparison with the complete solution to Richard's Equation, Eq. 4.1, at two successive times. The upper graph illustrates the rainfall flux imposed. K_u for the soil was 0.02 m/hr (from Smith, 1983)

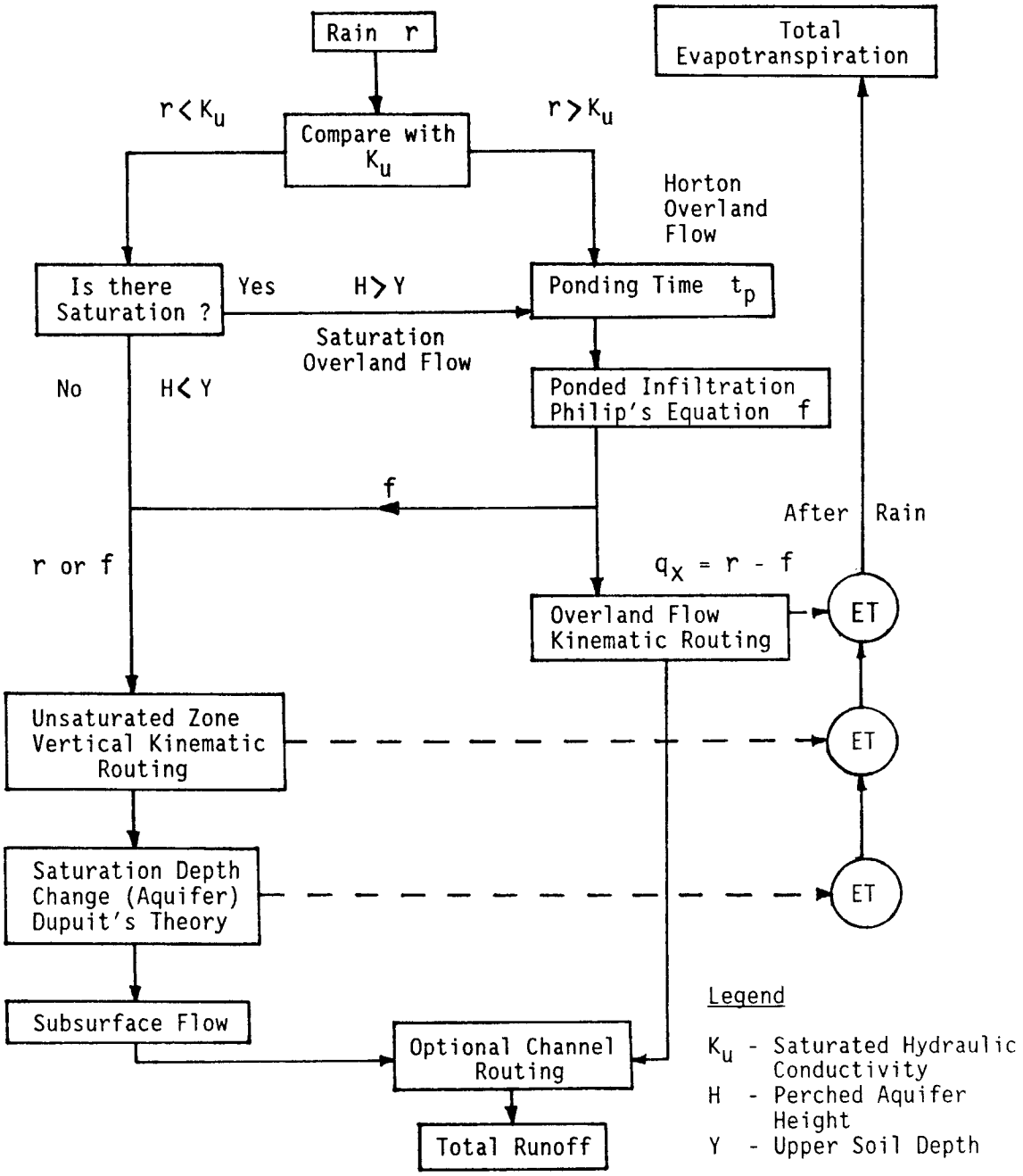

Figure 4.3 Flow diagram of Smith-Hebbert model S-H

(1) It is only applicable to two-layer, hillslope mantles composed of homogeneous, anisotropic/isotropic soils with symmetrical geometry.
(2) The snowmelt runoff process is not included.
(3) It is suitable for hillslopes having grassland surface and so it cannot handle forested catchments.
(4) It cannot account for the influence of depression storage, macropores (plant root pores that induce cracks) and clayey soils that have significant swelling.
(5) Subsurface flow is assumed to be sufficiently parallel to the lower boundary for Dupuit's theory to be applicable. For slopes equal to or greater than 0.30, this assumption becomes poor.

4.2 Conceptual Rainfall-Runoff models

In general, a conceptual r-r model is designed to give a useful quantitative description of the hydrologic cycle, such that the dominant components of the cycle are adequately represented. Conceptual models often are applied to simulate sequential rainfall-runoff events for a time frame of several years or more. To make the computations manageable and to reflect available measured data, a lumped parameter approach is used. The two most widely used conceptual r-r models, Stanford Watershed model (SWM) and Sacramento model (SMA), are described below. The former, though not used here, is included because it is the first major conceptual model from which many offspring came into existence.

4.2.1 Stanford Watershed Model (SWM)

The SWM developed by Crawford and Linsley (1966) conceptualizes a drainage basin as one composed of five major conceptual storages as shown in Fig. 4.4. Inputs to the model are lumped parameter values, short-interval precipitation data (hours or minutes) and daily evaporation data which together contribute to the changes of moisture in the storages and the resultant runoff hydrographs. The physical characteristics of the basin under study are represented by the model's lumped parameters.

As shown in Fig. 4.4, rain falling on any impervious area of the basin (connected directly to a channel) is diverted overland to the channel, while rain falling over pervious areas is subject first to interception. Once the interception storage is filled, water overflows as input to the ground surface. This water is either diverted to surface detention (delayed infiltration) or direct infiltration, in proportions determined by the basin infiltration capacity which varies spatially according to an assumed linear cumulative distribution function. Water that is stored as surface detention will contribute to overland flow, or interflow storage, or will enter belatedly the upper zone storage which represents depression storage and storage in surface soils. The moisture entering the upper zone is depleted either by evapotranspiration (ET) or percolation to the lower zone storage or a combination of the two. Water that infiltrates directly into the soil profile is distributed between interflow storage, lower zone storage, and groundwater storage. Moisture in the interflow storage moves

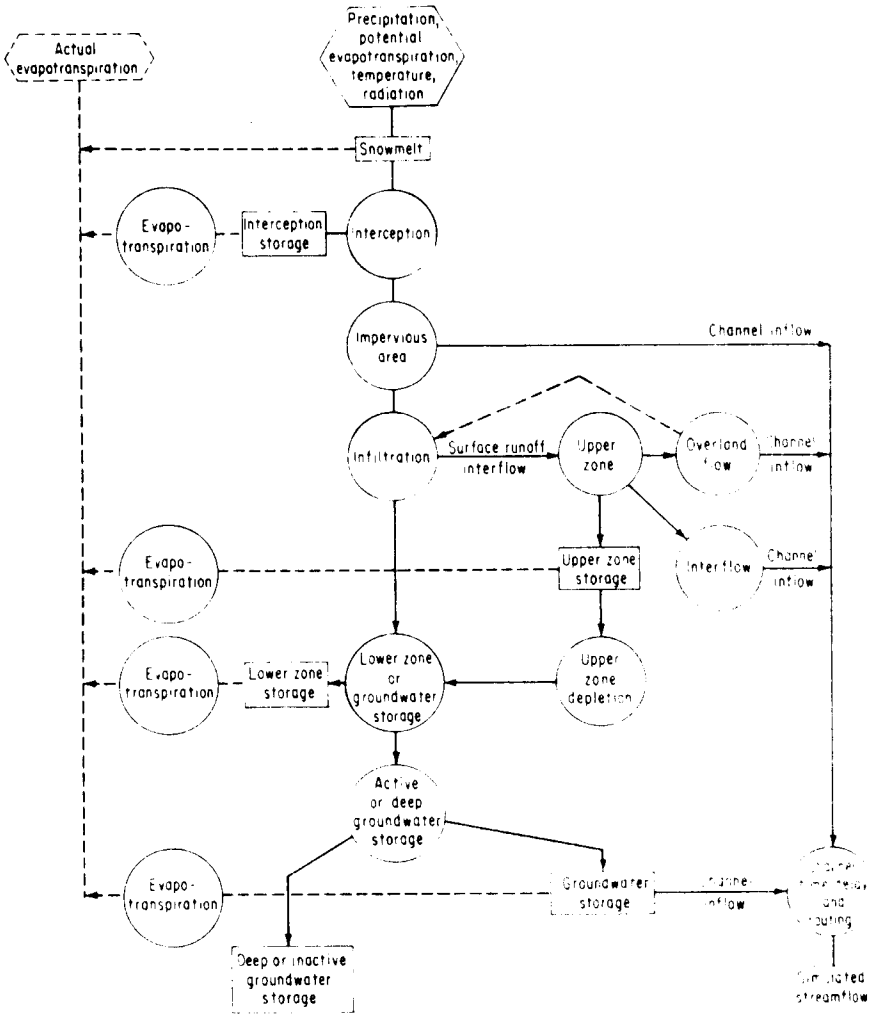

Figure 4.4 Flow diagram of Stanford Watershed Model IV (from Linsley et. al, 1982)

laterally through the upper soil layer until it enters the channel. The groundwater storage contributes runoff as baseflow to the channel.

ET acts upon interception and upper zone storages at the potential rate. Once these two storages are depleted, ET occurs from the lower zone and groundwater storages. Variations in response to the uptake and release of water in these conceptual storages depend on two main factors. One of them is the catchment characteristics, specified by the input parameters, and another is the relative contents of the interacting storages, accounted for by four empirical functions.

Overland flow, groudwater flow, and interflow enter the channel and are routed empirically to the catchment outlet as runoff hydrographs. Discharge is usually computed on an hourly basis. While the model structure of SWM, the first general conceptual r-r model written, is discussed here, a similar but slightly more complex model, the Sacramento model, is used in the rest of the work.

4.2.2 Sacramento Model

The Sacramento Model was developed by Burnash et al. (1973) and has become the U. S. National Weather Service's basic catchment hydrologic response model for operational forecasting (SMA-NWSRFS). It is also a deterministic, lumped parameter, conceptual model but has a "variable impervious area" and an increase of lower zone free water when tension water is not filled. The original model was built for daily precipitation input but later versions of finer time increments have been introduced (6-hour, 1-hour or less).

Input to the model includes precipitation data, pan evaporation data, and lumped parameters that conceptualize the basin physical characteristics. By treating a basin as a closed system whereby all rainfall input returns as either storm runoff or ET, initial values for some of the basin parameters can be determined from inspection and analysis of observed runoff hydrographs.

The framework of the Sacramento model moisture-accounting processes is similar to SWM. When rain occurs over a basin, it is considered to fall on two types of basin covers: (1) a permeable soil mantle, and (2) lakes, channel networks, and impervious areas. Rain falling on impervious areas always becomes direct runoff, whereas that which falls on the permeable soil mantle undergoes a complicated sequence of water movements. Below the permeable soil mantle, the soil moisture storage is conceptually made up of upper and lower zones (Fig. 4.5). Each zone stores moisture in two forms, "tension moisture" and "free moisture". "Tension moisture" denotes water closely bound to the soil particles while "free moisture" is the moisture that fills up the interstitial soil pores.

The upper zone represents topsoils and the basin interception layer. Its tension water, bound closely to the soil particles, must be filled before moisture can be stored as free water. Upper zone free water generates vertical drainage (percolation) to the lower zone and lateral drainage (interflow) to the channel. If the precipitation rate exceeds the sum of lateral and vertical drainage rates, and the upper zone free water capacity is completely filled, excess surface runoff

will result. The actual percolation rate to the lower zone is governed by the interrelationship between soil drainage characteristics and the relative soil moisture conditions of the two zones.

The lower zone, which represents a groundwater reservoir, has a tension water storage and two free water storages (called primary and secondary). Water goes to the tension water zone first and then to the two free water zones, which generate primary and secondary baseflow. The reason for using three water components is to allow a wide range of groundwater recession rates in an attempt to model baseflow.

ET extracts moisture from the upper and lower tension zones and from free water surfaces. Actual basin ET occurs either at the potential rate, for areas covered by surface water or phreatophyte vegetation, or at a daily mean rate (usually obtained from pan evaporation data), adjusted by seasonal adjustment coefficients. Other factors that influence the basin ET include the hierachy of moisture extraction priority and the water available in each zone.

The model produces five runoff components, namely: direct runoff from impervious and water surfaces, surface runoff and interflow from the upper zone free water, and primary and secondary baseflows from the lower zone free waters. Runoff volumes from these five components feed to a channel and are routed down the channel by one of several available techniques.

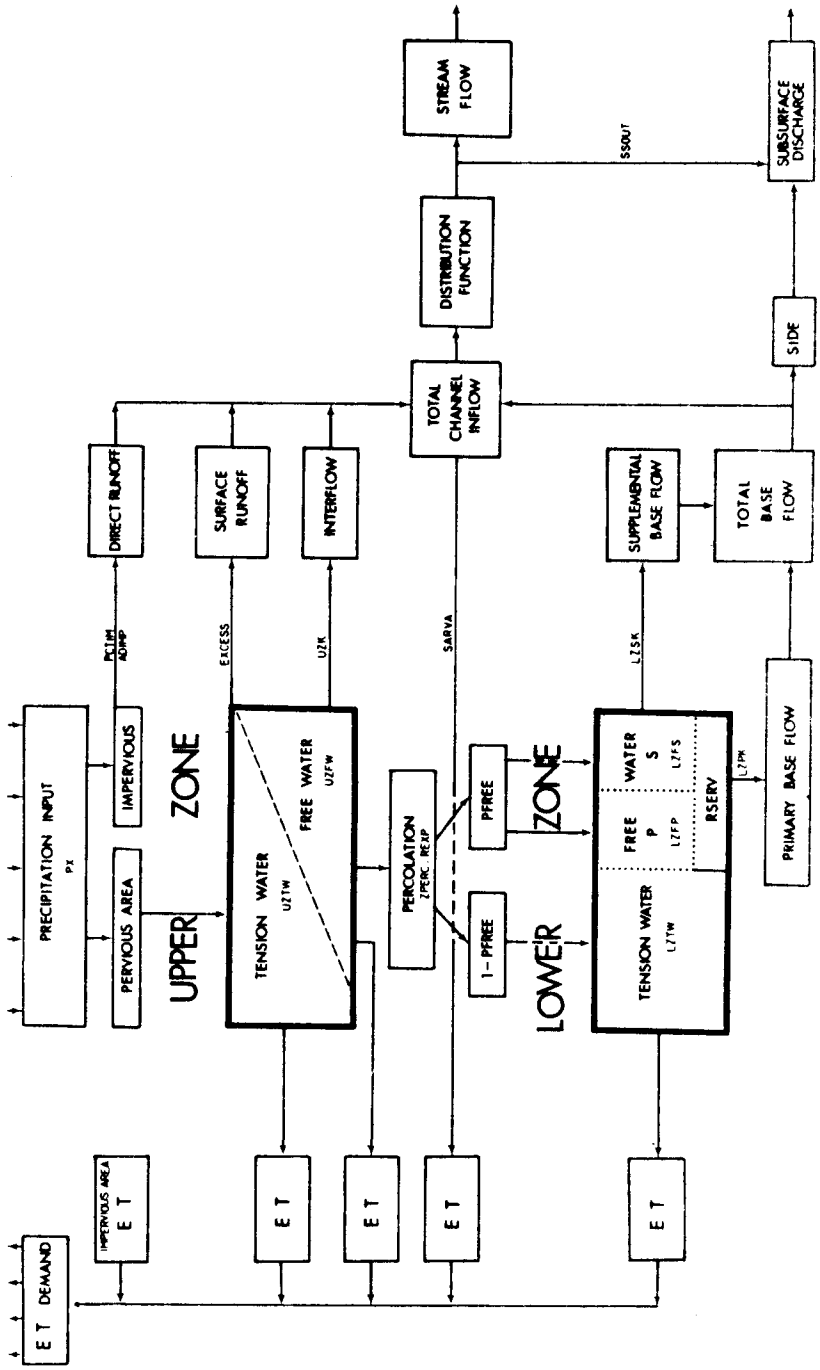

Figure 4.5 Schematic representation of the Sacramento Model (from Peck, 1976)

The manual calibration program (MCP3) of the National Weather Service (NWS) which contains subroutines for the Sacramento Soil Moisture Accounting Model and many other optional operation routines is used here. MCP3 is versatile in that the sequence of operations can be arbitrarily selected by the user. Hence, it can be used for the hydrologic simulation of many types of basin-channel network configurations. It is also currently the latest version available from the NWS. To meet the needs of the present work, MCP3 was extended to incorporate automatic calibration and to handle fine time step computations.

If MCP3 is converted from a fixed time step to a variable time-step model, its computational efficiency can be enhanced because larger time steps are justified for computing baseflows in the dry months. To do that, the original programming structure of MCP3, subtly designed to operate in a versatile manner, must be drastically changed. Moreover, it is difficult or impractical to handle large variably sized direct-access data files; a systematic constant size input-output (I/O) format is embeded in MCP3. For these reasons, the fixed time-step feature of MCP3 is retained even though an effort was initiated to modify its programming structure.

4.3 The Extended Manual Calibration Program, SMA

The original MCP3 program of NWS was written to take hourly data . The soil moisture accounting component can handle time intervals of 1,2,3,4,6,8,12 or 24 hours. Since the size of catchments for this study are relatively small, 0.1 to 0.5 Km^2, the lag time from

the start of a storm to the hydrograph peak, being closely related to catchment area, is short. For the model to keep track of changes in runoff versus time accurately, small time steps, on the order of minutes must be used. To meet these requirements, MCP3 was modified to perform computations at minutes as well as hours. The upper limit is still 24 hours but the lower limit is now one minute instead of one hour. The actual allowable hourly time steps are the same as before while the allowable fixed finer increment data input time steps are 1,2,3,4,5,6,10,12,15,20,30 and 60 minutes. The fine time increment model is referred to hereafter as SMA (Soil-Moisture Accounting).

Using the original version of MCP3, SMA was tested for its credibility in both "hourly" and "minute" domains. A set of hourly precipitation and stream flow data of one year duration for the West Branch Watershed (9 square miles) of the Upper Soquel Creek, California, was used for the test. The data were collected by Linsley, Kraeger Associates, Ltd. for the Soquel Creek Water District to estimate the streamflow at two proposed reservoir sites. The daily potential ET values were taken from a gaging station at Leroy Anderson Dam, located near Soquel Creek. Using hourly time steps, MCP3 was calibrated manually. From the set of parameters obtained and with the same rainfall data, SMA was used to simulate streamflow hydrographs at a time step of one hour. The hydrographs generated by both versions are identical, which confirms that SMA and MCP3 are equivalent to each other in the "hourly" domain.

SMA was then tested in time steps less than one hour. The same hourly rainfall data were divided uniformly into data of 30-minute time intervals and used as input. Again, with the same set of lumped parameters, SMA was operated to produce streamflow hydrographs at 30-minute time increments. The mean monthly flow volumes in CMSD (Table 4.1) of both time-frame cases agree with each other closely.

Table 4.1 Comparisons of monthly mean flows simulated by MCP3 and SMA

Month	Simulated Mean Monthly FLow	
	MCP3 and SMA at 1-hour (CMSD)	SMA at 30-minute (CMSD)
October	0.032	0.033
November	0.550	0.558
December	1.224	1.234
January	0.461	0.453
February	0.329	0.330
March	0.346	0.346
April	0.137	0.136
May	0.074	0.073
June	0.054	0.054
July	0.042	0.042
August	0.033	0.034
September	0.027	0.028
Annual	0.275	0.277

Using MCP3 as a baseline model, the modified model (SMA) conserves mass when operated at one half the time increment of the baseline model. It is assumed that mass is conserved when a finer time increment (several minutes) is used.

4.4 S-H Model Verification and Modification

S-H is built upon current scientific theory and is designed to model the physics of hillslope hydrology. It must again be pointed out S-H is limited to hillslopes composed of homogenous soil layers with uniform geometry. Hence it can not be expected to replicate real flow data accurately because natural basins are made up of nonuniform heterogeneous soil layers. Validation of the model is constrained, therefore, to hypothetical basins which comply with its limitations.

Even for hypothetical hillslopes, a complete model verification is elusive because closed form solutions for transient flow movement are unavailable. Hence, model verification includes testing the essence of S-H's kinematic approximation to unsaturated infiltration and the numerical scheme to compute the perched aquifer profile. The former aspect of S-H has been verified by Smith (1983), for soils with saturated hydraulic conductivities equal to or greater than 0.02 m/hr. Additional tests are performed here to verify S-H's capability in representing the growth of a steady-state phreatic surface.

4.4.1 Perched Aquifer Configuration

It is essential to the main thrust of the research work that subsurface flow be modelled accurately. In the model, streamlines of subsurface flow on a sloping, leaky aquifer are assumed parallel to the lower boundary such that Dupuit-Forchheimer's theory can be applied. Hence the subsurface flow rate Q, given in equation 4.11 , is governed by the horizontal hydraulic conductivity K_h, slope of the aquifer bottom (sin γ), depth of aquifer outlet ($H_{out}+z_b$) and the water surface gradient dh/dx, ie:

$$Q = K_h(H_{out}+z_b)(\text{Sin } \gamma - \text{Cos } \gamma \, dh/dx) \tag{4.11}$$

A central-in-space, backward-in-time finite difference scheme (Eq. 4.13) for Dupuit flow given by Eq. 4.12 is used to obtain the relevent terms for computing dh/dx numerically. The grid configuration is illustrated in Fig. 4.6.

$$-K_h[H\text{Cos}\gamma d^2h/dx^2 + \text{Cos}\gamma(dh/dx)^2 - dh/dx(G_i - (H/W)\text{Cos}\gamma dW/dx) - G_i(H/W)(dW/dx)] + \phi_e dH/dt = q_n(x,t) \tag{4.12}$$

where

$H = H_{out} + z_b$,

ϕ_e = soil porosity,

$q_n(x,t)$ = influx to aquifer at node x, time t

W = Width of the section

G_i = Sin γ

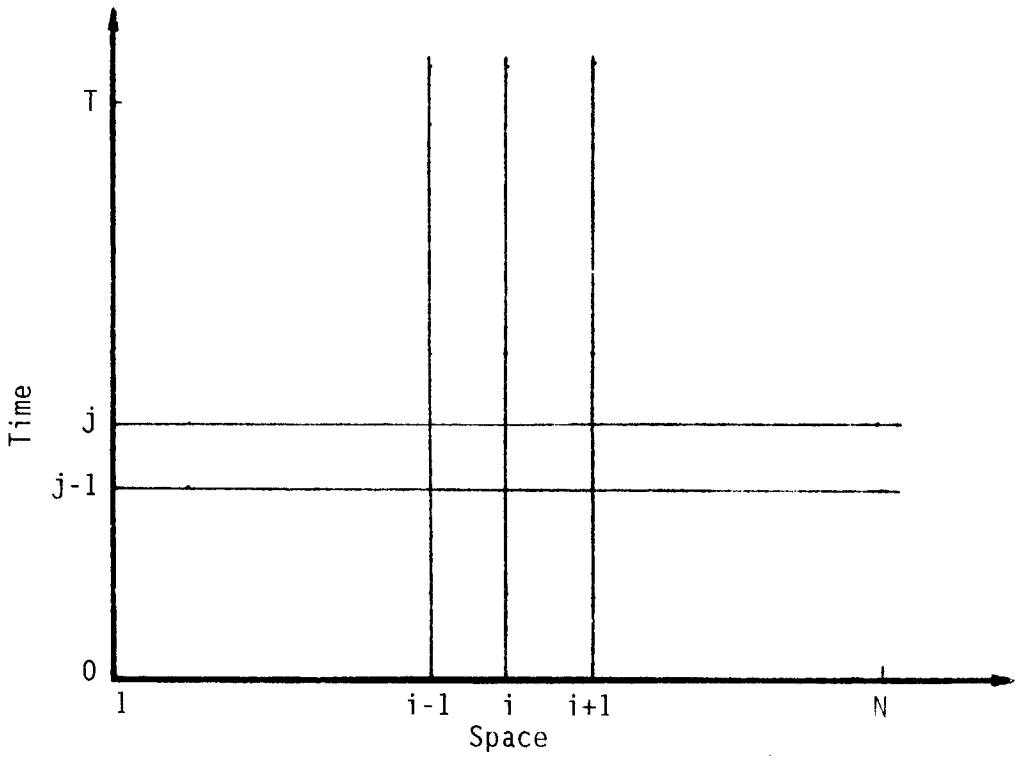

Figure 4.6 Finite difference scheme (central in space, backward in time) for the Dupuit flow equation for unconfined aquifers

The numerical approximation scheme yields:

$$-(K_h/dx^2)\{H_pB[\alpha(h_{i+1}-h_i)^j + \beta(h_{i+1}-h_i)^{j-1}] - H_mB[\alpha(h_i-h_{i-1})^j + \beta(h_i-h_{i-1})^{j-1}]\} + K_h/2dx(G_i - b_cH_iB/W_i)[\alpha(h_{i+1}-h_{i-1})^j + \beta(h_{i+1} - h_{i-1})^{j-1}] + K_hH_iG_ib_c/W_i + \phi_e/dt(h_i^j-h_i^{j-1}) = \alpha q_n^j + \beta q_n^{j-1} \quad (4.13)$$

in which $B = \text{Cos } \gamma$

$$H_m = 0.5(h_{i-1} + h_i + z_{bi-1} + z_{bi})^{j-1}$$

$$H_p = 0.5(h_i + h_{i+1} + z_{bi} + z_{bi+1})^{j-1}$$

$$H_i = (h_i + z_{bi})^{j-1}$$

$$b_c = dW/dx$$

$$\alpha = 1 - \beta$$

i,j = space and time steps

Analytical solutions for Dupuit problems under simplified and steady state conditions are available (Beven 1981,1982; Yates et. al, 1985). The exact analytical solution by Yates et. al for steady flow in a shallow soil layer overlying a sloping bedrock (a nonlinear Dupuit-Forchheimer problem) provides an excellent check for validating the S-H model.

For a given set of soil properties, bedrock slope, input flux and appropriate boundary conditions, the steady state phreatic surface configuration can be readily derived by the analytical model. For the same hillslope under the same input flux, S-H is operated until

equilibrium is reached, ie. when input flux and subsurface discharge are equal. The phreatic surface profiles of both models are compared graphically. Four test cases A,B,C and D (Fig. 4.7) that cover a wide range of bedrock slope, soil properties, input flux and aquifer configurations are shown. The data for the test conditions are given in Table 4.2.

Both S-H and the analytical model produced almost identical water surface profiles except for Case B where the slope is high (slope=0.30). Some of the differences observed in Case B are attributable to the fact that the x-coordinate for the analytical model is the horizontal axis while that of S-H is along the slope. For large slopes, the discrepencies between the two coordinate systems become significant and flow may not be sufficiently parallel to the lower boundary for the Dupuit theory to be valid. While the fidelity of S-H for computing steady-state phreatic surface profiles numerically has been shown here, unfortunately there is no analytical solution for appropriate transient problems to verify the transient aspects of the S-H scheme.

4.4.2 Mass Balance

Continuity, is one of the basic criteria that any scientific model of mass fluxes must satisfy. Initial tests conducted on the original

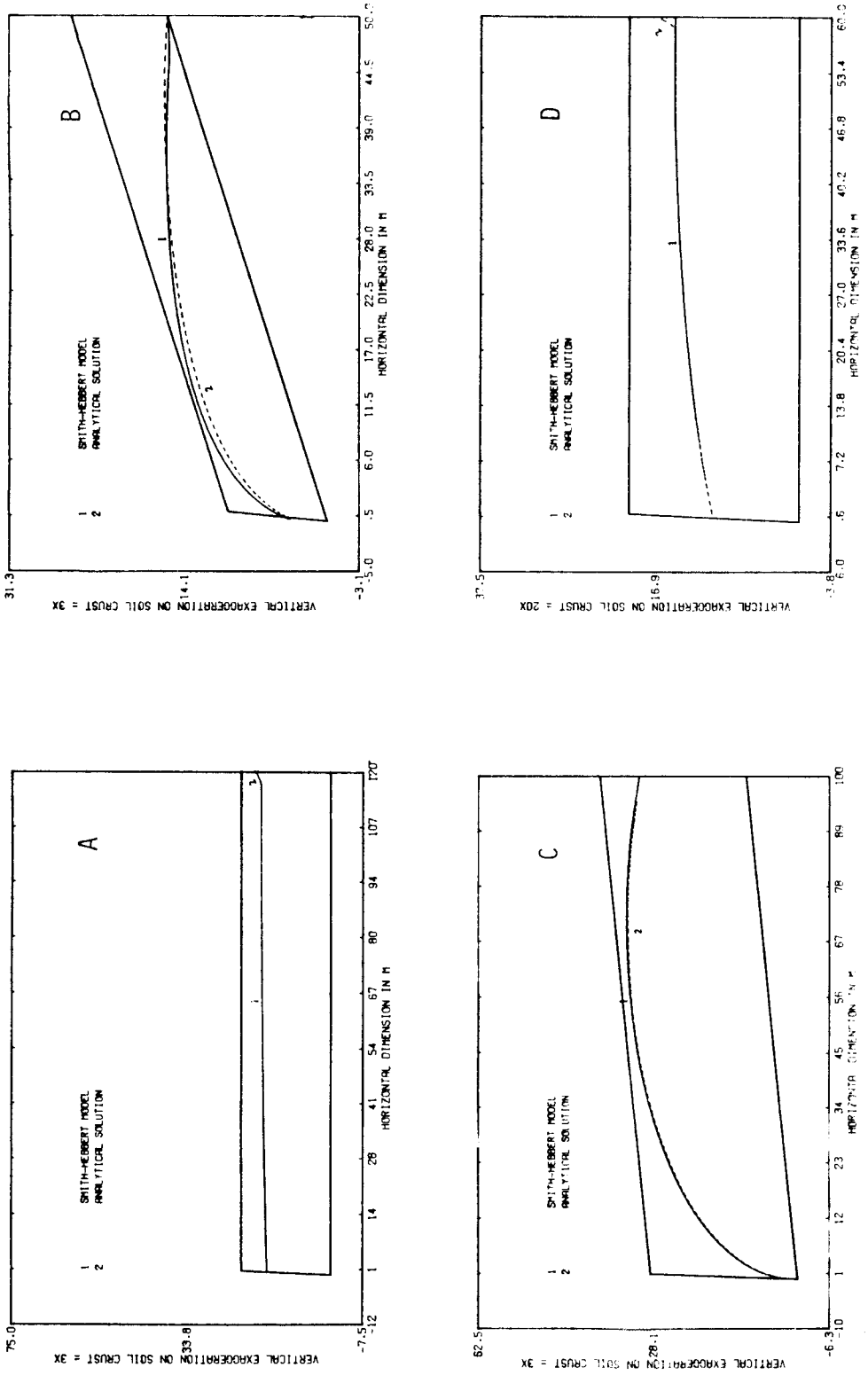

Figure 4.7 Comparisons between steady-state perched aquifer configurations Computed by S-H and an analytical model (Yates et. al, 1985)

Table 4.2 Test conditions for four steady-state perched aquifer configurations (refer to Fig.4.7)

Test Conditions	Case A	B	C	D
Hillslope length (m)	120	50	100	60
Saturated Hydraulic Conductivity (m/hr)	0.25	0.10	0.5	1.0
Soil Thickness (m)	7.0	3.0	9.5	1.0
Slope of Hill	0.001	0.3	0.10	0.001
Rainfall rate (mm/hr)	0.10	2.25	10.0	0.10

version of S-H showed that there were flaws and program 'bugs' in the code. As the simulation continued, the discrepancy in mass balance escalated quickly. Hence at the initial stage of this study, many man-months of tedious effort were devoted to resolving these problems.

S-H uses an iterative, under-relaxation method to compute the perched aquifer profile (Eq. 4.13). After many experiments, it was found that a convergence criterion of 0.01 to 0.005 (ratio of change in water depth over previous depth $\Delta h_i^j / h_i^{j-1}$) and a relaxation factor of approximately 0.5 produce good results within reasonable computing time. Keeping track of the balance between input and output fluxes gives a general idea of the state of simulation. When the S-H model fails to perform satisfactorily, the error in mass balance quickly deteriorates into an unacceptable value, eg: from 2 % to 30 %, so the mass balance error is useful as a warning signal whenever S-H runs into problems.

4.4.3 Modifications to S-H

The original version of the S-H model was configured to simulate flow from elementary hillslope segments and simple basins of rectangular shape to a single channel. Basins that possess realistic catchment features are those drained by a simple channel network (instead of just a single channel), pear-shaped, with runoff from the land entering the receiving channel at consistent, acute angles. S-H

was modified and extended to handle hypothetical basins that have more resemblance to natural catchments. Because of the present limited computer capability (S-H was written specifically for use on a Vax 11/780 digital computer and the ability for regular interchange with its originators was an important constraint), S-H was extended to handle only relatively small catchments, comprising three separate subbasins connected by a simple channel network, to minimize data storage and computation time. Some of the catchment characteristics mentioned above are simplified. These subbasins of a catchment are still rectangular in shape and water drains to the channel at right angles but they can have different hillslope geometries and soils. The channel network has three simple, straight, connected prismatic channels. Figure 5.8 shows a catchment with two subbasins.

4.5 Data interpolation with cubic spline function

Although S-H operates with a basic time step (DT) specified by the user, the actual time intervals used vary in the computation process. During wet periods, When the rainfall rate changes quickly, the time steps taken are reduced to keep track of the changes in soil infiltration accurately. During dry periods, the computation time interval is gradually increased until it reaches a predetermined upper limit to reduce simulation time.

Since SMA is designed to handle uniformly spaced temporal data, it is necessary to interpolate from the S-H flow data for comparison with SMA outputs. After examining both linear and cubic spline interpolation methods, and by comparing results obtained through both methods, it was obvious that the latter is a better choice. In the cubic spline method, a smooth curve is fitted through desired points according to the elastic property of a flexural French curve. The mathematical analog to the law of this elastic bar is that the slope and the curvature for the pair of cubics that join at each point of the curve are the same. Figure 4.8 shows a typical pair of flow hydrographs for a particular wet month. The first plot represents the original S-H hydrograph data while the second represents the data interpolated from the original by the cubic spline scheme at regular intervals. Close inspection of Figure 4.8 shows that other than the interpolated peak labelled A being relatively low, both curves appear to be virtually identical as they should be.

The cubic spline technique is further investigated on short time-interval storm hydrographs shown in Figure 4.9 in which the original S-H hydrograph data and the interpolated data are plotted together. The 24-hour plot (III) shows that both hydrographs agree with each other perfectly except at point B. A 4-hour plot (IV) containing the peak flow in (III) shows that the discrepancy at B is insignificant. Data interpolation by the cubic spline method maintains the characteristics

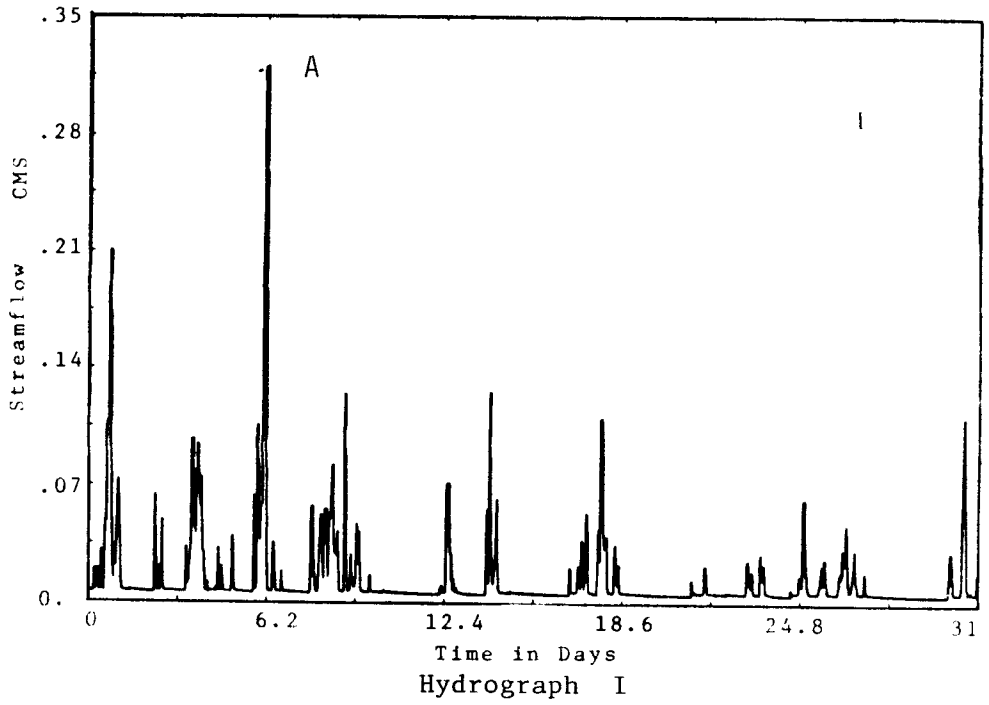

Hydrograph I

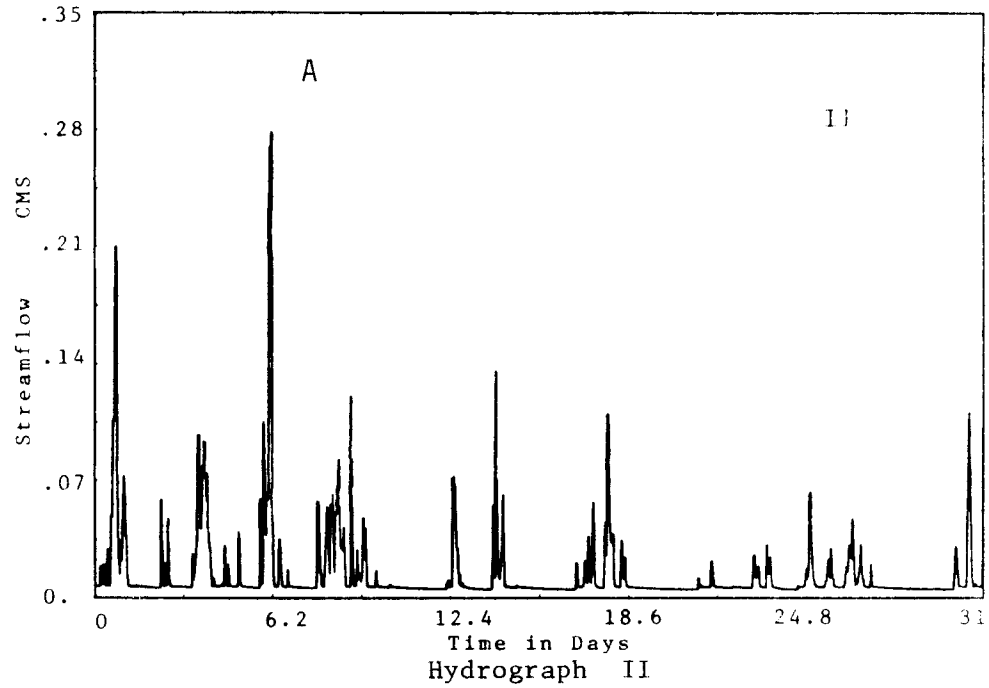

Hydrograph II

Figure 4.8 Comparisons between hydrographs I and II in which II was interpolated from a cubic spline curve fitted through I

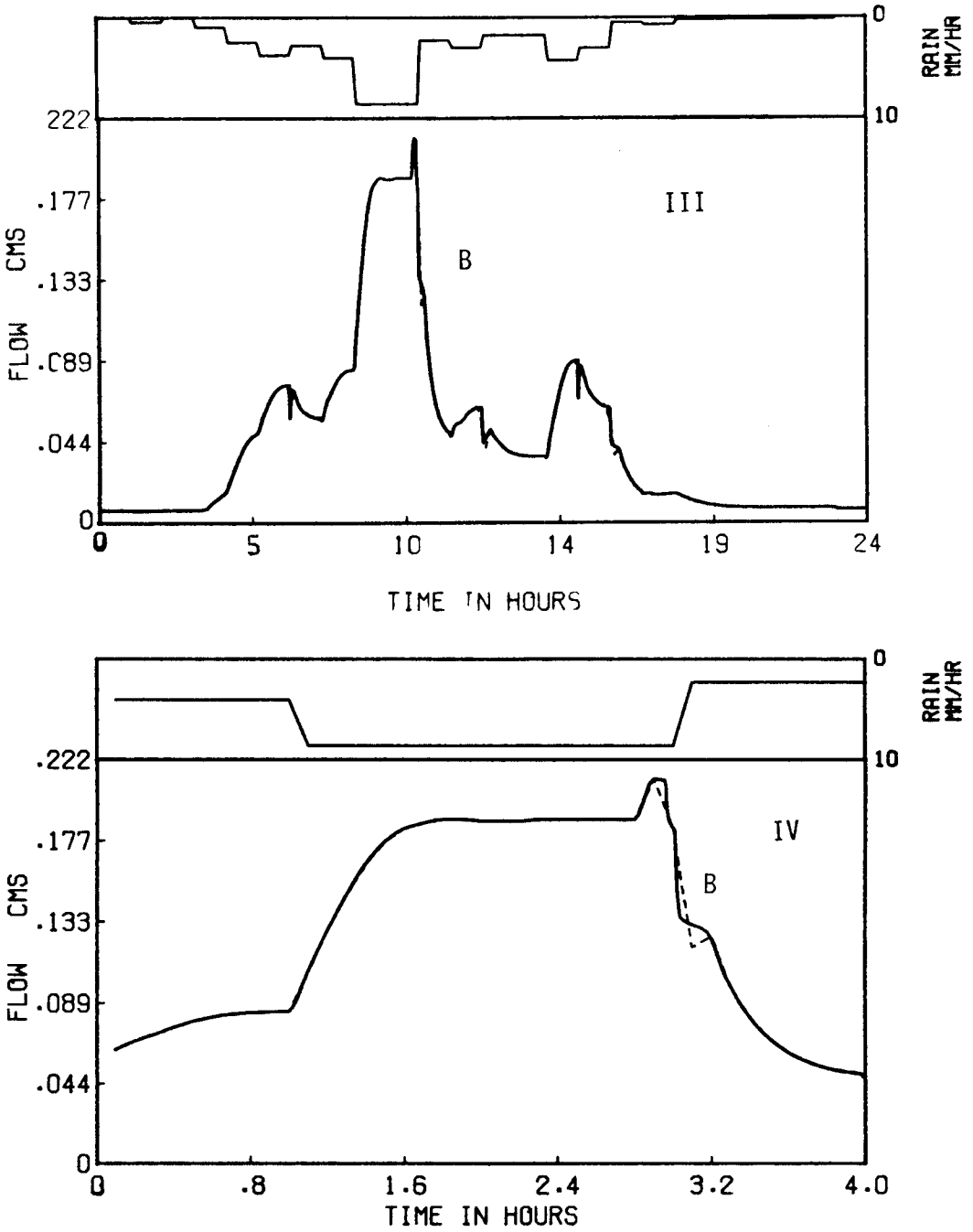

Figure 4.9 Hydrographs showing results from Smith-Hebbert model (solid) and cubic spline interpolation (dashed) such that (IV) is the 4-hour period containing the peak flow of (III).

of the original S-H flow data adequately. Pertinent details of the spline interpolation scheme are as follows:-

Let (Q_1,t_1), (Q_2,t_2),.....(Q_i,t_i), (Q_{i+1},t_{i+1}), (Q_n,t_n) be a set of n pairs of flow vs time data, and (Q,t) is the value of interest that lies between (Q_i,t_i) and (Q_{i+1},t_{i+1}) where

$$Q = L_i(t-t_i)^3+M_i(t-t_i)^2+N_i(t-t_i)+P_i \tag{4.15}$$

Let $Z_1,Z_2,.....,Z_n$ be the time differences between Q's so that

$$\begin{aligned} Z_1 &= t_1 \\ Z_2 &= t_2-t_1 \\ Z_i &= t_i-t_{i-1} \\ Z_n &= t_n-t_{n-1} \end{aligned} \tag{4.16}$$

and S_1, S_2,....., S_n be the slopes of the common cubics.

$S_1,S_2,.....,S_n$ are related to each other by

$$Z_{i-1}S_{i-1}+2(Z_{i-1}+Z_i)S_i+Z_iS_{i+1}=6\left[\frac{Q_{i+1}-Q_i}{Zi} - \frac{Q_i-Q_{i-1}}{Zi-1}\right] \tag{4.17}$$

$$\forall \quad i = 1,2,..... ,n-1$$

There are (n-2) such equations but n unknowns and so two end conditions are needed to solve the equations. For the current work, values of S_1 and S_n were chosen arbitrarily as linear extrapolation from S_2 and S_3, S_{n-2} and S_{n-1} respectively.

The relations for the end conditions are:

$$S_1 = \frac{(Z_1-Z_2)S_2 - Z_1S_3}{Z_2} \tag{4.18}$$

$$S_n = \frac{(Z_{n-2}+Z_{n-1})S_{n-1} - Z_{n-1}S_{n-2}}{Z_{n-2}}$$

From Eq. 4.15 and Eq. 4.17, a set of (n-2) equations are formed which written in matrix notation are:

$$\begin{bmatrix} \frac{(Z_1+Z_2)(Z_1+2Z_2)}{Z_2} & \frac{Z^2_2-Z^2_1}{Z_2} & & & \\ Z_2 & 2(Z_2+Z_3) & Z_3 & & \\ & Z_3 & 2(Z_3+Z_4) & Z_4 \cdots & \\ & & \vdots & & \\ & & \frac{Z^2_{n-2}-Z^2_{n-1}}{Z_{n-2}} & \frac{(Z_{n-1}+Z_{n-2})(Z_{n-1}+Z_{n-2})(Z_{n-1}+2Z_{n-2})}{Z_{n-2}} & \end{bmatrix} \begin{bmatrix} S_2 \\ S_3 \\ \vdots \\ S_{n-1} \end{bmatrix} = 6 \begin{bmatrix} \frac{Q_3-Q_2}{Z_2} - \frac{Q_2-Q_1}{Z_1} \\ \frac{Q_4-Q_3}{Z_3} - \frac{Q_3-Q_2}{Z_2} \\ \vdots \\ \frac{Q_n-Q_{n-1}}{Z_{n-1}} - \frac{Q_{n-1}-Q_{n-2}}{Z_{n-2}} \end{bmatrix}$$

The matrix is tridiagonal which needs little computer memory space to store and can be solved readily. After solving for the slopes, the cubic coefficients L_i, M_i, N_i and P_i are calculated from

$$L_i = \frac{S_{i+1} - S_i}{6Z_i}$$

$$M_i = \frac{S_i}{2}$$

$$N_i = \frac{Q_{i+1} - Q_i}{Z_i} - \frac{2Z_iS_i + Z_iZ_{i+1}}{6}$$

$$P_i = Q_i$$

and finally Q is interpolated between Q_i and Q_{i+1} from Equation 4.15.

CHAPTER 5

RESEARCH DESIGN

The unresolved question regarding valid usage of conceptual models in extreme hydrologic applications has been alluded to in the previous chapters. A causal model (S-H) and a conceptual model (SMA) appropriate for the needed comparisons have been identified. Part of Chapter 4 describes efforts made to test the credibility of S-H, and to modify and upgrade both models for meeting the needs of this research. This chapter concentrates on the methods undertaken for the fulfillment of the research objectives stated in Chapter 2.

The tasks carried out are summarized under four main categories:

(1) Preparation of climatic input data;

(2) Design of hypothetical drainage basins;

(3) General testing method; and

(4) Conceptual model evaluation procedure.

5.1 Climatic Input Data

Climatic input includes daily pan evaporation data and external storm events. Both the areal variation of rainfall and storm movement were ignored. Hourly precipitation data for different rain stations throughout the United States are available from the National Climatic Data Center, Asheville, North Carolina. The data were recorded hourly precipitation taken from four stations (two are located in Washington State and one each in Georgia and Florida) representing three different

climatic regions of the United States. The locations of these stations are given in Table 5.1 and Figure 5.1.

Table 5.1 Precipitation Station Locations

Station	Index No.	Latitude	Longtitude	Elevation above MSL
Quillayute Washington	94240	47° 57'N	124° 33'W	179 ft
Aberdeen NNE Washington	0013	47° 16'N	123° 49'W	435 ft
Tray Mountain Georgia	8860	34° 48'N	83° 42'W	4430 ft
Niceville Florida	6240	30° 31'N	86° 30'W	60 ft

MSL = Mean sea level

A 6-minute time interval was used in the simulations to represent hillslope dynamics accurately. Two years of data were used for calibrating SMA, one year for validating and another year for testing the calibrated model in operational mode. While this may seem restrictive, the number of storms per year range from 79 to 232 so the hillslopes experienced a wide range of hydrologic states and fluxes. A discussion on the length of data appropriate for calibrating SMA is given in Section 6.2. The rain data selected for prediction tests were much wetter than those data used for calibration and validation. For test cases using Georgia and Florida rain, data were taken from the same stations, Tray Mountain and Niceville, respectively. This was not so for Washington. Both Aberdeen and Quillayute are closely located to

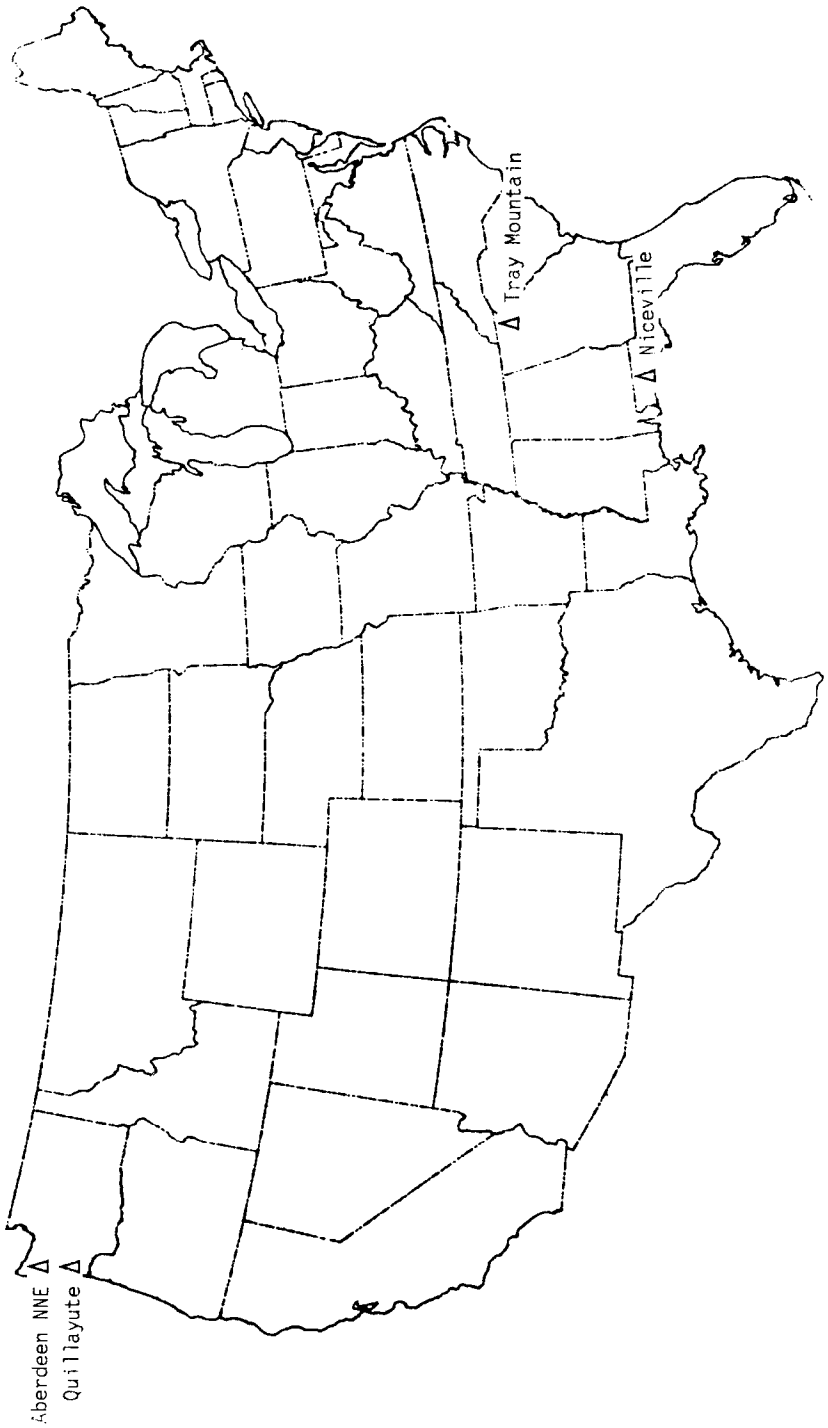

Figure 5.1 Geographical locations of rain stations Aberdeen NNE and Quillayute (Washington), Tray Mountain (Georgia) and Niceville (Florida)

each other on the coastal plain between the Pacific Ocean and the Olympic Mountains. Their rain patterns are usually of moderate intensity (Aberdeen has higher intensity) with long storm durations. Because they have similar rain structure, Quillayute rain was used for calibration and validation while Aberdeen rain for operational prediction. Properties of the rainfall data such as rainfall duration, volume, intensity and interarrival times are tabulated in Appendix F.

In contrast to the Washington rain structure, the Florida rain data have short storm durations, long interarrival time with occasional bursts of intense rain. The Georgia rain data have more uniform storm properties and are less extreme than the Washington and Florida data. In terms of total annual volumes, the stations ranked in descending order are Aberdeen NNE, Quillayute, Tray Mountain and Niceville. Figs. 5.2, 5.3, 5.4 and Table 5.2 provide information on monthly and annual precipitation depths at each station, respectively.

Table 5.2 Annual precipitation volumes

Rain Station	Annual Precipitation Volume (mm)			
	Calibration Year 1	Calibration Year 2	Validation Year 1	Prediction Year 1
Quillayute, WA	2645.5	3144.8	2657.0	-
Aberdeen NNE, WA	-	-	-	4688.9
Tray Mountain,GA	2052.8	2109.3	2024.3	2759.2
Niceville, FL	1573.8	1448.31	1343.92	2384.0

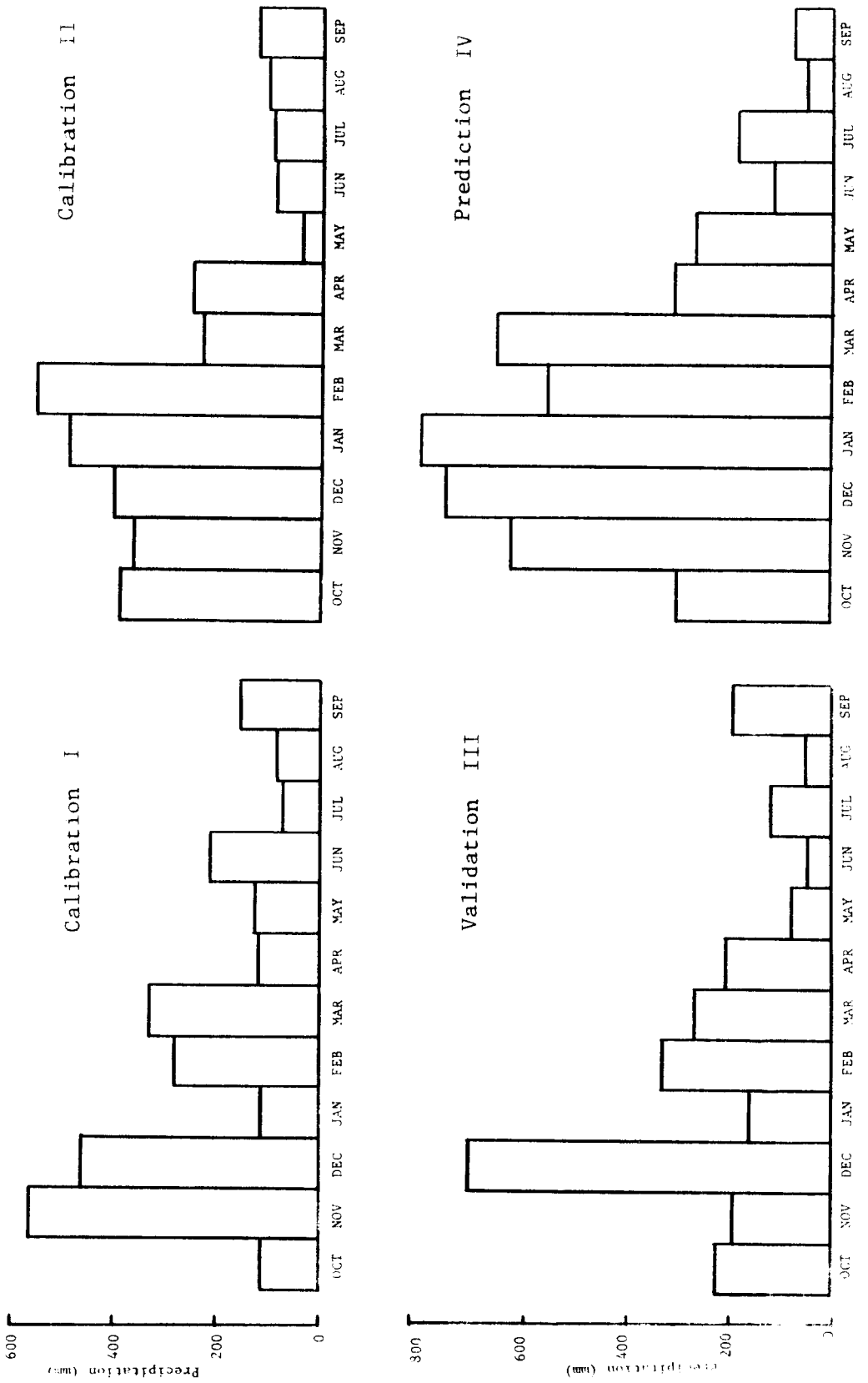

Figure 5.2 Monthly precipitation volumes at rain stations Quillayute (I,II,III) and Aberdeen NMF (IV), Washington

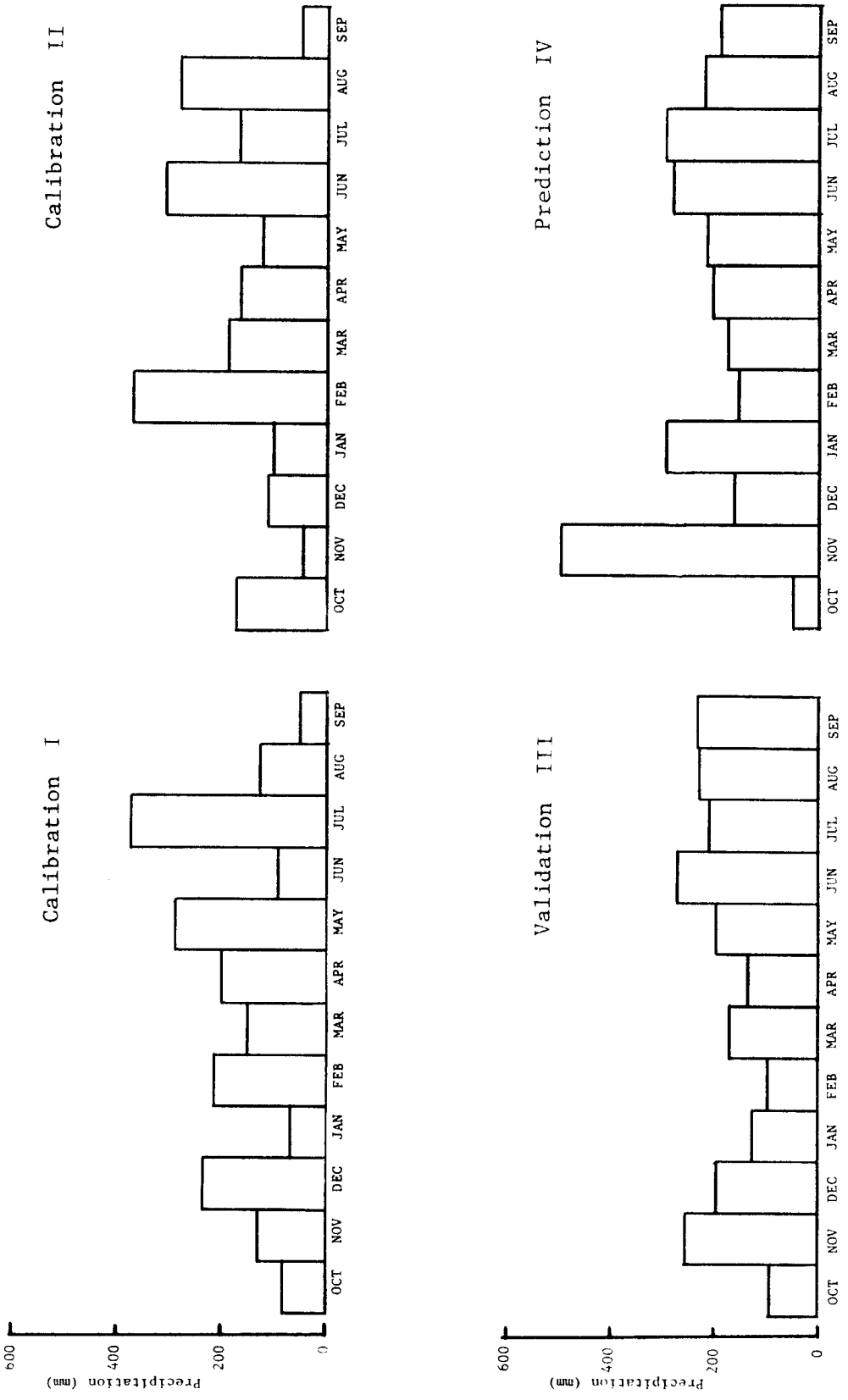

Figure 5.3 Monthly precipitation volumes at rain station Tray Mountain (I,II,III,IV), Georgia

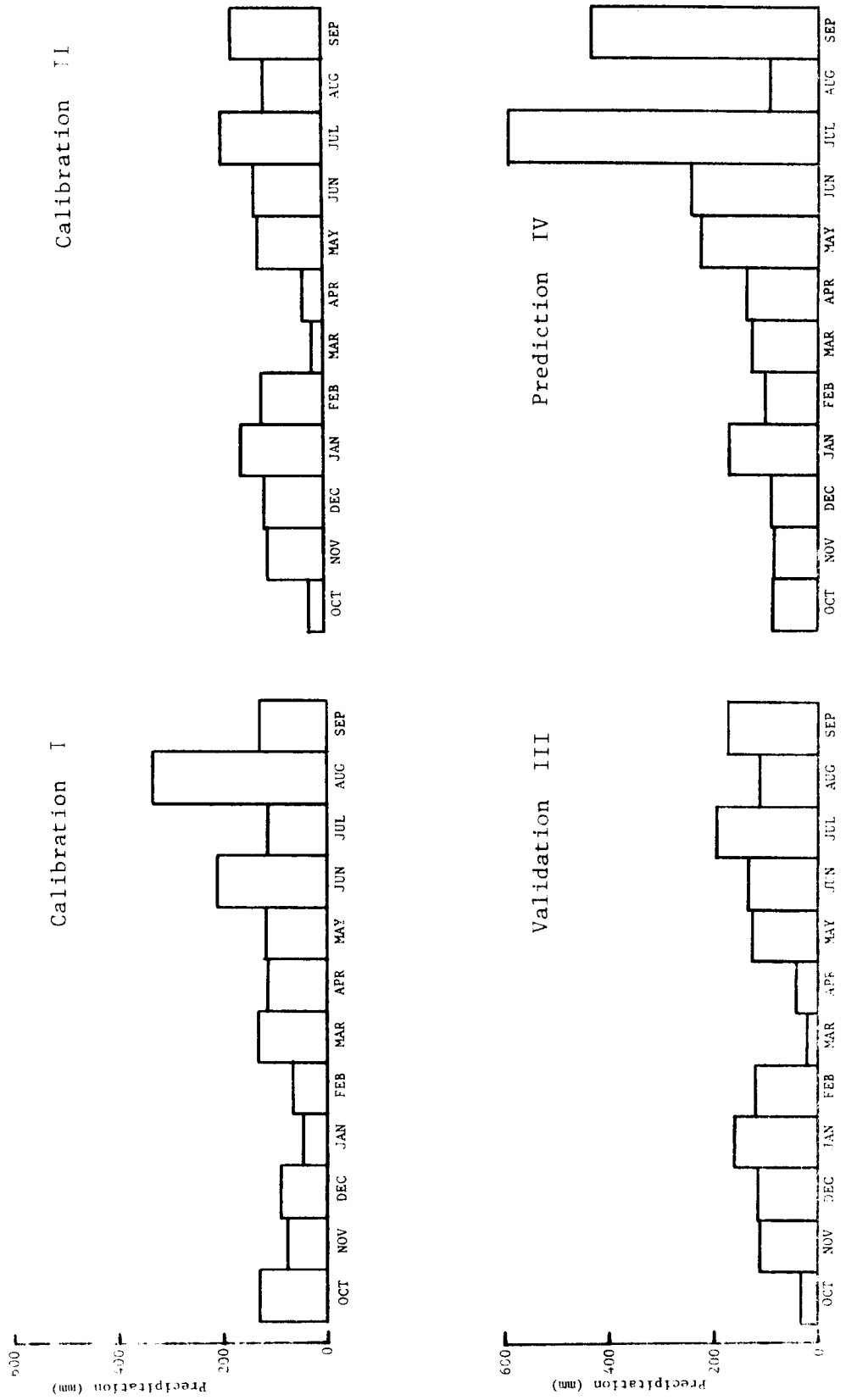

Figure 5.4 Monthly Precipitation Volumes at Rain Stations Niceville (I,II,III,IV), Florida

Table 5.3 Daily mean potential evapotranspiration (measured Class A Pan data x 0.7 (refer to Equation 5.1)), mm/day

		Class A Pan Station		
		Seattle/Tacoma Washington	Allatoona Dam Georgia	Milton Exp. Sta. Florida
	Index No.	7473	0181	5793
	Latitude	47°26'N	34°10'N	30°47'N
	Longtitude	122°18'W	84°44'W	87°08'W
DAILY MEAN POTENTIAL ET	January	.66	0.6	1.4
	February	1.0	1.3	2.0
	March	1.32	2.2	2.8
	April	1.89	3.0	3.7
	May	2.91	3.3	4.0
	June	3.43	3.7	4.1
	July	4.01	3.7	3.7
	August	3.17	3.4	3.4
	September	2.08	2.7	3.1
	October	1.14	1.9	2.6
	November	0.73	1.0	1.8
	December	0.58	0.3	1.3

Pan evaporation data were taken from three Class A pan stations (Seattle/Tacoma, Washington; Allatoona Dam, Georgia ; Milton Experimental Station, Florida) monitored by the National Weather Service (NWS, 1982). Monthly averages of observed Class A pan evaporation measurements were transformed by Equation 5.1 to mean daily potential ET values. By linearly interpolating these mean values, daily potential ET data were obtained.

$$\text{ET (mm/day)} = \frac{\text{Pan Evaporation x 0.7 x 25.4}}{\text{Days per month}} \qquad (5.1)$$

Table 5.3 provides information on the stations and the mean daily potential ET values in mm/day.

5.2 Design of Hypothetical Basins

To achieve the objective of assessing the reliability of a conceptual r-r model, an essential aspect of the work involved setting up hypothetical catchments that possess realistic characteristics of nature. Here the work of geomorphologists on the study of drainage basins, generally perceived as geomorphological systems (Chorley, 1962; Leopold et al. ,1964), was helpful. Topographic parameters of drainage basins relevant from the perspective of geomorphology are discussed briefly in Section 5.2.1. The assumptions and detailed design procedure are summarized in Sections 5.2.2 and 5.2.3, respectively.

5.2.1 Geomorphic Parameters for Drainage Basins

Many topographic characteristics have been related to basin hydrology by various researchers (Horton, 1932; Langbein,1947; Strahler, 1958). For this research, relevant geomorphic parameters can be broadly categorized in terms of land aspects, and channel aspects of drainage basins. These parameters were selected on the basis of widely accepted geomorphic principles that explain many phenomena observed in nature. A range of relevant values for these parameters are given in Appendix E, Table E.2.

The land aspects of a drainage basin are sufficiently specified by indices such as basin area, basin shape, valley slopes, hillslope soils and vegetation cover. Among these indices, basin shape is probably the most elusive topographic property to be described or measured well. Until now, Hack's (1957) relationship that relates the mainstream length (L) and basin area (A) by a simple power function written as

$$L = CA^{.6} \qquad (5.2)$$

where C is a constant, was found to hold for various major river basins in the world by Leopold et al.(1964), and demonstrated statistically by Shreve (1974) and others. The exponent of the basin area varies between 0.5 and 0.7. An exponent greater than .5 indicates a trend of basin elongation as the basin grows downstream, which is in line with the observed pear-shaped characteristics of the average basin (Horton, 1945). Because of constraints imposed by the S-H model, hypothetical catchments have to be formed from 2-D or pseudo 3-D elementary

hillslope segments arranged together (Fig. 4.1). Consequently, Hack's relationship was employed only as a guiding index to relate the mainstream length with a given basin area. Hillslope segments must be arranged so that flows between adjacent segments either did not occur or were negligible, a limitation imposed by the S-H model. This implies that hillslope gradients should be much larger than channel gradients.

Hillslope soils contribute another significant influence on basin hydrology. In S-H, a two-layer soil mantle is considered which is a simple, yet realistic approximation of the progressive decrease in soil permeabilities with depth. Whipkey and Kirkby (1978) found that one of the prerequisites for subsurface flow to be significant is the presence of one or more impeding soil layers. This concept is adopted here in modeling subsurface flows via the formation of a perched aquifer on top of the intersoil surface (refer to Fig. 4.1). Only homogeneous, isotropic soil layers were considered.

Though they occur less frequently in nature, there are soil profiles that vary in a direction parallel to that of the basin channel (Figure 5.4). The pattern of stratigraphic sequences of the hillslopes located on the S.E. Brazilian Plateau is one such example (De Meis and De Moura, 1984). The same phenomena were found by Dietrick and Dunne (1978) in forested mountains in the Oregon coast range. With reference to Fig. 5.5, the soil types only change from one subbasin to the next, i.e., from Z to A. S-H was modified to handle hypothetical basins with

such soil profiles employed in Test II and III (described in Section 5.3.1 and 5.3.2).

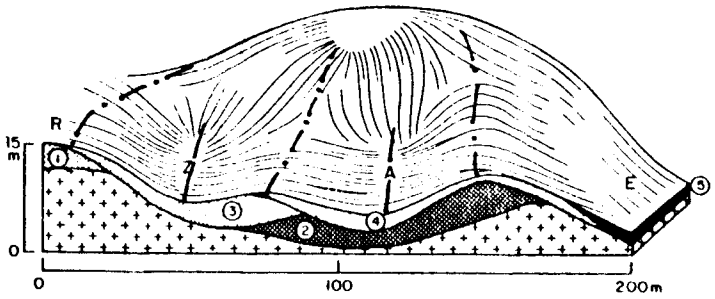

Figure 5.5 Sketch of morphostratigraphical relationships of hillslope environment located at S.E. Brazilian Plateau (from De Meis and De Moura, 1984)

Soil properties were taken from the major soil texture classes identified by the American Society of Agriculture Engineers (see Appendix E, Table E.3), reported by Rawls et al. (1981).

Overland flow directions, with given valley-side and channel slopes, could be derived from Horton's (1932) model, but were taken to be orthogonal to the receiving channel because the momentum contributed by lateral inflow to channel routing is normally insignificant. Moreover, if they were taken into consideration, elementary segments that form hypothetical catchments would become unsymmetrical. Also, to avoid an excessively complicated dynamic hydrologic cycle, vegetation was restricted to being uniformly distributed short grasses whose root systems did not penetrate beyond the top soil layer. The presence of

the grass is assumed not to change the properties of the top soil layer in any way.

Another class of geomorphic indices for a drainage basin are those that describe its channel system. Elements of channel networks that influence the basin hydrologic response include drainage density, channel network configuration, channel slopes, channel hydraulic geometry, and channel junction angles. Brief descriptions for some of these elements are given herein.

Drainage density is the average length of streams per unit basin area and thus reflects the spacing of the drainage ways. It is important because it affects both sediment and water yields significantly. However, channel network configuration is a broader descriptive term that cannot be precisely defined by a single parameter. Factors affecting channel network configuration are basin scale, climatic conditions and basin geology. Basin scale is a measurement that is usually specified by the order of the channel network in the basin (Appendix C).

Several methods for describing channel networks have been proposed (Horton, 1945; Strahler, 1952; Shreve, 1967). Shreve defines the number of first order channels of a basin as the magnitude (U) of the basin. While many basic channel patterns have been identified (Howard, 1967), the more complicated systems of Test II were restricted to two subbasins (U = 2) drained by two channels that entered the

parent channel at the downstream junction in a systematic manner (a simple fork-shaped channel network).

Channel slopes are directly related to valley slopes (Strahler, 1964) but have a smaller range compared with valley slopes and hence have lesser impact on the storm hydrographs (Table E.2). The channel routing scheme plays a very minor role in the prediction of the flood peaks except in large catchments. While channel junction angles (between tributaries and the mainstream) can be determined by Horton's (1945) or Howard's (1971) model, they were not required in this work.

Lastly, instead of using empirical channel hydraulic geometry introduced by Leopold and Maddock (1953),selections of channel cross-sections were based on charts of channel bankfull dimensions versus drainage areas of natural channels in the United States (Miller, 1958; Dunne and Leopold, 1978; Madej, 1982).

5.2.2 Assumptions of Hypothetical Basins and Channels

The salient elements of drainage basins from the standpoint of geomorphology have been discussed. Because of computational constraints, data availability and model limitations, hypothetical basins used were simplified versions of nature. While eight simplifying assumptions regarding basins given below were made, they posed minimal restrictions.

The constraining assumptions used are:

(1) The basin is a closed system in that no flow occurs across the basin divide and hence no groundwater loss or recharge occurs.

(2) There is no gully, surface depression or impervious area present on the hillslope surface.

(3) Uniform short green vegetation (grass) covers the ground surface and has a constant depth root system within the top soil.

(4) Soils in both layers are homogeneous and isotropic, and soil thickness remains constant along the flow direction. The hydraulic properties of the soil-grass system are the same as for the soil alone.

(5) The underlying basin geology is uniform and free from any significant tectonic influence.

(6) Hillslopes are straight and stable, suffer no erosion, rilling, earthslide, creep or failure of any kind.

(7) All soil hydraulic conductivities $K(\theta)$ are related to moisture content, θ, according to the Brooks and Corey formula (1964), ignoring hysteretic effects.

(8) Rain falling on the basin (or subbasin) has no spatial variation.

Assumptions made for the channel network (with U = 2) shown in Figure 5.8 are such that they comply with the requirements for applying a 1-D kinematic wave model for channel flow routing:

(1) Channel links are straight, not braided and are equal in length.

(2) Channel shapes are trapezoidal and are free from any significant scouring or sediment deposition.

(3) Flow variations in one channel at junction J (see Figure 5.8) have negligible effects upon the water surface elevation and velocity of the other channel.

(4) Channel slopes are sufficient to prevent backwater effects at J.

(5) The cross-sections of channels remain constant so that a 1-D channel routing model can be applied.

(6) Flows from rectangular basins enter the channels at right angles.

5.2.3 Procedure for Setting up Hypothetical Basins with Channel Networks

A flow chart for this procedure is presented in Figure 5.6.

(1) Select a basin area A;

(2) For Test II (Section 5.3.2) basins, estimate the mainstream length L (diameter) using Hack's (1957) relation given by Eq. 5.2 where C =1.4 if A is in $mile^2$ and C =1.27 if A is in Km^2. (Mainstream lengths L are confined to 500 m only so that time lags in peak flows due to routing are insignificant.) Adjust area A if necessary.

(3) Fix the magnitude U;

(4) Check drainage density D by

$$D' = \frac{LU}{A} \tag{5.4}$$

where LU is the total channel length. If D′ is not approximately equal to D, try another area A and return to Step (2), otherwise proceed;

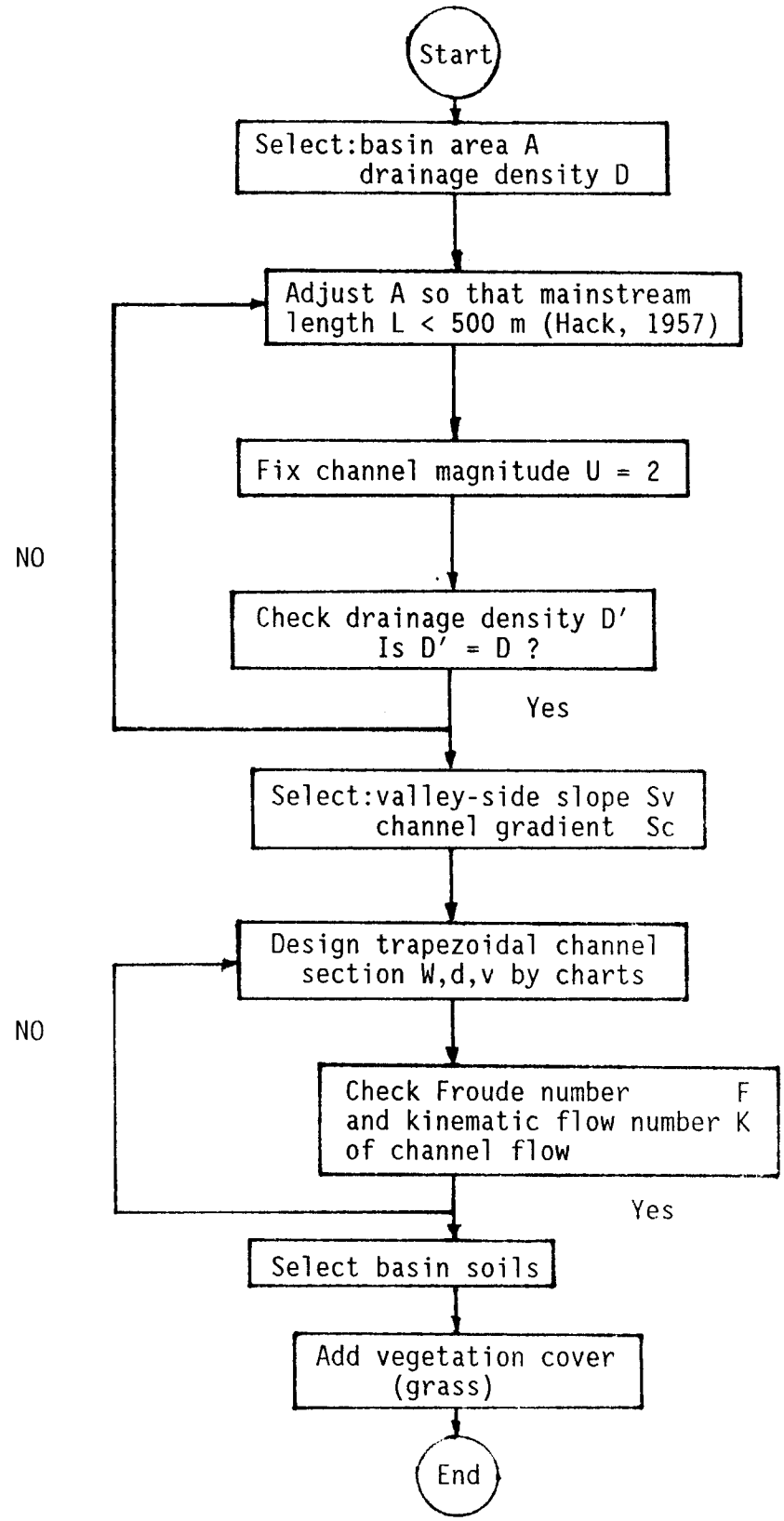

Figure 5.6 Flow chart for creating a hypothetical basin and channel

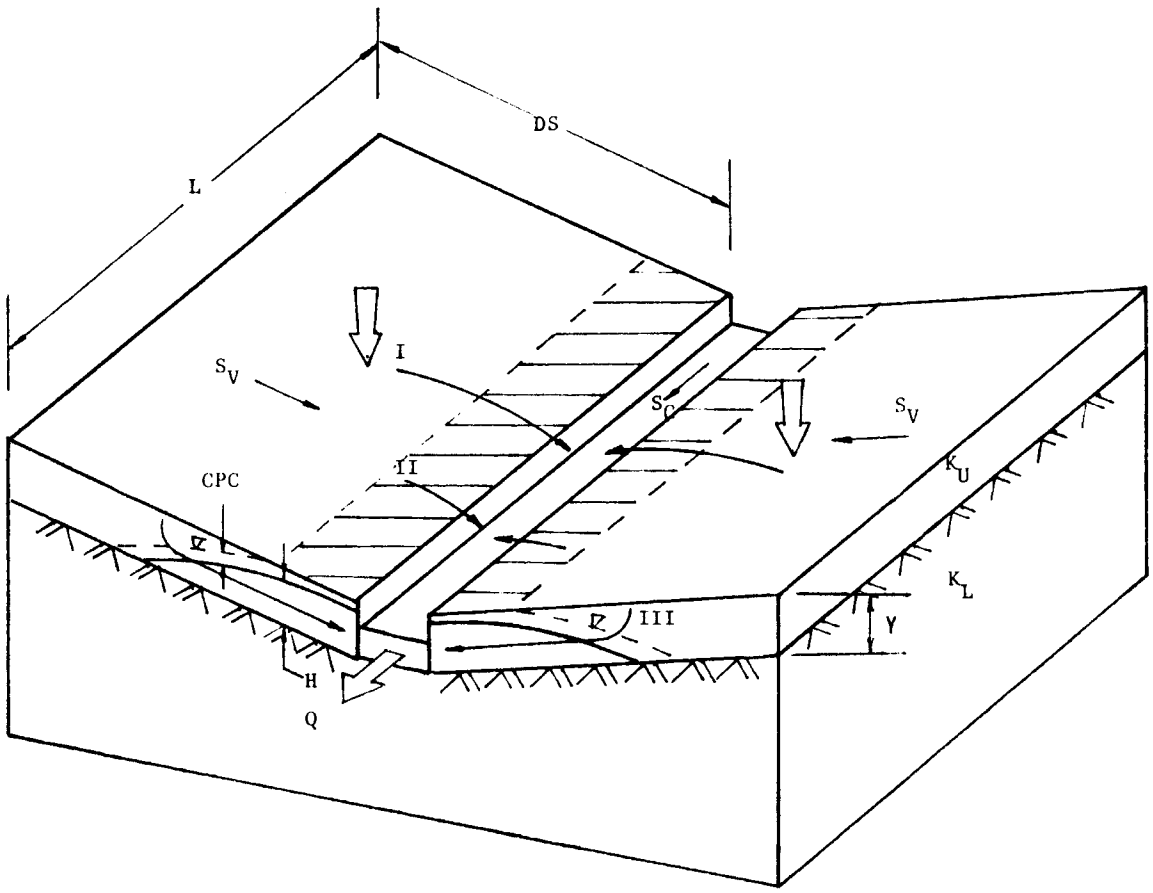

Figure 5.7 A symmetrical, single-channel elementary basin

Table 5.4 Parameters of Elementary Hypothetical Catchments depicted in Figure 5.7

Case	Catchment Parameters DS m	Y m	S	K_U m/hr	ϕ_u	$K_L \times 10^{-6}$ m/hr	L m	A km^2
HIL101	100	0.8	0.1	0.2	0.44	5	500	0.1
HIL102	100	0.8	0.1	0.02	0.40	5	500	0.1
HIL103	100	1.6	0.1	0.2	0.44	5	500	0.1
HIL104	250	0.8	0.1	0.2	0.44	5	200	0.1
HIL105	100	0.8	0.04	0.2	0.44	5	500	0.1
HGL102 HFL102	100	0.8	0.1	0.06	0.44	1	500	0.1
HGL103 HFL103	100	1.6	0.10	0.2	0.44	1	500	0.1
HGL104 HFL104	250	0.8	0.1	0.2	0.44	1	200	0.1
HGL105 HFL105	100	0.8	0.04	0.2	0.44	1	500	0.1

Legend

DS = Hillslope length (m)
Y = Upper soil thickness (m)
S = Slope
K_U = Upper soil saturated hydraulic conductivity (m/hr)
K_L = Lower soil saturated hydraulic conductivity (m/hr)
L = Catchment width (m)
A = Catchment area (km^2)
ϕ_u = Upper soil total porosity
HIL = Washington Data
HGL = Georgia Data
HFL = Florida Data

(5) Choose valley-side slope S_v and channel gradient S_c such that $S_v >> S_c$;

(6) For each basin area drained, determine the channel dimensions from charts on natural channels;

(7) For using Manning's equation, check that the Froude number of estimated peak flow F is less than 1.5 (Miller and Cunge, 1975) and the kinematic flow number K exceeds 10 (Woolhiser and Ligget, 1967), where

$$F = \frac{V}{\sqrt{gh}} \tag{5.5}$$

$$K = \frac{S_c L}{hF^2} \tag{5.6}$$

V and h are the velocity and depth of flow.

(8) Select soil types and the top soil thickness;

(9) Select the grass root system depth.

Two main classes of hypothetical catchments were tested. The first type (Test I catchments, section 5.3.1) was a rectangular basin of "open-book" shape composed of uniform soils with flows entering the channel at right angles (see Fig. 5.7). However, for Test I catchments, the channel routing component was ignored because here only the land aspects of catchments were under investigation. Next, two of the above elementary basins were selectively combined to form the second type of catchments for Tests II and III. The effects of channel

routing were considered in Test II. In the course of experiments, it was found that channel routing played a very minor role in basin outflow while it was computationally prohibitive (it increased the S-H simulation time by an average factor of 3). Hence, channel routing was ignored in Test III. Table 5.4 gives the single-element basin dimensions and soil types used in the various tests.

5.3 General Method

For a specified climatic input, soil types, hillslope topography and channel system, S-H was used to generate "error free" flow hydrographs for calibrating, validating and testing the conceptual r-r model, SMA, in two modes: operational prediction, and forecasting. The former test is relatively long-term in that a one year period of rain data was used. On the other hand, the latter is short-term for only an extremely heavy storm of 6 to 48 hours duration (on the order of a probable maximum precipitation, PMP, event) was used. Chapter 7 gives a detailed account of the results of all the tests conducted.

Graphical comparisons and statistical analysis of runoff produced by S-H and the calibrated SMA for the same climatic series and extreme event provided indications on the reliability of the latter when extrapolated beyond its calibration and verification experience. Figure 5.9 summarizes the process. All the tests conducted are categorized under three general areas described below.

5.3.1 Test I: Elementary Basins (No Channel)

For a basin comprised only of two symmetrical hillslopes, the relevant geomorphic variables such as soil thickness and types, valley-side slopes, hillslope lengths, and basin area were specified such that either one or more of the three basic flow mechanisms (Horton overland, saturation overland, and subsurface) dominated runoff production. Other than geomorphic factors, flow generation processes also depend upon the climatic conditions. Basin shapes were rectangular and soil profiles were uniform.

The key issue that these experiments address is whether a conceptual r-r model can capture the fundamental physics of the hillslope hydrologic behavior. Test I comprises cases HIL101 to HIL105, HGL102 to HGL105 and HFL102 to HFL104.

5.3.2 Test II:Basins with Channel Networks of Magnitude U = 2

A basin with a network of magnitude 2 (Fig. 5.8) was made up of two subbasins as shown in Fig. 5.7, and each subbasin was drained by a single channel. In order that runoff enters the channels at right angles, a limitation of S-H, the two subbasins are respectively replaced by two rectangular segments assumed to be independent of each other. A substantial effort was devoted in adapting S-H for this purpose. The subbasins had different geomorphic properties and produced flow from different flow mechanisms. These tests were conducted to address possible ambiguities when modeling basins possessing widely disparate soil mantles where lumped parameters are

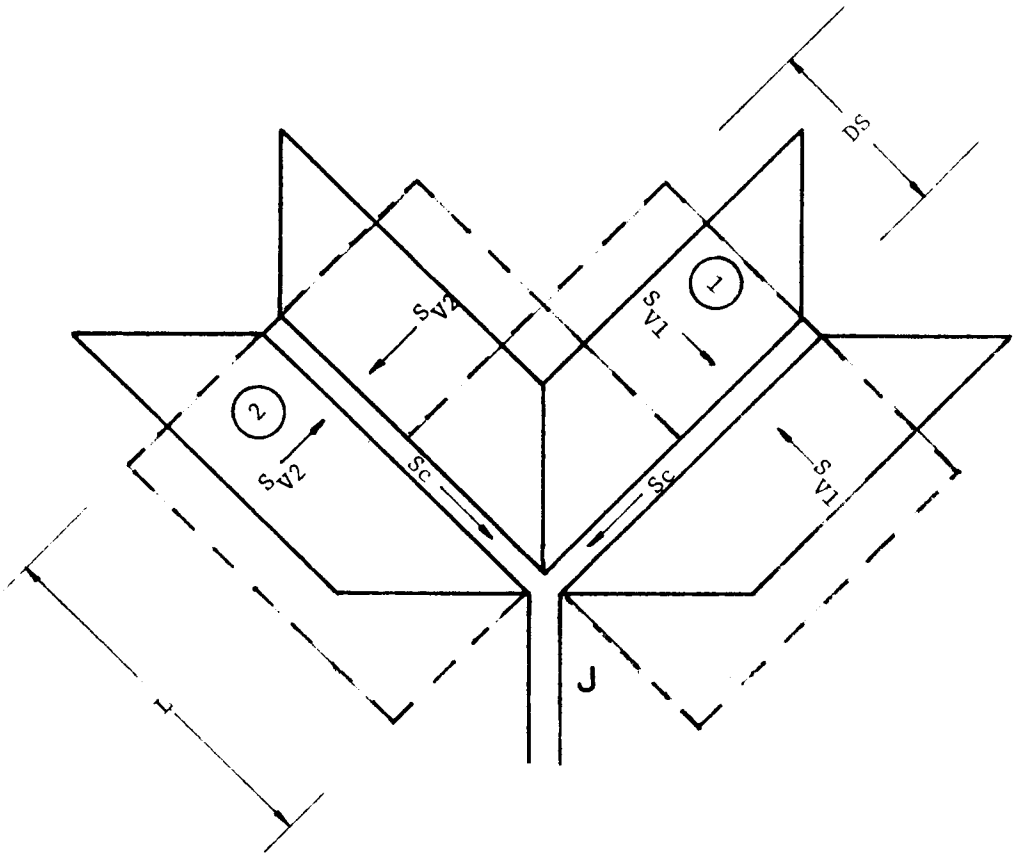

Figure 5.8 A hypothetical catchment with two subbasins (1 & 2) which are replaced by rectangular segments (dotted lines) so that flows enter the channels at right angles (Test II).

used. Hydrographs from the two subbasins were routed to the channel junction and superimposed as the basin outflow. The channels used have a constant bedslope of 0.004, a trapezoidal cross-section of bottom width 2.25 m and 1:1 side slopes. The streamflow data generated by S-H were used for calibrating, validating, and testing the conceptual model.

The tests here demonstrate some of the effects basins with greater land complexities have on conceptual modeling. They explore how spatial variability in basin geomorphology influences the values of estimated lumped parameters. Test II comprises cases HL223, HG223 and HF223.

5.3.3 Test III: Basins subjected to spatially variable storm input

In addition to basin complexities dealt with in Test II, the effects of storm spatial variability were considered here. Again, tests were confined to catchments with two subbasins only.

Rain input on an individual subbasin was uniform but differed from the other subbasin. Rainstorms from one of the rain stations were applied to one subbasin. Then the storm depths of the same set of storms were "perturbed" by a noise component, assuming the time distributions of rainstorms remained unchanged. This was achieved by adding to the storm depths scaled random numbers generated from a uniform distribution. These "contaminated" rainstorms were applied to the second subbasin. S-H outflows reflect these separate inputs while SMA used a single input, the noise contaminated rainfall.

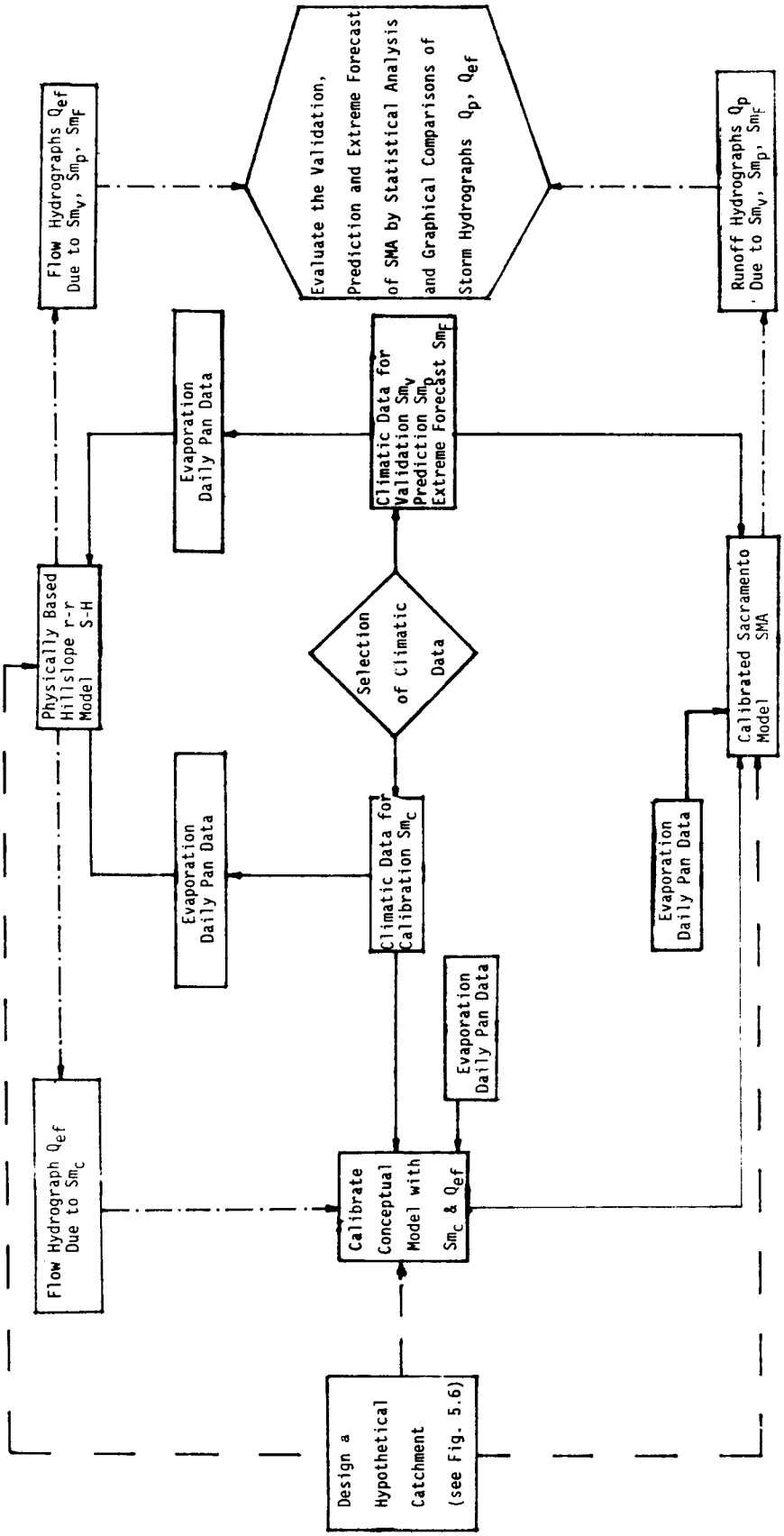

Figure 5.3 Flow Chart for the Overall Research Methodology

The noise term represents the variations in rain falling at different points of a basin caused by wind circulation or other effects. In a limited sense, this series of tests examined some of the effects of rainfall spatial variability on the calibration and use of conceptual models. The complex interactions of basin parameters and climatic input variations also help to examine issues concerning the number of rain gages required to monitor rain depth. Test III comprises cases HUL104, HUG105 and HUF45.

5.4 Evaluation of Conceptual Model Performance

Conventional methods of evaluating hydrologic model performance were given by Pilgrim (1975), James and Burges (1982) and Green et al. (1986). Willmott (1981, 1982) commented on the evaluation of geographic and atmospheric science models. They generally advocated the use of statistical measures between observed and simulated variates as the quantitative approach to model evaluation. However, they differ in opinions as to which statistical indices are more useful than others. James and Burges emphasized the utility of graphical comparisons. Willmott also recommended statistical graphics to describe visually the relationships between the two variates being compared.

SMA is a continuous streamflow simulation model. However, the overall model performance was assessed on the basis of both continuous and single events. In a broad sense, the former includes model calibration, validation and prediction tests. Its evaluation approach comprises statistical mesures, comparisons of graphical plots of "error free" flow hydrographs (Q_{ef}) against simulated flow hydrographs (Q_p),

and the comparison of volumes of various flow mechanisms. For the extreme rain tests using the calibrated model (SMA) (Section 7.4) comparisons of graphical plots and event summary variables (flow volume, peak flow, and time to peak) were made.

5.4.1 Statistical Summary

Moments of flow data used included the mean and standard deviation. Instead of checking for significance by hypothesis tests, these summary statistics are tabulated for simple comparisons between "error free" Q_{ef} and simulated Q_p variates. $\underline{Q}_{ef}$ is the mean of Qef.

Other than moment estimates, residues were analyzed for trends such as systematic over or under simulations. Several measures were used for the analysis of residues:

Maximum error, QME, (CMSD),

$$QME = \text{Max } (Q_{pj} - Q_{efj}) \Big|_{j=1}^{M_j} \tag{5.8}$$

Root mean square error, RMSE, (%)

$$RMSE = \left[\frac{\sum_{j=1}^{M_j} (Q_{pj} - Q_{efj})^2}{M_j} \right]^{0.5} \times \frac{100}{\underline{Q}_{ef}} \tag{5.9}$$

Coefficient of determination, R^2,

$$R^2 = \frac{\sum_{j=1}^{M_j} (Q_{efj} - \underline{Q}_{ef})^2}{\sum_{j=1}^{M_j} (Q_{pj} - \underline{Q}_{ef})^2} \tag{5.10}$$

Modeling efficiency, E_f,

$$E_f = \frac{\sum_{j=1}^{M_j} (Q_{efj} - \underline{Q}_{ef})^2 - \sum_{j=1}^{M_j} (Q_{pj} - Q_{efj})^2}{\sum_{j=1}^{M_j} (Q_{efj} - \underline{Q}_{e}f)^2} \tag{5.11}$$

Coefficient of residual mass, RM,

$$RM = \frac{\sum_{j=1}^{M_j} Q_{efj} - \sum_{j=1}^{M_j} Q_{pj}}{\sum_{j=1}^{M_j} Q_{efj}} \tag{5.12}$$

Some of these statistics, calculated for both the original flow sequence at a time interval of six minutes and for their mean daily averages, are given in Table 7.2. The coefficient of determination, R^2, measures the proportion of the total variance of "error free" data explained by SMA. While the root mean square error, RMSE, is sensitive to a few big errors, it does not identify the types of errors, systematic or random, that are present in Qp. The modeling efficiency E_f is also affected by a few extreme errors and could be biased if a wide range of flow events are experienced. E_f is less than 1 and can be negative as seen in Table 7.2. A negative modeling efficiency shows

that the model's simulated value is worse than simply using the observed mean. James and Burges (1982) suggested that E_f should exceed 0.97 together with other measures for satisfactory model performance when modeling hydrographs in natural catchments.

5.4.2 Graphical Displays

Traditional methods of evaluating model performance by statistical measures have limitations. Numbers are not effective in communicating qualitative information such as trends, types of errors and distribution patterns. Graphical display is important. It is a visual display of quantitative as well as qualitative information. The ability of the human visual system to decode information, to detect geometric patterns, and to assess magnitudes encoded on graphs make graphical methods a powerful tool for analyzing scientific data. Two types of graphics, statistical, and hydrographs, were plotted. Statistical graphics plotted were box-plots and bivariate scattergrams. Though simple in nature, they display succinctly the relationships between the two variates of interest, Q_{ef} and Q_p.

Box plots compare several distributions of flow differences (Q_p - Q_{ef}) grouped in terms of Q_{ef} flow intervals. The horizontal line inside the box is the 50^{th} percentile, the top and bottom are the 25^{th} and 75^{th} percentiles. The upper and lower ends of the dashed lines are the maximum and the minimum values within the respective measurement groups.

Scattergrams of Q_p were plotted against Q_{ef} on a $\log_{10}$ scale because of the range of flow rates generated from a given hillside. Graphing on a linear scale produces a graph of poor resolution because a few extreme values caused most of the data to cluster near the origin. Even on a logarithmic scale, some cases (Figs. 7.10 and 7.12) still display this problem. The principal value of each scattergram is to observe under- or over- simulation as a function of flow magnitude.

Plots of streamflow hydrographs of "error free" (Q_{ef}) and simulated (Q_p) data are used to display model quality. For single-event plots, Q_p was superimposed on Q_{ef} (Figs. A.1 to A.23). The same approach could not be used for continuous hydrograph plots which had many peaks to be plotted within a small space. Therefore, for continuous hydrographs, the "error free" hydrographs Q_{ef} were plotted with the difference (Q_p - Q_{ef}) plotted directly below (Figs. 7.1 to 7.18).

CHAPTER 6

Calibration of The Sacramento Model

Then I applied myself to the understanding of wisdom,
and also of madness and folly,
but I learned that this, too,
is a chasing after the wind.

Ecclesiastes 1:17

Calibration is one of the most important aspects of the overall conceptual modeling process. A poorly calibrated conceptual model will inevitably produce erroneous flow even though the model itself may be conceptually realistic.

For a range of soil types, basin geometries, and climatic input, the S-H model was operated to produce flow time series which, together with the same input data set, were used for calibrating the Sacramento model (SMA). Snow was not considered so the snow accumulation and ablation component of SMA was removed from the model. A set of values was assigned initially to the model parameters which were adjusted through a combination of manual and automatic calibration processes. Throughout the processes, comparisons between the "error free" and the "simulated" streamflow values were the basis for determining the stage of parameter optimization. From time to time, parameters were also inspected and any value found to be physically unrealistic was manually replaced. The quality and effectiveness of the final calibration was assessed by verification summary statistics and graphical comparisons of another period of flow data generated by S-H and SMA. Sections 5.4 and 7.3 describe, respectively, the statistical indices and graphs used.

6.1 Initial Estimates of Model Parameters

A list of model parameters, grouped in terms of the sequential phases of the soil moisture accounting processes, is presented in Table 6.1. For each case study, out of 17 model parameters, only 10 are to be determined (labelled as type V) since the rest (Type F) have either zero or nominal values which are not optimized. Use of accurate initial parameter estimates expedites the calibration process. If the initial estimates are poor, instead of converging to optimality, automatic calibration might cause parameters to diverge to unrealistic values.

Techniques have been developed to estimate initial parameter values primarily from observed streamflow hydrograph and catchment information (Burnash et. al, 1973; Peck, 1976). Parameters which can be readily estimated are those concerned with SMA's lower zones (LZFPM, LZPK, LZFSM and LZSK). A new approach for estimating these parameters was developed during the current work. It is difficult to estimate parameters such as the lower zone tension storage LZTWM and the upper zone moisture parameters UZFWM, UZTWM and UZK. UZFWM and UZK are two upper zone parameters primarily concerned with interflow (return flow) and surface flow mechanisms. Some rules of thumb based on calibration experience for the hypothetical small catchments modeled here are given below.

For catchments having quick and sizeable surface flow response to heavy storms, UZFWM should be kept small, on the order of 5 to 20 mm but UZK on the order of 0.5 to 0.9. If a catchment produces substantial

Table 6.1 Soil moisture accounting parameters of the Sacramento model (SMA)

Soil moisture phase	No	Parameters	Type	Description	Range
Direct	1	PCTIM	F	Minimum impervious area %	0.0
runoff	2	ADIMP	F	Additional impervious area %	0.0
	3	RIVA	F	Riparian vegetation area %	0.0
	4	EFC	F	Effective forest cover %	0.0
Upper	5	UZTWM	V	Upper zone tension water capacity mm	5 - 250
zone	6	UZFWM	V	Upper zone free water capacity mm	3 - 30
	7	UZK	V	Daily upper zone free water withdrawal rate	.06 - .98
Perco-	8	ZPERC	V	(ZPERC+1)xPBASE = the maximum percolation rate	10 - 130
lation	9	REXP	V	Exponent for the percolation equation	1 - 3
Lower	10	LZTWM	V	Lower zone tension water capacity mm	20 - 200
zone	11	LZFSM	V	Lower zone supplemental freewater capacity mm	10 - 350
	12	LZFPM	V	Lower zone primary freewater capacity mm	50 - 900
	13	LZSK	V	Daily supplemental withdrawal rate	.008 - .10
	14	LZPK	V	Daily primary withdrawal rate	.005 - .03
	15	PFREE	F	% percolation water goes directly to LZFM storages	.30

Table 6.1 Continued

	16	RSERV	F	% lower zone free water not transferable to LZTW	.30
	17	SIDE	F	Ratio of non-channel baseflow to channel baseflow	0.0
Initial	18	UZTWC	V	Upper zone tension water content mm	0 - 250
water	19	UZFWC	V	Upper zone freewater content mm	0 - 50
	20	LZTWC	V	Lower zone tension water content mm	0 - 200
	21	LZFSC	V	Lower zone supplemental free water content mm	0 - 350
	22	LZFPC	V	Lower zone primary free water content mm	0 - 900
	23	ADIMC	V	Tension water contents of the ASIMP area mm	0 - 250
Climatic	24	PXADJ	F	Precipitation adjustment factor	1.0
Index	25	PEADJ	V	ET-demand adjustment factor	0.7 - 1.0

Legend

F = parameters with fixed user specified values
V = parameters with values determined through calibration

baseflow but little surface flow even during wet periods, UZFWM and UZK should have initial values in the reverse order. UZFWM should range between 20 to 75 mm and UZK 0.08 to 0.4.

By keeping the above guidelines in mind, and after examining the streamflow hydrographs from the S-H model (truth), initial values for UZFWM and UZK are assigned accordingly. Initial values of the percolation parameters ZPERC and REXP are usually based on values obtained from calibration of the model for a similar catchment. ZPERC ranges between 50 to 130 and REXP between 1.0 to 3.0. According to Burnash et. al (1973) and Peck (1976), if no such information is available, REXP can be given an initial nominal value of 1.8.

Armstrong (1978) developed a procedure for obtaining initial parameters from catchment soil properties. Because the soil properties of hypothetical catchments are homogeneous and clearly defined, his method should be applicable here. After applying his technique on one of the test catchments, initial parameters derived were found to be unrepresentative; with these values as the starting point, the calibration process was inefficient and his approach was not pursued. Table 6.2 shows the wide contrast between initial parameters derived from Armstrong's method and the optimal parameters that were obtained separately from other techniques.

Table 6.2 Initial parameters from Armstrong's method compared with optimized parameters for case HIL101

Parameters	Initial parameters by Armstrong's method (mm)	Optimized Parameters (mm)
UZTWM	75.	154.
UZFWM	21.	6.
UZK	0.06	0.66
ZPERC	198.	55.
REXP	1.5	2.1
LZTWM	97.	80.
LZFSM	15.	108.
LZFPM	50.	272.
LZSK	0.022	0.028
LZPK	0.004	0.021

An alternative procedure for estimating initial lower zone SMA parameters for hillslope catchments is described below.

Initial Estimates of Lower Zone Parameters

Select a dry period with minimum or no precipitation so that the (S-H) hydrograph is predominantly baseflow . The initial and the final baseflows Q_0 and Q_t, separated by t days, are noted (Fig. 6.1).

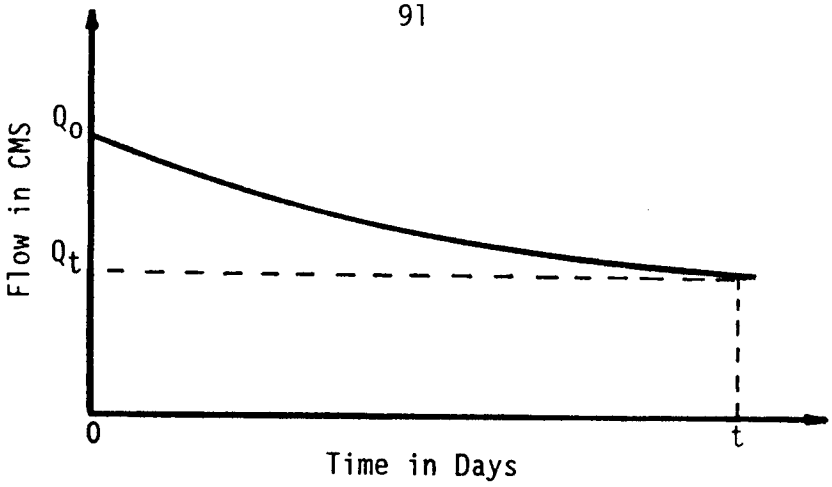

Figure 6.1 A baseflow curve

Assume Q_o and Q_t are entirely attributed to the primary and secondary base flows Q_p and Q_s, such that

$$\begin{aligned} Q_o &= Q_{po} + Q_{so} \\ Q_t &= Q_{pt} + Q_{st} \end{aligned} \tag{6.1}$$

where Q_{po}, Q_{so}, Q_{pt} and Q_{st} are the primary and secondary flow components at time o and t, respectively. Let LZPK and LZSK be the primary and secondary recession coefficients so that

$$\begin{aligned} Q_{pt} &= [\ 1 - LZPK\ ]^t\ Q_{po} \\ Q_{st} &= [\ 1 - LZSK\ ]^t\ Q_{so} \end{aligned} \tag{6.2}$$

From equations 6.1 and 6.2,

$$\begin{aligned} Q_{po} + Q_{so} &= Q_o \\ [\ 1 - LZPK\ ]^t\ Q_{PO} + [\ 1 - LZSK\ ]^t\ Q_{so} &= Q_t \end{aligned} \tag{6.3}$$

Or expressed in matrix form,

$$\begin{bmatrix} 1 & 1 \\ [\ 1 - LZPK\ ]^t & [\ 1 - LZSK\ ]^t \end{bmatrix} \begin{bmatrix} Q_{po} \\ Q_{so} \end{bmatrix} = \begin{bmatrix} Q_o \\ Q_t \end{bmatrix} \tag{6.4}$$

For the indeterminate system of Equation 6.4, LZPK, LZSK, Q_{po} and Q_{so} are unknown. By assigning values to the former two parameters, the

latter two are determined. If values assigned to LZPK and LZSK are poor, either Q_{po} or Q_{so} could be negative. Using a trial and error approach, a set of values for LZPK and LZSK is obtained. The pair which produce Q_{po} and Q_{so} that are more consistent than the rest with respect to the curvature of the baseflow hydrograph are selected as initial estimates. For example, if the hydrograph has a relatively mild slope, Q_{po} should dominate Q_{so} and vice versa.

The lower zone primary and secondary moisture contents LZFPC and LZFSC are related to Q_p and Q_s by

$$\begin{aligned} LZFPC &= K(Q_p \;/\; LZPK) \\ LZFSC &= K(Q_S \;/\; LZSK) \end{aligned} \qquad (6.5)$$

Where K is the conversion factor from m^3/sec to mm/unit area. Maximum primary and secondary baseflows are estimated from the S-H calibration hydrograph and using equation (6.5), the corresponding maximum value of LZFPC and LZFSC obtained should be closely related to LZFPM and LZFSM, their respective storage capacities. Initial estimates for LZFPM and LZFSM are based on the maximum LZFPC and LZFSC values obtained, and usually augmented by another 10 to 20 %. An example is given below.

Catchment area = 0.10 km^2

Q_0 = 0.002 m^3/s

Q_t = 0.00114 m^3/s

t = 23.66 days

From Equation (6.2)

$$\begin{bmatrix} 1 & 1 \\ [\ 1 - LZPK\ ]^{23.66} & [\ 1 - LZSK\ ]^{23.66} \end{bmatrix} \begin{bmatrix} Q_{po} \\ Q_{so} \end{bmatrix} = \begin{bmatrix} 0.002 \\ 0.00114 \end{bmatrix}$$

Table 6.3 Initial estimates of LZPK and LZSK by a trial and error method

No.	LZPK	LZSK	Q_{po}	Q_{so}
1	.007	.010	-.00744	.00944
2	.010	.030	.00055	.00145
3	.011	.058	.00124	.00076
4	.01	.05	.00111	.00089
5	.02	.05	.0017	.00031
6	.015	.05	.00136	.00064
7	.020	.03	.00125	.00075
8	.010	.07	.00128	.00072

A brief description of the selection procedure is given here. Estimate No. 1 was ruled out because Q_{po} is negative. Based on the relatively flat curvature of the baseflow hydrograph for this case, Q_{po} should be dominant, hence No. 2 and No. 4 were also discarded. No. 5 was also not accepted because Q_{po} is proportionally too high. Estimates No. 3, 6, 7 and 8 have comparable values for Q_{po} and Q_{so}. However, No. 8 where LZPK = 0.01, LZSK = 0.07, Q_{po} = 0.00128 and Q_{so} = 0.00072 was chosen for the initial parameter set because based on calibration experience, for cases similar to this, LZPK should be significantly smaller than LZSK.

For the selected estimate No. 8,

LZFPM = (864 x .00128 x 1.2) / .01 = 264 mm

LZFSM = (864 x .00072 x 1.2) / .07 = 24 mm

Where, 864 (= 3600 x 24 x 10^3 x 10^{-5}) which is K in Equation 6.5, converts m^3/s to mm and 1.2 is used to scale the estimates by an additional 20%. The initial estimates and the optimized values are given in Table 6.4 which shows that the contention of LZSK being much larger is not accurate.

Table 6.4 Initial lower zone parameters compared with the optimized values

Parameters	Initial Estimates	Optimized Values
LZPK	0.01	0.014
LZSK	0.07	0.030
LZFPM	264.	231.
LZFSM	24.	47.5

6.2 Automatic Calibration

Following the estimation of initial parameters and some preliminary manual calibration, automatic algorithms can be used to optimize the model parameters. Automatic calibration aids, such as a hill climbing method (Monro,1971; Burnash, 1973), gradient search algorithm (Sorooshian and Gupta,1983; Sorooshian et al,1983), or a simplex for function minimization, (a pattern search method, Nelder and

Mead, 1965), are a few of the many algorithms used for calibrating hydrologic models automatically.

Despite recent advances in automatic calibration techniques, there is still no guarantee that optimal parameters would be obtained. The high degree of interacton between parameters and the complex model structures of SMA make unique estimation of parameters almost impossible. The Nelder and Mead simplex method was found to be the most effective scheme available and was used throughout this work.

An automatic calibration procedure has three elements. The first element concerns the length of record used for calibration. A sensitivity analysis of the effects of data record length, using one, two, and three years of data for the case HIL101 was carried out (Fig. 6.2). For these three cases, the same set of initial values for SMA parameters was used. In Fig. 6.2, each calibration represents one complete cycle, which can be either one, two, or three years of computations. Among the three cases, parameters that converge to almost the same optimum values are UZFWM, UZK, LZFPM and LZPK. Parameters whose convergence are not as close are ZPERC, REXP and LZSK. LZFSM, LZTWM and UZTWM are three parameters that have significantly different optimized values because for case HIL101, they are relatively insensitive. Apparently, NMS is more effective in optimizing sensitive parameters that have most influence on model predicted streamflows. For parameters which have little influence on model generated streamflows and hence on the objective function, NMS has problems producing optimal values.

Figure 6.3 shows that the extreme flood hydrographs for dry antecedent conditions computed by S-H and SMA for the three cases are basically the same. This offers little surprise since peak flows are dictated by the upper zone parameters which among the three cases are almost the same. Fig. 6.2 shows that the one-year case requires more calibration runs than the two-year case to arrive at convergence for the upper zone parameters. Even though the former effectively represents about the same amount of computation as the latter, it is subjected to greater influence by the initial conditions which can be significant. The three-year data case has no obvious advantage. The test case explored here produced a mix of surface and subsurface responses to rainfall and reflects the range of experience that will be encountered by SMA for its upper and lower zone storages. Given that the most influential parameters are estimated adequately with two years of calibration, that amount of calibration data appeared appropriate for all subsequent work. Consequently, SMA was calibrated for all eighteen cases using a two-year long climatic record.

Two years of data include two different annual cycles of dry and wet seasons. Though a longer data set (three to five years) would be more appropriate for a large catchment, the calibration period was restricted because of data handling limitations (two years of data at a 6-minute time step comprise 175200 numbers). Calibration data used were ideal because they were simulated error free from catchments with homogeneous soils and uniform topography. Therefore problems of missing and unrepresentative data did not exist.

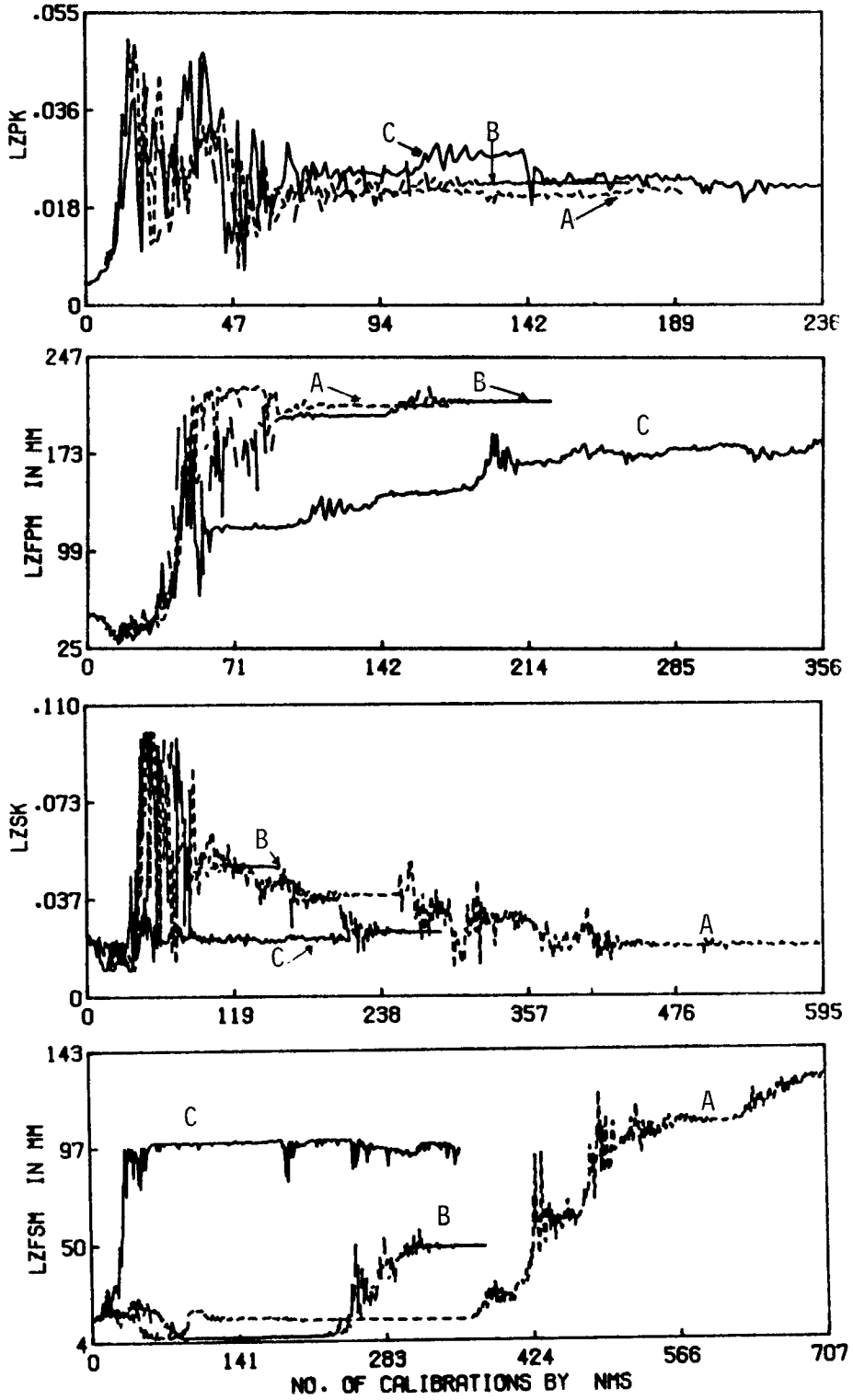

Figure 6.2 Sensitivity analysis of the effects of data length (one (A), two (B), and three (C) years) on automatic calibrations of SMA using NMS for HIL101

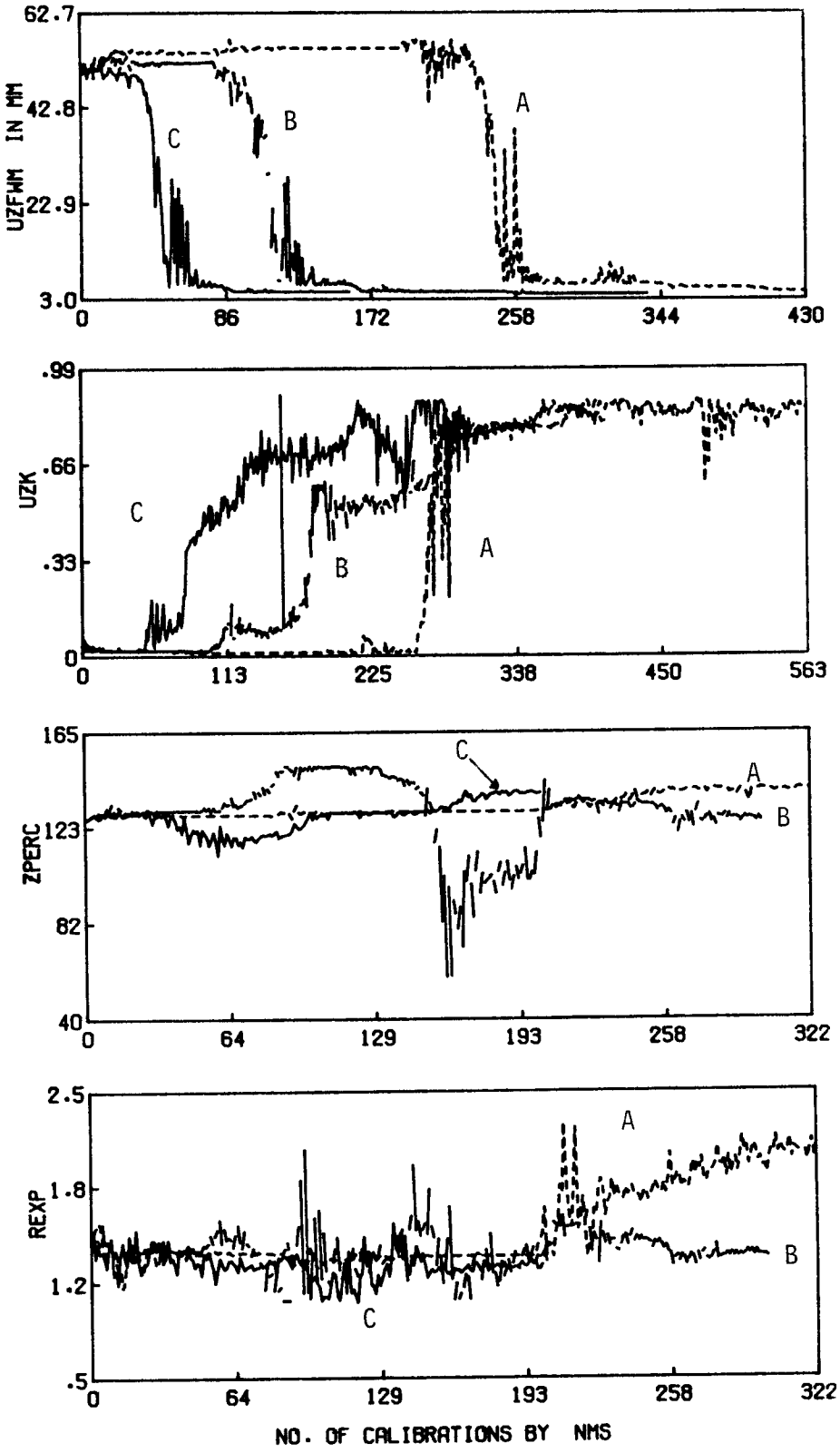

Figure 6.2 Continued

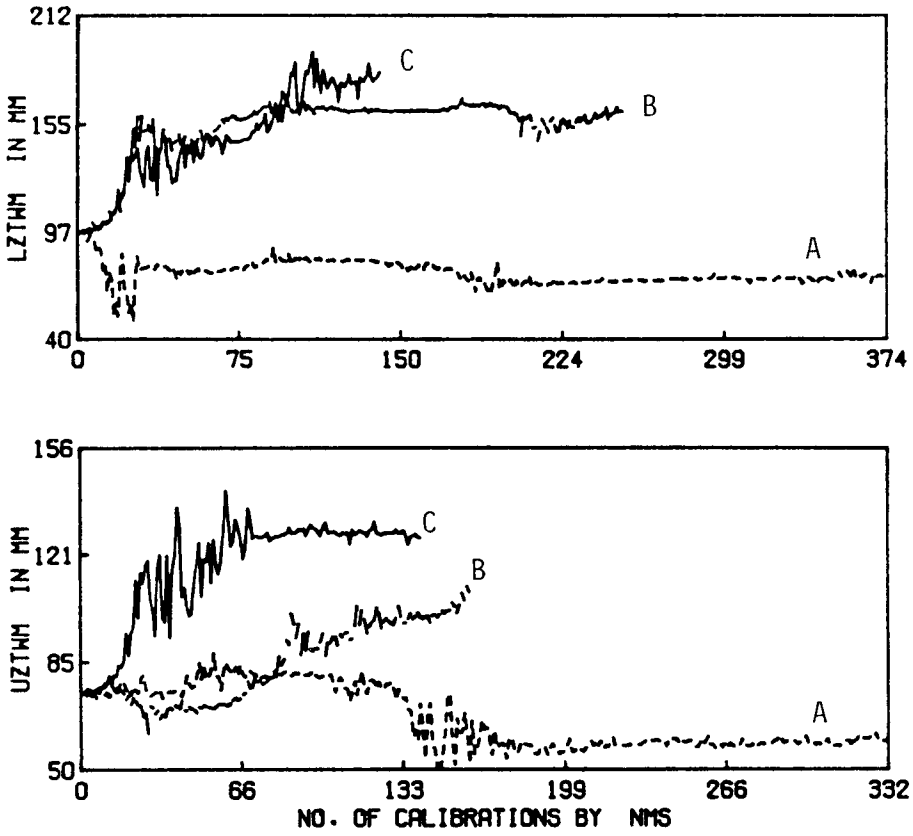

Figure 6.2 Continued

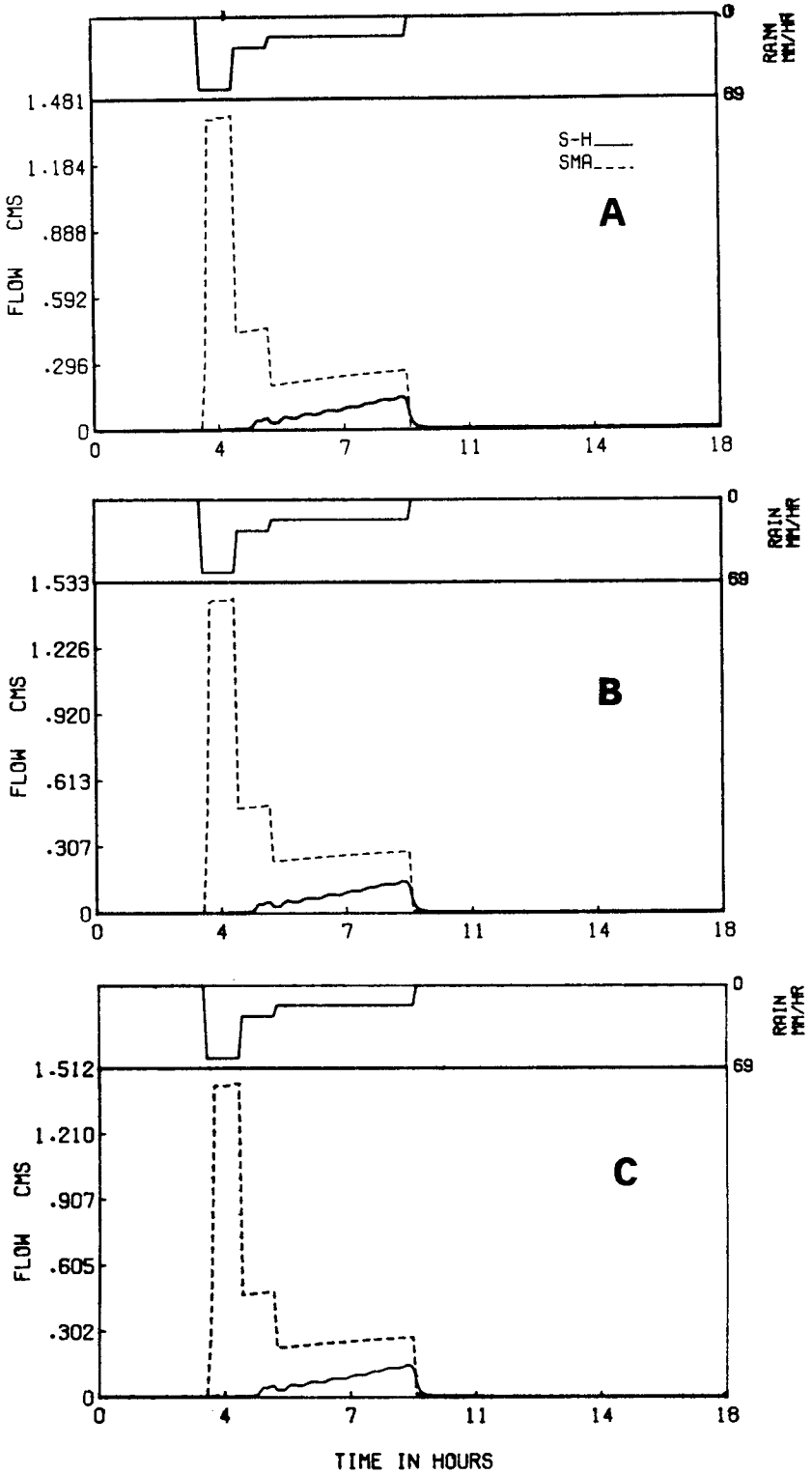

Figure 6.3 Comparisons of extreme flood hydrographs (storm PMP I) under dry antecedent conditions computed by S-H and SMA when SMA was calibrated using one year (A), two (B) and three (C) years of calibration data (case HIL101)

The second element concerns objective functions which, in essence, minimize differences between observed and predicted data. The optimization algorithm adjusts the values of the unknown parameters according to changes in the values of a prespecified objective function. What objective function should be used?

Five objective functions (Equations 6.6 to 6.10) were studied.

$$OF_1 = \frac{\sum_{j=1}^{N} (\log_e Q_{efj} - \log_e Q_{pj})^2}{N} \tag{6.6}$$

$$OF_2 = \frac{\sum_{j=1}^{N} \left| \log_e Q_{efj} - \log_e Q_{pj} \right|}{N} \tag{6.7}$$

$$OF_3 = \frac{\sum_{j=1}^{N} (Q_{efj} - Q_{pj})^2}{N} \tag{6.8}$$

$$OF_4 = \frac{\sum_{j=1}^{N} \left| Q_{efj} - Q_{pj} \right|}{N} \tag{6.9}$$

$$HMLE = \left(\sum_{j=1}^{N} W_j d_j^2 \right) \left(N \left(\prod_{j=1}^{N} W_j \right)^{-N} \right)^{-1} \tag{6.10}$$

where $d_j = Q_{efj} - Q_{pj}$

$W_t = Q_{efj}^{2(\eta-1)}$

η is an unknown transformation parameter which stabilizes the variance, estimated by

$$\left(\sum_{j=1}^{N} \ln(Q_{efj})\right)\left(\sum_{j=1}^{N} W_j d_j^2\right) - N\left(\sum_{j=1}^{N} W_j \ln(Q_{efj}) d_j^2\right) = 0 \qquad (6.11)$$

The first four follow either the conventional simple least square or absolute least value method on natural or logarithmically transformed data. The fifth objective function, however, is a maximum likelihood estimator (HMLE) that assumes the presence of heteroscedastic errors in the data (inhomogeneous variance). Sorooshian et al.(1983) claimed that HMLE provides more consistent parameter estimates than the usual least square approach and is less sensitive to the influence of calibration data length and variability. Preliminary experiments were conducted to determine the most effective objective function among these five.

In the course of these experiments, HMLE was found to be an "expensive" estimator. While minimizing the objective function, at every iterative step, the parameter η (Equation 6.10) must also be estimated iteratively, giving rise to an almost exponential situation in the number of computations. The influence of heteroscedasticity, when it exists, might be minimized by logarithmic transformation of data (Trontman, 1985). Apart from being costly to use, no apparent advantage was found in parameter estimation so HMLE was abandoned.

Of the four objective functions the first (Equation 6.6) was found to give parameters that are more plausible physically. This is no surprise because the influence of several large errors on the

magnitude of the objective function is reduced when data used for computing objective functions are transformed logarithmically.

After calibrating with OF_1, OF_4 (Equation 6.9) can be used for refining upperzone parameters (UZK and UZFWM) which influence primarily peak flows. Since OF_4 gives more weight to large flows, by minimizing OF_4, peak flows can be replicated more accurately. Care is taken to ensure that this is not achieved at the expense of low or intermediate flows. When OF_4 is used, only the upperzone parameters are optimized while the rest are kept fixed at the optimized values obtained by using OF_1.

The optimization algorithm constitutes the third element of automatic calibration. Sorooshian and Gupta (1983) chose initially an efficient pattern search method developed by Hooke and Jeeves (1961). In subsequent work for a simple, six-parameter, hydrologic model, Sorooshian and Gupta found that a Newton-Raphson (derivative based) optimization method is more efficient, especially when the number of parameters to be optimized is large (Gupta and Sorooshian, 1985). In recent work, Hendrickson et. al (1986), using the full Sacramento model, demonstrated that though the "gradient search" technique is computationally more effective than the Nelder and Mead simplex algorithm (NMS), it lacks robustness because it sometimes diverges to non-feasible solutions (three out of thirteen test cases diverged). However, for the same tests, NMS always faithfully converged to optimal solutions.

Parkinson and Hutchinson (1972) investigated the efficiency of variants on the simplex method and confirmed its reliability. They reported that out of thousands of test runs, NMS converged in all except six cases when apparently convergence was reached at false solutions. In summary, they said that many researchers quoted that among many favored direct search algorithms on unconstrained optimizations, NMS is the most reliable of all (Schnabel, 1966; Kowalik and Osborne, 1968; Box et. al, 1969), though Box (1966) cautioned that NMS becomes less efficient as the number of dimensions increases.

A literature search and personal investigation provide ample evidence to accept NMS as the present most robust direct search algorithm for model calibration. The relevant details of NMS are included here for completeness.

6.3 Automatic Optimization Algorithm

$P_1, P_2, \ldots$ and P_n are n parameters to be optimized such that

$$LP_i < P_i < UP_i, \qquad i=1,2,\ldots,n$$

where P_i is constrained between the upper UP_i and the lower LP_i bounds. UP_i and LP_i prevent P_i from diverging to unrealistic values. Let ΔP_i be the initial increment made to P_i. Since NMS is an unconstrained optimizing algorithm, it is necessary to transform the P_i's into an unconstrained space, denoted as R_i, where

$$R_i = \sin^{-1}\left[\frac{P_i - LP_i}{UP_i - LP_i}\right]^{.5} \tag{6.12}$$

and the equivalent increment ΔR_i in the unconstrained space is given by

$$\Delta R_i = R_i - \sin^{-1}\left[\frac{P_i + \Delta P_i - LP_i}{UP_i - LP_i}\right]^{.5}$$

Next an initial simplex array A is set up as

$$A = \begin{bmatrix} R_1+\Delta R_1 & R_2 & \cdots & R_n \\ R_1 & R_2+\Delta R_2 & \cdots & R_n \\ R_1 & R_2 & R_3+\Delta R_3 & R_n \\ & \vdots & & \\ R_1 & R_2 & & R_n+\Delta R_n \\ R_1 & \cdots\cdots & & R_n \end{bmatrix}_{(n+1)\times n}$$

Such that

$$A_0 = (R_1+\Delta R_1, R_2, \ldots, R_n)$$

$$A_1 = (R_1, R_2+\Delta R_2, \ldots, R_n)$$

$$\vdots$$

$$A_{n-1} = (R_1, R_2, \ldots, R_n+\Delta R_n)$$

$$A_n = (R_1, R2, \ldots, R_n)$$

From here on, proceed to the pattern search procedure of Nelder and Mead (1965).

6.3.1 Pattern Search Procedure of Nelder and Mead (1965) (NMS)

$A_0, A_1, A_2, \ldots, A_n$ are the (n+1) points in n-dimensional space defining the current "simplex" of n variables such that

OF_i = function value at A_i

OF_h = max (OF_i)

OF_l = min (OF_i)

Let $\underline{A}$ be the centroid of the points with i = h and

[A_iA_j] be the distance from A_i to A_j. Three operations (reflection, contraction, and expansion) are used in which A_h is replaced at each stage by a new point as follows:-

(1) A_1, Reflection of A_h by a ratio α

so that $A_1 - \underline{A} = \alpha(\underline{A} - A_h)$

If $OF_7 < OF_1 < OF_h$, replace A_h by A_1 and start again with a new simplex.

If $OF_1 < OF_7$, proceed to step (2).

(2) A_2, expansion of A_1 by a ratio γ ($\gamma > 1$)

so that $A_2 - \underline{A} = \gamma(A_1 - \underline{A})$

If $OF_2 < OF_7$, replace A_h by A_2 and restart the process

If $OF_2 > OF_7$, expansion fails; Replace A_h by A_1 before restarting the process.

If $OF_2 > OF_i$ for all $i = h$, define A_h to be either the old A_h or A_1, whichever has the lower OF value and proceed to step (3).

(3) A_2, contraction of A_h by a ratio β ($\beta < 1$)

If $OF_2 < OF_h$, replace A_h by A_2 and restart.

If $OF_2 > \min (OF_h, OF_1)$, contraction fails;

replace all the A_i's by $(A_i + A_1)/2$

The convergence criterion is either

$$\frac{1}{n} \sum_{i=0}^{n} (OF_i - \underline{OF})^2 < \epsilon$$

or if the total number of iterations has reached the maximum specified (MAXN).

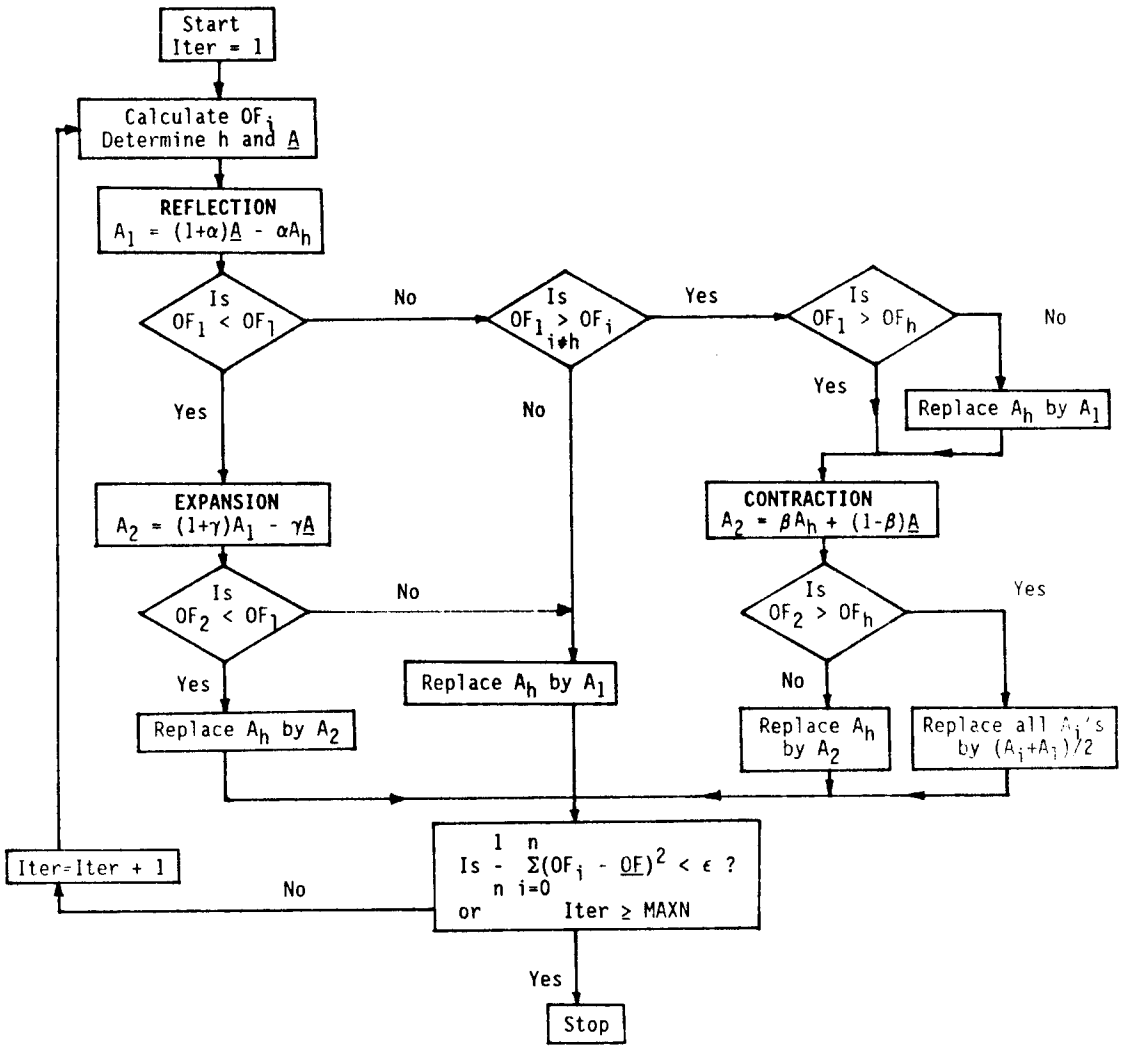

Figure 6.4 Flow chart of the Simplex Optimization Algorithm by Nelder and Mead (1965)

After reaching the end of the pattern search process, the final A_h is re-transformed to the original space to get the final set of parameters P^*_i where i = 1,2,.... ,n. Sets of α, β and γ used in the experiments were (1.0, 0.5, 2.0) and (0.8, 0.5, 0.8).

6.4 Principles of Effective Manual-Automatic Calibration

Questions that are asked frequently regarding calibrating hydrologic models can be summarized as :-

(1) Which calibration approach should be used, manual or automatic?

(2) When operating in automatic mode, how many parameters should be optimized and what are they?

(3) In manual calibration, what parameters should be changed and by how much?

(4) How should one determine that the parameters have reached "optimality" and that further effort to improve them, either manual or automatic would only result in marginal return?

(5) What guidelines should be used in determining whether a set of parameters is "final" or not?

A set of calibration principles resulting from the experience gained in calibrating SMA for eighteen hypothetical catchments is outlined below. The skill, experience, and intuition of the hydrologist and his or her knowledge of the hydrologic model play a great part in the calibration process, in particular when the manual approach is employed.

The World Meteorological Organization, WMO (1975), conducted a project on intercomparisons of conceptual models. They recommended that a combination of manual and automatic procedures should be adopted in model calibration. If the manual approach alone is adopted, it will be tedious in terms of man hours required to obtain a good set of parameters, not to mentioned that skill and experience of the hydrologist are also indispensable. Automatic methods, on the other hand, are simple to use but they do have some inherent disadvantages. They are computationally expensive and they rely totally on one pre-specified objective function. Possible divergence in parameters if initial values selected are poor, failure of automatic methods to recognize the effect of perturbing a group of parameters concurrently and for the pattern search methods, the presence of a concave or a discontinuous response surface at portions of the parameter simplex, are among many problems commonly encountered in this approach. By taking advantage of the merits of both methods together, one could at least overcome partially the pitfalls of each method applied alone. Morever, the chances of obtaining a good set of parameters within a reasonable length of time is substantially increased.

The experience gained in calibrating SMA automatically for the small catchments used here indicates that parameters should be optimized in groups according to the following order:

(1) Lower zone parameters LZPK, LZFPM, LZSK and LZFSM;

(2) Percolation parameters ZPERC and REXP;,

(3) Upper zone parameters UZK and UZFSM;

(4) Tension water parameters LZTWM and UZTWM.

Even though these suggestions are based on hypothetical situations, they are likely to be useful for natural catchments too.

The main idea is to subdivide the calibration process in a manner so that three hydrologic phases, baseflow, the percolation process, and peak flows are modelled separately and in the right order. Depending on the situation, it might be more effective to optimize parameters from two categories together to keep track of their interactions. For example, sometimes by optimizing the upper zone and the percolation parameters concurrently instead of separately, better results are obtained.

Below are steps suggested for the combined manual-automatic calibration procedure:-

(1) Derive initial estimates of parameters (Section 6.1) and start the calibration process manually. Based on preliminary runs, study the differences between S-H and SMA hydrographs. Alter some parameters to improve the fits between hydrographs, primarily baseflow and then peak values. To correct a situation where baseflow is insufficient but surface responses are excessive, increase percolation by enlarging LZFPM or LZFSM or both. Very often, ZPERC is increased and REXP decreased to augment percolation to the lower zone for more baseflow to occur. When a reverse situation occurs, the relevant parameters are changed in the opposite direction. During dry spells, if the baseflow recedes too quickly, the recession coefficients LZPK and

LZSK are reduced. If peak responses to heavy storms are too high, enlarge UZFWM and decrease UZK to reduce surface flow and interflow. If the surface responses oversimulate volumes but not peak flow rates, either manipulate UZFSM and UZK as before or increase the percolation or do both. If the total flow volume is low due to excessive evapotranspiration (ET), decrease PEADJ. However if ET is approximately correct (consistent with S-H values), reduce the tension storages UZTWM and LZTWM or both. Sometimes it is necessary to manipulate the initial state variables LZTWC, UZTWC, UZFWC, LZFPC and LZFSC to produce more flow in the initial months.

(2) After one has manually adjusted the parameters to a stage where the direction to proceed for further refining the parameters becomes unclear, it is time to let the automatic optimization aid (NMS) take over. Two to five parameters are optimized concurrently. At the end of each optimization run, which comprises many iterations, the new values are compared with the original and the fits between recorded and simulated hydrographs and the summary statistics are studied. Based on the results, a decision for the next step is made. One can either make another optimization run on the same set of parameters with the new values from the last run as the starting point, or optimize a different set of parameters, or return to step (1) to adjust some parameters before embarking to step (2) again. Normally, the last alternative is chosen.

(3) In between step (1) and step (2), the state variables UZTWC, LZTWC, UZFWC, LZFPC and LZFSC which are initial storage levels are adjusted manually to improve the initial simulation conditions. NMS could be used to optimize the state variables but it is seldom used because it was found that manual adjustments are faster. Moreover, substantial saving in computer time is achieved if NMS is not used.

(4) The whole process is terminated when further attempts to refine the parameters result in marginal or even negative return. The quality of the final calibration is assessed according to the methodology given in Sections 5.4, 7.2 and 7.4.

Several salient points related to automatic calibration are addressed below.

First of all, the number of parameters (n) optimized per simulation run should generally not exceed 5 . If more than 5 parameters are adjusted simultaneously, the response surface of the parameter space might be too uneven for the pattern search method to be effective. In other words, high dimensionality in the parameter space should be avoided. On the other hand, n should not be less than 2 in usual circumstances since most parameters are closely interrelated to at least one other parameter, if not more. If closely related parameters are not optimized concurrently, consistent values are difficult to obtain and the capability of NMS is not utilized fully.

As mentioned before, optimize parameters related to baseflow first, then percolation, and finally surface responses. Hence, it is not advisable to optimize variables such as UZK and UZFSM unless lower zone parameters are more or less optimized. After all parameters have been optimized, it is normally a good practice to refine those parameters until there is no gain in simulation quality.

In general, a set of parameters comprise those parameters related to the same hydrologic processes. For example, ZPERC and REXP or UZK and UZFWM should be optimized together. The optimal number of iterations per run was found to be between 30 and 70. After a certain number of iterations, changes assigned to the parameters by NMS dwindle in magnitude. If the convergence criterion CONVG specified happens to be too stringent or the maximum number of iteration MAXN is too high, the process would continue even though parameters are more or less stabilized. Each iteration involving two years of simulation at a 6-minute time step requires approximately 5 minutes of Vax 11/780 CPU time. Hence each run takes at least two and half to six hours of real time; the two criteria for terminating the process should be selected carefully.

6.5 Calibration Experience

In the initial stage, improvements are usually fast but after a certain degree of refinement is reached, progress becomes slow and tedious. Experience shows that the process will reach a point after

which any attempt to improve parameter estimates, whether it is manual or automatic, will be fruitless.

In terms of relative total volumes of surface and subsurface flow dynamics, the eighteen test cases for which SMA was calibrated can be divided into three broad classes:-

(1) predominantly surface flow,

(2) similar amount of surface and subsurface flow, and

(3) predominantly subsurface flow.

Test cases falling under Class (1) are HIL102, HGL102 and HFL102 (the case labels are used for reference to data sets given in Table 5.4) which have relatively impermeable soils (saturated hydraulic conductivity K_u ranges from 0.02 to 0.06 m/hr) and steep slope (gradient equal to 0.1). Difficulties were encountered in attempting to replicate peak flows accurately. While the peak flow rates were both over and under simulated during calibration, the calibrated models performed excellently in many extreme rain tests for reasons described in Section 7.4.

Many of the tests fall into Class (2) and they are HIL101, HIL104, HIL105, HGL104, HGL105, HFL104, HL223, HG223 HF223, HUL104, HUG105 and HUF45. Good calibrations were difficult to achieve. Two man months were spent in calibrating HIL101 (the first case) yet flow volumes for dry months were not adequate. Some cases were better than others but in general, there were more problems during dry than wet months. Gross errors (as much as 100 % or more) in monthly volumes

during dry periods were encountered. On the whole, peak flows were more accurate than the intermediate flows. Apparently, parameters identified could not keep track of the changes in the moisture contents during the transition periods between low and high flows. Unlike the results of extreme rain tests on Class (1) catchments, the results of such tests were less predictable.

Among the cases under Class (2), HL223, HG223, HF223 and HUF45 are the four catchments made up of two subbasins each. For the former three catchments, one of the subbasins was taken from those under Class (1) and so it responded to rain primarily with surface dynamics. The second subbasin which belong to those under Class (3), responded to the same rain only with baseflow. It was an interesting experience to attempt to identify a set of parameters that could replicate high flows and at the same time kept a high profile of baseflow. Unfortunately the parameters obtained did not give rise to adequate high flows and low flows tended to be over-simulated. Many high flow events were either over or under simulated by a significant amount.

HIL103, HGL103 and HIL103 were three cases with deep and highly permeable soils (K_U = 0.2 m/hr, upper soil depth = 1.6m) so the dynamics of flow responses was dominantly subsurface. They are grouped under Class (3). With practically no flood events (a few occurred in HIL103), they were easily calibrated . Without peak flows to complicate the response surface of the parameter space, lower zone parameters were readily identified by the automatic procedure. Unfortunately, with a few or no flood events, there was no basis to

identify upper zone parameters, so all the extreme flood events were grossly over-forecasted (Figures 7.19 to 7.21). HIL103 was subjected to a wetter set of rain data (Quillayute, Washington) and so surface mechanisms did occur. Even then, without an adequate number of flood events, parameters identified were still poor in predicting peak flows.

The last three cases, HUL104, HUG105 and HUF45 that incorporated spatial distribution in the rainfall data were harder to calibrate especially HUF45 because it was made up of two different subbasins. The search for better sets of parameters by NMS became more tedious and more search operations (reflection, contraction, and expansion) were involved in each iteration.

Chapter 7

An Evaluation of the Sacramento Model

"There are three things that are too amazing for me,
four that I do not understand: .... "

Proverbs 30:18

The performance of SMA was examined for 18 cases. These 18 cases, outlined in previous chapters, were taken from five elementary hillslopes and three sets of climatic data. They were designed to explore the two objectives defined in Chapter 2:

(1) To determine the relative sensitivity of the flow mechanisms to changes in hillslope topographic parameters, to climatic data variability (from wet to dry conditions), and to spatial distributions of rainfall data, and

(2) To assess the fidelity of SMA in both prediction and extreme forecasting modes under a wide range of hydrologic and climatic conditions.

The evaluation of the SMA's performance is based upon the following measures.

(1) Statistical plots (boxplots and scattergrams), hydrograph plots, and comparisons of summary variables and flow volumes to assess SMA's ability to simulate S-H output in calibration, validation, and prediction modes.

(2) Analysis of flood hydrographs and comparisons of summary variables (48-hour flow volume Q_v, flood peak Q_p, time to peak Q_t) to assess

SMA's credibility when used to predict (forecast) catchment response to extreme rainfall for known catchment initial conditions.

(3) The physical plausibility of the final lumped parameters obtained from calibrations.

(4) The effects of calibration data variability and catchment characteristics on the estimated parameters.

7.1 Effects of hillslope characteristics and climatic data on flow dynamics

Even for small scale, idealized catchments such as the hypothetical hillslopes used here, the dynamics of flow is a complicated hydrologic process. The hypothetical hillslope indices (Figs. 4.1 and 5.7) that are pertinent to flow dynamics are hillslope length DS, upper layer soil depth Y, hill slope S, and saturated hydraulic conductivity K_u. The input data (precipitation and evapotranspiration) play an important role in determining the relative magnitude of surface and subsurface responses. Among the three sets of climatic data used, Quillayute (Washington) is the wettest location, followed by Tray Mountain (Georgia) and lastly Niceville (Florida) (Table 5.2).

Causal interactions that occur between climatic data and small scale catchment characteristics are discussed in this section. A better understanding of the cause-and-effect relationships that exist between variables in hydrologic processes can be developed from here.

The discussions are given with reference to cases involving elementary hillslopes only (Test I).

7.1.1 Rainstation - Quillayute (Washington)

For the same climatic input data, a total of five elementary hillslopes (HIL101 to HIL105) were tested. HIL101(saturated hydraulic conductivity K_u = 0.2m/hr, total soil porosity ϕ_u = 0.44, soil depth Y = 0.8m, slope length DS = 100m and slope S = 0.10) is the baseline case for discussion. One of these four indices was changed in each of the remaining 4 cases, while all others were kept constant, to study the effects of each hillslope index on flow mechanism.

HIL101

It has a highly permeable soil and steep slope. Subsurface flow dominated except during heavy rain (primarily in the prediction mode).

HIL102

K_u was changed from 0.2m/hr to 0.02m/hr, ϕ_u from 0.44 to 0.40 and all else remained unchanged. The rate of soil infiltration was drastically reduced, and so was the subsurface flow. This caused significant rainfall excess (Horton mechanism) to take place, hence surface runoff.

HIL103

K_u was restored to 0.2m/hr and the upper soil depth Y was doubled tc 1.6m. Baseflow dominated flow from this deep, highly permeable upper soil layer on a steep slope. Since the perched aquifer (water table) rarely reached the ground surface, saturation overland flow did

not occur, neither did the Horton mechanism because no rainfall intensity exceeded K_u.

HIL104

The conditions of the first case (HIL101) were maintained but the hillslope length DS was increased to 250 m. With a long, steep hillslope, the perched aquifer tended to rise up to ground surface at and near the downstream location, making saturation overland flow a major contributor to the total flow volume.

HIL105

An intermediate situation between HIL101 and HIL104 was created by reducing the slope S to 0.04. All other conditions of HIL101 were maintained. With a hillslope smaller than that of HIL101, the subsurface flow velocity was reduced, giving rise to higher perched aquifer profiles and more saturation overland flow occurred, but less than that occurring on the long slope of HIL104.

7.1.2 Rainstation - Tray Mountain (Georgia)

Four cases were tested: HGL102 to HGL105, which have the same hillslope properties as their counterparts, HIL102 to HIL105. Similar flow mechanisms were observed but the surface response was proportionally lower than the subsurface response. This offers little surprise since Tray Mountain is drier than Quillayute and experiences higher ET rates, so there was less rainfall excess to generate surface responses.

7.1.3 Rainstation - Niceville (Florida)

Here only three cases were tested: HFL102 to HFL014, which also have the same hillslope properties as HIL102 to HIL104. Among the three rain stations, Niceville is the driest and experiences long storm-interarrival times and low storm intensity, but sometimes experiences some heavy storms of short duration. The ET demand at this location is the highest of the three locations. Subsurface flow was the primary flow mechanism even for the case HFL102 (low K_u =0.02m/hr), except for the wetter prediction year when the Horton or saturated or both overland flow volumes were higher.

While a causal model such as S-H can simulate the basic hydrologic response of a small hypothetical catchment accurately, it requires formidable computer resources. Unless computer technology can continue to progress at the pace it has for the past two decades, and relevant field data are obtainable and available for scientific analysis, it is unlikely that causal models will be used routinely in the near future. A critical question is: can computationally less intense conceptual models offer a viable, alternative ?

7.2 Can the Sacramento model represent fundamental flow mechanisms ?

It is important to know if complex conceptual models of form similar to the Sacramento model (SMA) can, at least on the average, represent the several known flow mechanisms. Comparisons of annual flow volumes between the two models will help to answer this question. A perusal of Table 7.1 reveals that on an annual basis SMA responded to two of the three input climatic data series with appropriate flow

mechanisms. However on an event by event basis, it sometimes fails to do so for reasons to be expanded upon in Section 7.3. A brief summary of SMA's performance in terms of preservation of flow volumes and ET estimates on an annual scale is given below.

Test I: HIL101 to HIL105 (Rain station - Quillayute (Washington))

SMA and S-H total annual flow volumes agree well in all stages, calibration, validation, and prediction. The largest difference is found in the validation stage of HIL104 where SMA flow volume is 7 % higher than S-H. Subsurface and surface flow volumes have greater discrepancies. SMA either over- produced subsurface volumes at the expense of surface volumes or vice versa. For example, in the calibration stage of HIL105, its subsurface volume is about 0.8 times the S-H volume but its surface flow volume is 1.14 times that of S-H. The ET predicted by SMA differed from that of S-H with a mean error of about 5 %.

Test I: HGL102 to HGL105 (Rain station - Tray Mountain, (Georgia))

Annual flow volumes do not agree as well as before with the largest error of about 8 % (HGL105, prediction stage). SMA generally produced slightly low surface volumes. It performed better in subsurface flows except in the calibration stages of HGL104 and HGL105 where the subsurface volumes are about 1.12 times those of S-H. Again, annual ET volumes are close.

Test I: HFL102 to HFL104 (Rain station - Niceville (Florida))

SMA no longer performed satisfactorily in these three cases. The poor results are attributable to SMA's inability to respond with adequate surface flows. HFL103, which is dominated by baseflow, is the best case here. However, subsurface flow volumes at all validation stages are high, up to 20 % in HFL104. On the average, the surface flow volumes of SMA are 40 % too low. Annual ET volumes are satisfactory with one exception, a 17 % error for the prediction stage of HFL102.

Test II: HL223, HG223 and HF223

These three cases are for a two-subbasin catchment subjected to three different sets of climatic data (Quillayute, Tray Mountain and Nicevile). Each of the two subbasins have the same hillslope properties as HIL102 and HIL103 respectively. Hence each subbasin responded differently to climatic inputs, and so annual flow volumes are proportional mixes of surface and subsurface flows. Apart from the validation stage for HF223 (29 % too high), annual flow volumes are fairly good. The subsurface flow volumes for HL223 are between 7 to 16 % too low but surface volumes are about 9 % too high. For HG223 and HF223, surface volumes are low (between 7 to 31 %). As before, HF223 which was subjected to the Florida climatic data, gave the worst results.

Test III: HUL104, HUG105 and HUF45

The effect of rainfall variability (section 5.3.3) at the subbasin scale is demonstrated here. All three cases are for catchments comprising two-subbasins. The first two catchments have two identical subbasins (taken from HIL104 and HGL105 respectively) while the third catchment has two different subbasins (HFL104 and HFL105). Compared with previous cases, annual flow volumes are marginally affected by the noise component added to the rain data. As before, the annual volume error for HUF45 for the validation stage (53 % too high) is partly due to the Florida data used. However, the effects of the noise component on surface and subsurface volumes is higher, especially in HUL104. The subsurface flow volumes for HUL104 are 12 to 20 % lower and surface flow volumes are 5 to 20 % too high (poorer than HIL104). The performance of HUG105 is comparable to HGL105. With reference to HFL104, the performance of HUF45 is worse in the validation stage (subsurface volume is 40 % too high) but slightly better in the prediction stage.

7.3 Performance of the Sacramento Model in calibration, validation and prediction modes

General comments on the statistical and hydrograph plots (a set for each case) are given to highlight important summary information and some trends. Frequent reference to the respective figures (Figures 7.1 to 7.18) and Table 7.2 is necessary when reading this section. From the mean daily flow plots contained in each figure, the reader can judge the quality of performance of SMA.

Table 7.1 Annual average flow and evapotranspiration(ET) volumes of S-H and SMA (in mm)

Case Stage	Model	Calibration(Two-year period) Total R.O.	Subsf	Surf	E.T.	Validation(One-year period) Total R.O.	Subsf	Surf	E.T.	Prediction(One-year period) Total R.O.	Subsf	Surf	E.T.
HIL101	S-H	2448	1408	1027	474	2158	1280	768	545	4143	1584	2558	534
	SMA	2376	1524	852	550	2049	1393	655	550	4178	1571	2607	545
HIL102	S-H	2425	290	2135	498	2347	304	2042	496	4424	300	4124	491
	SMA	2392	252	2142	468	2183	241	1942	471	4261	263	3998	458
HIL103	S-H	2437	2278	149	544	2086	2036	55	548	3880	2986	894	563
	SMA	2407	2329	78	511	2083	2029	55	520	4189	2939	1250	513
HIL104	S-H	2299	639	1660	486	1979	659	1320	507	4090	675	3415	488
	SMA	2321	652	1670	500	2123	640	1483	511	4210	705	3505	504
HIL105	S-H	2398	1116	1283	522	2110	1064	947	544	3972	1247	2725	513
	SMA	2347	892	1455	510	2104	870	1234	520	4207	1010	3197	510
HGL102	S-H	1462	351	1111	676	1454	358	1096	681	2127	366	1761	644
	SMA	1368	381	987	669	1353	395	958	674	2031	441	1590	681
HGL103	S-H	1447	1447	0	718	1283	1283	0	715	1876	1876	0	706
	SMA	1482	1475	7	723	1327	1321	6	706	1909	1898	11	723
HGL104	S-H	1525	658	867	667	1410	649	761	683	2196	694	1502	630
	SMA	1404	581	824	652	1369	640	729	649	2067	715	1352	665
HGL105	S-H	1469	811	658	698	1432	824	608	707	2169	928	1241	663
	SMA	1341	723	619	696	1324	781	543	692	2004	928	1076	709

Table 7.1 Continued

HFL102	S-H	654	394	260	907	377	293	84	919	1646	440	1206	819
	SMA	567	395	172	940	449	345	104	880	1277	549	728	955
HFL103	S-H	790	790	0	890	442	442	0	806	1167	1111	57	928
	SMA	773	781	1	885	501	500	1	805	1100	1066	34	883
HFL104	S-H	591	499	92	903	385	368	17	911	1408	574	834	870
	SMA	550	497	54	914	487	446	41	859	1196	738	458	929
HL223	S-H	2425	1257	1169	523	2193	1134	1059	517	4226	1604	2622	513
	SMA	2398	1129	1269	506	2100	1060	1040	512	4221	1352	2869	503
HG223	S-H	1455	884	571	700	1379	811	568	709	2020	1110	910	679
	SMA	1413	880	533	696	1333	890	443	689	1975	1117	858	701
HF223	S-H	737	582	156	897	401	354	47	864	1382	741	641	908
	SMA	677	569	108	885	517	438	79	777	1300	729	571	888
HUL104	S-H	2314	619	1669	480	1969	661	1307	505	4242	780	3529	772
	SMA	2349	552	1797	476	2109	542	1567	482	4279	592	3687	477
HUG105	S-H	1407	745	637	695	1413	792	621	704	2096	886	1210	659
	SMA	1266	706	560	702	1320	779	542	700	1934	933	1001	712
HUF45	S-H	611	508	95	907	303	296	0	913	1327	590	729	903
	SMA	594	483	111	907	461	413	48	830	1222	666	556	895

Total R.O = All Sources of Runoff From Catchment.
Subsf = Subsurface Runoff From Catchment.
Surf = Surface Runoff From Catchment.

For every test case, additional hydrograph plots for a selected wet month for each modeling stage are given in appendices A.1 to A.18 where two plots for the same selected wet month are presented. One of the plots is for daily mean flow values and the other shows the original 6-minute time step flow values. Finally, a 48-hour period is picked from the 6-minute time series for a third plot to highlight peak events of that month. For some cases, plots of certain dry months are also included in the appendices (Figs. A.19 to A.23) to demonstrate the performance of SMA during primarily baseflow situations.

Each of the figures numbered 7.1 to 7.18 contains nine parts. Three plots (a scattergram, boxplot, and time series plot) are given for each of calibration, validation, and prediction modes. Consider the results for catchment HIL102 (Figure 7.2). The scattergram and boxplot show that some low flows in the calibration stage were over-simulated. From the hydrograph plot of "error free" Q_{ef} values from S-H with the residues (Q_p-Q_{ef}) plotted directly below, it is clear that over simulation of low flows primarily occurred during the dry periods. Some flows in all modes were under-simulated as revealed by scattering below the 45^0 line of the scattergrams and some parts of the boxplots lying in the negative domain. The hydrograph plots reveal the times when under simulation occurred. Careful study of individual hydrograph plots (48-hour period) such as those given in Figure A.2 show that part of the residues portrayed in the daily hydrograph plots are caused by the differences in the hydrograph shape of Q_p and Q_{ef} and not by gross simulation errors. The overall performance of SMA in each of the three modes is similar.

Rain station - Quillayute (Washington)

Hypothetical catchments: HIL101 to HIL105 (Figures 7.1 to 7.5, Tables 7.1 and 7.2)

The means of SMA flows are close to the means of S-H flows. However, the standard deviations of SMA are always slightly higher than for S-H. Some gross over-simulation errors occurred in the dry to wet transition periods, especially in HIL104 (long hillslope) and HIL105 (mild slope) where some simulated flows are more than 10 times larger than S-H flows. Several excessive responses by SMA to heavy storms are observed in HIL103. Conversely, some high flows were badly under-simulated (HIL101 and calibration mode of HIL105) but overall, under-simulation occurred less frequently than did over simulation.

Many low flows were either over-simulated (HIL101 and HIL102) or under-simulated (HIL102), though the errors are less severe. High flows were generally subjected to larger errors, as indicated by the larger spread in the boxplots. Table 7.2 shows that except for HIL103, in particular during validation, the coefficients of efficiency values E_f are close to unity. E_f values can be deceptive because they do not reveal gross simulation errors that are clear in the corresponding hydrographs. Apparently, SMA performed better in the prediction stage than the calibration and validation stages mainly because wet climatic conditions are more favorable for SMA. This trend is confirmed by smaller RMSE values in the prediction stage.

Rain station - Tray Mountain (Georgia)

Hypothetical catchments - HGL102 to HGL105 (Figures 7.6 to 7.9, Tables 7.1 and 7.2)

A perusal of the plots and the summary values reveal similar trends present in these four cases. For example, the means of SMA flows are close to those from S-H, but the standard deviations are always higher. Also some serious over-simulation errors occurred in the dry to wet transition periods (HGL102, HGL104 and HGL105), some high flows were under-simulated (HGL105) and low flows in many instances were too low (HGL102, HGL104 and HGL105). Unlike HIL103, however, no severe error is detected in HGL103 except the overall simulation was slightly high. Comparisons of E_f and RMSE values reveal that for the same hypothetical catchments, SMA performed better with the Quillayute than the Tray Mountain rainfall.

Rain station - Niceville (Florida)

Hypothetical catchments - HFL102 to HFL104 (Figures 7.10 to 7.12, Tables 7.1 and 7.2)

The performance of SMA in these three cases is much poorer than all previous cases. Trends are difficult to detect; both the mean and standard deviations of SMA are poorly related to those from S-H. The simulated means of the calibration and prediction stages are consistently low and those during validation stage consistently high. In the former two stages, under simulations prevail in the high flow regions as demonstrated in the respective boxplots. Serious over-

simulation problems are also found during the dry months and are most noticeable in Figures 7.10 and 7.11.

Errors during low flow conditions differ from case to case and stage to stage. For example, low flows in the first two stages of HFL103 are too high but those in the prediction stage are better. Careful perusal of the plots and the summary statistics show that baseflows are generally over-simulated, at the expense of high flows. Apparently, the relatively severe climatic conditions, low precipitations and high ET rates made the task of calibration very difficult. The ET rates were so high that flows no longer constituted the dominant fluxes and so they became less effective as the sole calibration signal. Moreover, there were either very few flood events or none (HFL103) for the calibration of high flows to be carried out properly.

Since the rain data for the validation stage is the driest, baseflows became the dominant flow response which, as mentioned earlier, tended to be high. This explains why the simulated means at the validation stages are always larger than S-H means. SMA demonstrated little predictive power for these climatic conditions. Low and negative E_f values and very high RMSE values characterize the poor results here.

Rain Stations - Quillayute, Tray Mountain and Niceville

Hypothetical catchments - HL223, HG223 and HF223 (Figures 7.13 to 7.15 and Tables 7.1 and 7.2)

These three cases are designed to test the capability of SMA in modeling a catchment comprised of two substantially different subbasins connected by a channel network. For the same catchment, the three rain-station data series were applied separately to explore the influence of climatic data on estimated SMA parameters.

Other than flows in the peak regime, fairly good results are obtained in the first two cases, HL223 and HG223. In fact, SMA performed slightly better in HL223 than in HIL102 and HIL103 separately even though in modeling HL223, one set of lumped parameters had to emulate the flow mechanisms from two subbasins. The problem of huge positive errors in the dry months was less severe but many peak events were either too high or too low.

Again the worst result comes from the case involving the Florida rain and ET data (HF223). Close examination of the plots and summary variables show that with one exception, similar types of defects from HFL102 to HFL104 are present in HF223. The exception was that the peak flows in the calibration stage were generally under-simulated but in the prediction stage, the reverse situation happened. In terms of E_f and RMSE values, the performance of HF223 is comparable to HFL102 and HFL104 but is poorer than HFL103 because HFL103 is predominantly baseflow; the error statistics are affected only by a few large simulation errors.

Though more tedious calibration efforts were involved in the multi-basin cases, the overall performance of SMA in the low flow regimes are similar to the single-basin cases. However, the quality of flood simulations deteriorated; a single set of lumped parameters cannot model the surface responses from two different subbasins consistently. Considering all the results (Figure 7.1 to 7.18), in practically all modeling stages, the climatic conditions play a bigger role than catchment characteristics on SMA's performance.

Rain Stations - Quillayute, Tray Mountain and Niceville

Hypothetical catchments - HUL104, HUG105 and HUF45 (Figures 7.16 to 7.18 and Tables 7.1 and 7.2)

For HUL104 and HUG105, catchments with two identical subbasins taken from HIL104 and HGL105 respectively, spatial variations in rain data at the subbasin level have marginal impact on the overall simulation. By comparing summary variables of these two cases with HIL104 and HGL105 (both subjected to spatially uniform rainfall), respectively, the means and standard deviations of SMA and S-H are still related to each other in the same fashion: the means are close but the standard deviations of SMA are higher than for S-H. E_f and RMSE values are about the same. The only noticeable difference is that boxplots for the high flows of HUG105 have wider spread than for HGL105.

A different situation is observed in HUF45 which is made up of two different subbasins (HFL104 and HFL105). This case was designed to

test the combined effects of rain spatial variability and subbasins with different hillslope properties. HUF45 was subjected to the Florida climatic data. Calibration of SMA under these conditions was difficult and so the quality of the overall simulation, as compared to point-rainfall cases such as HFL104 and HF223, is much poorer. High flows were often too low and low flows were generally over-simulated. The validation stage exhibited some gross over-simulation errors with E_f equals -67.9 and the standard deviation from SMA is 0.0095 but that of S-H is only 0.00114. It is the worst among the eighteen cases tested.

Summary

(1) Test cases involving the Florida data demonstrate larger errors compared to cases using the other two climatic data sets. The former has high ET demand, a more variable rain pattern, and an occasional short-duration heavy storm. It appears that severe climatic conditions are not conducive to modeling with a conceptual model of structure similar to SMA. When the ET demand is high, flow fluxes become less effective as the sole calibration signal.

(2) Droughts, and in particular the transition period from dry to wet seasons are difficult to model correctly because SMA cannot represent the ground moisture state adequately under dry conditions. Under such conditions, SMA has a tendency to over-simulate low flows.

(3) While SMA has predictive power that is generally good, especially for catchments that experience wet climatic conditions, it sometimes exhibits serious errors in predicting peak events.

(4) Climatic conditions appear to have a larger role than catchment characteristics on conceptual model output. More extensive experiments would be needed to generalize this observation beyond the hypothetical cases examined here. The situations might be different if spatial features of natural catchments are considered.

Table 7.2 Summary statistics of flow sequences of S-H and SMA

Case	Statistics Mode	Mean CMS S-H	Mean CMS SMA	Std. Dev. CMS S-H	Std. Dev. CMS SMA	E_f 6-min.	E_f Daily	RMSE Percentage 6-min.	RMSE Percentage Daily
	C	.00754	.00747	.0164	.0174	.810	.965	94.5	26.6
HIL101	V	.00934	.0094	.0201	.0213	.831	.973	88.5	24.0
	P	.0129	.0132	.0257	.0270	.843	.978	78.6	20.4
	C	.00753	.00758	.0242	.0261	.825	.976	135.0	30.9
HIL102	V	.00729	.00692	.0229	.0240	.856	.989	191.0	21.6
	P	.0139	.0135	.0340	.0356	.880	.992	85.1	14.0
	C	.00759	.00763	.00722	.00878	.527	.869	65.5	28.8
HIL103	V	.00649	.00661	.00525	.00630	.0257	.653	79.8	43.1
	P	.0122	.0133	.0153	.0210	.574	.865	82.1	36.2
	C	.00714	.00736	.020	.0222	.781	.969	131.0	32.5
HIL104	V	.00611	.00673	.0171	.0199	.665	.931	162.0	52.8
	P	.0128	.0133	.0295	.0319	.809	.969	101.0	28.2
	C	.00741	.00744	.0206	.0211	.695	.964	153.0	31.7
HIL105	V	.00620	.00667	.0159	.0183	.697	.935	141.0	46.1
	P	.0123	.0133	.0267	.0306	.824	.960	91.0	29.8
	C	.00454	.00434	.0310	.0338	.864	.965	252.0	51.4
HGL102	V	.00451	.00429	.0235	.0261	.826	.953	217.0	57.0
	P	.0066	.00644	.0337	.0376	.832	.971	209.0	39.4
	C	.00445	.00470	.00131	.00135	.780	.797	13.8	13.2
HGL103	V	.00394	.00421	.00085	.00096	.632	.649	13.1	12.7
	P	.00581	.00605	.00141	.00149	.818	.837	10.3	9.7
	C	.00467	.00445	.0252	.0280	.762	.950	264.0	51.9
HGL104	V	.0043	.00434	.0165	.0201	.425	.870	292.0	73.9
	P	.00676	.00655	.0263	.0286	.715	.955	208.0	43.6
	C	.00447	.00425	.0240	.0282	.788	.954	247.0	46.8
HGL105	V	.00435	.00420	.0156	.0196	.436	.888	268.0	63.4
	P	.00665	.00635	.0257	.0292	.754	.959	192.0	40.1
	C	.00203	.00180	.0123	.0142	.218	.689	538.0	123.
HFL102	V	.00116	.00142	.0052	.0098	-1.83	-.149	757.0	189.0
	P	.00514	.00405	.0363	.0333	.780	.918	331.0	95.9
	C	.00248	.00245	.00143	.00126	.838	.840	23.3	23.0
HFL103	V	.00138	.00159	.00092	.00069	.714	.717	35.7	35.5
	P	.00367	.00349	.00674	.00792	.210	.826	163.0	43.1

Table 7.2 Continued

HFL104	C	.00184	.00174	.00615	.0044	-0.218	.426	368.0	91.1
	V	.00119	.00154	.00179	.0030	-2.450	-.120	278.0	78.1
	P	.00441	.00379	.0282	.0245	.63	.83	388.0	145.0
HL223	C	.0153	.0152	.0287	.0280	.779	.954	87.9	27.5
	V	.0139	.0133	.0247	.0234	.685	.861	100.0	45.9
	P	.0268	.0268	.0478	.0456	.801	.958	79.7	25.9
HG223	C	.00917	.00896	.0306	.0373	.480	.891	240.0	46.5
	V	.00870	.00845	.0232	.0163	.652	.880	158.0	49.2
	P	.0128	.0125	.0330	.0376	.542	.907	175.0	38.1
HF223	C	.00462	.00429	.0134	.0165	-0.712	.677	300.0	65.5
	V	.00256	.00328	.00589	.0107	-1.63	-0.133	374.0	116.0
	P	.00871	.00825	.0392	.0544	0.405	.918	347.0	64.7
HUL104	C	.0362	.0372	.102	.111	.802	.961	125.0	37.0
	V	.0307	.0334	.0845	.0945	.715	.928	147.0	52.3
	P	.0653	.0678	.150	.160	.812	.961	99.3	31.2
HUG105	C	.00866	.00803	.0459	.0526	.771	.922	254.0	59.4
	V	.00868	.00837	.0316	.0393	.470	.882	265.0	68.2
	P	.0129	.0123	.0491	.0543	.748	.925	191.0	54.3
HUF45	C	.00381	.00376	.0119	.0212	-2.14	-0.246	555.0	129.0
	V	.00188	.00293	.00114	.0095	-67.9	-3.85	503.0	132.0
	P	.00828	.00775	.0535	.0554	.655	0.923	379.0	96.8

Legend

C - Calibration mode
V - Validation mode
P - Prediction mode

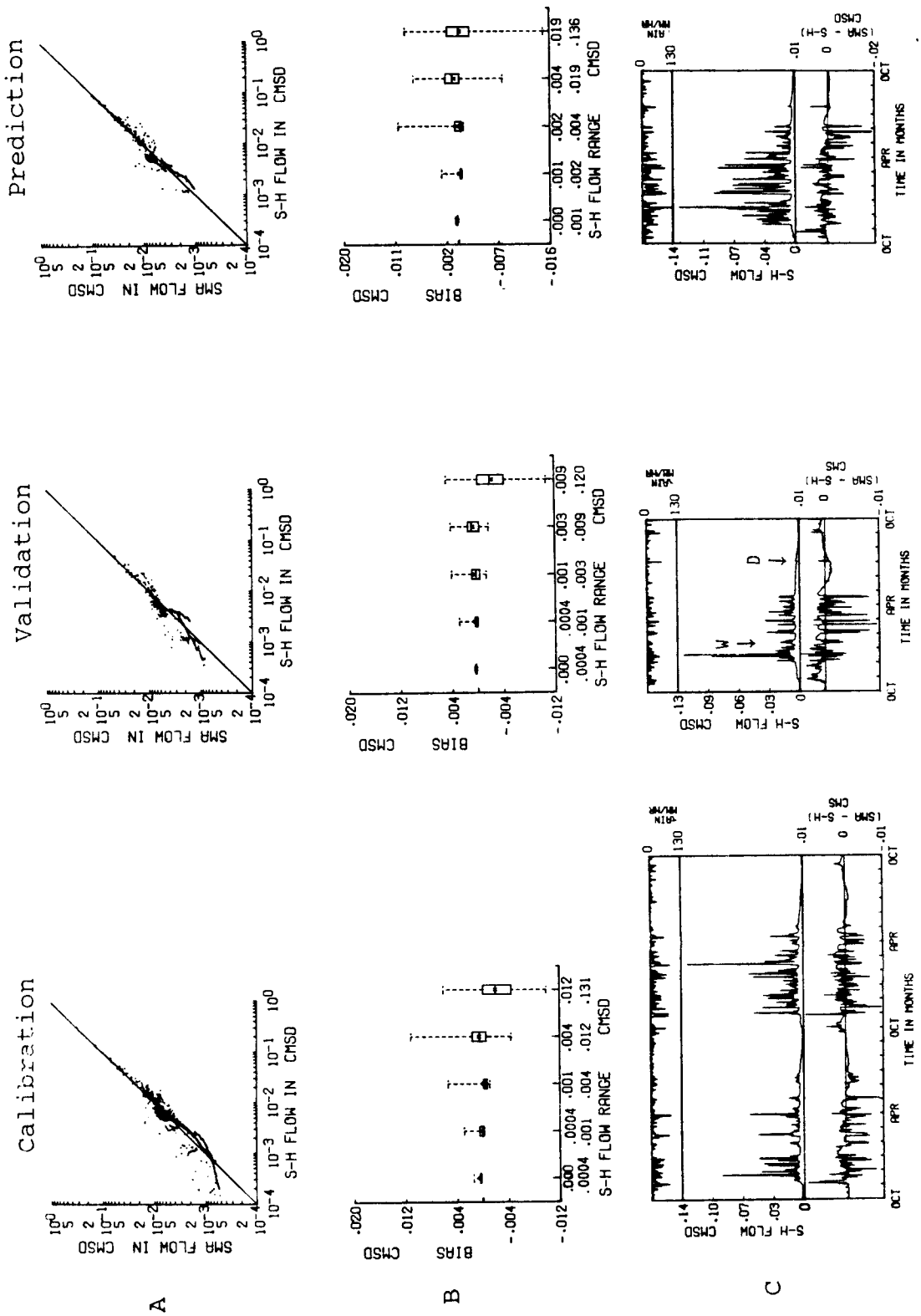

Figure 7.1 Scattergrams (A), boxplots (B) and mean daily hydrographs (C) for HIL101

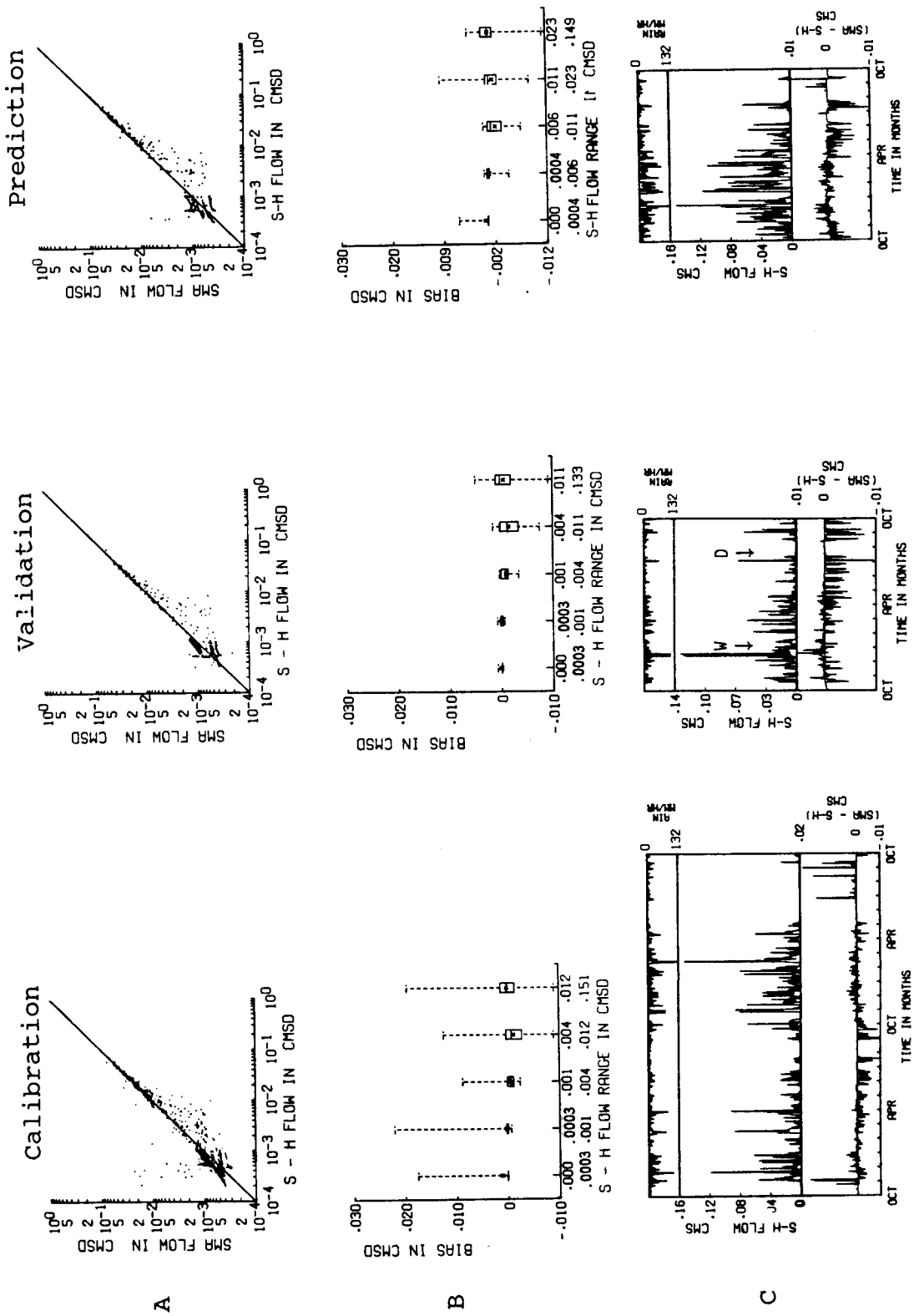

Figure 7.2 Scattergrams (A), boxplots (B) and mean daily hydrographs (C) for HIL102

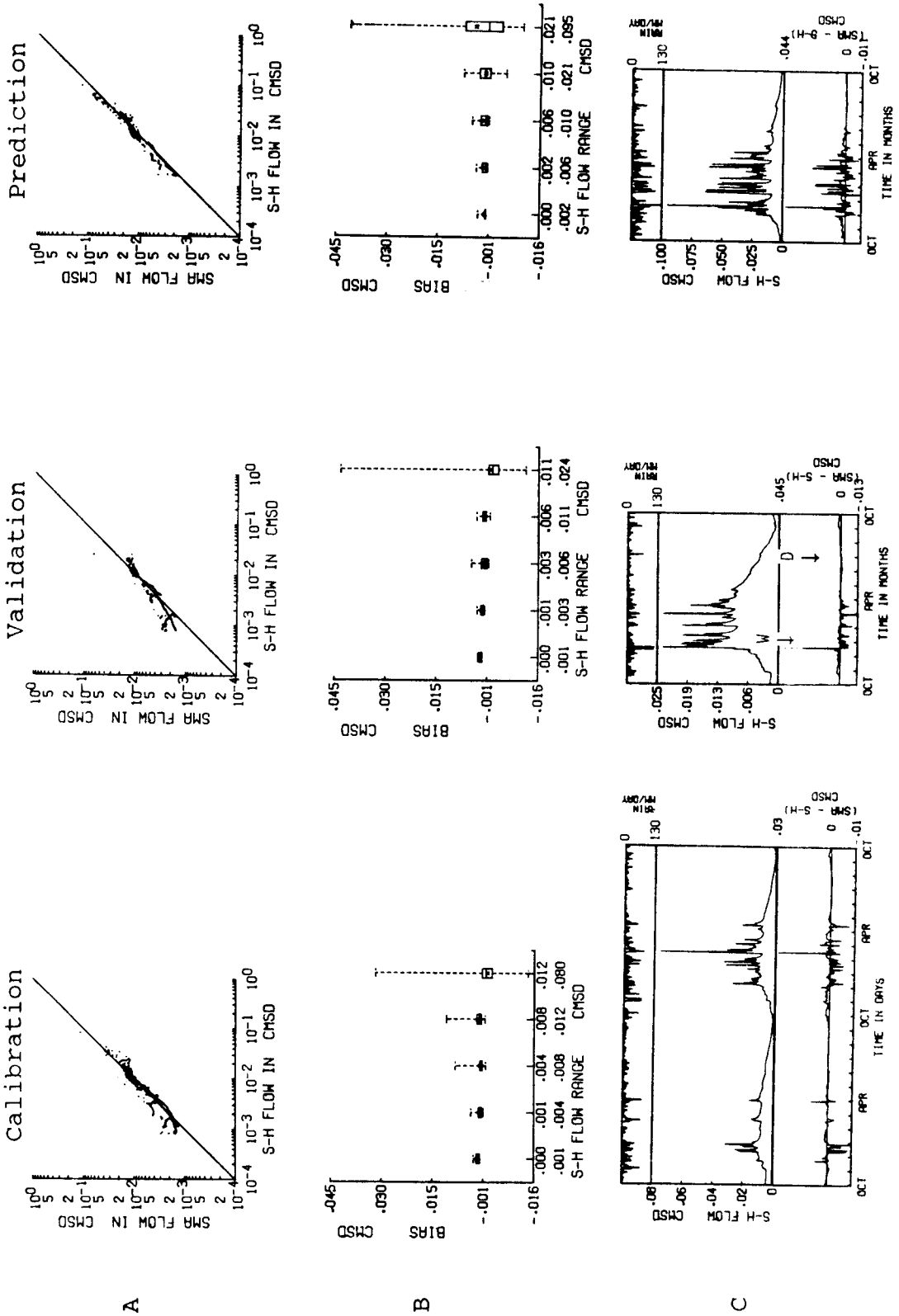

Figure 7.3 Scattergrams (A), boxplots (B) and mean daily hydrographs (C) for HIL103

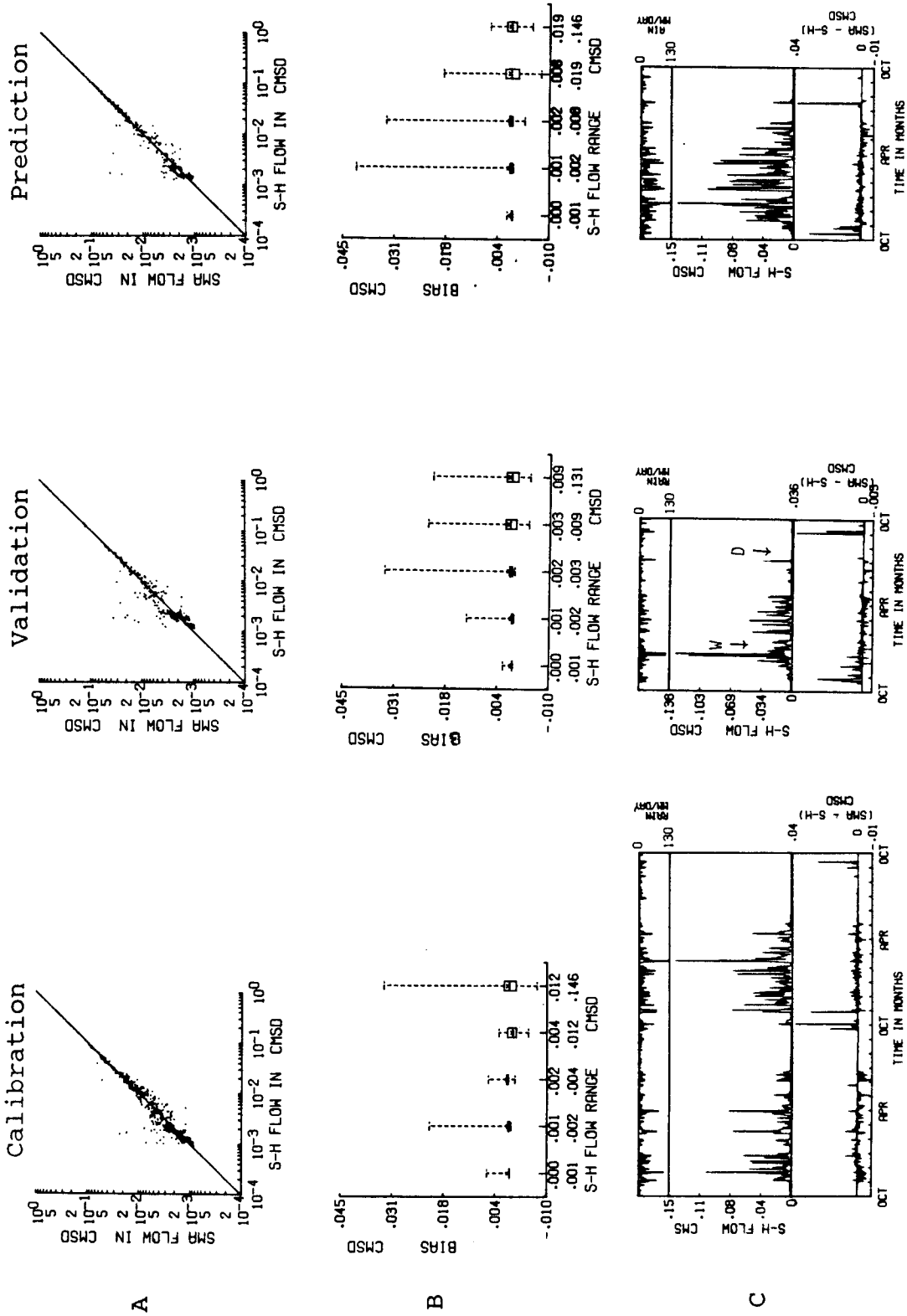

Figure 7.4 Scattergrams (A), boxplots (B) and mean daily hydrographs (C) for HIL104

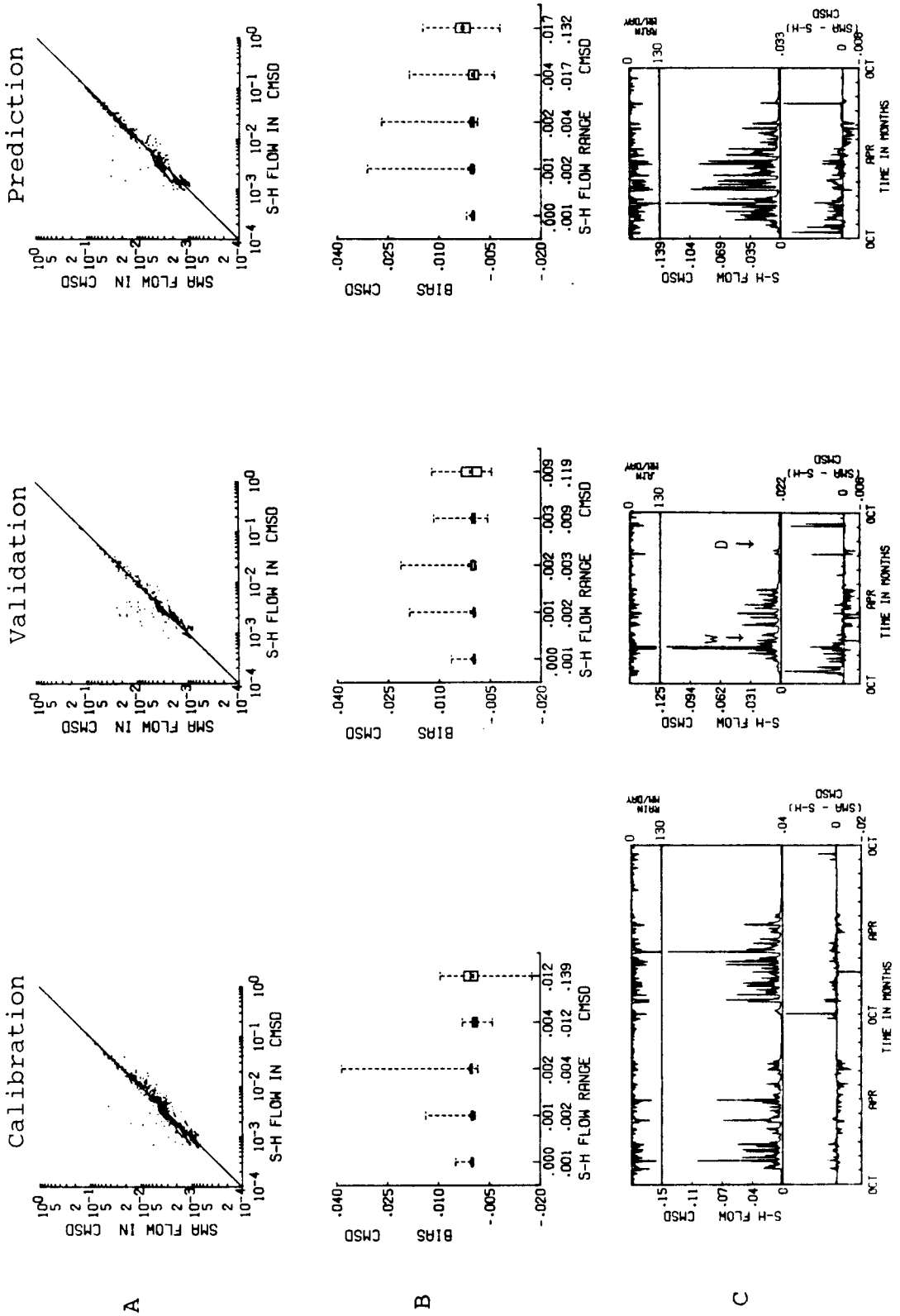

Figure 7.5 Scattergrams (A), boxplots (B) and mean daily hydrographs (C) for HIL105

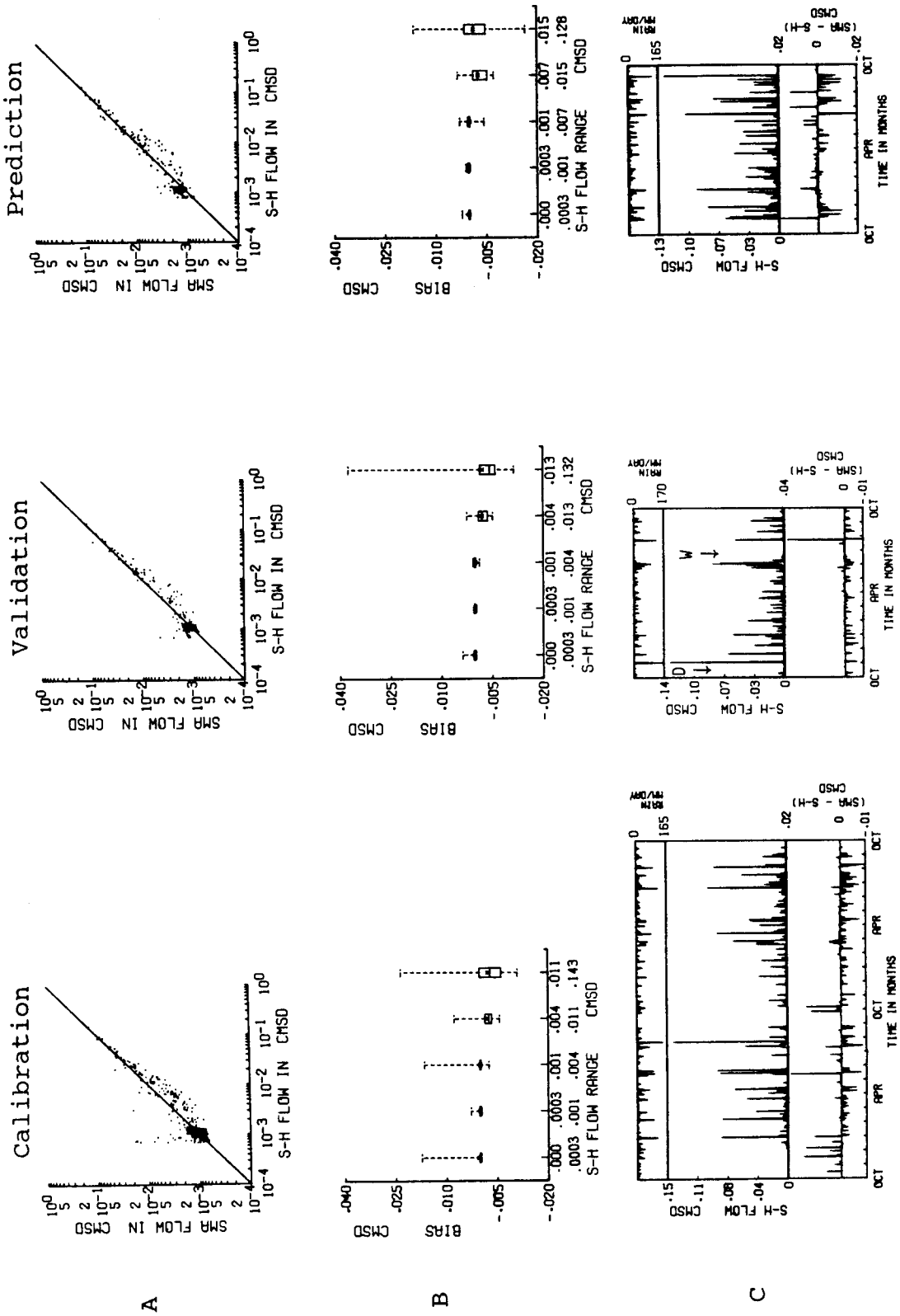

Figure 7.6 Scattergrams (A), boxplots (B) and mean daily hydrographs (C) for HGL102

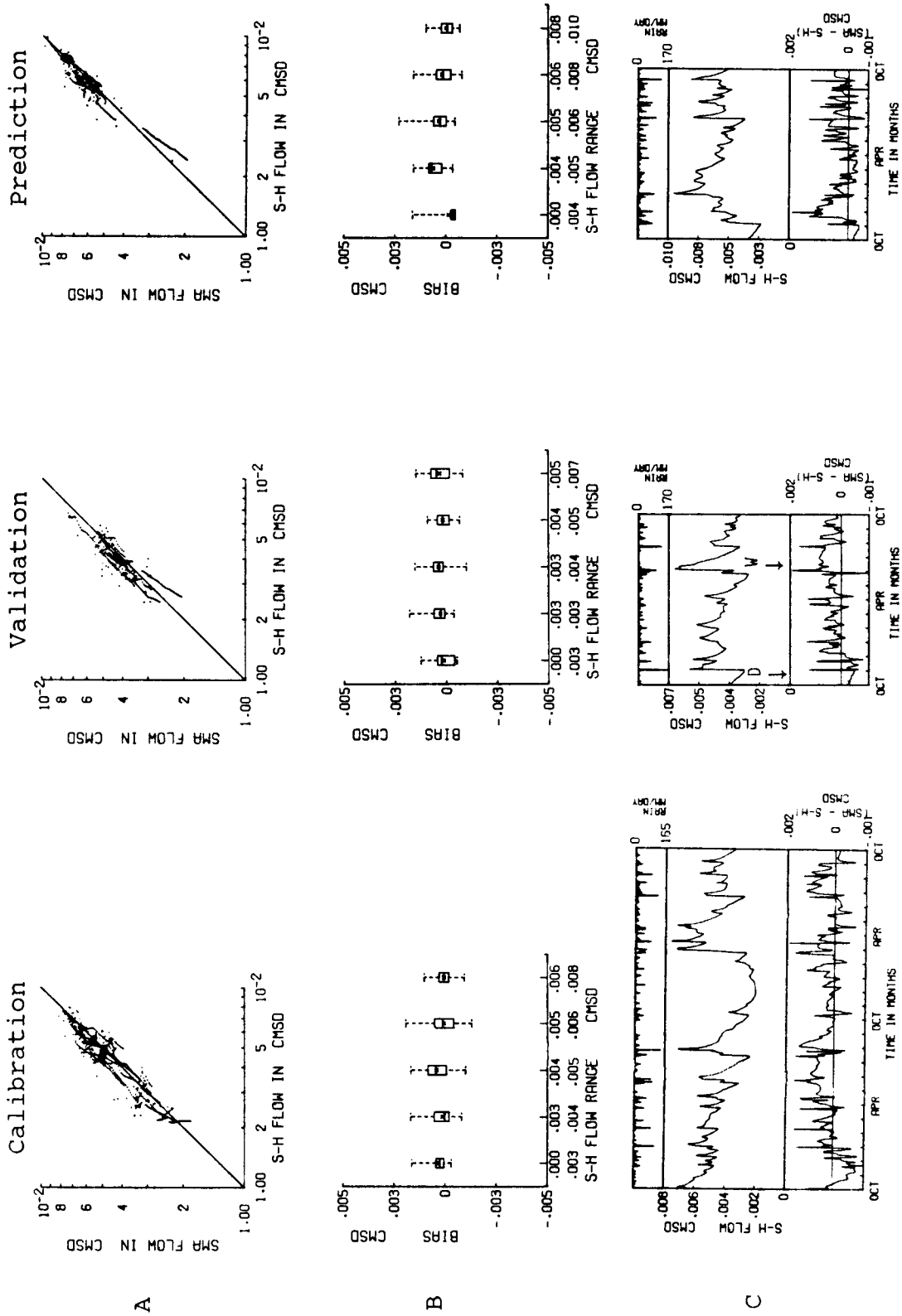

Figure 7.7 Scattergrams (A), boxplots (B) and mean daily hydrographs (C) for HGL103

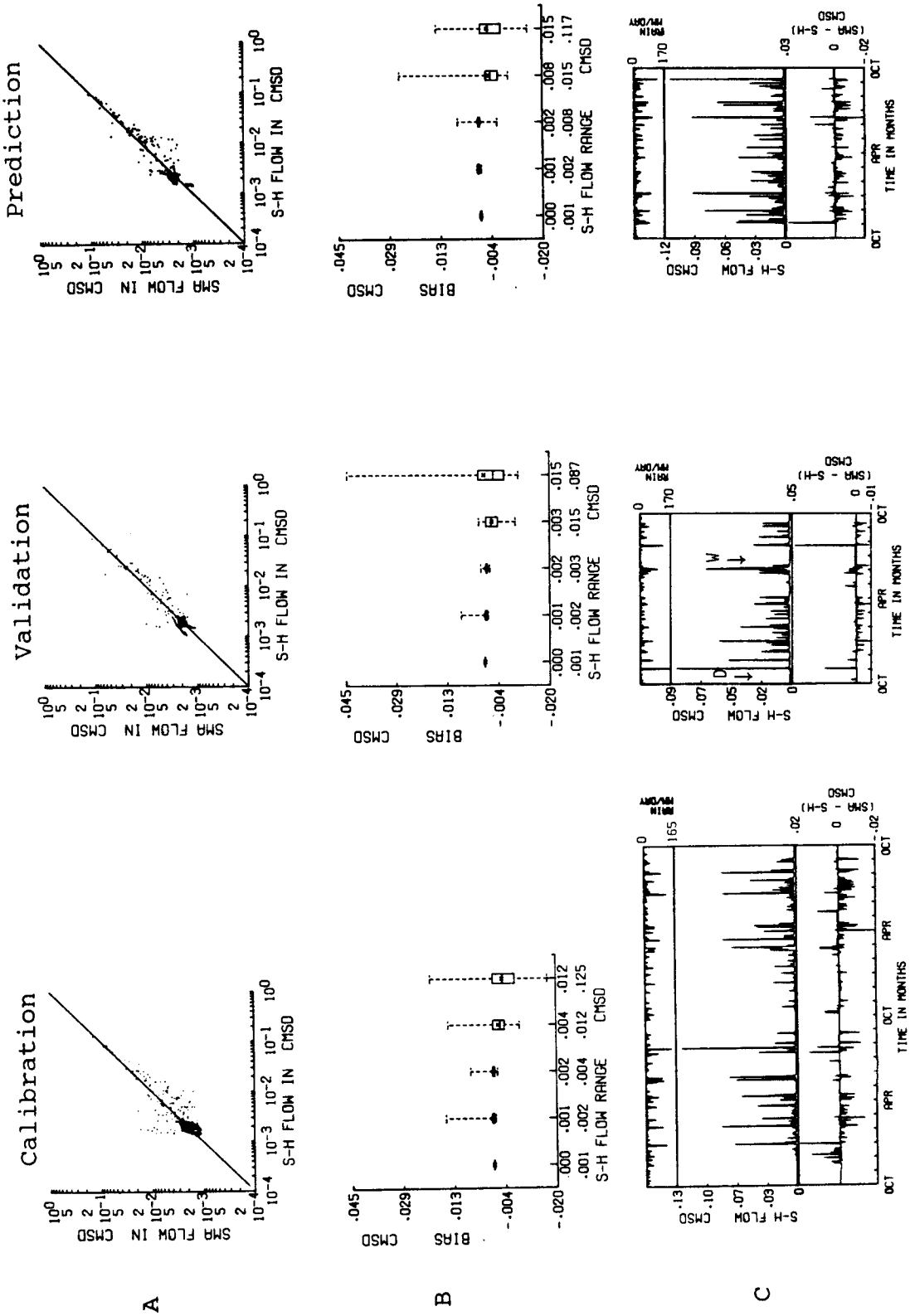

Figure 7.8 Scattergrams (A), boxplots (B) and mean daily hydrographs (C) for HGL104

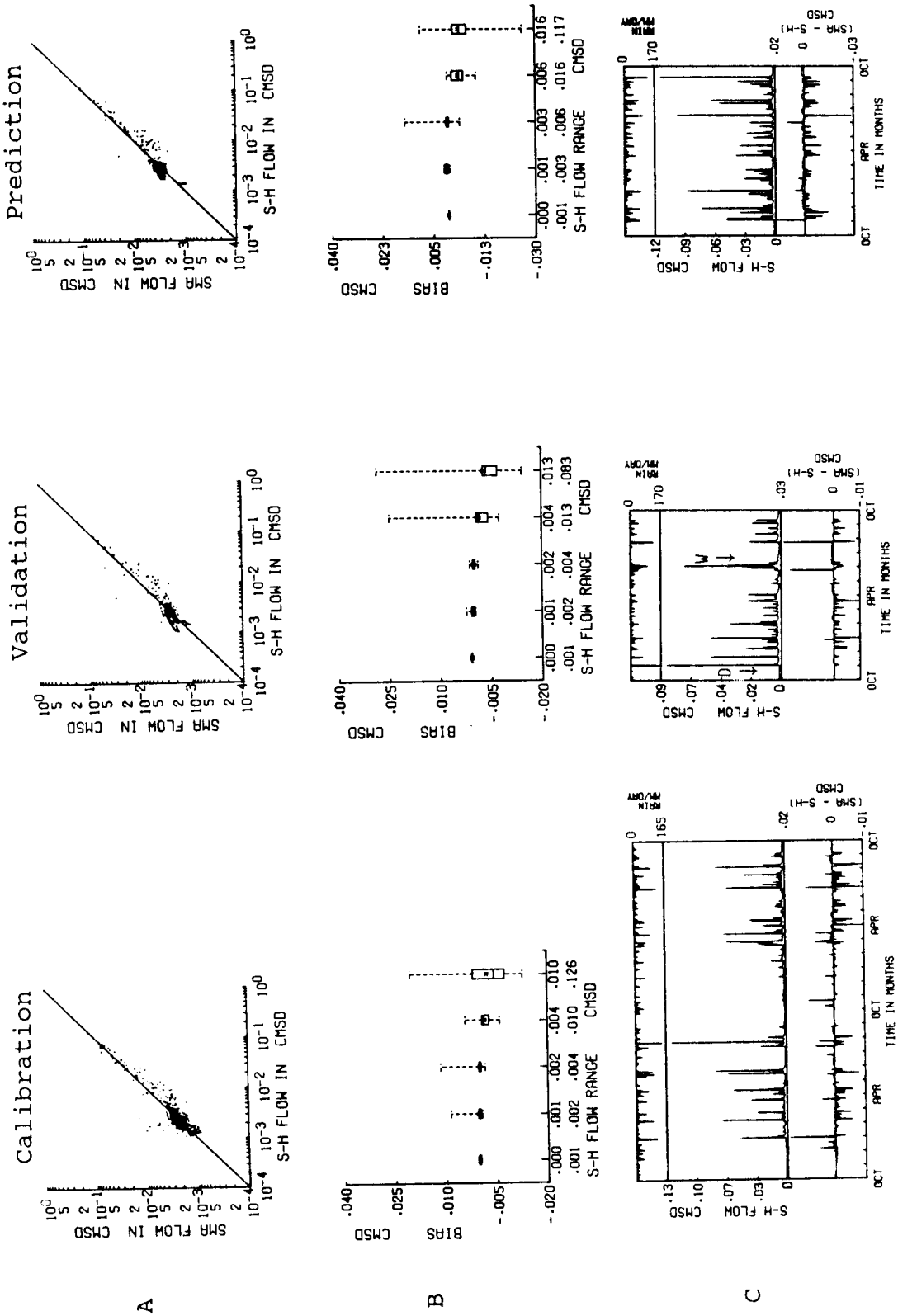

Figure 7.9 Scattergrams (A), boxplots (B) and mean daily hydrographs (C) for HGL105

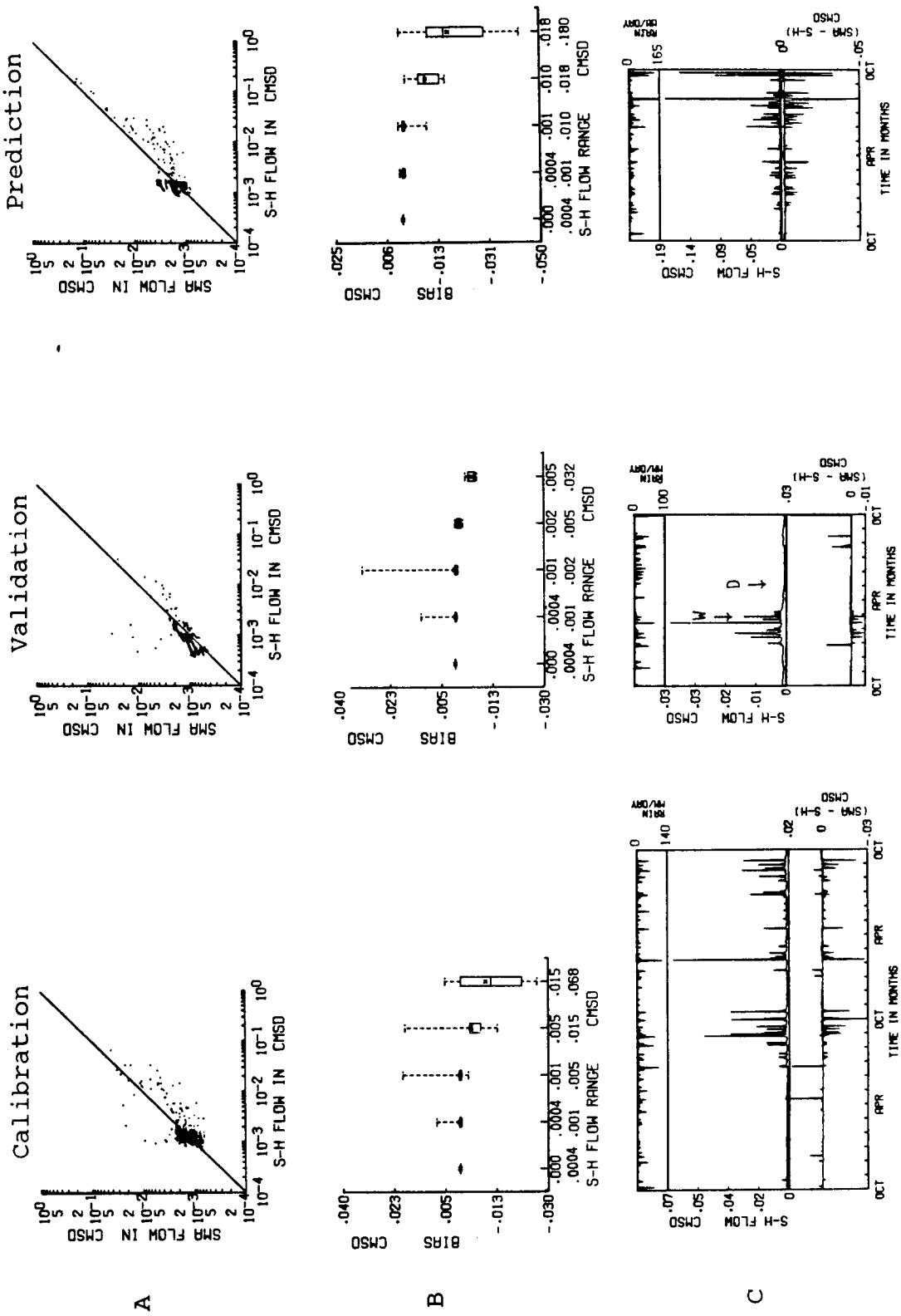

Figure 7.10 Scattergrams (A), boxplots (B) and mean daily hydrographs (C) for HFL102

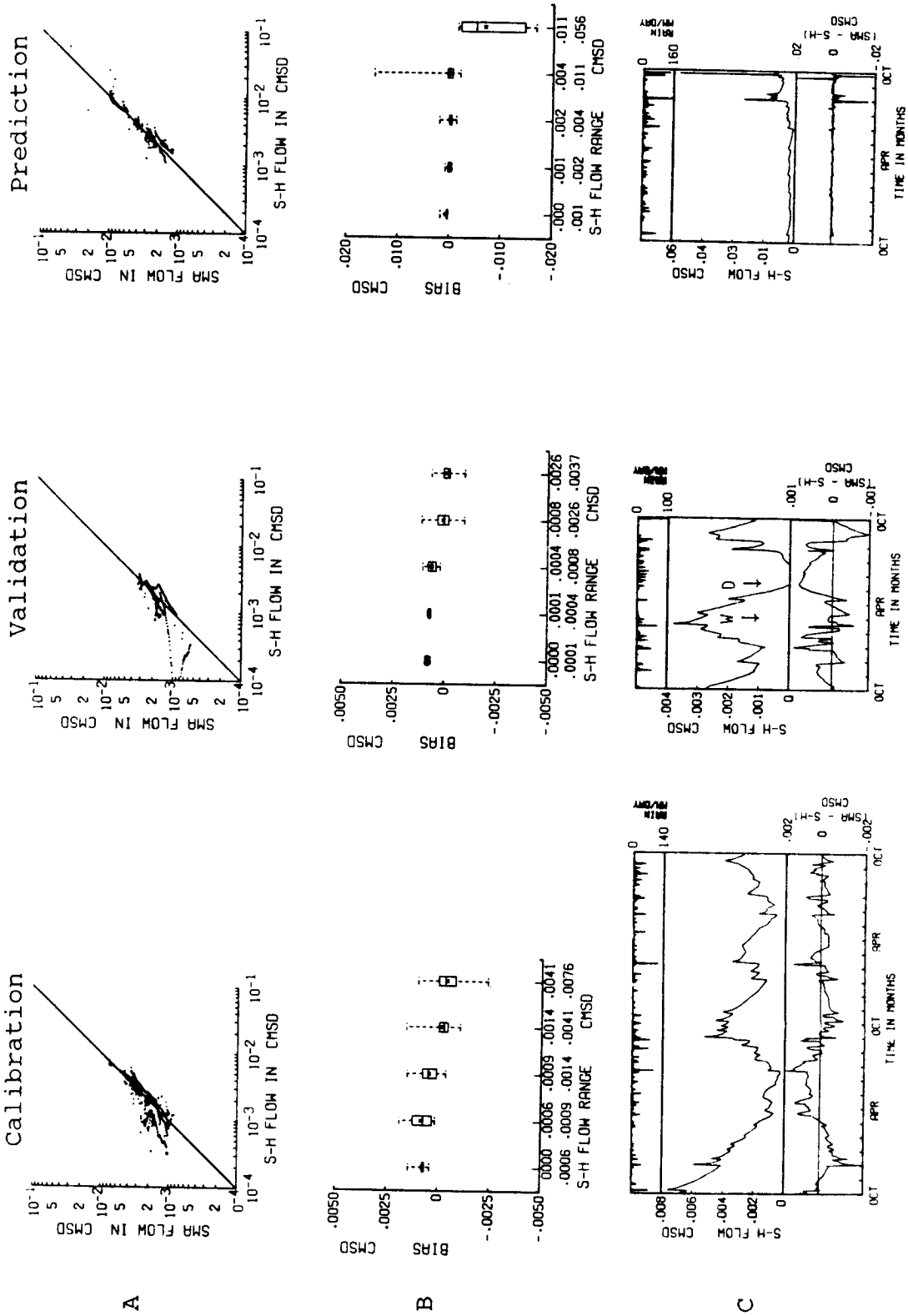

Figure 7.11 Scattergrams (A), boxplots (B) and mean daily hydrographs (C) for HFL103

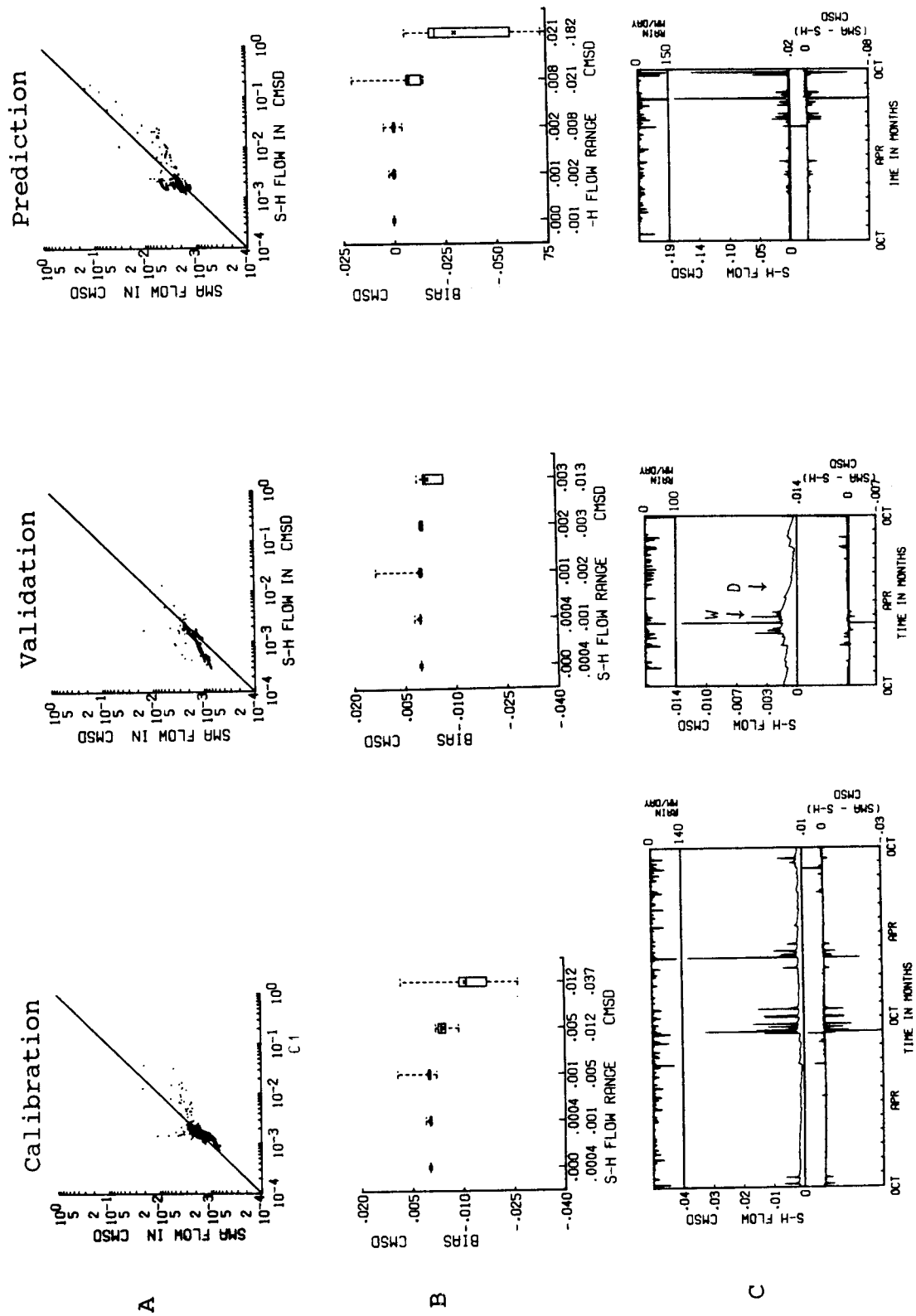

Figure 7.12 Scattergrams (A), boxplots (B) and mean daily hydrographs (C) for HFL104

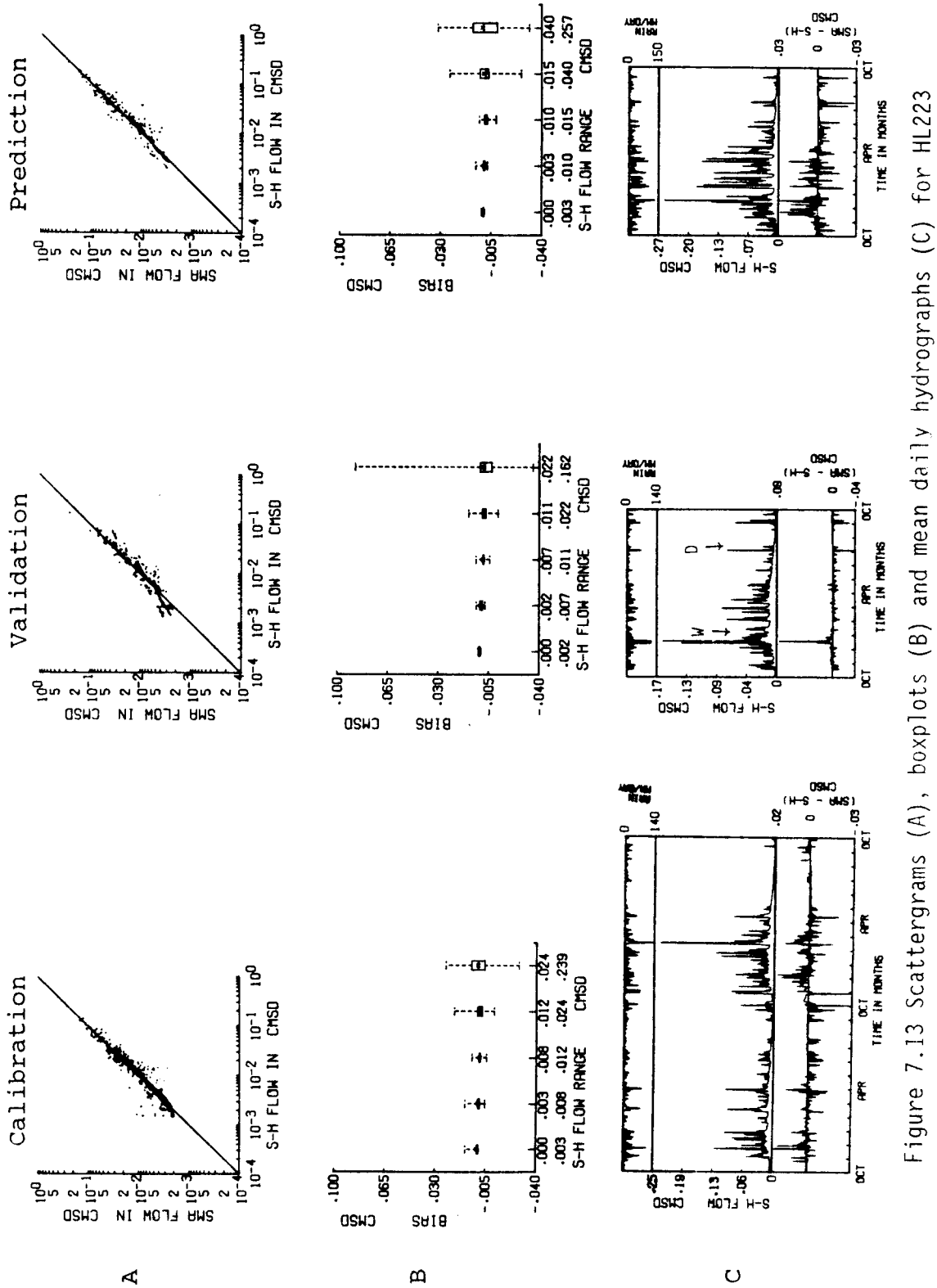

Figure 7.13 Scattergrams (A), boxplots (B) and mean daily hydrographs (C) for HL223

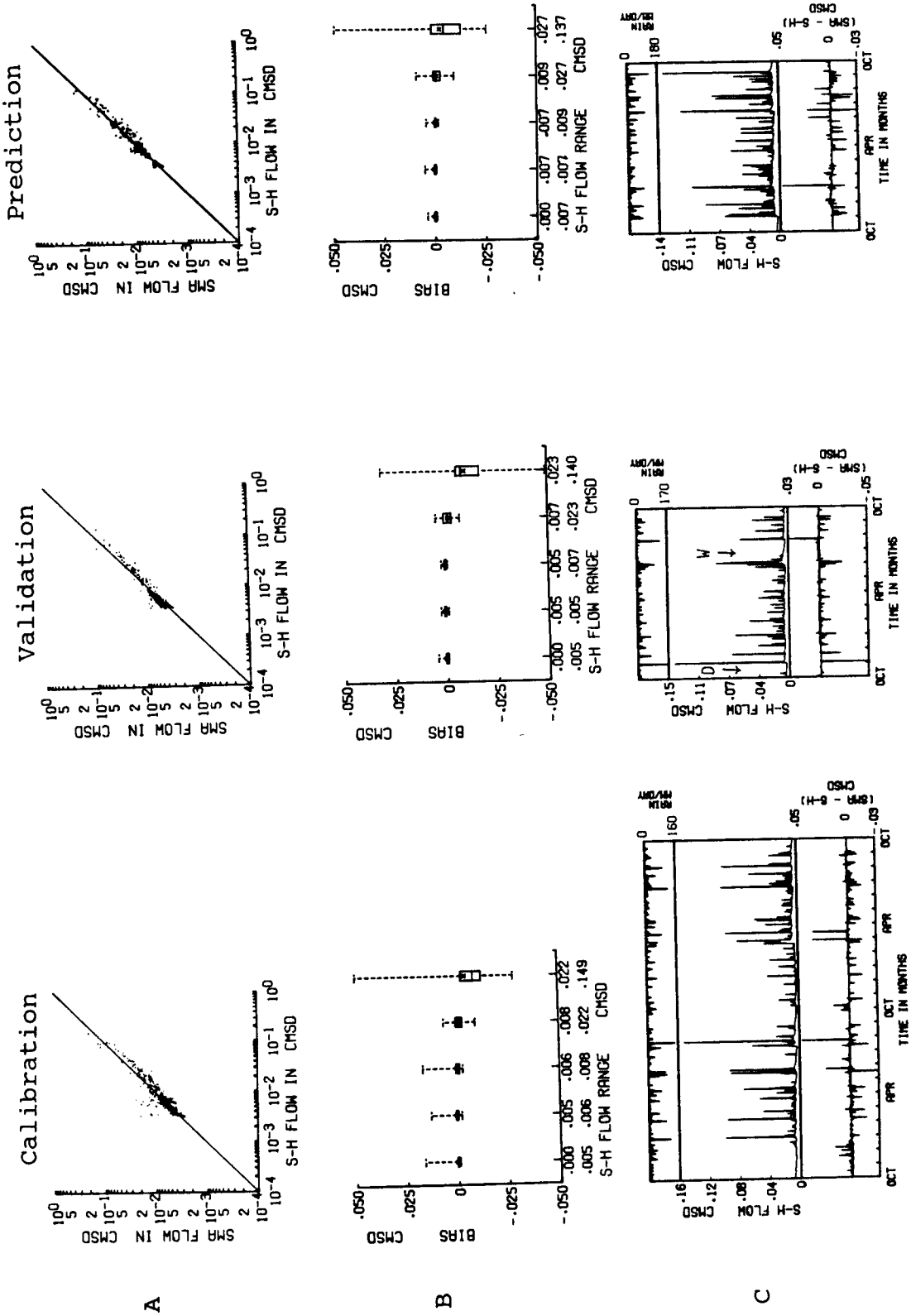

Figure 7.14 Scattergrams (A), boxplots (B) and mean daily hydrographs (C) for HG223

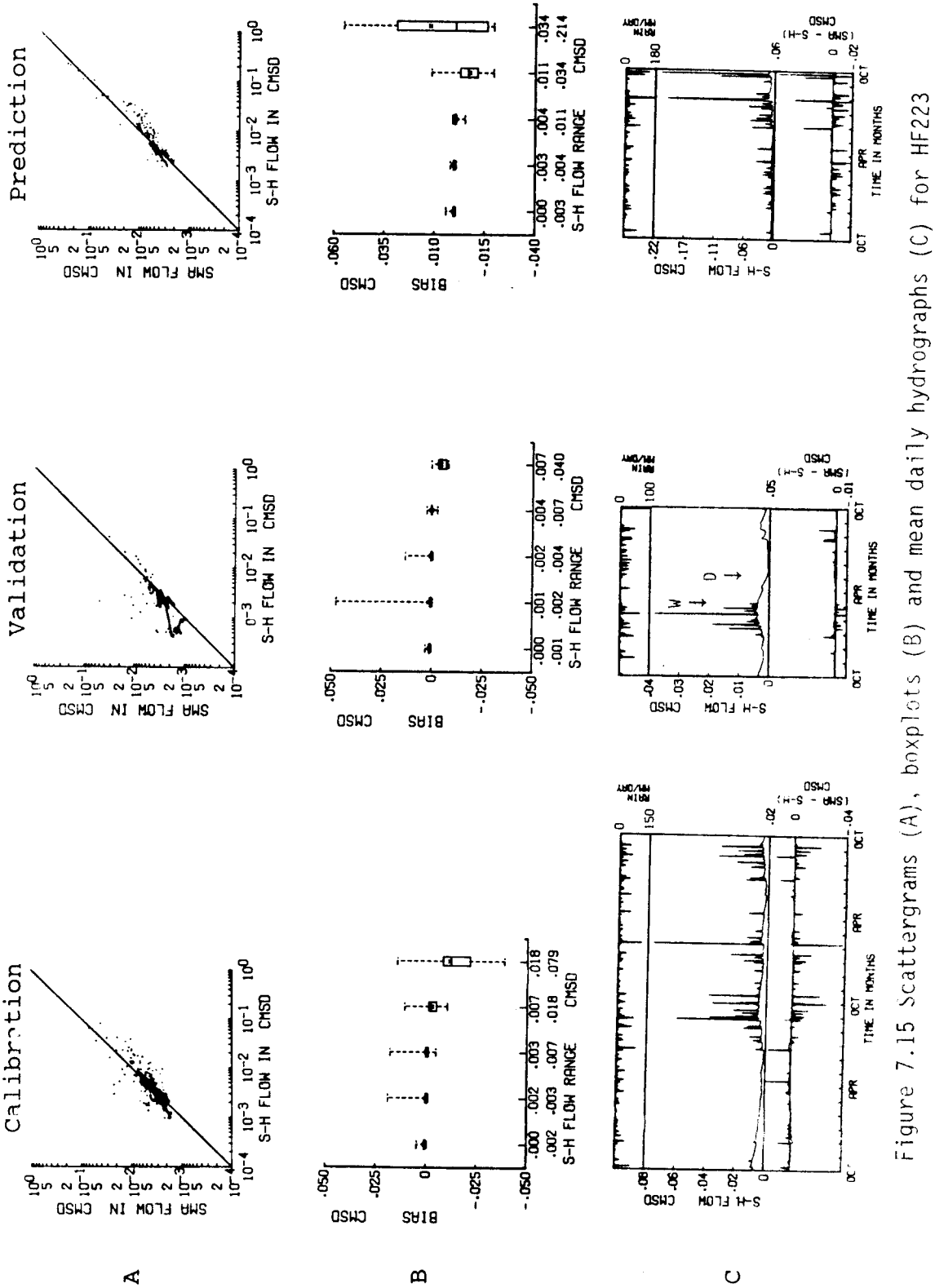

Figure 7.15 Scattergrams (A), boxplots (B) and mean daily hydrographs (C) for HF223

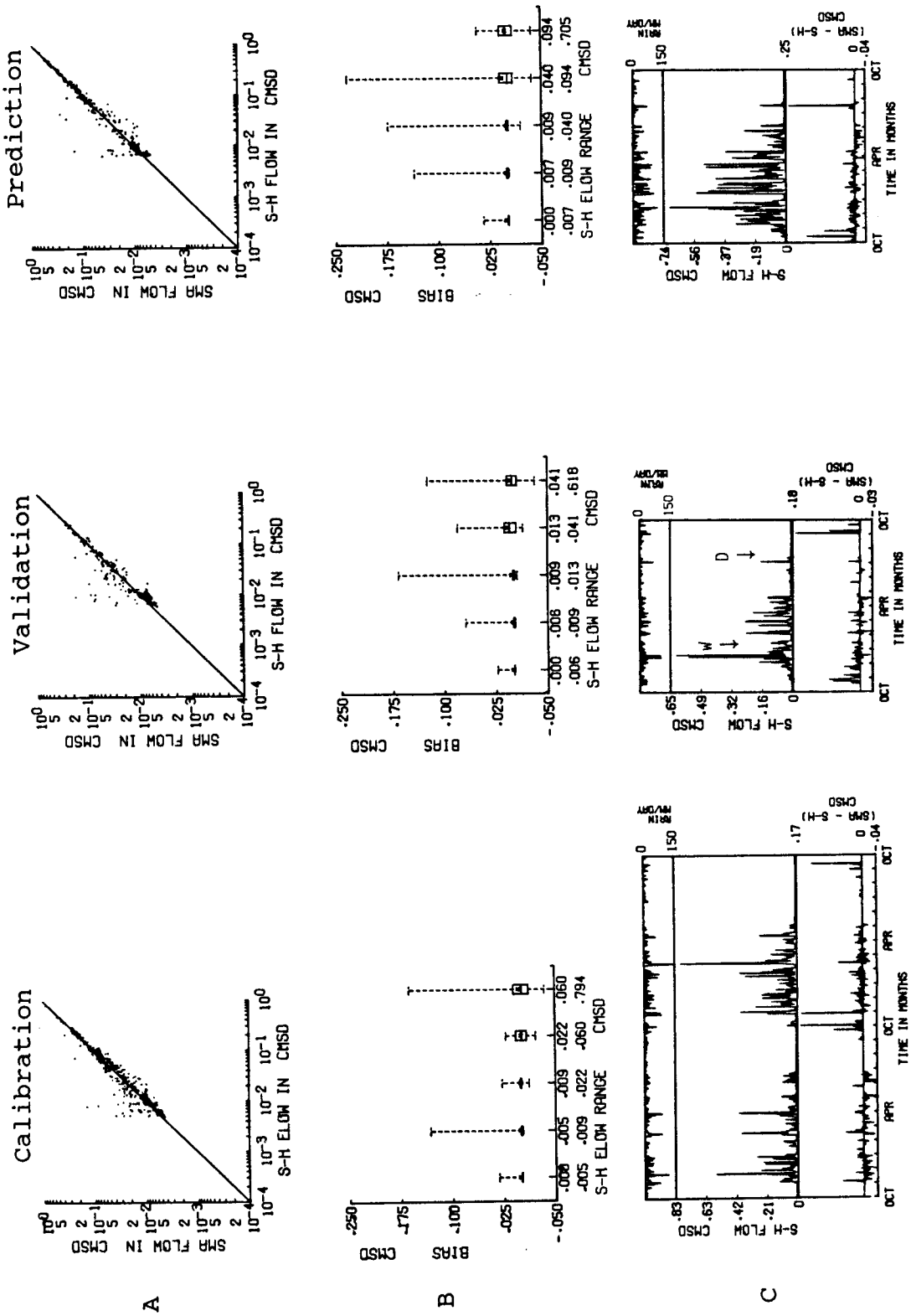

Figure 7.16 Scattergrams (A), boxplots (B) and mean daily hydrographs (C) for HUL104

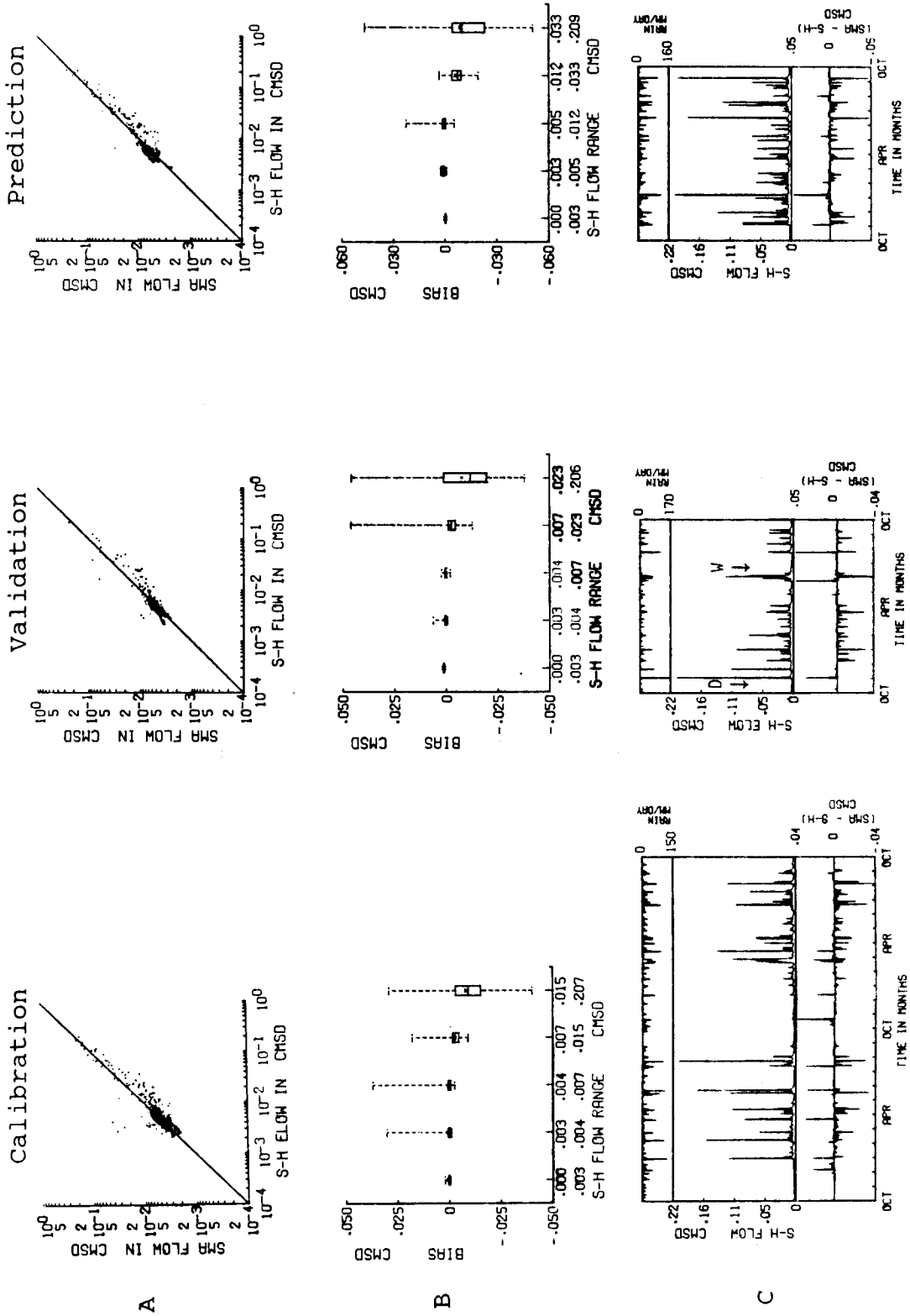

Figure 7.17 Scattergrams (A), boxplots (B) and mean daily hydrographs (C) for HUG105

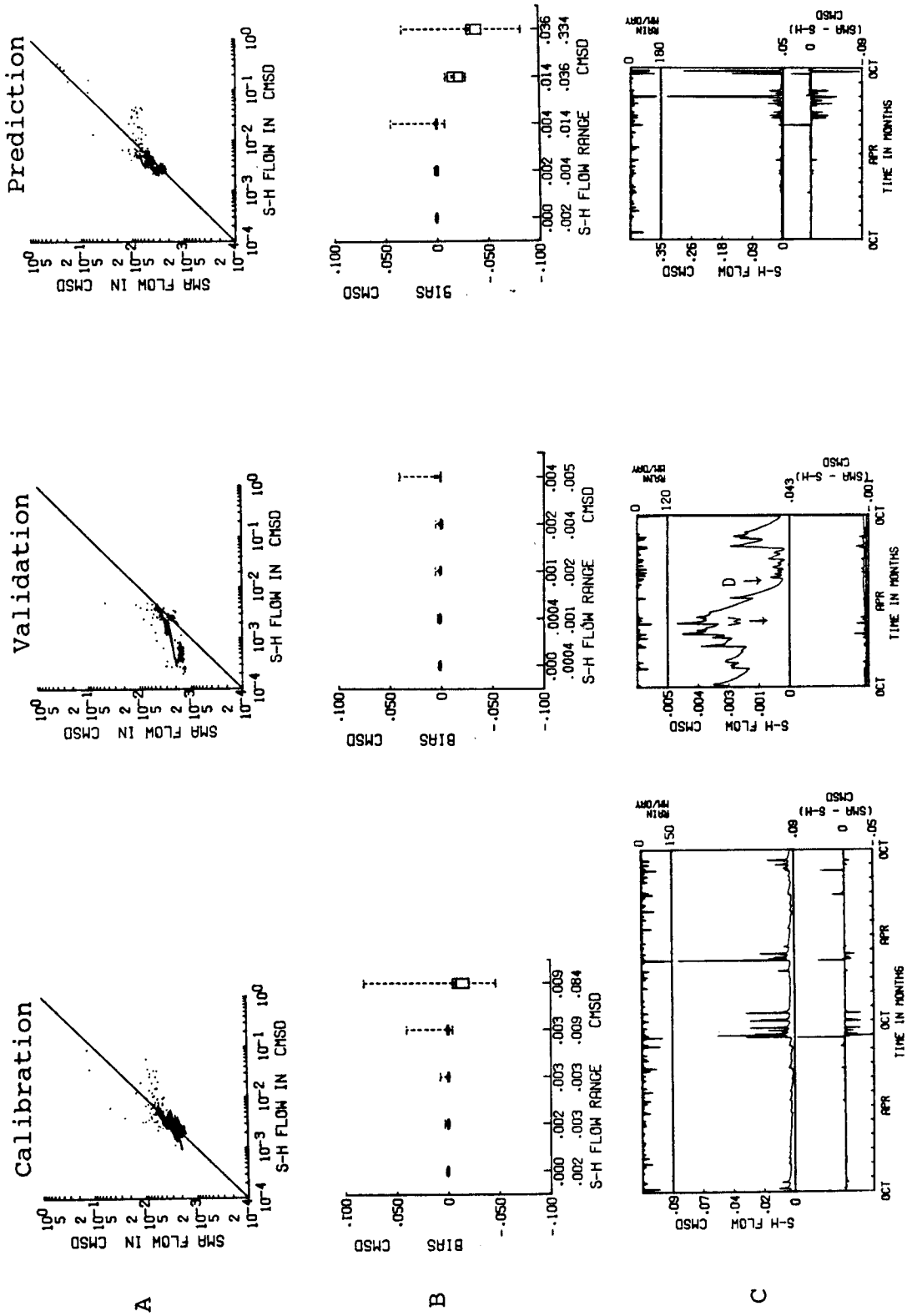

Figure 7.18 Scattergrams (A), Boxplots (B) and Mean Daily Hydrographs (C) for HUF45

7.4 Extreme Rain Tests on Calibrated Sacramento Model

For the design of major hydraulic structures in which failure could mean loss of human life and damage to property, hydrologists use what is called probable maximum precipitation (PMP), which is supposed to be the worst storm that can possibly occur, to estimate extreme flood response for a catchment. Myers (1967) defined PMP as: "that magnitude of rainfall over a particular basin which will yield the flood flow of which there is virtually no risk of being exceeded."

Generalized charts and techniques to define PMP for selected sites in the U.S have been developed (U.S. Bureau of Reclamation, 1977; Schreiner, 1978; Miller et al, 1984.) and used by federal agencies for decades. PMP is transformed to the rainflood hydrograph, usually known as the probable maximum flood (PMF). Catchment parameters involved in traditional estimation techniques are the hydraulic efficiency coefficients C, flood wave travel times, loss rate (to compute rainfall excess) and basin unitgraphs. Bullard (1986) reported that from his comparison study of 61 recorded extreme flood events, 9 had peaks that represent at least 80 percent of the estimated PMF peaks for those locations. Thirty-nine floods had peaks less than 50 percent of estimated PMF peaks. It is natural that the credibility of hydrologists' estimates of PMF's might be questioned.

The high peak flow rates of a PMF are attributed to low loss rates, commonly assumed, which imply that either the catchment is impermeable or it had just experienced heavy rains before the PMP. Some hydrologists recommend the use of conceptual r-r models to predict

extreme flood hydrographs (Linsley et al, 1982). Hence, there is a need to study the forecast ability of conceptual models when used under extreme climatic and antecedent conditions.

A series of extreme rain (on the order of estimated PMP depths) tests was conducted under well defined physical and climatic settings to evaluate the calibrated SMA model's effectiveness. Three sets of PMP depths (Table 7.3, 7.4 and 7.5) were used for the extreme rain tests. They cover three climatic regions in the USA, where the three rain stations selected for this study are located,

One procedure for computing the PMP is found in U.S Bureau of Reclamation (1977, Chapter 3). With a PMP included at a specified time in the rain data time series, S-H was activated to provide the PMP-induced flood event for comparison with that simulated by the calibrated SMA model. For every case, two separate tests were conducted in which the same PMP was applied at time periods representing dry and wet antecedent moisture conditions respectively. For cases HGL102 to HGL105, the differences in moisture conditions between the two tests periods were less distinct. For wet antecedent conditions a flood event on the order of the PMF can be expected from PMP rainfall. In contrast, depending on the situation, for (dry antecedent conditions) there may be no flood at all (Table 7.6 and Figs. 7.19 to 7.23). The times at which extreme rains assumed to occur for experiments using Washington, Georgia and Florida data are shown in Figs. 7.1, 7.6 and 7.10 respectively (W = wet antecedent condition, D= dry antecedent condition).

Table 7.3 Extreme Storm, PMP I (100% of 6-hr PMP) for Quillayute, Washington

Time in hours	Cumultive Rainfall Depth in mm
0	0.
1	61.
2	86.9
3	103.4
4	119.9
5	136.4
6	152.9

Table 7.4 Extreme storm, PMP II (50% of 48-hr PMP) for Tray Mountain, Georgia

Time in hours	Cumulative Rainfall Depth in mm
0	0.0
1	30.5
2	63.5
3	104.1
4	289.6
5	345.4
6	375.9
12	447.5
24	484.1
48	520.7

Table 7.5 Extreme storm, PMP III (50% of 48-hr PMP) for Niceville, Florida

Time in hours	cumulative Rainfall Depth in mm
0	0.
1	30.5
2	63.5
3	104.1
4	289.6
5	345.4
6	375.9
12	426.2
24	487.2
48	548.1

Results of the series of extreme rain tests are presented in the format of graphical plots (Figs. 7.19 to 7.23) and event summary variables, 48-hour flow volume Q_V (mm), discharge peak Q_p(CMS), and time to peak T_p(hour), (Table 7.6). Based on visual comparisons of the flood hydrographs and the summary variables, the forecast of each test is classified either as good, fair, or poor. Comments on the general features observed from the forecast results are given below.

Among cases that during normal rain are dominated by surface flows such as HIL102, HFL102 and HGL102 (relatively impermeable soil), forecasts are generally good under both moisture conditions. In contrast, for cases which under normal circumstances are almost only amenable to subsurface responses such as HIL103, HGL103 and HFL103 (deep, permeable soils) most of the forecasts are poor or at best, fair. In terms of flow mechanisms, for cases that fall between these two extremes, the trends are less definite but in general, forecasts made under wet antecedent moisture conditions are much better than those under dry conditions, as shown in Table 7.6. There is also an obvious trend of over forecasting by substantial amounts, in particular under dry conditions. Only in a few instances were SMA's forecast peak flows slightly below the S-H flood events. These features are summarized in Table 7.7.

Table 7.6 Summary Variables For Extreme Rain Tests on Calibrated Sacramento Model (SMA)

PMP	Case	Model	Antecedent Catchment Moisture: Dry Q_v mm	Dry Q_p m^3/s	Dry T_p hr	Wet Q_v mm	Wet Q_p m^3/s	Wet T_p hr
I	HIL101	S-H	7.8	.025	8.5	158.1	1.61	3.6
		SMA	65.7	1.43	4.0	163.3	1.69	3.1
I	HIL102	S-H	146.0	1.65	4.0	161.6	1.55	4.9
		SMA	136.5	1.71	3.1	162.4	1.68	4.3
I	HIL103	S-H	1.7	0.006	8.1	117.5	1.20	4.3
		SMA	25.9	1.10	4.0	140.0	1.70	3.8
I	HIL104	S-H	14.7	0.13	9.1	151.2	1.72	3.7
		SMA	123.6	1.62	3.2	154.7	1.72	3.3
I	HIL105	S-H	13.0	.14	7.9	151.2	1.70	3.8
		SMA	112.3	.59	4.0	154.7	1.70	3.2
II	HGL102	S-H	462.2	4.99	3.8	442.4	4.98	3.7
		SMA	425.9	5.07	3.1	432.0	5.08	3.1
II	HGL103	S-H	49.3	0.14	5.7	77.8	.27	5.9
		SMA	178.0	4.16	3.9	184.0	4.25	4.0
II	HGL104	S-H	407.8	4.19	4.0	400.9	4.60	3.9
		SMA	419.0	5.05	3.4	398.3	5.08	3.1
II	HGL105	S-H	406.9	5.04	3.9	398.3	5.00	3.9
		SMA	381.0	4.99	3.4	368.1	5.04	3.1
III	HFL102	S-H	343.0	4.31	4.0	499.4	5.12	3.7
		SMA	280.8	4.90	3.3	414.7	5.03	3.1
III	HFL103	S-H	12.1	0.009	7.5	134.8	0.48	5.8
		SMA	168.5	4.05	4.0	206.5	4.33	3.9
III	HFL104	S-H	297.2	2.43	4.0	474.3	5.08	3.9
		SMA	252.3	4.85	3.6	340.4	4.95	3.1
I	HL223	S-H	75.6	1.64	3.9	140.0	2.93	4.0
		SMA	73.4	2.97	4.0	161.1	3.35	3.4

Table 7.6 Continued

II	HG223	S-H 257.0	4.99	4.0	261.8	4.99	4.0
		SMA 337.8	9.69	3.8	358.6	9.80	3.9
III	HF223	S-H 182.3	4.36	4.0	321.4	5.12	3.8
		SMA 276.1	9.42	4.0	370.2	9.86	4.0
I	HUL104	S-H 25.6	0.70	8.8	160.0	8.38	3.9
		SMA 135.1	8.14	3.4	162.6	8.46	3.1
II	HUG105	S-H 406.5	9.99	3.9	400.9	10.00	3.9
		SMA 387.8	10.00	3.0	371.1	10.1	3.0
III	HUF45	S-H 285.6	3.11	4.8	461.8	10.2	3.9
		SMA 292.0	9.91	3.6	420.3	10.1	3.0

Legend

Q_v - Total 48-hour flow volume

Q_p - Peak flow

T_p - Time to peak flow

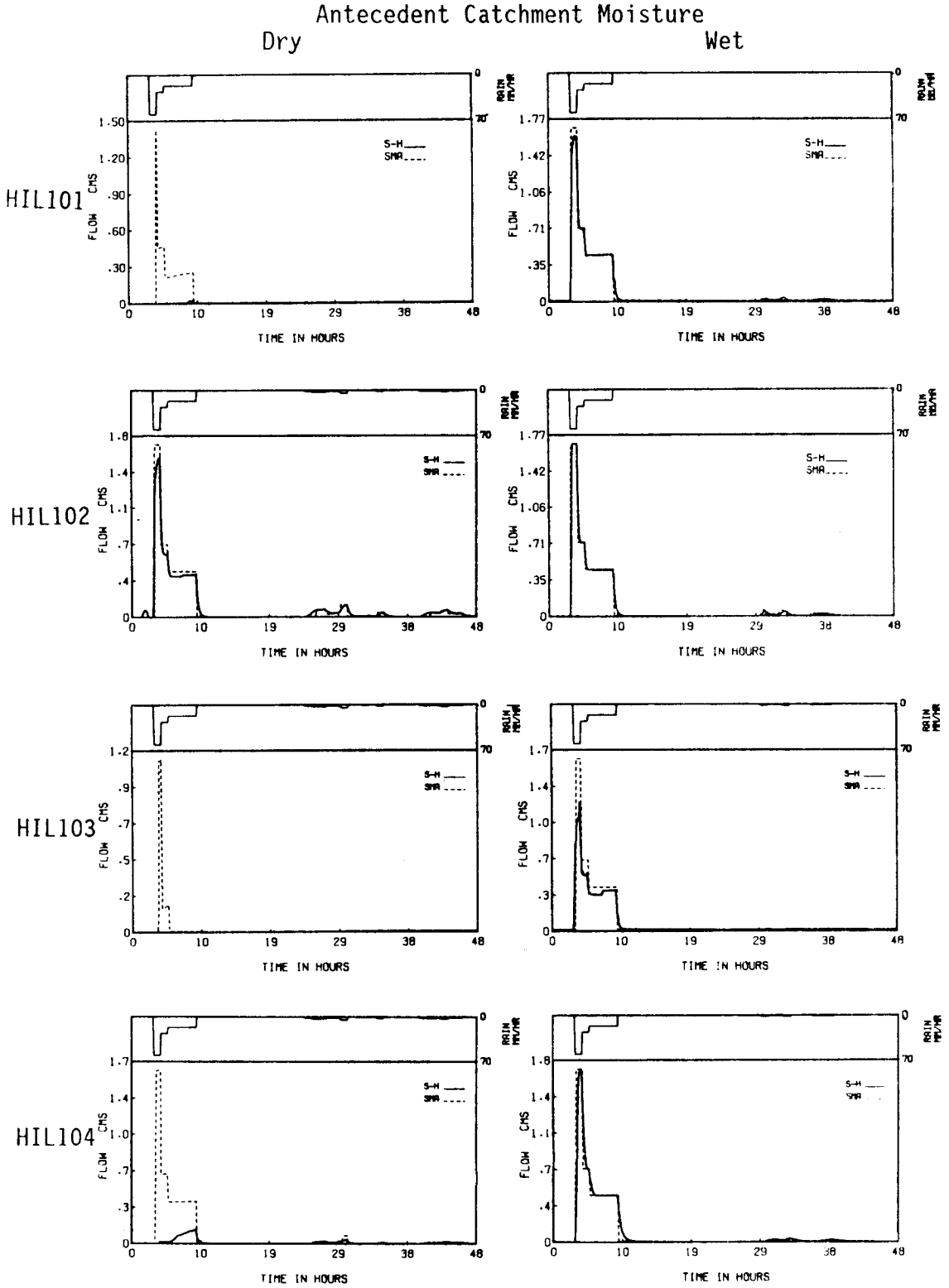

Figure 7.19 Comparisons of extreme flood hydrographs computed by S-H and SMA for five elementary basins (HIL101 to HIL105) subjected to a 6-hour, 153 mm storm (PMPI Washington)

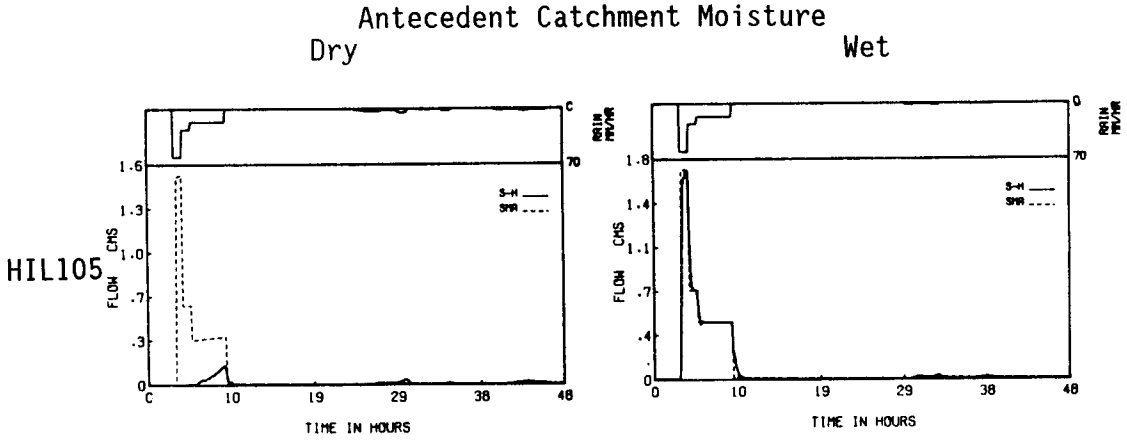

Figure 7.19 Continued

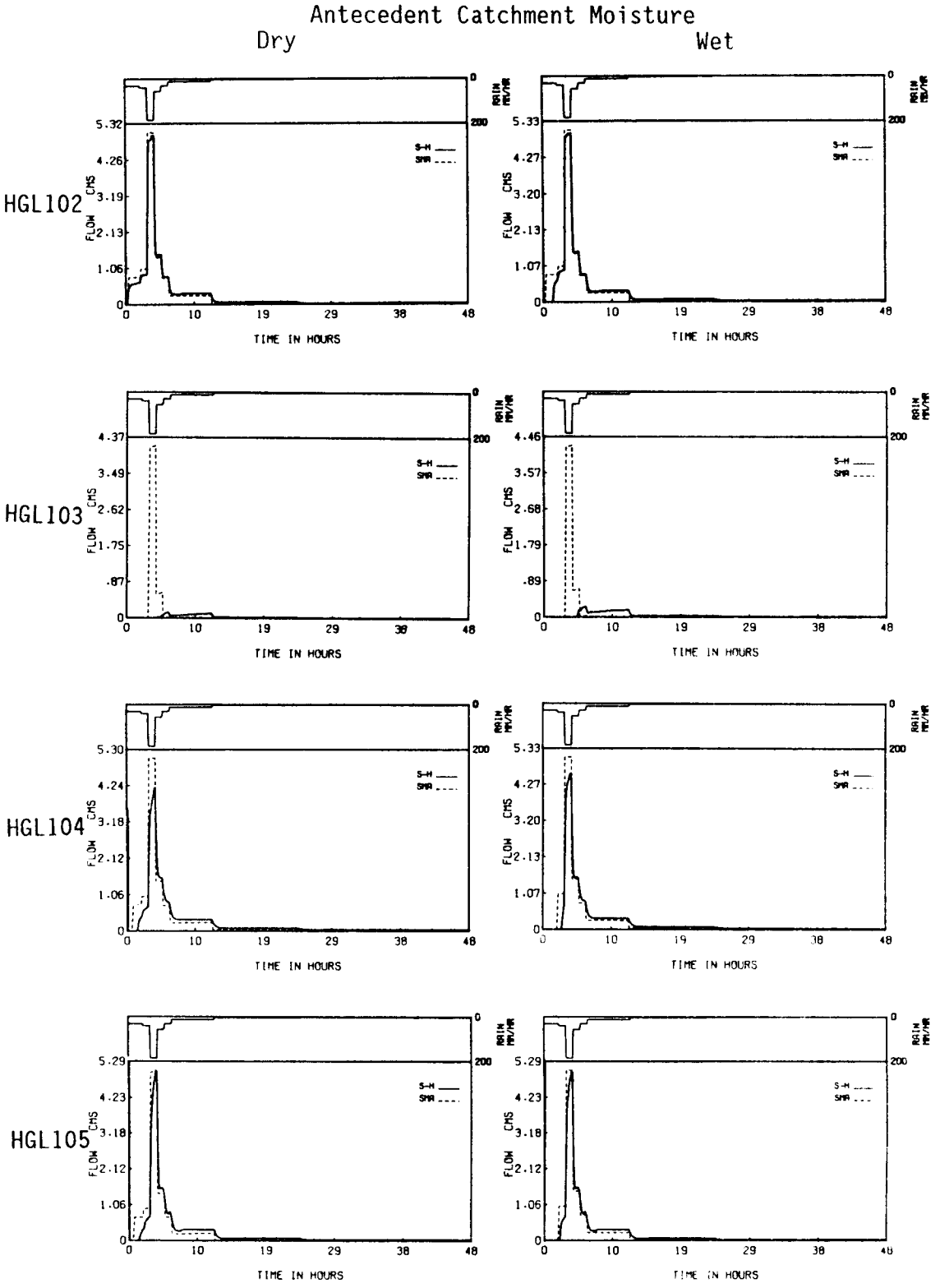

Figure 7.20 Comparisons of extreme flood hydrographs computed by S-H and SMA for four elementary basins (HGL102 to HGL105) subjected to a 48-hour, 520.7 mm storm (PMPII Georgia)

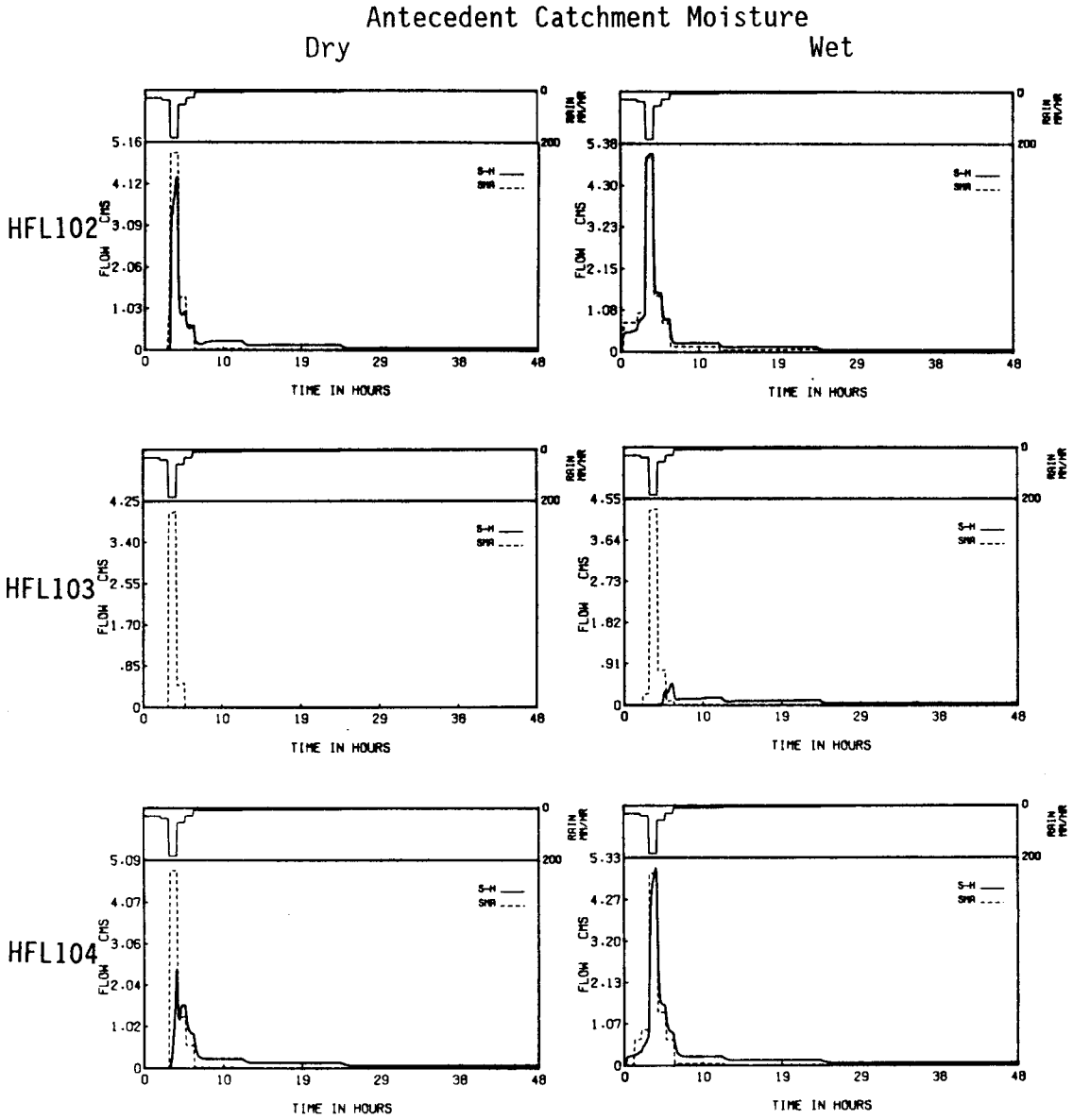

Figure 7.21 Comparisons of extreme flood hydrographs computed by S-H and SMA for three elementary basins (HFL102 to HFL104) subjected to a 48-hour, 548 mm storm (PMPIII Florida)

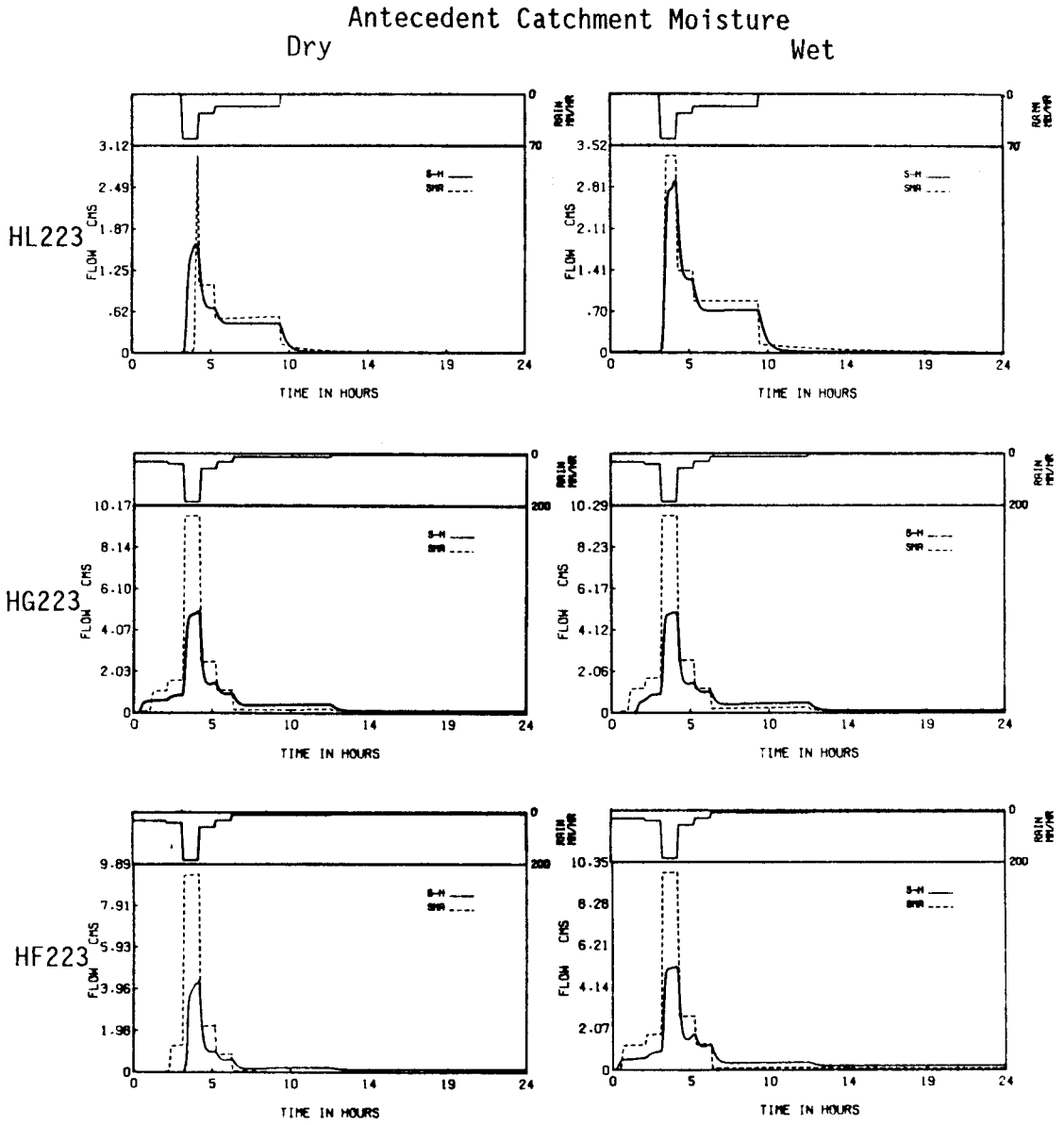

Figure 7.22 Comparisons of extreme flood hydrographs computed by S-H and SMA for three 2-subbasin catchments (HL223, HG223 and HF223) subjected to storms PMPI, PMPII and PMPIII respectively

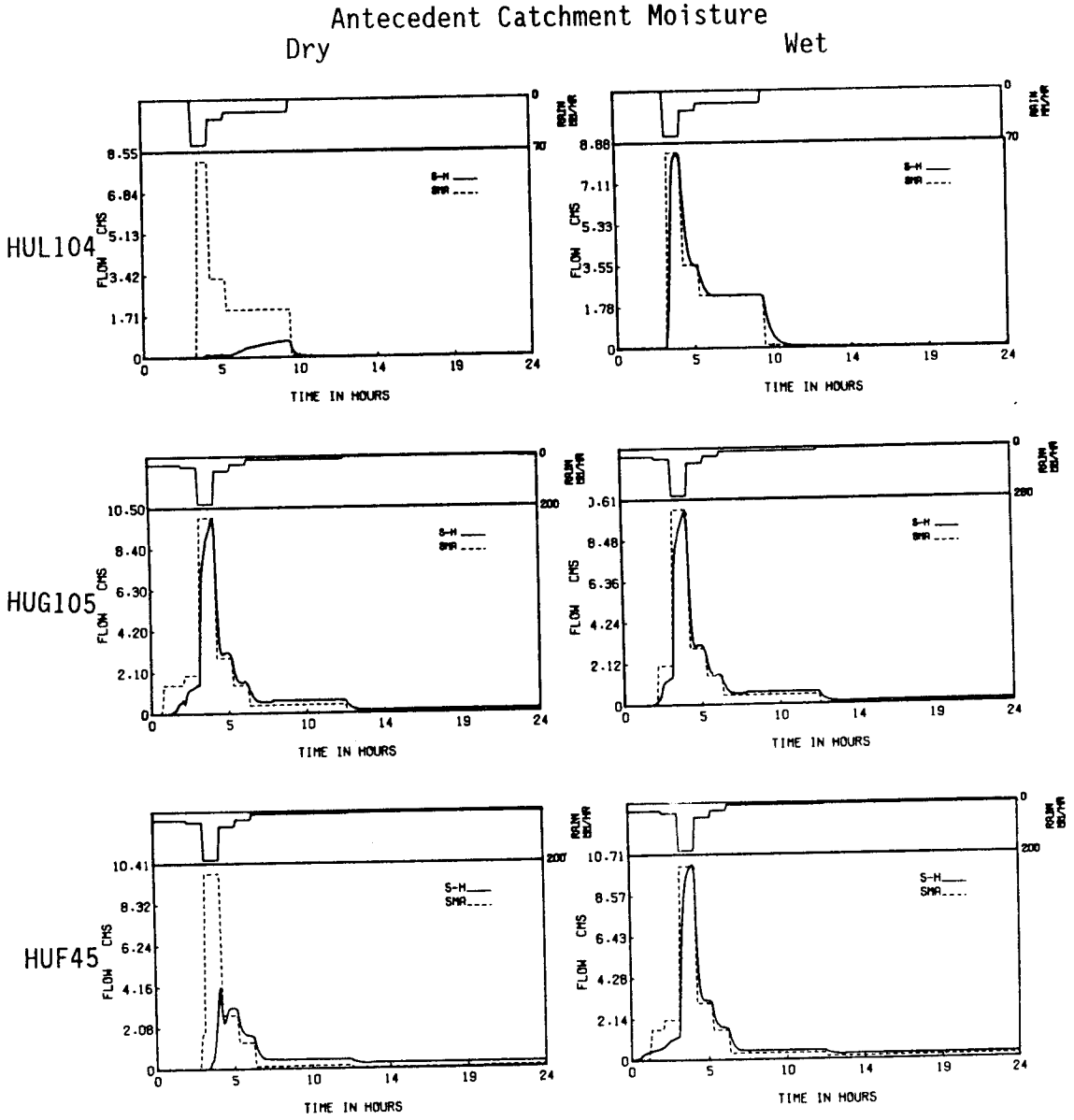

Figure 7.23 Comparisons of extreme flood hydrographs computed by S-H and SMA for three 2-subbasin catchments (HUL104, HUG105 and HUF45)subjected to storms PMPI, PMPII and PMPIII respectively

Table 7.7 Summary of catchment responses for extreme rain falling on dry and wet catchments

Performance	Number of cases Antecedent Moisture Condition	
	Dry	Wet
Good	4	10
Fair	3	2
Poor	11	6

The scope of this research is confined to simple, idealized, small catchments only. Hence, complicating factors and their combined effects on PMF such as channel storage and attenuation effects, depression storage, vegetation, undulating terrain, and heterogeneities in soil layers found in natural catchments were not considered. For the simple catchments explored, the factors that govern a hypothetical catchment's response to heavy rain were its antecedent moisture condition, the soil infiltration rate and depth of the upper soil layer.

There are two major reasons attributed to good forecasts in cases HIL102, HGL102, and HFL102. For catchments with low saturated hydraulic conductivity (K_u = 0.02m/hr to 0.06m/hr), overland flow would be the major flow mechanism when subjected to intense rain because loss rates due to infiltration are small, even under dry antecedent conditions. For these three cases, S-H always produced flood events of significant magnitude in all extreme rain tests. The SMA was

calibrated with flow sequences for these cases that were dominated by many peak values and so the parameters primarily responsible for surface flows, UZK, UZFWM and UZTWM (Fig. 4.5) were estimated accurately. With such favorable factors, when heavy rain was applied, SMA would respond with great floods as S-H did. In essence, both models produced either Horton or saturation overland flows for these cases.

The situations in HIL103, HGL103 and HFL103 are quite different. With thick, highly permeable soils (Depth = 1.6m, K_u = 0.2m/hr), they had large capacities to absorb rainfall. Without the presence of impermeable surfaces and microtopography, and with all the extreme rain pulses having intensities lower than K_u, surface response was only possible when the water table reached the ground surface. Out of 6 tests, only in HIL103 (under wet antecedent conditions) did S-H produce a significant flood event. The flow traces used for calibrating SMA were predominantly baseflows. It is no surprise, therefore, that upper zone parameters UZFWM, UZTWM and UZK were estimated poorly. Under high percolation rates (for highly permeable soils), the rain pulses experienced in the calibration stage were not large enough to cause the upper zone free moisture content UZFWC to build up to exceed UZFWM and so no surface flow would be predicted by SMA. In SMA, interflow (UZFWC x UZK) also seldom occurred. Estimated values of UZFWM range between 20 mm and 40 mm which was sufficient to prevent overland flow during the calibration stage. However, when the rain pulses became exceedingly large, the calibrated model's percolation rates would not be fast enough to drain all the moisture to the lower zones and the

moisture remaining in the upper zone exceeded UZFWM, giving rise to surface flow. Hence, most forecasts by SMA for cases HIL103, HGL103 and HFL103 were too high.

In terms of flow mechanisms, the remaining cases fall in between the 6 cases discussed above. Except for half of the six two-subbasin catchment cases, they had a common soil hydraulic conductivity of 0.2m/hr, but they differ in other hillslope characteristics. Poor forecasts under dry antecedent conditions for most of these cases are attributed to two main causes. Under dry antecedent conditions, with K_u higher than the flux rates of all extreme rain pulses, S-H would not produce either saturation or Hortonian responses. Though the upper zone parameters were now calibrated on a better basis than previous cases, they were still inadequate to cope with extreme rain pulses not experienced in the calibration stage. Whenever the calibrated UZFWM is too small, surface flows occur for sufficiently heavy rain. The conceptual model was not able to emulate the soil moisture condition of the catchment continuously (in terms of 5 "conceptual storages"). At certain periods, the contents of the 5 conceptual storages were suitable for accurate simulations but the threshold values (capacities) were determined incorrectly and could not accommodate extreme inputs (Figs. A.1 and A.25).

This phenomenon was observed in many cases and could occur practically in any modeling stage, namely calibration, validation, and prediction. This finding, that forecasts for dry conditions were poor, complements what was discovered by the r-r models inter-

comparison study conducted by the World Meteorological Organization (1975); all models tested performed badly for dry catchments, including the more complicated explicit soil moisture accounting models.

The influence of catchment characteristics on forecasts was further explored by combining elementary hillslopes from the first two "extreme" groups to form 2-subbasin catchments for cases in Test 2: HL223, HF223, and HG223. For the same rain data applied, two highly contrasting flow responses, one surface and the other subsurface, resulted from each subbasin. Hence, the resulting flood hydrographs produced by S-H were moderate in peaks and volumes. Again, essentially for the same reasons, forecasts made by the calibrated SMA models were poor, though the quality of forecast fell in between the first two groups.

Three cases under Test III (HUL104, HUG105, HUF45 of Section 5.3.3) were conducted to study the effects of rain spatial distributions . With respect to the corresponding cases subjected to point rainfall only, the parameters derived are different but the differences are not enough to make any significant impact on extreme flood events. When operated in forecast modes, the same factors dominated the performance of SMA (Fig. 7.23). A more rigorous approach is needed to study the effects that the natural spatial character of rainfall has on calibration.

Within the framework of this research, there is enough evidence gathered to draw conclusions regarding the reliability of the SMA when

used for conditions not experienced during calibration. The results are limited because the tests were conducted under simplified assumptions but they give indications regarding the quality of conceptual modeling for soils on the order of 1 meter deep and saturated hydraulic conductivity larger than 0.02 m/hr.

(1) It is nearly impossible for conceptual r-r models to keep a realistic soil moisture profile continuously, especially during droughts and in particular when a series of storms occurs after prolonged dry periods.

(2) How much does a calibrated conceptual r-r model, represented by a set of parameters, capture of the hydrologic processes of the catchment modeled ? Based on flood hydrographs, the calibrated model could replicate some phases of the processes well at certain time periods but very poorly at others, depending on the climatic condition and catchment characteristics. This implies that global optimal parameters, if they exist, are nearly impossible to obtain through model calibration. The parameters are "fitted" values and their interpretation is open to question.

(3) Conceptual models are more reliable for modeling the hydrograph response of wet than dry catchments.

(4) The results are not wholly conclusive since they are based on idealized situations which ignore the complicated effects of soil heterogeneities and many spatial variabilities of natural catchments.

7.5 Physical interpretation of parameters

It has been a common practice to assess the credibility of a hydrologic model by comparing the simulated data with the observed. For this research, an extra means of assessment is the physical interpretation of the set of lumped parameters that represent the calibrated conceptual model. Each set of parameters was obtained by calibrating SMA prediction to S-H streamflow data, which was simulated by S-H for a precisely defined hypothetical catchment and error free climatic input. If SMA represents hydrologic processes well the parameters which represent conceptual storages should add up to the effective soil water capacity of the hypothetical catchment. Table 7.8 gives the actual soil water capacity and the corresponding sum of the five conceptual storages for all 18 cases studied. Variables representing the capacity of each of the five conceptual SMA storages are UZFWM, UZTWM, LZFPM, LZFSM and LZTWM (Fig. 4.5).

Table 7.8 Maximum physical soil water capacity of hypothetical catchments and total estimated conceptual storage capacities

Physical soil water capacity (mm/unit area)	Case	Total conceptual storages (mm/unit area)
	HIL101	620
	HIL104	591
	HUL104	599
	HIL105	422
	HGL102	380.7
352	HGL104	474
	HGL105	477.9
	HUG105	608.8
	HFL102	696.6
	HFL104	867
	HUF45	673
360	HIL102	140
528	HF223	605
	HG223	515
532	HL223	555
	HIL103	1085
704	HGL103	1102.4
	HFL103	1027.0

Table 7.8 (continued)

Note: Cases with headings HIL's, HL's and HUL were subjected to Quillayute, Washington rain data; HGL's, HG's and HUG to Tray Mountain, Georgia rain data; and HFL's, HF and HUF to Niceville, Florida rain data.

Examination of Table 7.8 reveals that none of the total conceptual storages is close to the respective effective physical soil storage with the exception of HGL102 (380.7 against 352). HIL102 has the lowest total conceptual storage. This is intuitively understandable because it produced predominantly surface flows (refer to Table 7.1), governed mainly by the upper zone storages, UZFSM and UZTWM, which should be small to trigger significant surface response.

On the other hand, HIL103, HGL103 and HFL103 are the three cases which were dominated mostly by base flows. Of course, their lower zone storages LZFPM and LZFSM responsible for base flows should be large to maintain high subsurface flow rates. Their calibrated storages differ by less than 10% but they are all much higher than the effective catchment soil water storage of 704mm.

Next, when hypothetical catchments with effective physical soil water capacity of 352mm experienced eleven different combined climatic and physiographic conditions, only two cases had cumulative conceptual storage (HGL102 and HGL105) remotely close to reality. HFL's have biggest storages, then HIL's and lastly HGL's. This is rather surprising because if conceptual storages could be related to the annual

precipitation or other storm parameters, the order should in fact be HIL's, HGL's and HFL's.

With respect to their effects on model output, some parameters are more influential than others. The five maximum storages ranked according to influence are UZFWM, LZFSM, LZFPM, UZTWM and lastly LZTWM. Experiments show that a wide range of values could be used for LZTWM or UZTWM without affecting the simulated flows. Therefore, the starting parameter values and the sequence of operations in the Nelder and Mead optimization scheme have significant influence on the "optimium" values of the less sensitive parameters.

The contention that conceptual lumped parameters should be rain invariant and only depend on catchment characteristics has been found to be false. By introducing 20 to 30% of a uniformly distributed [-.5, .5] random noise to the rain data in case HUL104 , the total conceptual storages obtained differ from those in HIL104 by 1.3%. A similar phenomenon was observed between HGL105 and HUG105. The five conceptual storages for HUG105 are 78.5% larger than HGL105. It is no surprise to find the parameters from cases using different rain data for the same catchments being very different from each other. They are not the same simply because they have to replicate different flow dynamics produced by the S-H model. For these experiments, the estimated values of the parameters depend primarily on the flow sequence and climatic data used for calibration, rather than on catchment properties.

While conceptual storages depend on climatic inputs, the crucial question is how well (or poorly) SMA approximates the real hydrologic system ? If it cannot emulate a simple, idealized situation, what is its chance in the natural world ? The explicit soil moisture-accounting technique when calibrated to a streamflow signal does not emulate the physical processes of a simple system adequately and therefore it generally cannot be expected to do better for a complex natural system. However, catchments that are closer representations of nature need to be tested to get more conclusive results.

7.6 Difficulties in Calibration

The model itself is not entirely responsible for parameters that lack a physical basis. Part of the problem lies in the calibration technique employed. It has been found that different sets of optimized parameters were derived from different sets of observed data for a given catchment, or from different sets of starting values of the parameters.

While the Nelder and Mead scheme (NMS) is a robust, reliable automatic tool, it has inherent difficulties in searching for the minimum of an objective function for the following reasons.

(1) A large number of combinations of parameter values give comparable low values of the objective function. Optimization search makes little or no progress along the floor of an "extended valley" response surface of the parameter simplex (Sorooshian and Arfi, 1982).

(2) Insensitive parameters make little difference to the simulated flow data and the objective function.

(3) Imperfect representation of hydrologic processes by the model leads to difficulties in optimization.

(4) Attempts to constrain conceptual storages to the physically known soil water capacity of a catchment resulted in poor calibration and validation for SMA. It is not clear that some constrained optimization schemes will lead to improvements in calibration.

Difficulties encountered in calibrating conceptual r-r models seem universal. Johnston and Pilgrim (1976) failed to find a true set of optimal parameters after two years of full time effort on just calibrating the Boughton model on a catchment in Australia. The discouraging outcome of attempts to correlate parameters with physical information could be partly attributed to the question of achieving optimality in calibration.

7.7 Model structure differences between S-H and SMA

The intention of identifying an optimal set of parameters that are physically meaningful and consistent is complicated primarily by the differences in the model structure between S-H and SMA. Some qualitative observations to this dilemma are offered.

Dry period

In S-H, even when there is no rain, water still percolates to the perched water table (though at a slower rate), thus supplementing the subsurface flow. The amount of moisture reaching the perched water table at a particular instant depends on the magnitude of the "oldest" rain pulse that is just above the water table and its velocity. The computation process for SMA is quite different. During dry periods, the upper zone tension water is usually less than the maximum allowable (UZTWC < UZTWM) and the upper zone free water is negligible. Whenever such a situation occurs, SMA does not allow moisture to percolate to the lower zone. Hence at the end of the dry period, there will be "proportionally" more upper zone tension moisture in SMA than the moisture in the unsaturated soil layer of S-H. A reverse situation happens between the lower zone moisture contents of SMA and the saturated soil layer (perched water table) of S-H. This is just one of the many possible situations that can cause the moisture representation in SMA to deviate from that of the catchment modeled by S-H.

Wet period

For SMA, as long as the upper zone free water UZFWC is greater than zero, there will be interflow (UZFWC x UZK) which may be thought of as the equivalent of the return flow in hydrologic processes. It is to be expected that the arrival of a storm after a lengthy dry period

would cause UZTWC and UZFWC to be filled in a shorter time frame than to bring the water table of the aquifer in S-H to the ground surface. For example, if the SMA upper zone free storage capacity, UZFWM, is small, say 5 to 10 mm, and a rain pulse is greater than UZFWM, surface flow would take place which is equivalent to either Hortonian or saturation overland flow. After a prolonged dry period, it takes much more rain for saturation overland flow to occur in S-H, unless the same rain pulse has an intensity greater than K_u which often does not happen when K_u is as large as 0.2 m/hr.

Evapotranspiration

The evapotranspiration component of SMA is a particularly simple approximation of a complex process. The algorithm for computing ET extraction rates is based on a linear ratio of tension water storages versus maximum tension storages. There is only one factor, PEADJ, for adjusting the final ET extracted. However in S-H, when the soil suction pressure Psc exceeds a pre-specified value, say 0.33 m, ET is adjusted by a factor FE based on the work of Denmead and Shaw (1962), given by Equation 7.1

$$FE = \left[\frac{0.33}{Psc}\right]^{1.33} \qquad (7.1)$$

which is a closer representation of nature. In the course of the present experiments, by adjusting PEADJ to values between 0.7 and 1.0, ET volumes from both models could only be matched on an annual basis.

Percolation process

The percolation process of SMA is governed by Eqs. 7.2 and 7.3

$$\text{Percolation} = \text{Perc}[1 + \text{ZPERC}\ (\text{Deficiency})^{\text{Rexp}}] \tag{7.2}$$

$$\text{Perc} = \frac{[\text{LZFPM} \times \text{DLZP} + \text{LZFSM} \times \text{DLZS}]\text{UZFWC}}{\text{UZFWM}} \tag{7.3}$$

which contain eight adjustable parameters. Even though many "knobs" are available for adjustments, it is unlikely that one can arrive at a stage of refinement where Eqs. 7.2 and 7.3 can emulate continuously the vertical routing process of rain pulses through unsaturated soils according to known scientific theories (section 4.1) in S-H, let alone other complications that are involved.

While only four major issues regarding model differences are raised here, they are far from being comprehensive. If more experiments under different settings are conducted, more "trouble spots" are probably going to emerge in SMA and models of similar structure.

Chapter 8

Summary and Conclusions

"...No one can comprehend what goes on under the sun.
Despite all his efforts to search it out,
man cannot discover its meaning.
Even if a wise man claims he knows,
he cannot really comprehend it."

Ecclesiastes 8:17

8.1 Summary

The primary contribution of this work is an objective evaluation of the performance of a widely used complex conceptual rainfall-runoff model in operational prediction and forecasting responses to extreme rainfall. The model evaluation is unique in that it is based on synthetic streamflow data which for idealized catchments, can be regarded as error free because they are generated by a physically sound, causal model (S-H), developed by Smith and Hebbert (1983).

Since there is hardly any reliable recorded extreme flood data available, synthetic data provide a sound alternative for determining the validity of a conceptual model when used to estimate hydrologic response to extreme rainfall. Moreover, this approach relates the reliability of a conceptual model with respect to clearly defined physical and climatic settings. This is crucial because only then can the model structure and the calibrated parameters be assessed objectively.

After reviewing two major conceptual r-r models, the Stanford Watershed Model and the Sacramento Model (SMA), the latter was selected for this study mainly because of its present wide use within the United States. The original hourly version of SMA was modified to accommodate inputs at minute intervals for use in small catchments. Input data were selected from three locations representing different climatic regions in the USA. Experiments were conducted on small catchments (five hypothetical hillslopes) carefully designed to incorporate geomorphic features pertinent to the mechanics of streamflow generation. A combined manual-automatic procedure was adopted for calibrating SMA. Several automatic algorithms were studied before the pattern search simplex method NMS was selected because of its robust quality.

For a given hypothetical catchment, a set of climatic and streamflow data, SMA was calibrated, validated and tested in prediction and extreme event forecasting modes. The latter tests were based on extremely heavy storms (on the order of probable maximum precipitation) applied at different antecedent moisture conditions (both dry and wet) to evaluate SMA's performance when extrapolated beyond its calibration and verification experience. The eighteen test cases conducted are classified under three categories:

(1) Test I: Elementary basins without channel;
(2) Test II: 2-subbasin catchments with channel networks of magnitude 2;

(3) Test III: Elementary basins subjected to spatially distributed rain data.

The performance of SMA was assessed in terms of visual display of plots including, boxplots, scattergrams, and hydrographs and through comparisons of summary statistics of streamflow including mean, standard deviation, coefficient of efficiency, E_f, and root mean square error, RMSE.

S-H demonstrated the relative sensitivity of the flow mechanisms (Horton overland, saturation overland, and subsurface flows) to changes in hillslope characteristics and climatic data. The SMA has shown some ability to represent fundamental flow dynamics and predict flood events on a continuous and operational basis. It gave better performance under Quillayute, Washington and Tray Mountain, Georgia precipitation data than Niceville, Florida data. Based on the experiments, wetter environments are more favorable than drier environments for conceptual modeling. The SMA creates gross simulation errors especially during droughts and in the dry-wet transition periods for most cases.

Extreme rain tests show that SMA is not reliable in forecasting extreme events for hypothetical small basins. In particular, the outcome of its application is very unpredictable under dry antecedent moisture condition and for catchments that on the average generate flow primarily by saturated groundwater flow (base flow). SMA performed poorly in 11 of the 18 tests conducted under dry conditions. For wet antecedent conditions, the result is much better: 10 out of 18 cases are good; the phenomenon of model "divergence" or gross simulation error is clear in the work reported here.

8.2 Conclusions

(1) The calibrated SMA simulates fundamental flow mechanisms but generally over-simulates low flows during the dry-wet transition period. At times, it predicted peak events in operational mode poorly.

(2) SMA was unreliable in predicting hydrologic response from extreme rainfall. The chances for a successful application under extremes and operational prediction is higher if the calibration experience encompasses a broad spectrum of flow dynamics. For such situations, the calibrated model predicts extreme hydrograph response best for wet antecedent conditions.

(3) SMA's performance in forecasting extreme events is largely dictated by the adequacy of soil moisture conditions represented at that period and by the physical basis of lumped parameters. Extreme rain test results and comparisons of parameter values with catchment properties show that the parameters obtained by calibration generally lack physical meaning. Instead, they are more of a set of "fitted" values, though in some cases they are consistent with soil moisture storage capabilities of hillslope soils.

(4) The lumped parameters appear to be time- and rain- dependent even though they are supposed to be constant since they represent physical properties (moisture storages) of watersheds modeled, such as thresholds of the soil water capacities, infiltration, and percolation rates.

(5) Even for idealized catchments, the lumped parameter concepts of SMA do not agree with known phenomena that are embodied in S-H. Within the scope of the experiments, the results indicate that SMA, represented by a set of lumped parameters, is a poor approximation to hydrologic reality. At its best SMA can still perform creditably (as long as it is not "stretched" beyond its calibration range) when representing the hydrograph of flow from a catchment.

(6) The class of causal models of the form of S-H are computationally intense and appear to be impractical for routine applications, e.g., single hillslope: 2.5 hours Vax 11/780 CPU time/year of simulation; 2-subbasin cases with channel routine: 10 hours/year of simulation.

(7) For single hillslope situations, the calibrated SMA executes 50 to 60 times faster than S-H though S-H is a relatively efficient causal model. Speeding up S-H type models for larger scale tests could be acheived by sacrificing the quality of physical representations.

(8) The experiments reported are confined to small scale, idealized catchments. Future similar research should be directed to catchments with more complex spatial features. The effects of spatial variabilities of rain data, catchment soil, and topographic properties on conceptual modeling needs to be explored.

Chapter 9

Recommendations for Future Work

"For with much wisdom comes much sorrow;
the more knowledge, the more grief."

Ecclesiastes 1:18

The reliability of a conceptual rainfall-runoff model, the Sacramento model SMA, has been investigated in operational and extreme-event forecasting modes. For a wide range of climatic and hillslope conditions, its performance had been evaluated with respect to the flow hydrographs generated by the physically-based S-H model. From the series of tests conducted, one comes to appreciate the combined effects rain patterns and hypothetical catchment characteristics had on the shape, peak and volume of flood hydrographs. In addition, the capability and limitations of SMA are now better known than before. This chapter contains suggestions for future work related to this topic.

9.1 Geomorphic Description of a Catchment

In view of the present capability of S-H and also of its large computational requirements, many simplifications of nature were made in the design of the hypothetical catchments used, but not at the expense of essential elements of causality. The catchments tested were small (areas range from 0.1 to 0.5 km^2), made up of hillslope sections of symmetrical topography, with uniform soil layers of homogeneous and isotropic properties and grass as vegetation cover. The highest order of these catchments was of magnitude 2.

The process of simplification necessitated the omission of some important geomorphic features of natural catchments which have significant influence on the dynamics of flow production. Their importance is apparent from the fact that many researchers have attempted to derive flood frequency distributions on the basis of catchment geomorphology (Eagleson, 1972; Cordova and Rodriquez-Iturbe, 1983; Beven, 1987). Therefore, hypothetical catchments for future work should include more basin hydrology related characteristics suggested by various scientists such as Horton (1932), Langbein (1947) and Strahler (1958).

9.1.1 Scale

The scale of catchments for future study should be extended to medium size (5 to 50 km^2). As the scale of catchments increases, the balance between different hydrological processes operating on different time scales and the effect of channel routing vary, leading to changes in the mechanisms of flow production. The complex rainfall-runoff relationships for a medium-sized catchment can be integrated by linking hillslope elements together with a channel network. The hillslope elements are divided according to soil types and topography, which serve as a means of reflecting the distributed effects of spatial variabilities found in natural catchments. As mentioned in Section 3.2, Beven and Kirkby (1978) applied this broad type of methodology to an 8-km^2 drainage basin in England with a simple, approximate physically-based model and obtained streamflow data that reasonably replicated the observed.

9.1.2 Drainage Pattern

The magnitude U of catchments should be extended from 2 to 5. As U increases, the effects of channel routing on the catchment outflow become more significant. For a given U, the concept of random topology on channel networks, pioneered by Shreve (1966,1967,1969,1974,1975), can be utilized to form many topologically distinct channel networks (TDCN). For example, if U = 5, TDCN = 14. The parameters needed to relate a TDCN to basin hydrologic response are magnitude U (number of first order channels), link length, total path length, and diameter. A topologic path length is the number of links traversed in a path, and a diameter is the largest path length or the main stream length of a basin. Since it is not possible to explore every conceivable channel network, drainage patterns to be adopted in designing multi-basin catchments should be confined to the following characteristics only:

(1) There are more tributaries on the upslope than the downslope of a catchment;

(2) A tributary valley has in general steeper side slopes than its parent channel valley;

(3) Channel slopes are gentler than valley slopes (Strahler, 1964).

9.1.3 Valley-Side Slopes

For simple catchments with fixed channel slopes, valley-side slopes play an important role in determining the shape of storm hydrographs and the magnitude of peak discharge. They depend on the

form and development of hillslopes and are functions of geomorphic variables such as climate, lithology, process and time. Convexo-concave slope profiles are more common in humid regions, and those in semi-arid and arid climates tend to be more angular. Only catchments of straight slope profiles have been investigated in the present work. To achieve a more realistic representation of hillslope geometry, convexo-concave slope profiles are recommended for future work. The Smith-Hebbert model can accommodate such hillslope geometries.

The design valley-slope had been confined only to values between 0.04 and 0.10. While it would be desirable to explore a wider range, limitations of S-H restrict slopes to less than about 15 degrees.

9.1.4 Soil Spatial Variability

This study did not deal with the issue of spatial variability in catchment soils. For simplicity, only a homogeneous, isotropic, two-layer soil mantle of uniform thickness was considered. Since an average hillslope has a soil mantle covering bedrock, water movement within a hillslope is confined within the permeable, heterogeneous, soil mantle of non-uniform thickness.

There have been many research studies on spatial variability of various soil properties and their effects on different hydrologic variables at different scales. Loague (1986) compiled a comprehensive list of spatial variability literature. Some of the studies addressed the effects of soil heterogeneities on flow responses (Luxmoore and Sharma, 1980; Moore and Clarke, 1981; Luxmoore, 1983; Koch, 1985;

Loague, 1986). Many of the studies describe soil variability either by the principles of soil scaling factors or by assuming a soil variable (such as the saturated hydraulic conductivity) as random with a probability density function (such as the lognormal distribution). To introduce soil heterogeneities into the investigation, the present S-H model would need substantial modifications and may prove unsuitable for such situations.

For a small scale catchment, soils usually vary in a way so that permeability increases with distance away from the catchment channel. Such kinds of soil profiles can be handled either by complicated, 3-D finite element hillslope models or possibly by modifying the S-H model. As a first attempt, this type of soil profile can be approximated by a single soil type that has the equivalent hydraulic permeability. Accurate physics based models of the hydrology of such hillsides are needed for more complete future comparison work.

9.1.5 Vegetation Cover

The presence of vegetation cover, depending on the type, affects the proportion of gross rainfall reaching the ground surface. Several components of the hydrologic cycle related to a vegetation cover such as forest are interception loss, throughfall, stemflow, ET, and infiltration. To avoid a complicated hydrologic cycle, vegetation in this research was restricted to uniformly distributed short grasses. For future work on larger scale catchments, forested hillslopes should be considered. The present S-H model uses daily pan evaporation data

and the ET extraction is corrected for moisture shortage by a simple reduction relationship based on the work of Denmead and Shaw (1962). To handle forest instead of grass cover, the ET component of S-H must be upgraded to include processes such as interception loss, throughfall and stemflow. The simple kinematic wave component of S-H may not be suitable to route overland flows on such hillslopes.

9.2 Calibration by Multiple Fluxes

The basis of automatic calibration in the present work depended entirely on minimizing the differences between "observed" and simulated flow sequences. For situations where the total ET exceeds more than about half the annual precipitation, it is insufficient to rely solely on the flow sequence for analysis, irrespective of whether manual or automatic calibration is used. The problem is probably more serious with the latter approach because of its total reliance on one objective function which is usually a simple least squares minimization of flow residuals only.

The relatively poor performance of SMA for cases involving the Florida climatic data may be attributed partly to large ET volumes which accounted for about 60 % of the total fluxes in the calibration and validation stages (Table 7.1). In future work, especially for dry catchments, ET should be a candidate flux, together with streamflow, to be used for the calibration signal.

9.3 Intercomparison of Conceptual Models

In 1975, the World Meteorological Organization (WMO) conducted an evaluation of rainfall-runoff models. Out of ten models tested, five belong to the explicit moisture accounting type and SMA was one of them. On four data sets tested by WMO, the performance of SMA was rated as good on two (humid conditions), and on the other two it was rated as fair (semiarid) and poor (arid). Those findings complement the findings of the present research which highlights some of the probable reasons for the limitations in performance.

In the course of the current work, several model structure problems have been detected in SMA (Section 7.7). Results show that SMA is more reliable for operational prediction than in extreme flood forecasting. Wetter climatic conditions seem to be more favorable for modeling.

Decision making for managing watersheds and resources are often influenced by the selection of a particular r-r model, conceptual or otherwise. According to conclusions arrived at in the study conducted by WMO, for wet climates simple models are just as good as more complicated models. In arid climates, practically all hydrologic models tested had difficulties modeling the basins. Further research directed to assess the performance of r-r models for a wide range of catchment scales and climatic settings is needed. More definite criteria need to be established to guide users in selecting a particular model in terms of the required application.

9.4 Rainfall Spatial Variability

The effect of spatial variability in rainfall patterns was addressed by applying a different rainfall data set to the subbasins of a catchment (maximum of two subbasins per catchment). For further exploration of the role that the spatial character of rainfall plays on catchment runoff, a more rigorous approach is necessary.

If the point rainfall approach is applied, where uniform rain is assumed throughout the basin area, only the storm exterior properties such as total rainfall depth, duration of storm, and interarrival time are required to characterize storms. Such information can either be supplied by records from a rain station or by a rainfall exterior model. However, to incorporate spatial variability, the interior properties of storms at selected points of interest must be included. A nonstationary rainfall model developed by Bras and Rodriguez-Iturbe (1976) is a model that can simulate storm interior properties. Within each storm event, the rainfall interior model generates the time distribution of the total depth at each point. Each point effectively represents a rain gage in the catchment.

The importance and effects of the spatial characteristics of rainfall on catchment hydrologic response have been addressed by authors including Wilson et. al (1979) and Beven and Hornberger (1982). It would be of great interest to see the impact such effects have on conceptual models. The question regarding the number of rain depth measurements required in a catchment can also be addressed rigorously.

While the computational burden of an approach similar to that undertaken for the present work when extended to scales needed to explore spatial variability adequately is prohibitive in the immediate future, it should not be considered impossible.

REFERENCES

Abrahams, A. D. 1984. Channel networks: A geomorphological perspective, Water Resour. Res., 20(2), 161-188.

Armstrong, B. L. 1978. Derivation of Initial Soil Moisture Accounting Parameters from Soil Properties for the National Weather Service River Forecast System, NOAA Technical Memorandum, NWS, HYDRO 37.

Beard, L. R. 1981. Toward scientific hydrology, in Fluid Mechanics Research in Water Res. Engr., edited by R. E. A. Arndt and M. H. Marsh, St. Anthony Falls Hydr. Lab., U. of Minnesota, Minneapolis, 63 - 70.

Betson, R. P. 1964. What is watershed runoff ?, J. Geophys. Res., 69, 1541-1551.

Betson, R. P. 1979. A geomorphic model for use in streamflow routing, Water Resour. Res., 15(1), 95-101.

Betson, R. P. , and C. V. Ardis. 1978. Implications for modeling surface-water hydrology, in Hillslope Hydrology, edited by M. J. Kirkby, Wiley-Interscience ,New York, 295-323.

Beven, K. 1977. Hillslope hydrographs by the finite element method, Earth Surface Processes, 2, 13-28.

Beven, K. 1982. On subsurface stormflow: Predictions with simple kinematic theory for saturated and unsaturated flows, Water Resour. Res., 18(6), 1627-1633.

Beven, K. 1983. Surface water hydrology-runoff generation and basin structure, Reviews of Geophysics and Space Physics, 21(3), 721-730.

Beven, K. 1987. Towards the use of catchment geomorphology in flood frequency predictions, Earth Surface Processes and Landforms, 12, 69-82.

Beven, K. J., and G. M. Hornberger. 1982. Assessing the effects of spatial pattern of precipitation in modeling streamflow hydrographs, Water Resour. Bull., 18(5), 823-829.

Beven, K., and M. J. Kirkby. 1979. A physically-based variable-contributing-area model of basin hydrology, Hydrol. Sci. Bull. 24, 27-53.

Bohm, D. 1957. Causality and Chance in Modern Physics, Routledge and Kegan Paul, London.

Box, M. J. 1966. A comparison of several current optimization methods, and the use of transformations in constrained problems, The Computer Journal, 9, 67-77.

Box, M. J., D. Davies, and W. H. Swann. 1969. Non-Linear Optimization Techniques, I.C.I. Monograph No. 5, Edinburgh.

Brazil, L. E., G. F. Smith, and J. W. LaBadie, 1986. A multi-level calibration strategy for National Weather Service hydrologic simulation models, Abstract in EOS Trans. AGU, 67(44), 930.

Bras, R. L., and I. Rodriguez-Iturbe. 1976. Rainfall generation: A nonstationary time-varying multidimensional model, Water Resour. Res., 12(3), 450-456.

Brooks, R. H., and A. T. Corey. 1964. Hydraulic properties of parous media, Hydrol. Paper 3, Colo. State University, Fort Colins, Colorado.

Bureau of Reclamation, 1977. Design of Small Dams, 2nd ed., rev. reprint, U. S. Government Printing Office, Washington, D.C., 816pp.

Burges, S. J. 1985. Rainfall-runoff model validation: The need for unambiguous tests, in Proceedings of 9th World Congress of the International Federation of Automatic Control, Budapest, Hungary, Elsevier.

Burnash, R. J. C., R. L. Ferral, and R. A. Mcguire. 1973. A generalized streamflow simulation system, Conceptual Modeling for Digital Computers, U. S. National Weather Service, Sacramento, CA.

Carson, M. A., and M. Kirkby. 1972. Hillslope Form and Process., Cambridge Univ. Press., London.

Chorley, R. J. 1962. Geomorphology and the general systems theory, U. S. Geol. Survey Prof. Paper 500-B.

Chow, V. T. 1959. Open-Channel Hydraulics, McGraw-Hill, New York.

Claborn, B. J. , and W. Moore, 1970. Numerical Simulation in Watershed Hydrology, Hydraulic Engineering Laboratory, Univ. of Texas, Rept. No. HYD 14-7001.

Clarke, R. T. 1973. A review of some mathematical models used in hydrology, with observations on their calibration and use, J. Hydrology, 19, 1-20.

Cleveland W. S., and R. McGill. 1985. Graphical Perception and Graphical Methods for Analyzing Scientific Data, Science, 229, 828-833.

Cordova, J. R. and I. Rodriguez-Iturbe. 1983. Geomorphoclimatic estimation of extreme flow probabilities, J. Hydrology, 65, 159-173.

Crawford, N. H., and R. K. Linsley. 1962. The Synthesis of Continuous Streamflow Hydrographs on a Digital Computer, Tech. Rept. No. 12, Dept. of Civil Engr., Stanford Univ., Stanford, CA.

Crawford, N. H., and R. K. Linsley. 1966. Digital Simulation in Hydrology: Stanford Watershed Model IV, Tech. Report No. 39, Dept. of Civil Engr., Stanford Univ., Stanford, CA.

Cundy, T. W. 1982. An analysis of the effects of spatial variability of point infiltration rates on the comparison of small and large plot rainfall-runoff, Ph.D. dissertation, Utah State Univ., Logan, Utah.

Curtis, D. C., and D. E. Colton. 1986. Recent experiences with real-time flood forecasting, Abstract in EOS Trans. AGU, 67(44), 934.

Day, G. N. 1985. Extended streamflow forecasting using NWSRFS, J. of Water Resour. Planning and Management, Am. Soc. Civil Engr. Tr., 111(2), 157-170.

De Meis, M. R. M. and J. R. D. S. De Moura. 1984. Upper Quaternary sedimentation and hillslope evolution: South-eastern Brazilian Plateau, American J. Sci., 284, 241-254.

Denmead, O. T., and R. H. Shaw. 1962. Availability of soil water to plants as affected by soil moisture content and meteorological conditions, Agron. J., 54, 385-389.

Dietrich, W.E., and T. Dunne 1978. Sediment budget for a small catchment in mountainous terrain, in Z. Gemorphol. Suppl. Bd., 29, 191-206.

Dunne, T. 1978. Field studies of hillslope flow processes, in Hillslope Hydrology, edited by M. J. Kirkby, Wiley-Interscience, New York, 227-293.

Dunne, T. 1980. Formation and controls of channel networks, Progess in Physical Geography, 2, 211-239.

Dunne, T. 1982. Models of runoff processes and their significance, Scientific Basis of Water-Resource Management, Nat. Academy Press, Washington, D.C., 17-30.

Dunne, T. 1983. Relation of field studies and modeling in the prediction of storm runoff, J. Hydrology, 65, 25-48.

Dunne, T., and R. D. Black. 1970. An experimental investigation of runoff production in permeable soils, Water Resour. Res., 6(2), 478-490.

Dunne, T., and W. E. Dietrich. 1980. Experimental study of Horton overland flow on tropical hillslopes 2. Hydraulic Characteristics and Hillslope Hydrographs, Z. geomorph. N. F., Berlin, Stuttgart.

Dunne, T., and L. B. Leopold. 1978. Water in Environmental Planning, W. H. Freeman and Company, San Francisco.

Eagleson, P. S. 1972. Dynamics of flood frequency, Water Resour. Res., 8(4), 878-898.

Eagleson, P. S. 1978. Climate, soil, and vegetation 2. The distribution of annual precipitation derived from observed storm sequences, Water Resour. Res., 14(5), 713-721.

Engman, E. T., and A. S. Rogowski. 1974. A partial area model for storm flow synthesis, Water Resour. Res., 10(3), 464-472.

Fiering, M. B., and G. Kuczera. 1982. Robust estimators in hydrology, Scientific Basis of Water Resource Management, Nat. Academy Press, Washington, D.C., 85-94.

Freeze, R. A. 1972a. Role of subsurface flow in generating surface runoff 1: Base flow contributions to channel flow, Water Resour. Res., 8(3), 609-623.

Freeze, R. A. 1972b. Role of subsurface flow in generating surface runoff 2: Upstream source areas, Water Resour. Res., 8(5), 1272-1283.

Freeze, R. A. 1974. Streamflow generation, Reviews of Geophysics and Space Physics, 12(4), 627-647.

Freeze, R. A. 1980. A stochastic-conceptual analysis of rainfall-runoff processes on a hillslope, Water Resour. Res., 16(2), 391-408.

Freeze, R. A. 1982. Hydrogeological concepts in stochastic and deterministic rainfall-runoff predictions, Geol. Soc. Am. Special Paper 189, in Recent Trends in Hydrogeology, edited by R. N. Narasimhan, 63-79.

Gardner, W. R., and C. F. Ehlig. 1963. The influence of soil water on transpiration by plants, J. Geophys. Res., 68(20), 5719-5724.

Gerald, C. F. 1980. Applied Numerical Analysis, Addison-Wesley publishing company, Reading, Massachusetts, 474-488.

Green I. R. A., and D. Stephenson. 1986. Criteria for comparison of single event models, Hydrolo. Sc. Jour., 31(3).

Gregory, K. J., and D. E. Walling. 1973. Drainage Basin Form and Processes, John Wiley and Sons, New York.

Gupta, V. K., and E. G. Waymire. 1983. On the formulation of an analytical approach to hydrologic response and similarity at the basin scale, J. Hydrology, 65, 95-123.

Gupta, V. K., and S. Sorooshian. 1985. The automatic calibration of conceptual catchment models using derivative-based optimization algorithms, Water Resour. Res., 21(4), 473-485.

Hawks, R. J., and G. L. Ashcroft. 1980. Applied Soil Physics, Advanced Series in Agricultural Sciences 8, Springer-Verlag, Berlon, Heidelberg.

Hendrickson, J., S. Sorooshian, and L. Brazil. 1986. Calibration of the Sacramento soil moisture accounting model using a gradient-type algorithm, Abstract in EOS Trans. AGU, 67(44), 930.

Hewlett, J. D., and A. R. Hibbert. 1967. Factors affecting the response of small watersheds to precipitation in humid areas, in Forest Hydrology, edited by W. E. Sopper and H. W. Lull, 275-290.

Holmes, R. M., and G. W. Roberton. 1959. A modulated soil moisture budget, Monthly Weather Review, 87, 101-105.

Holmes, R. M. 1961. Estimation of soil moisture content using evaporation data, Canadian Nat. Res. Council, Proc. Hydro. Symp., 184-196.

Hornbeck R. W. 1975. Numerical Methods, Prentice-Hall, New Jersey, 47-50.

Horton, R. E. 1932. Drainage basin characteristics, Am. Geophys. Union. Tr., 350-361.

Horton, R. E. 1945. Erosional development of streams and their drainage basins: Hydrophysical approach to quantitative morphology. Geol. Soc. Am. Bull., 56, 275-370.

Huang, S. L., and J. D. Keenan. 1987. Hydrologic simulation of the Brandywine Basin, Water Resour. Bull., 23(3), 403-421.

James , L. D., and S. J. Burges. 1982. Selection, calibration, and testing of hydrologic models, in Hydrologic Modeling of Small Watersheds, edited by C. T. Haan, H. P. Johnson, and D. L. Brakensieck, Am. Soc. Ag. Eng., St-Joseph, Mich. 437-472

Kibler, D. F., and D. A. Woolhiser. 1970. The Kinematic Cascade as a Hydrologic Model, Hydrol. Pap. 39, Colo. State Univ., Fort Collins, 27pp.

Klemes, V. 1978. Physically based stochastic hydrologic analysis, Advances in Hydroscience, 11, Academic Press, 285-356.

Klemes, V. 1982. Empirical and causal models in hydrology, Scientific Basis of Water-Resource Management, Nat. Academy Press, Washington, D.C., 95-104.

Kock, R. W., 1985. A stochastic streamflow model based on physical principles, Water Resour. Res., 21(4), 545-553.

Kowalik, J., and M. R. Osborne. 1968. Methods for Unconstrained Optimization Problems, American Elsevier, New York.

Krumbein, W. C., and R. L. Shreve. 1970. Some Statistical Properties of Dendritic Channel Networks, Tech. Rept. 13, ONR Task No. 389-150., Dept. Geog. Sci., Northwestern U., Evanston, Illinois, Spec. Proj. Rep. NSF Grant 6A-1137. Dept. Geog., UCLA, Los Angeles, CA.

Langbein, W. B. 1947. Topographic characteristics of drainage basins, U. S. Geol. Survey Water-Supply Paper 968-C.

Langbein, W. B. 1964. Geometry of river channels, J. of the Hydraulics Div., Am. Soc. Civil Engr., 90(HY2), 301-312.

Larcher, W. 1975. Physiological Plant Ecology, Springer-Verlag, New York.

Leopold, L. B. 1982. Field data: The interface between hydrology and geomorphology, Scientific Basis of Water-Resource Management, Nat. Academy Press, Washington, .D.C., 105-108.

Leopold, L. B., and W. B. Langbein. 1962. The concept of entropy in landscape evolution, U. S. Geol. Survey Prof. Paper 500-A.

Leopold, L. B., and T. Maddock. 1953. The hydraulic geometry of stream channels and some physiographic implications, U. S. Geol. Survey Prof. Paper 252.

Leopold, L. B., and M. G. Wolman. 1957. River channel patterns; braided, meandering and straight, U. S. Geol. Survey Prof. Paper 282-B.

Leopold, L. B., M. G. Wolman, and J. P. Miller. 1964. Fluvial Processes in Geomorphology, W. H. Freeman, San Francisco.

Lettenmaier, D. P. 1984. Synthetic streamflow forecast generation, J. Hydraul. Eng., Am. Soc. Civil Eng., 110(3), 277-289.

Linsley, R. K., and N. H. Crawford. 1960. Computation of a Synthetic Streamflow Record on a Digital Computer, Publ. No. 51, International Assoc. of Scientific Hydrology, 526-538.

Linsley, R. K., M. A. Kohler, and J. L. H. Paulhus. 1982. Hydrology for Engineers, Third Edition, McGraw-Hill, New York.

Liou, E. Y. 1970. OPSET: Program for Computerized Selection of Watershed Parameter Values for the Stanford Watershed Model, Research Rept. No. 34, Water Resource Institute, U. of Kentucky, Lexington.

Loague, K. M. 1986. An Assessment of Rainfall-Runoff Modeling Methodology, Doctoral dissertation, Univ. of British Comlumbia, Vancouver, Canada.

Loague, K. M., and R. A. Freeze. 1985. A comparison of rainfall-runoff modeling techniques on small upland catchments, Water Resour. Res., 21(2), 229-248.

Luxmoore, R. J. 1983. Infiltration and runoff predictions for a grassland watershed, J. Hydrology, 65, 271-278.

Luxmoore, R. J., and M. L. Sharma. 1980. Runoff responses to soil heterogeneity: Experimental and simulation comparisons for two contrasting watersheds, Water Resour. Res., 16(4), 675-684.

Madej, M. A. 1982. Sediment Transport and Channel Changes in an Aggrading Stream in the Puget Lowland, Washington, in Sediment Budgets and Routing in Forested Drainage Basins, USDA, General Tech. Rept. PN W-141, Pacific Northwest.

Miller, J. P. 1958. High mountain streams: Effects of geology on channel characteristics and bed material, State Bureau of Mines and Mineral Resources, New Mexico.

Miller W. A., and J. A. Cunge. 1975. Simplified equations of unsteady flow, Unsteady Flow in Open Channels, I, edited by K. Mahmood and V. Yevjevich, WRP, Fort Collins, Colorado.

McNaughton, K. G., and P. G. Jarvis. 1983. Predicting effects of vegetation changes on transpiration and evaporation, Water Deficits and Plant Growth, 7, Academic Press, 1-47.

Melton, M. A. 1958. Geometric properties of mature drainage systems and their representation in an E4 phase space, J. Geol., 66, 35-56.

Mock, S. J. 1971. A classification of channel links in stream networks, Water Resour. Res., 7(6), 1558-1566.

Molz, F. J., and I. Remson. 1970. Extraction term models of soil moisture use by transpiring plants, Water Resour. Res., 6(5), 1346-1356.

Moore, R. J., and R. J. Clarke. 1982. A distribution function approach to rainfall-runoff modeling, Water Resour. Res., 17(5), 1367-1382.

Myers, V. A. 1967. Meteorological estimation of extreme precipitation for spillway design floods, Weather Bureau Technical Memorandum, WBTM HYDRO-5, Washington, D.C.

Nelder, J. A., and R. Mead. 1965. A simplex method for functional minimization. The Computer Journal, 9, 308-313.

NWS. 1982. Mean Monthly, Seasonal, and Annual Pan Evaporation for the United States, NOAA Technical Rept., NWS 34.

Onstad, C. A., and D. G. Jamieson. 1970. Modeling the effect of land-use modifications on runoff, Water Resour. Res., 6(5), 1287-1295.

Parkinson, J.M. and D. Hutchinson. 1972. An investigation into the efficiency of variants on the Simplex Method, in Numerical Methods for Non-Linear Optimization, edited by F.A. Lootsma, Conference sponsored by the Science Research Council, University of Dundee, Scotland, 115-135.

Parlange, J. Y. 1972. Analytical theory of water movement in soils, in Joint Symposium on Fundamentals of Transport Phenomena in Porous Media, Univ. Guelph, Guelpa, Ontario, Canada.

Peck, E. L. 1976. Catchment modeling and initial parameter estimation for the national weather service river forecast system, NOAA, Tech. Memo., NWS HYDRO-31.

Penman, H. L. 1948. Natural evaporation from open water, bare soil and grass, Proc. Roy. Soc., Ser. A, 193, 120-145.

Philip, J. R. 1957a. The theory of infiltration: 1. The infiltration equation and its solution, Soil Sci., 83, 345-357.

Philip, J. R. 1957b. The theory of infiltration: 4. Sorptivity and algebraic infiltration equations, Soil Sci., 84, 257-264.

Philip, J. R. 1969. Theory of infiltration, Advances in Hydroscience, 5, 215-305, Academic Press.

Pilgrim, D. H. 1983. Some problems in transferring hydrological relationships between small and large drainage basins and between regions, J. Hydrology, 65, 49-72.

Rahn, P. H. 1975. Lessons learned from the June 9, 1972, flood in Rapid City, South Dakota, Bull. of the Assoc. of Eng. Geologists, 12, 83-97.

Rawls, W. J., D. L. Brakensiek, and K. E. Saxton. 1981. Soil water characteristics, Am. Soc. Ag. Eng., paper no. 81-2510.

Reeves, M., and J. O. Duguid. 1975. Water Movement Through Saturated Unsaturated Porous Media: A Finite-Element Galerkin Model, Oak Ridge National Lab. ORNL-4927, Oak Ridge, Tennessee, 236pp.

Ricca, V. T. 1972. The Ohio State University Version of the Stanford Streamflow Simulation Model, Part I - Technical aspects, Ohio State Univ., Columbus.

Richards, L. A. 1931. Capillary conduction of liquids through porous mediums, Physics, 1, 318-333.

Ritter, D. F. 1984. Process Geomorphology, Wm. C. Brown Company, Iowa.

Rubey, W. W. 1952. Geology and mineral resources of the Hardin and Brussels quadrangles (in Illinois), U. S. Geol. Survey Prof. Paper 218.

Schnabel, B. K. 1966. An Investigation into the Effects of Random Error on a Selection of Current Minimization Methods, M. Sc. thesis, University of Leeds.

Schumm, S. A. 1956. Evolution of drainage systems and slopes in Badlands at Perth Amboy, New Jersey, Geol. Soc. Am. Bull., 67, 587-646.

Sherman, L. K. 1932. The relation of hydrographs of runoff to size and character of drainage basins, Am. Geophys. Union Tr., 13, 332-339.

Shreve, R. L. 1966. Statistical law of stream numbers, J. Geol., 74, 17-37.

Shreve, R. L. 1967. Infinite topologically random channel networks, J. Geol., 75, 179-186.

Shreve, R. L. 1969. Stream lengths and basin areas in topologically random channel networks, J. Geol., 77, 397-414.

Shreve, R. L. 1974. Variation of mainstream length with basin area in river networks, Water Resour. Res., 10(6), 1167-1177.

Shreve, R. L. 1975. The probabilistic-topologic approach to drainage-basin geomorphology, Geol., 3, 527-529.

Smart, J. S. 1972. Channel networks, Advances in Hydroscience, 8, 305-346.

Smart, J. S., and J. R. Wallis. 1971. Cis and Trans Links in natural channel networks, Water Resour. Res., 7(5), 1346-1348.

Smith, R. E. 1983. Approximate soil water movement by kinematic characteristics, Soil Sci. Soc. Am. Proc., 47, 3-8.

Smith, R. E., and R. H. B. Hebbert. 1979. A Monte Carlo analysis of the hydrologic effects of spatial variability of infiltration, Water Resour. Res., 15(2), 419-429.

Smith, R. E., and R. H. B. Hebbert. 1983. Mathematical simulation of interdependent surface and subsurface hydrologic processes, Water Resour. Res., 19(4), 987-1001.

Smith, R. E., and R. H. B. Hebbert. 1984. Hillslope Model Users Manual, Fort Collins, Colorado (unpublished manuscript).

Smith, R. E., and J. R. Williams. 1980. Simulation of the Surface Water Hydrology, Creams, Conser. Res. Rept. no. 26, USDA.

Sorooshian, S. 1983. Surface water hydrology: On-line estimation, Reviews of Geophysics and Space Physics, 21(3), 706-721.

Sorooshian, S., and F. Arfi. 1982. Response surface parameter sensitivity analysis methods for postcalibration studies, Water Resour. Res., 18(5), 1531-1538.

Sorooshian, S., and V. K. Gupta. 1983. Automatic calibration of conceptual rainfall runoff models: The question of parameter observability and uniqueness, Water Resour. Res., 19(1), 260-268.

Sorooshian, S., V. K. Gupta, and J. L. Fulton. 1983. Evaluation of maximum likelihood estimation techniques for conceptual rainfall-runoff models: Influence of calibration data variability and length on model credibility, Water Resour. Res., 19(1), 251-259.

Strahler, A. N. 1952. Hypsometric (area-altitude) analysis of erosional topograpghy, Geol Soc. Am. Bull., 63, 1117-1142.

Strahler, A. N. 1964. Quantitative geomorphology of drainage basins and channel networks, in Handbook of Applied Hydrology, edited by. V. T. Chow, McGraw-Hill, New York. 4.39-4.76.

Thomas, H. A. Jr., and M. B. Fiering. 1963. The nature of the storage yield function, in Operations Research in Water Quality Management, Chp. 2, Harvard Univ. Water Program, Cambridge, Massachusetts.

Troutman, B. M. 1983. Runoff prediction errors and bias in parameter estimation induced by spatial variability of precipitation, Water Resour. Res., 19(3), 791-810.

Viessman, W. Jr., J. W. Knapp, G. L. Lewis, and T. E. Harbangh. 1977. Introduction to Hydrology, Harper and Row, New York, 584-588.

Vigier, J. P. 1957. Discussion of a paper by J. P. Vigier. The concept of probability in the frame of the probabilistic and the causal interpretation of quantum mechanics, Observation and Interpretation, edited by S. Korner, Butterworth, London.

Werner, C., and J. S. Smart. 1973. Some new methods of topologic classification of channel networks, Geogr. Analysis, 5, 271-295.

Whipkey, R. Z. 1966. Subsurface stormflow from forested slopes, Bull. Internat. Assoc. Sci. Hydrology, 10(2), 74-85.

Whipkey, R. Z. 1969. Storm runoff from forested catchments by subsurface routes, Internat. Assoc. Sci. Hydrology, Symposium of Leningrad, Publication 85, 773-779.

Whipkey, R. Z., and M. J. Kirkby. 1978. Flow within the soil, in Hillslope Hydrology, edited by M. J. Kirkby, Wiley-Interscience, New York, 121-144.

Willmott, C. J. 1981. On the validation of models, Physical Geography, 2(2), 184-194.

Willmott, C. J. 1982. Some comments on the evaluation of model performance, American Meteoro. Soc., 63(11), 1309-1313.

Wilson, C. B., J. B. Valdes, and I. Rodriguez-Iturbe. 1979. On the influence of the spatial distribution of rainfall on storm runoff, Water Resour. Res., 15(2), 321-328

Woolhiser, D. A., and J. A. Liggett. 1967. Unsteady one-dimensional flow over a plane- the rising hydrograph, Water Resour. Res., 3(3), 753-771.

World Meteorological Organization. 1975. Inter-comparison of conceptual models used in operational hydrology forecasting, Operational hydrology, Rept. 7, Geneva, Switzerland, 172pp.

Yates, S. R., A. W. Warrick, and D. O. Lomen. 1985. Hillside seepage: An analytical solution to a nonlinear Dupuit - Forchheimer problem, Water Resour. Res., 21(3), 331-336.

Appendix A

Selected hydrographs for Wet and Dry Months

Figures A.1 to A.23 show hydrographs for selected wet and dry months. For wet months, each figure contains nine graphs. Sufficient detail is given in the figures to show differences between SMA generated hydrographs and the corresponding "error-free" hydrographs from S-H. Examples are given from calibration, validation and prediction portions of the climatic record. Row A shows the mean daily hydrographs (cubic meters per second-day, CMSD) while Row B shows the same hydrograph plotted at 6-minute increments (cubic meters per second, CMS). In Row B, the S-H hydrograph is plotted with (SMA-SH) plotted below it, except for figures A.7 and A.11 where both SMA and S-H hydrographs are shown. Other than a few exceptions, row C of each figure shows S-H and SMA hydrographs together for a 48-hour period. The individual graphs within a given figure have different vertical scales.

Figures that show differences between SMA and S-H hydrographs for dry periods (Figs. A.19 to A.23) are all drawn for one month periods. Figures A.19 - A.23 are included to show differences between catchment and climate characteristics during dry conditions. The vertical scales of graphs within each figure differ. A description of the catchment features for each case is given in Table 5.4.

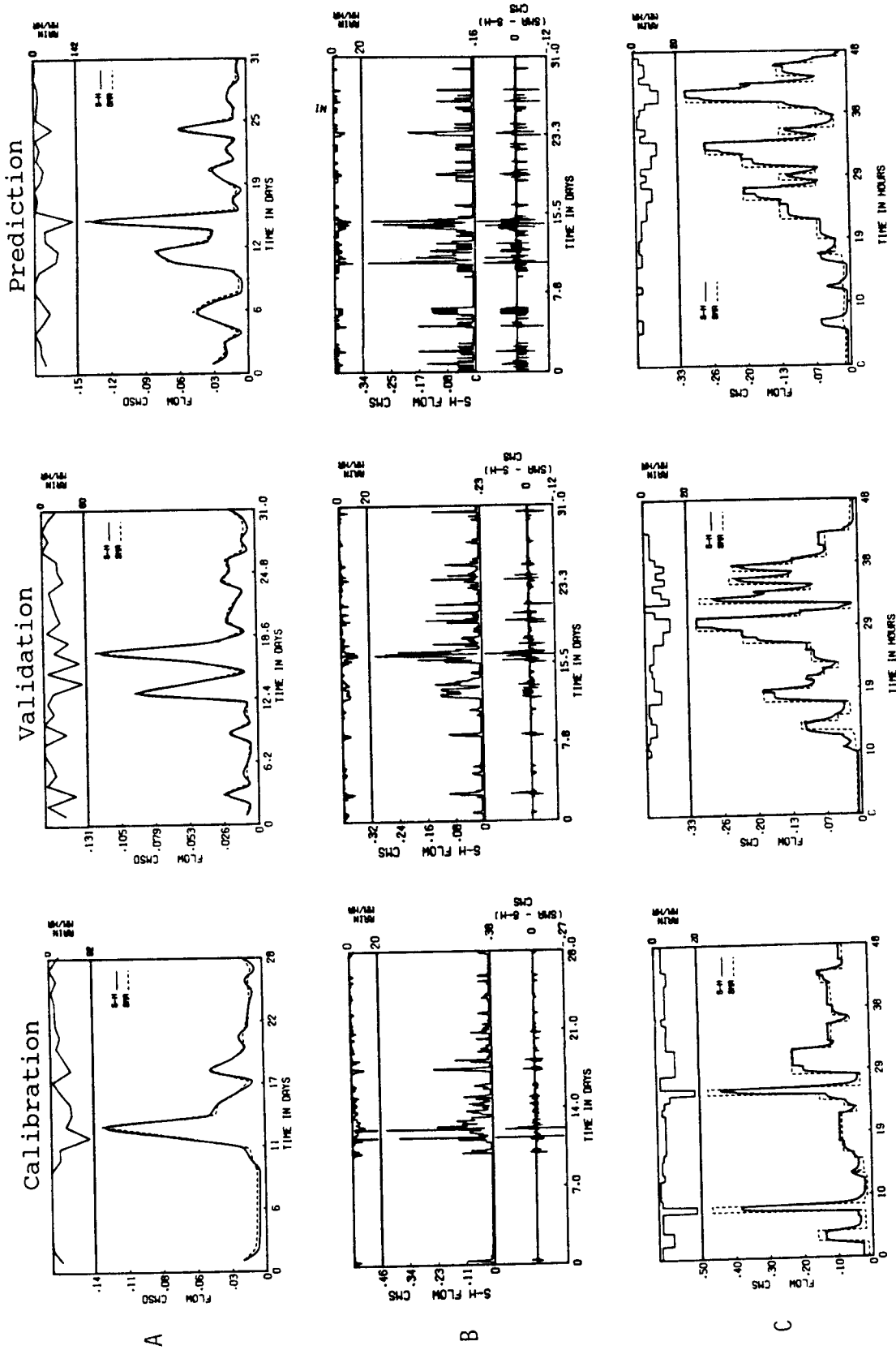

Figure A.1 Mean daily (A), 6-minute (B) and selected event (C) hydrographs for wet months for HIL101

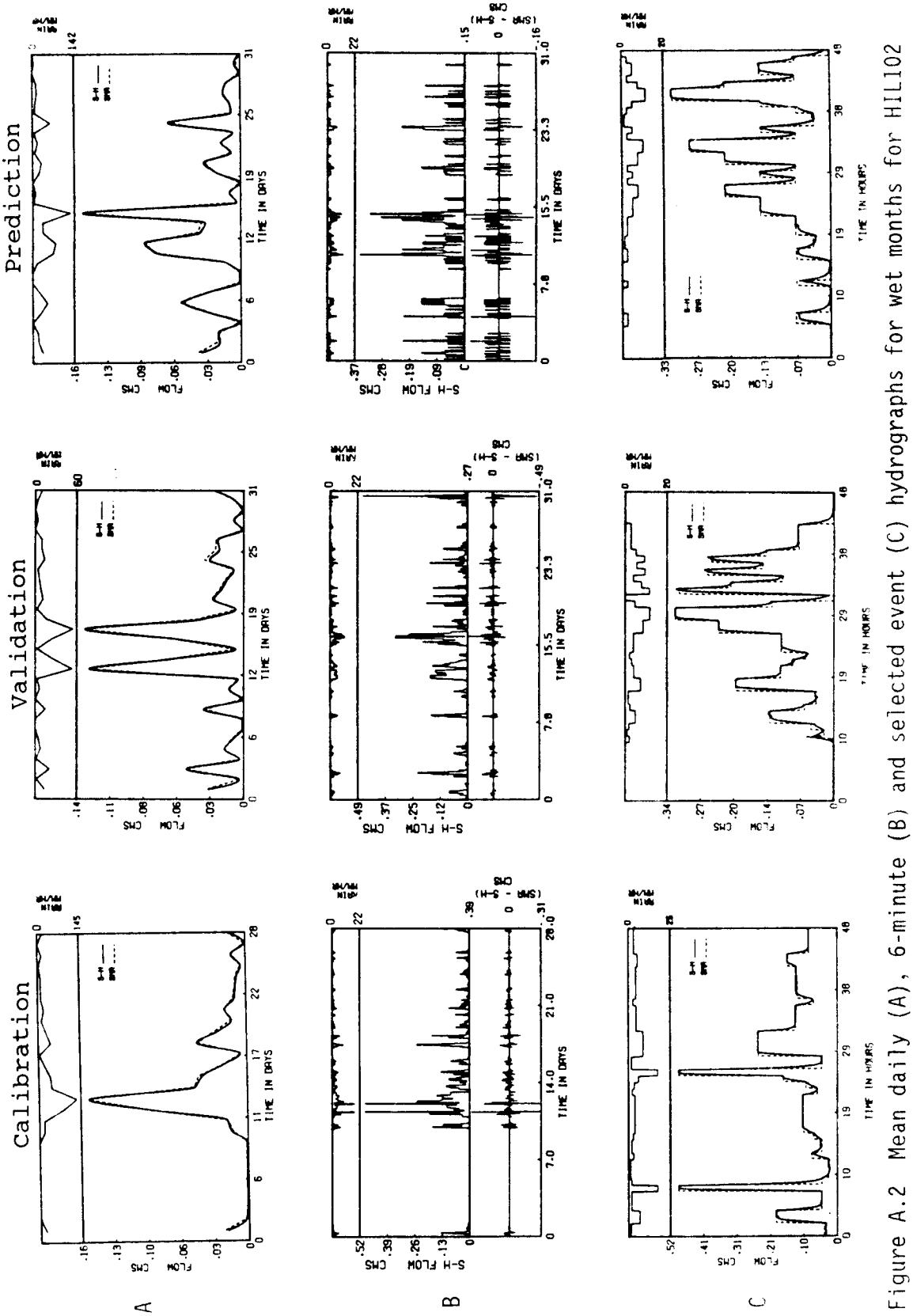

Figure A.2 Mean daily (A), 6-minute (B) and selected event (C) hydrographs for wet months for HIL102

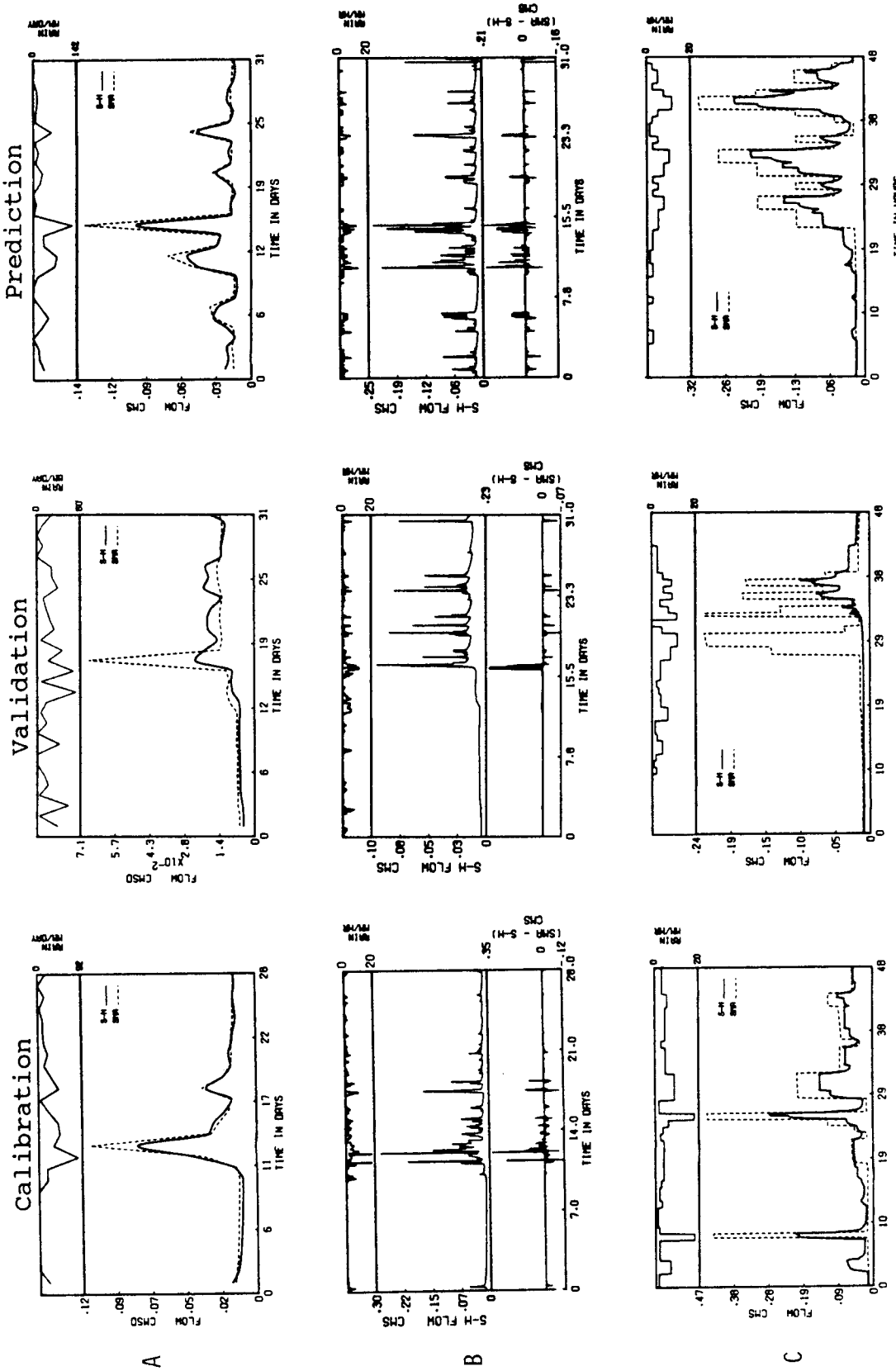

Figure A.3 Mean daily (A), 6-minute (B) and selected event (C) hydrographs for wet months for HIL103

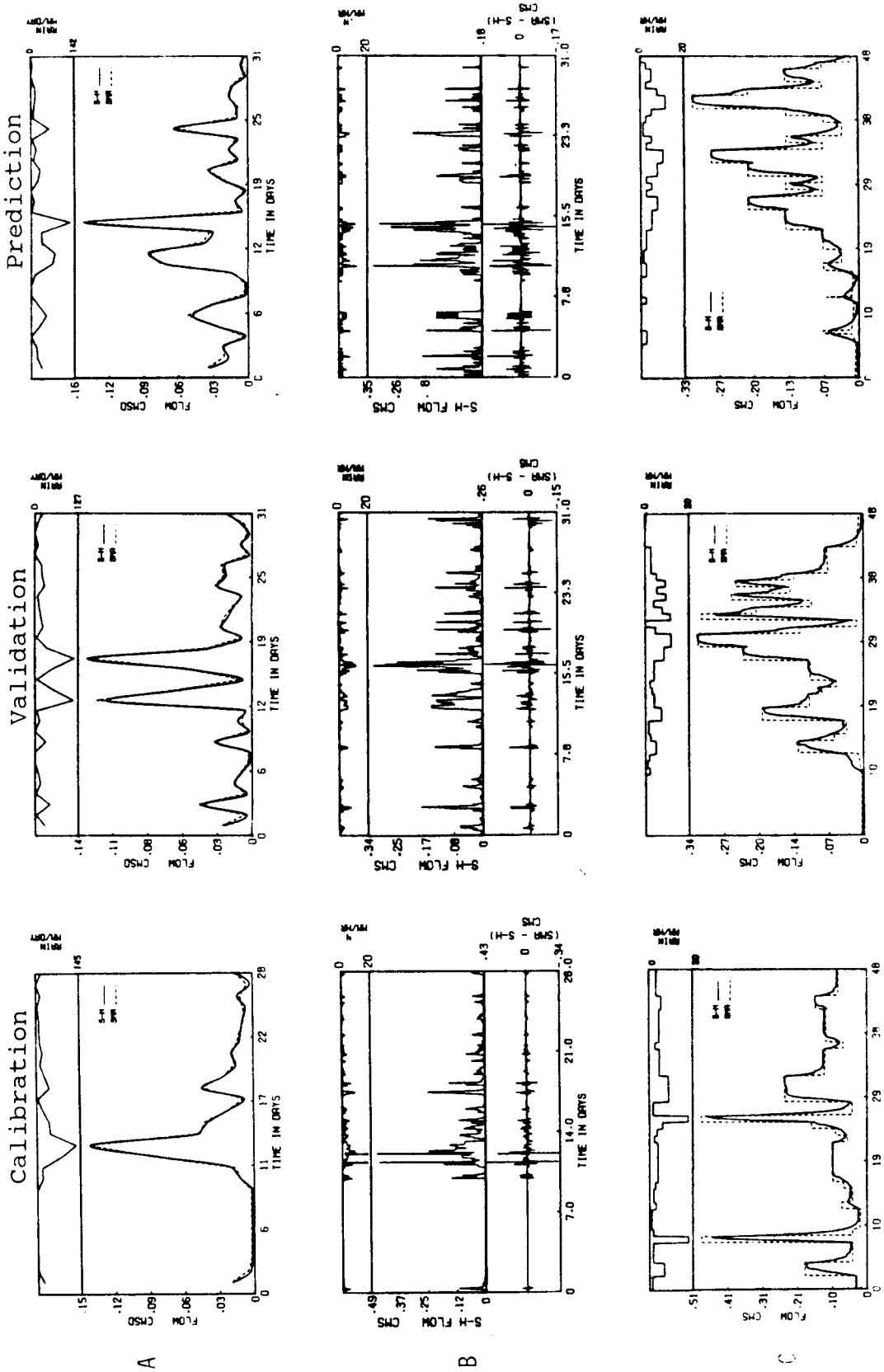

Figure A.4 Mean daily (A), 6-minute (B) and selected event (C) hydrographs for wet months for HIL104

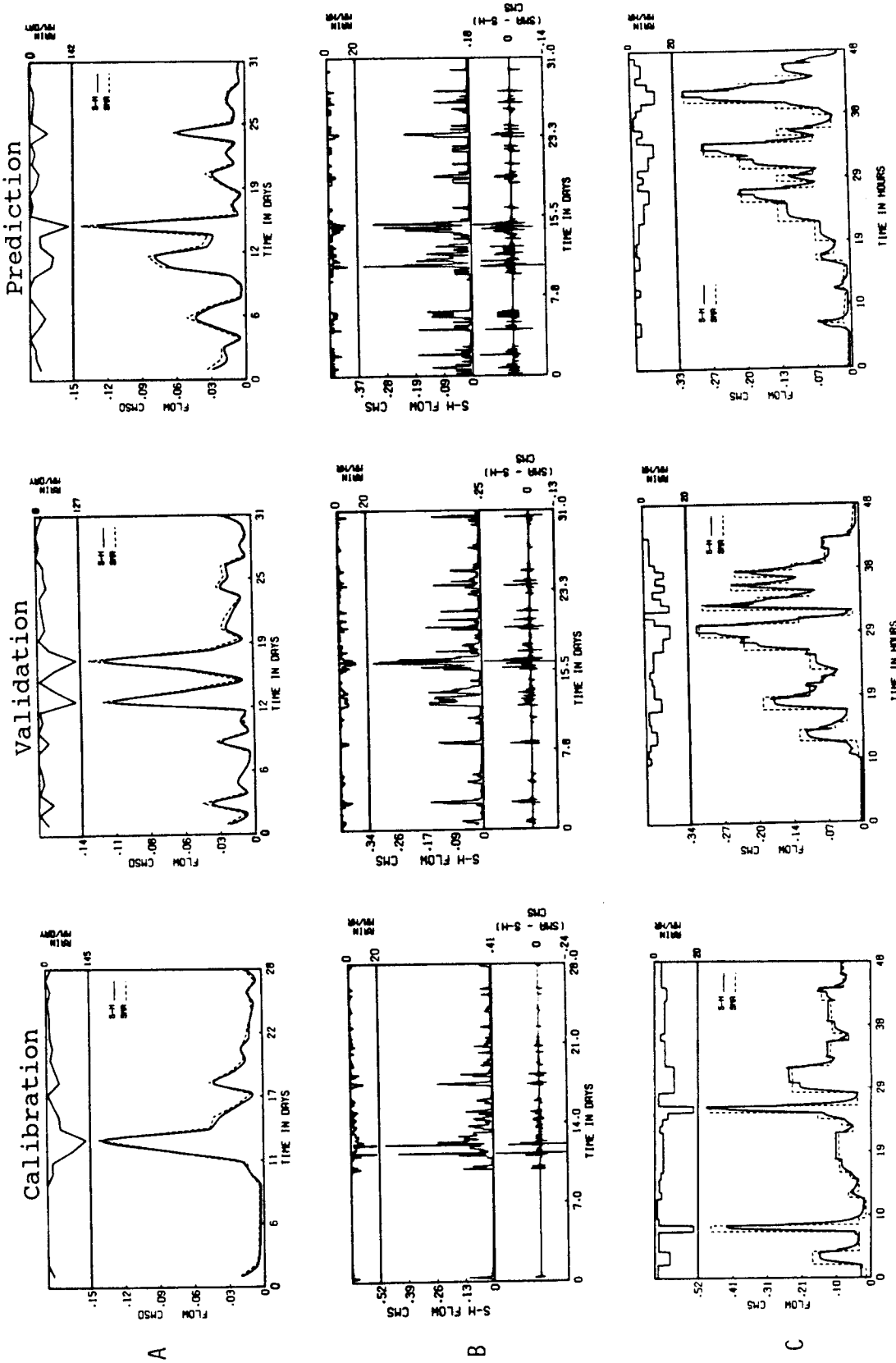

Figure A.5 Mean daily (A), 6-minute (B) and selected event (C) hydrographs for wet months for HIL105

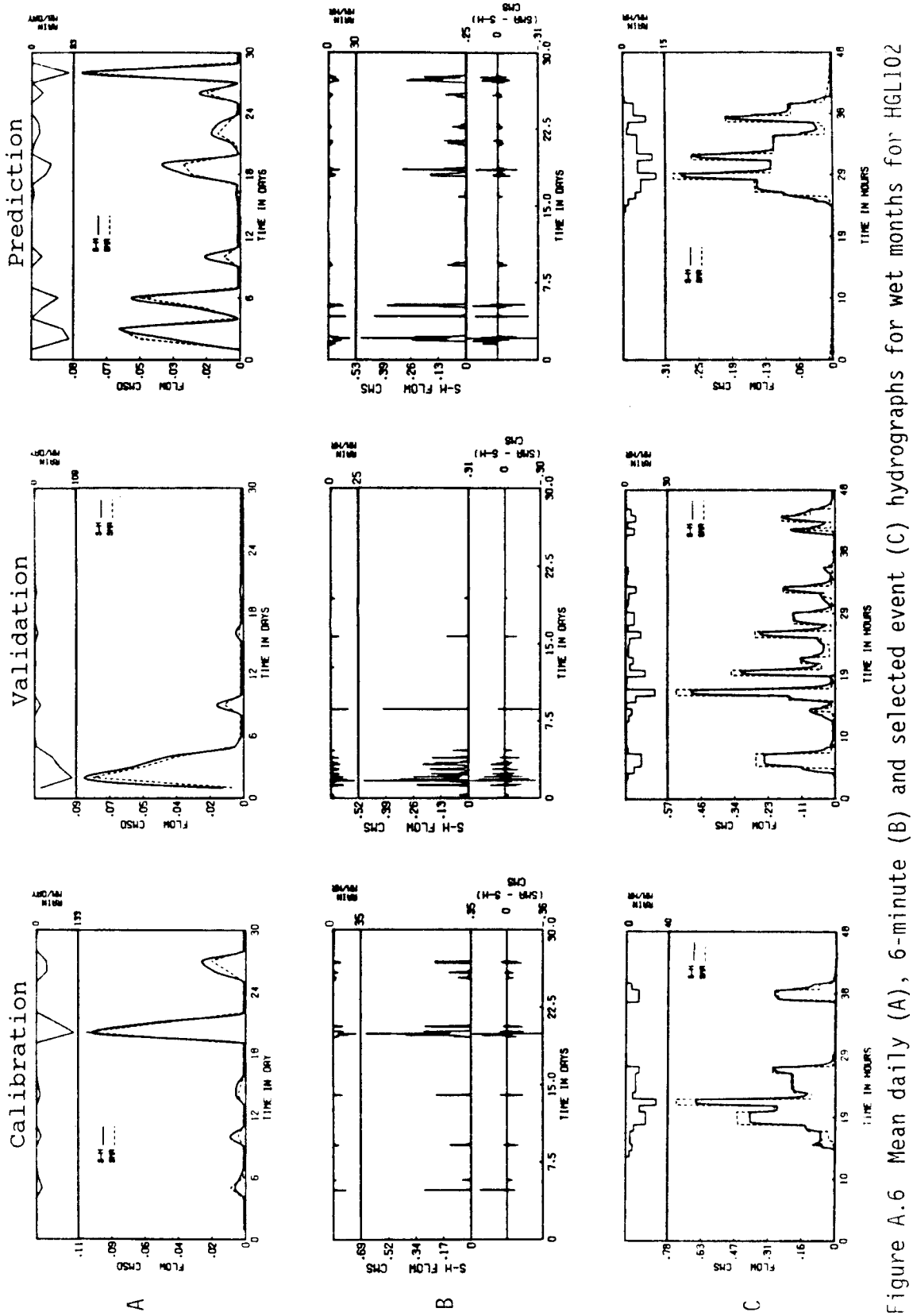

Figure A.6 Mean daily (A), 6-minute (B) and selected event (C) hydrographs for wet months for HGL102

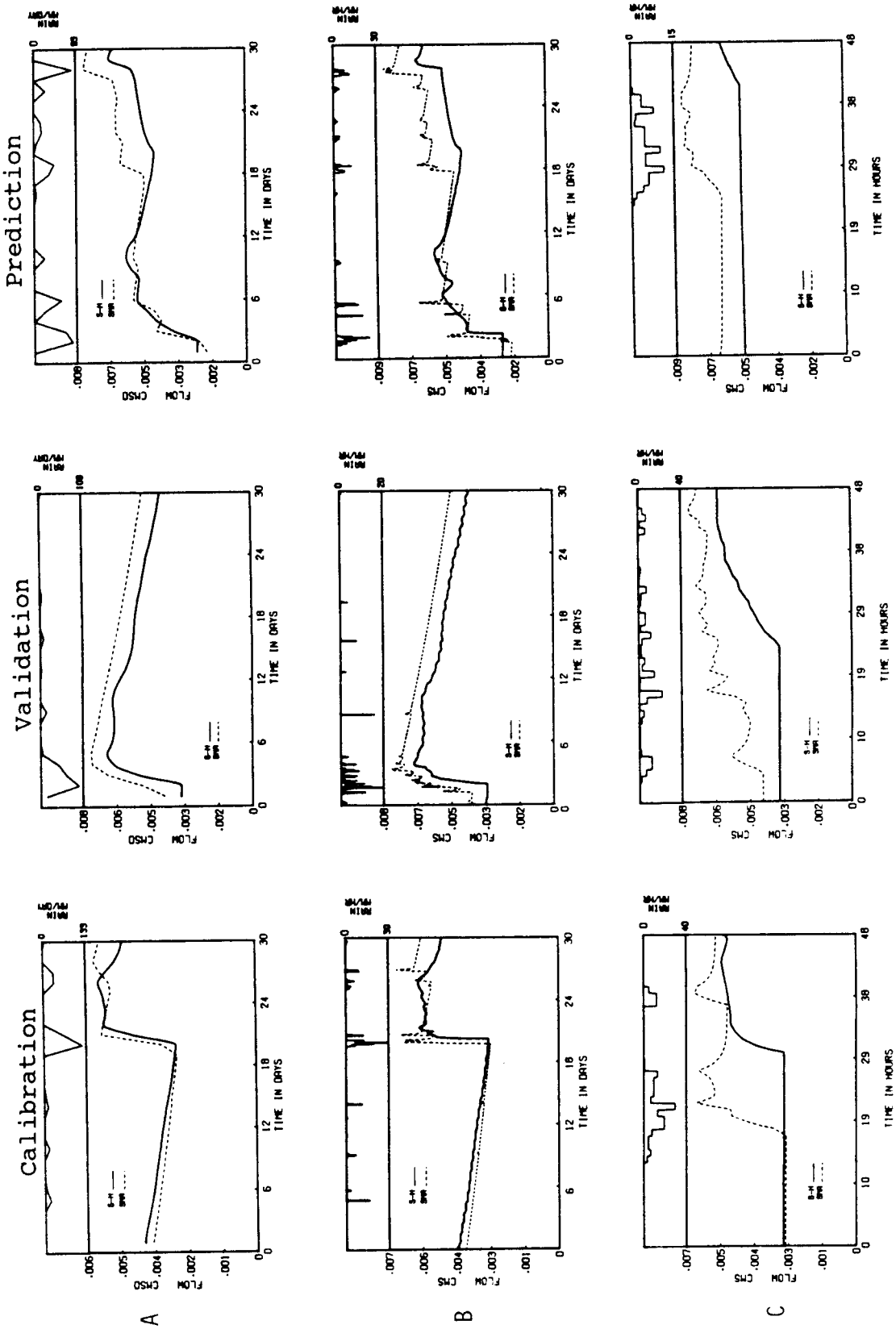

Figure A.7 Mean daily (A), 6-minute (B) and selected event (C) hydrographs for wet months for HGL103

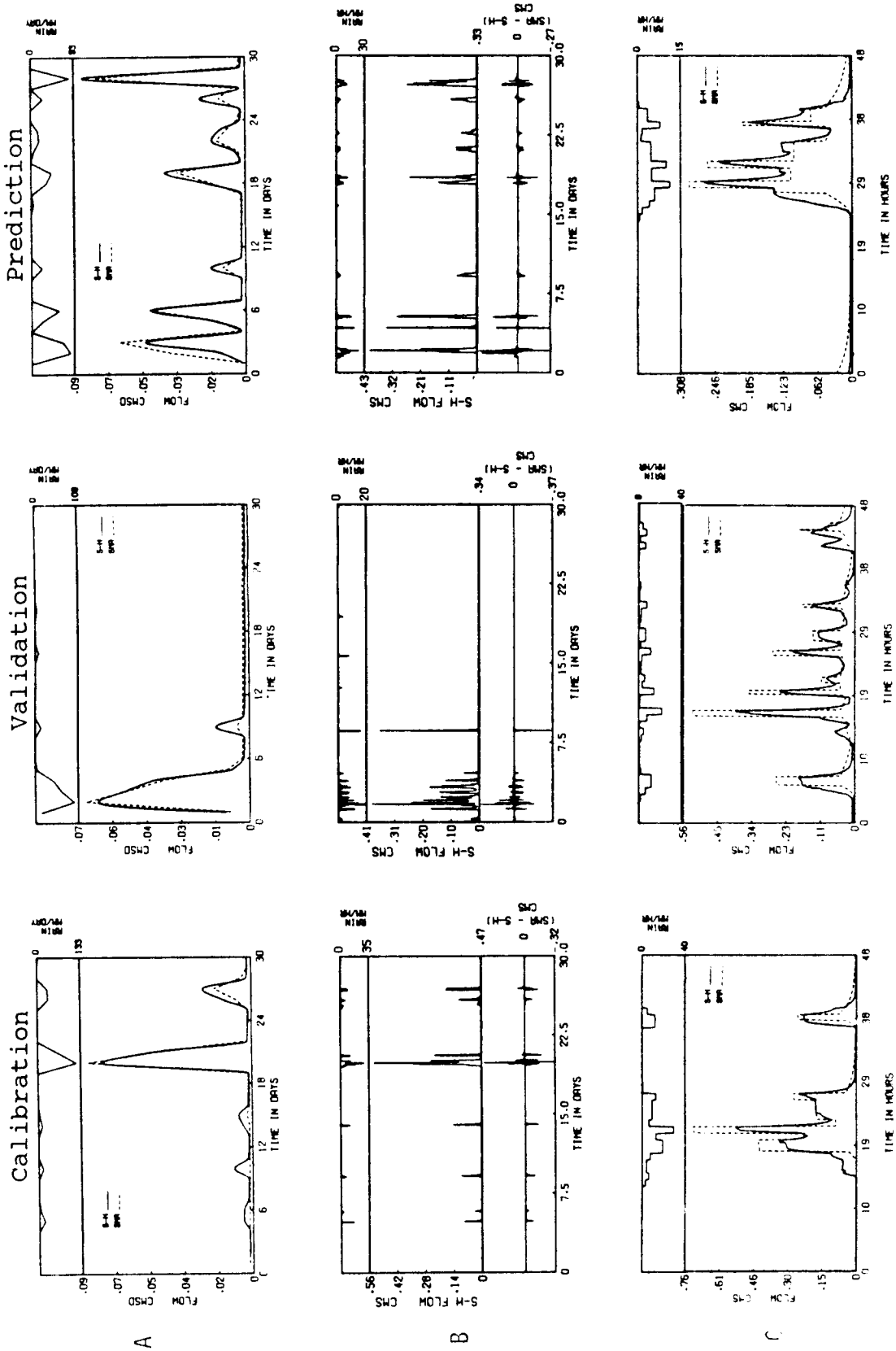

Figure A.8 Mean daily (A), 6-minute (B) and selected event (C) hydrographs for wet months for HGL104

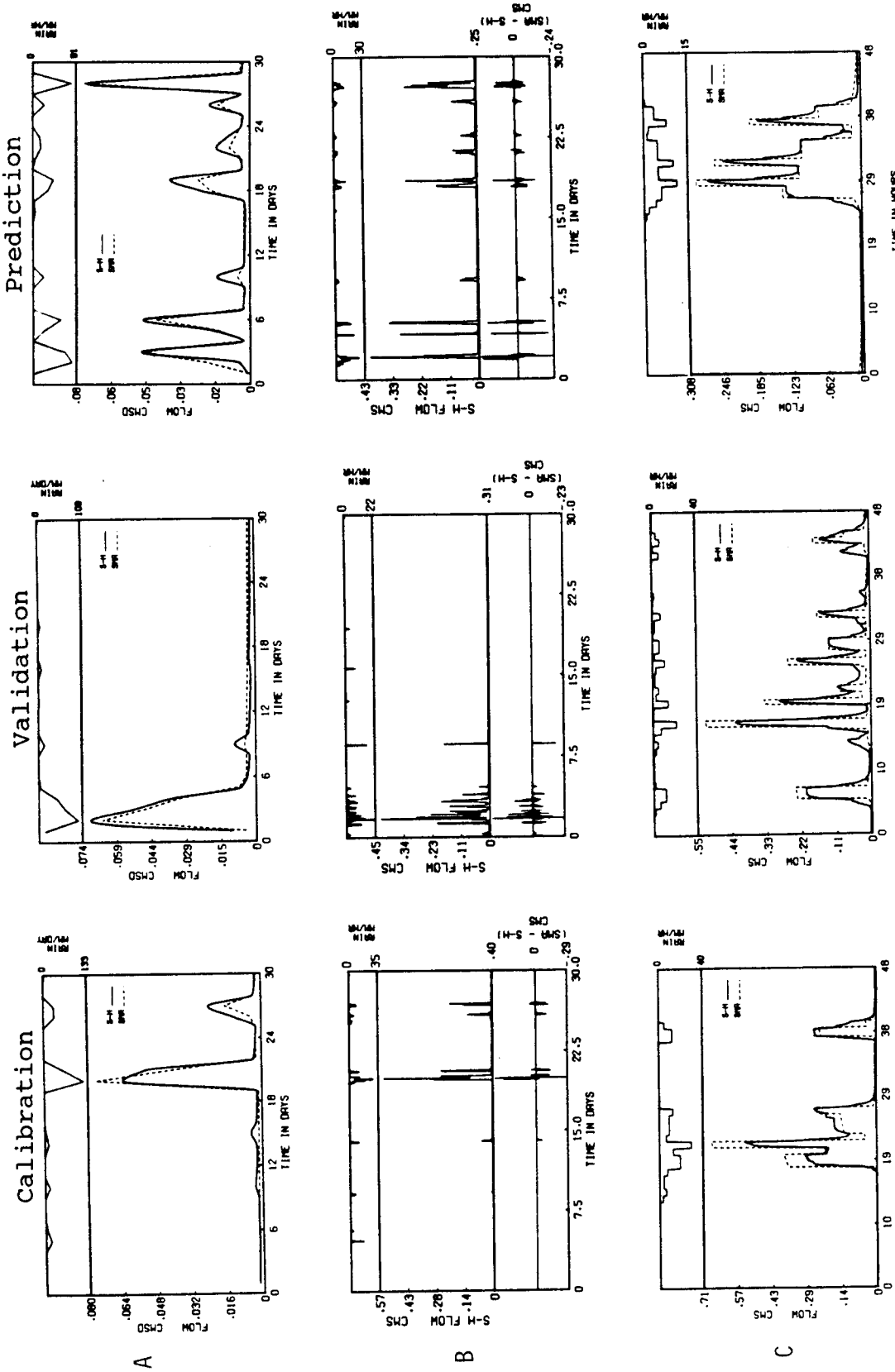

Figure A.9 Mean daily (A), 6-minute (B) and selected event (C) hydrographs for wet months for HGL105

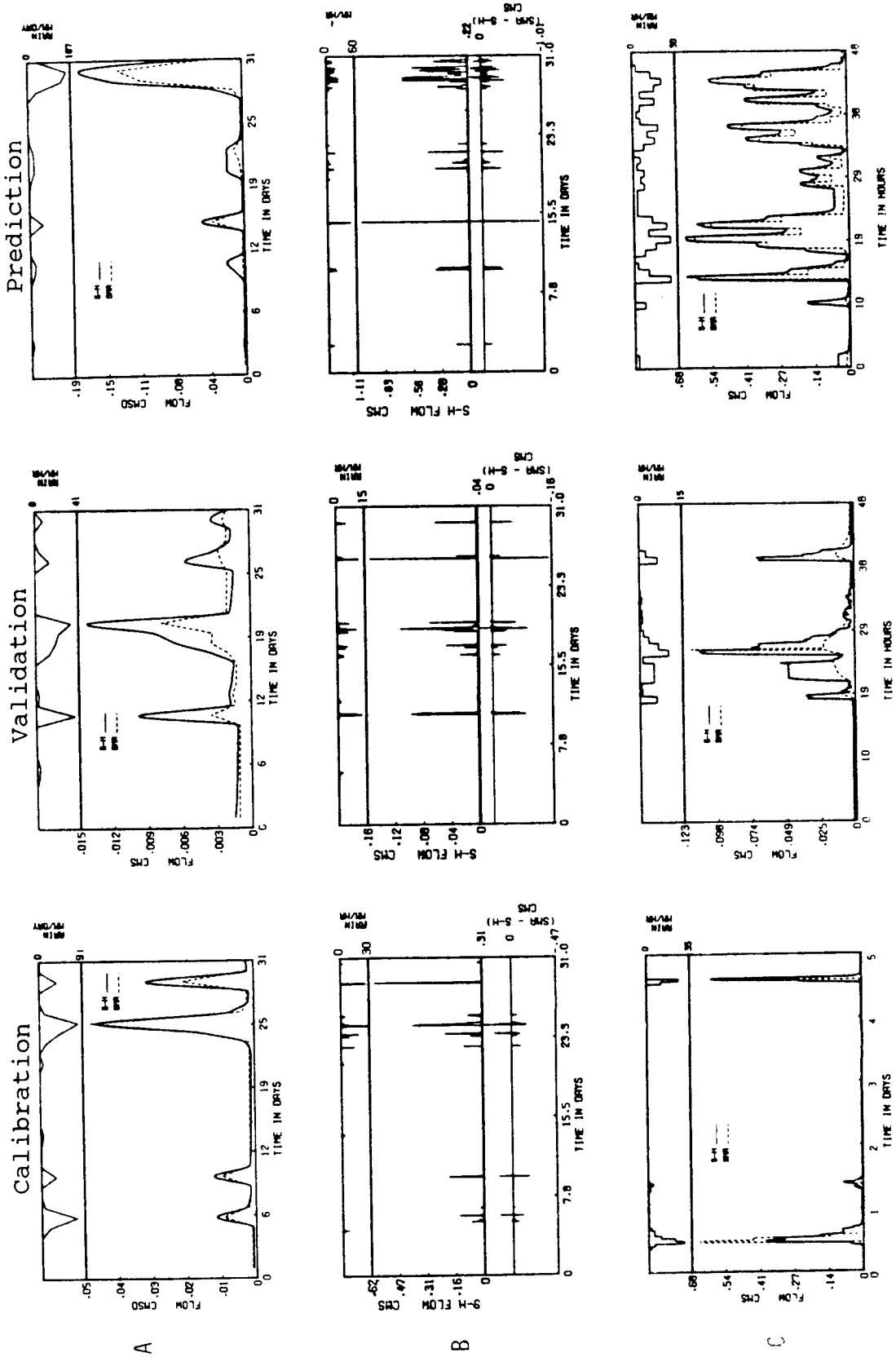

Figure A.10 Mean daily (A), 6-minute (B) and selected event (C) hydrographs for wet months for HFL102

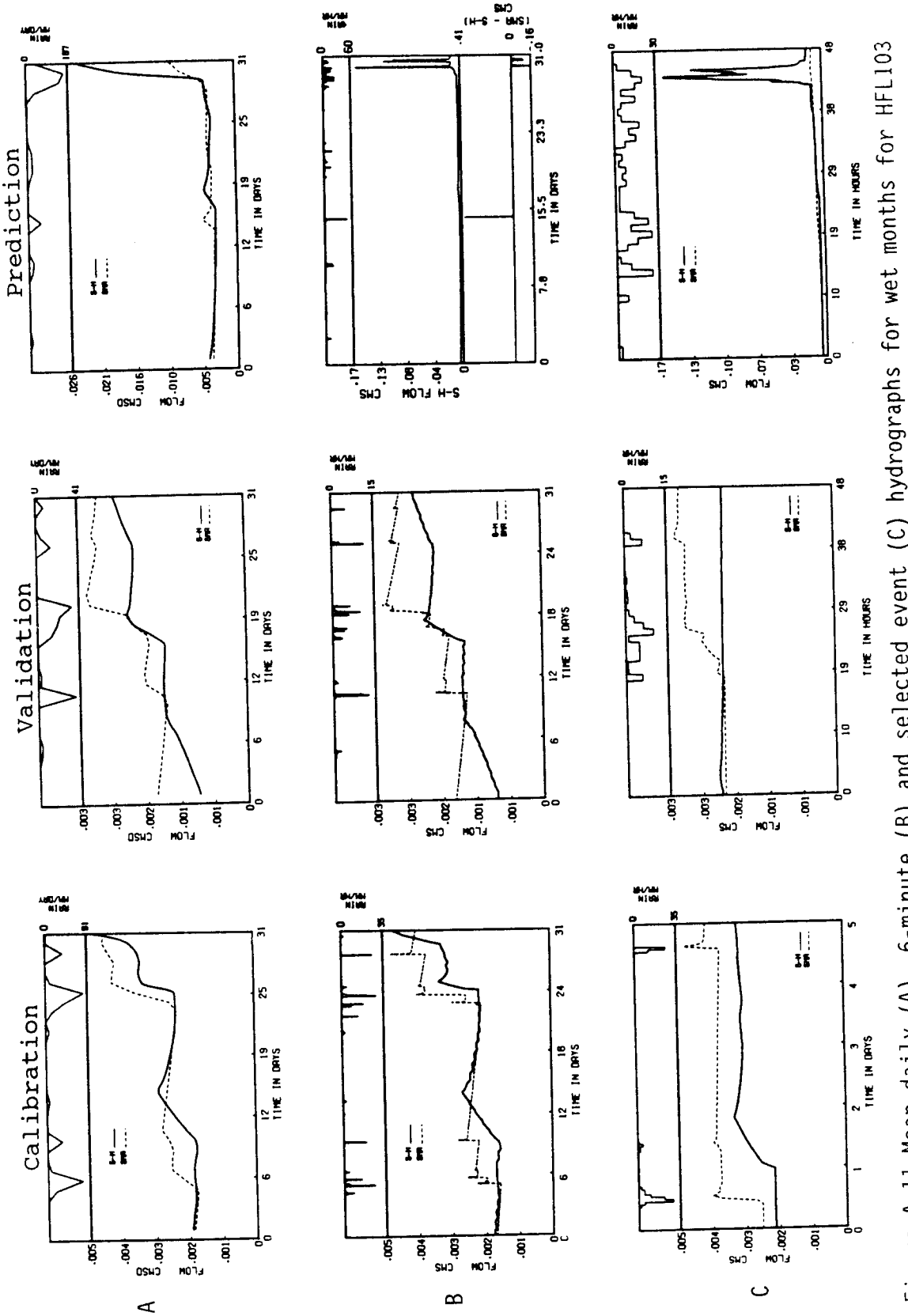

Figure A.11 Mean daily (A), 6-minute (B) and selected event (C) hydrographs for wet months for HFL103

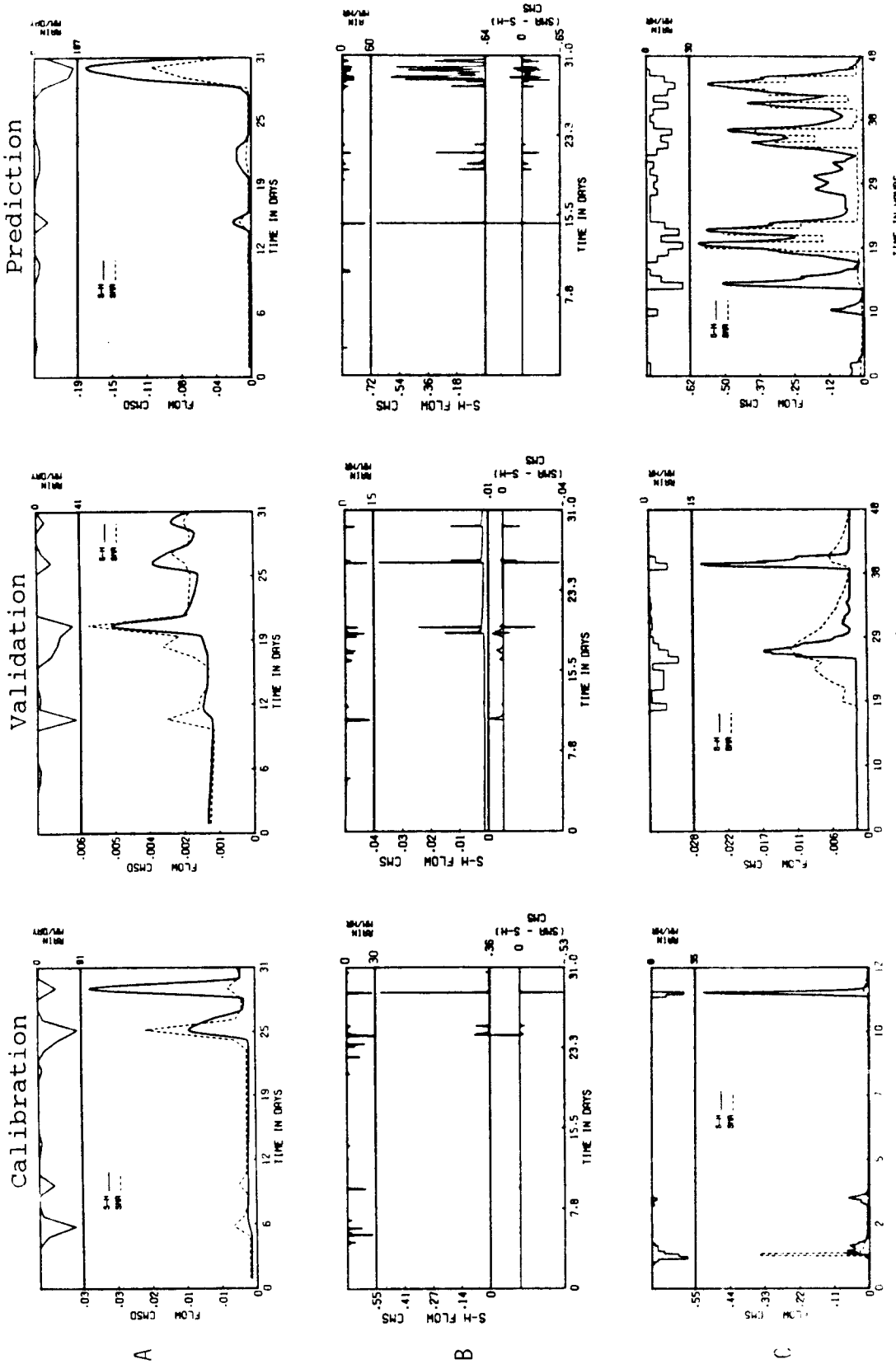

Figure A.12 Mean daily (A), 6-minute (B) and selected event (C) hydrographs for wet months for HFL104

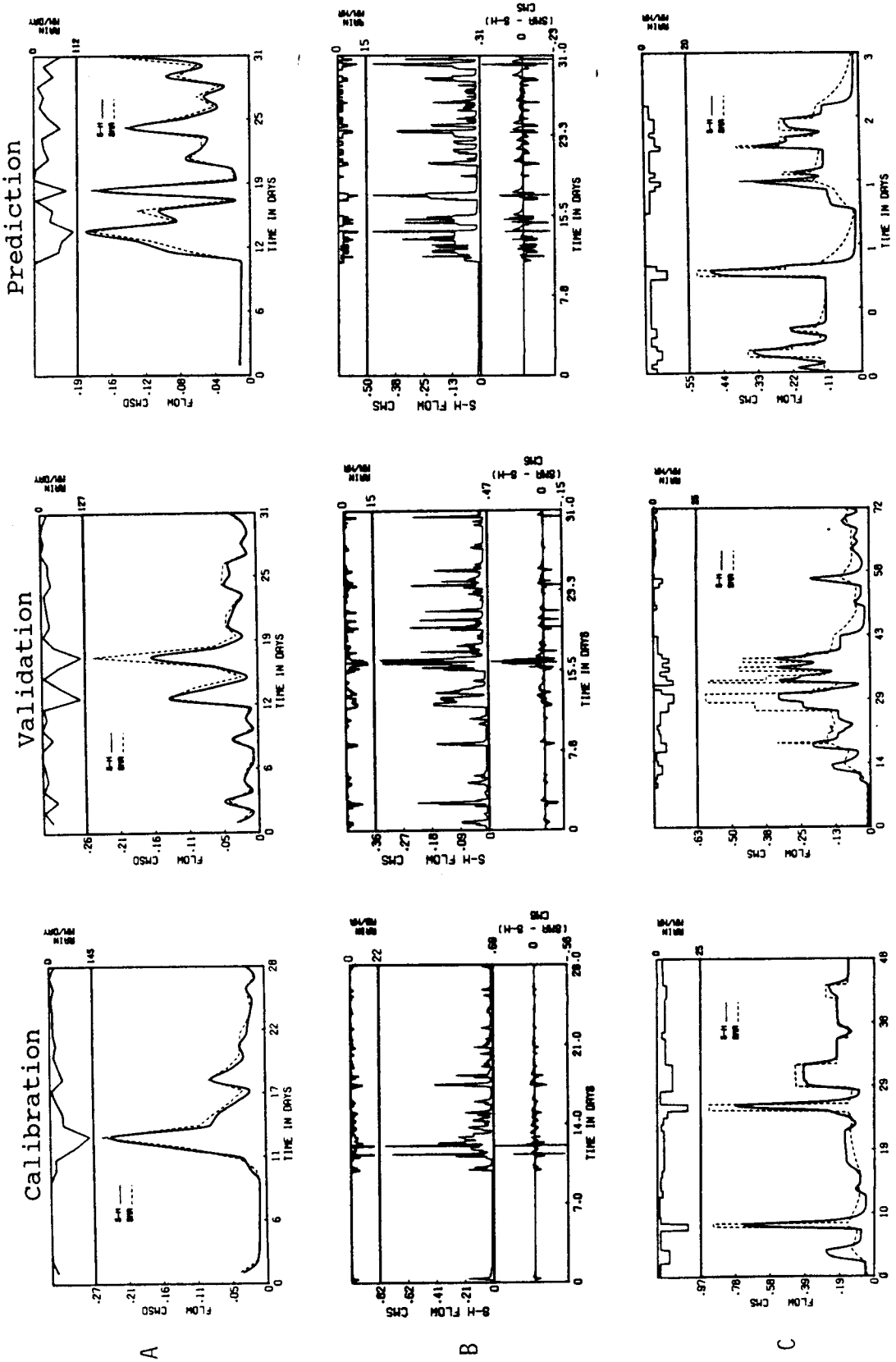

Figure A.13 Mean daily (A), 6-minute (B) and selected event (C) hydrographs for wet months for HL223

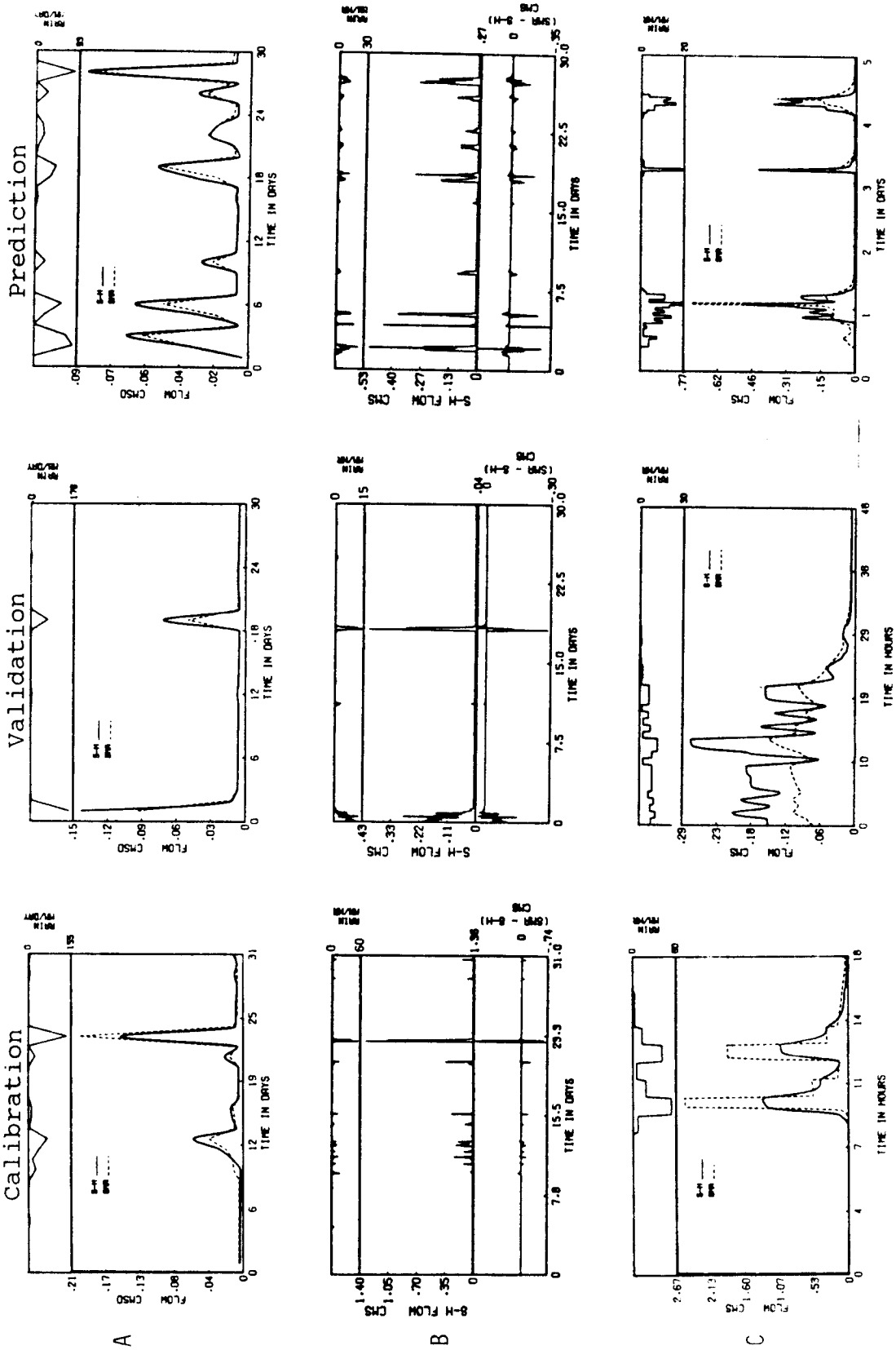

Figure A.14 Mean daily (A), 6-minute (B) and selected event (C) hydrographs for wet months for HG223

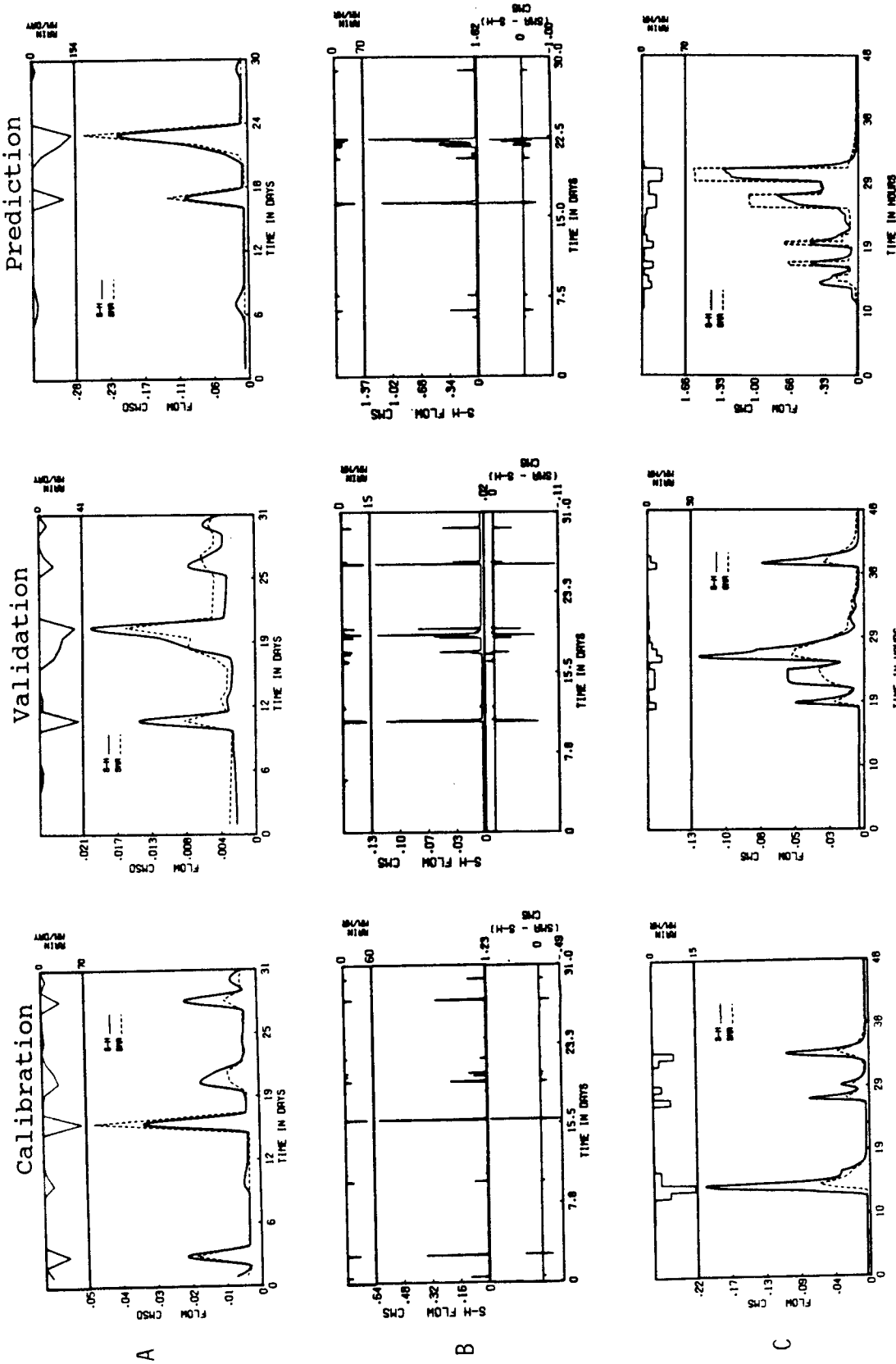

Figure A.15 Mean daily (A), 6-minute (B) and selected event (C) hydrographs for wet months for HF223

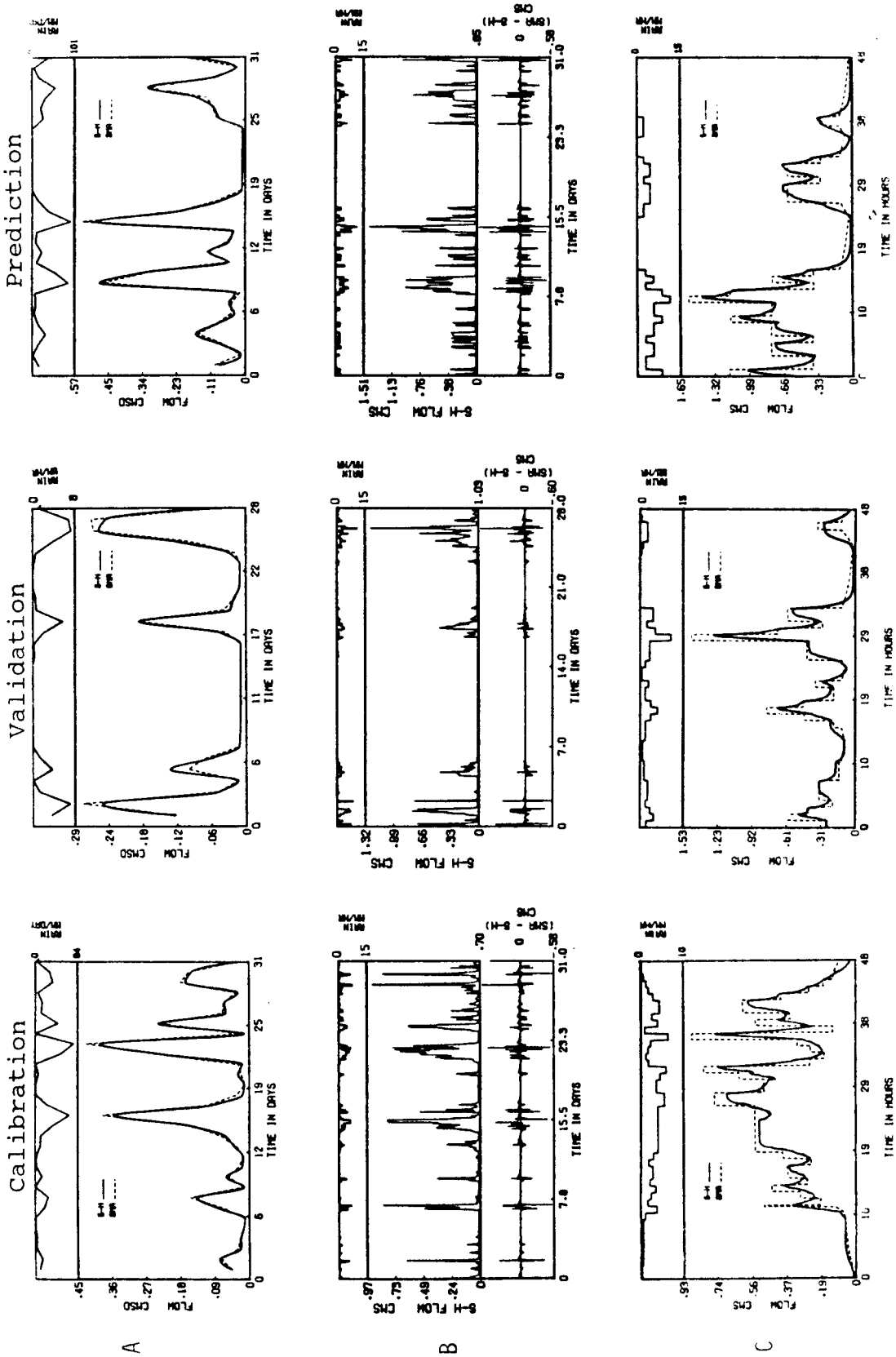

Figure A.16 Mean daily (A), 6-minute (B) and selected event (C) hydrographs for wet months for HULL10:

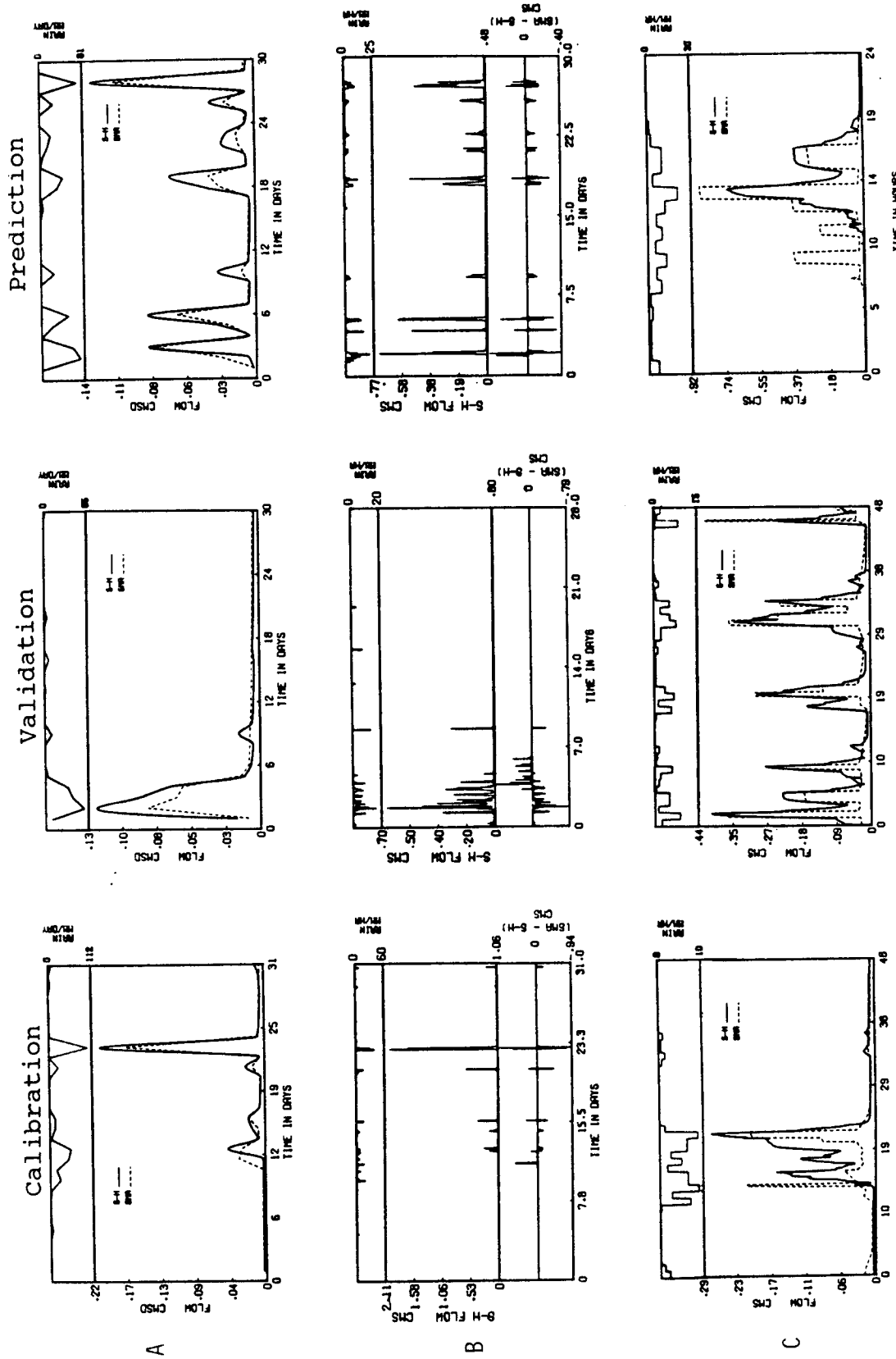

Figure A.17 Mean daily (A), 6-minute (B) and selected event (C) hydrographs for wet months for HUG105

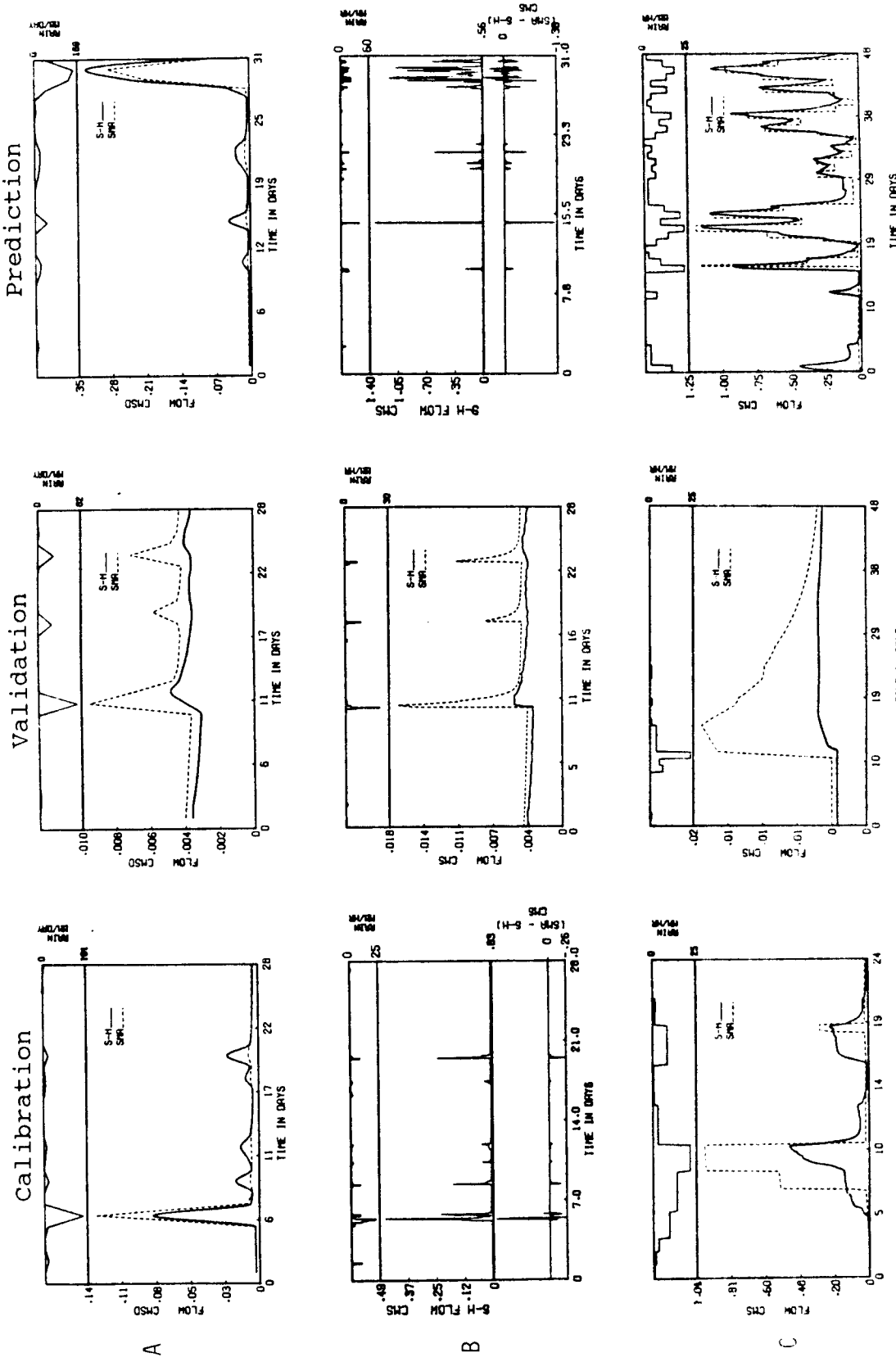

Figure A.18 Mean daily (A), 6-minute (B) and selected event (C) hydrographs for wet months for HUF45

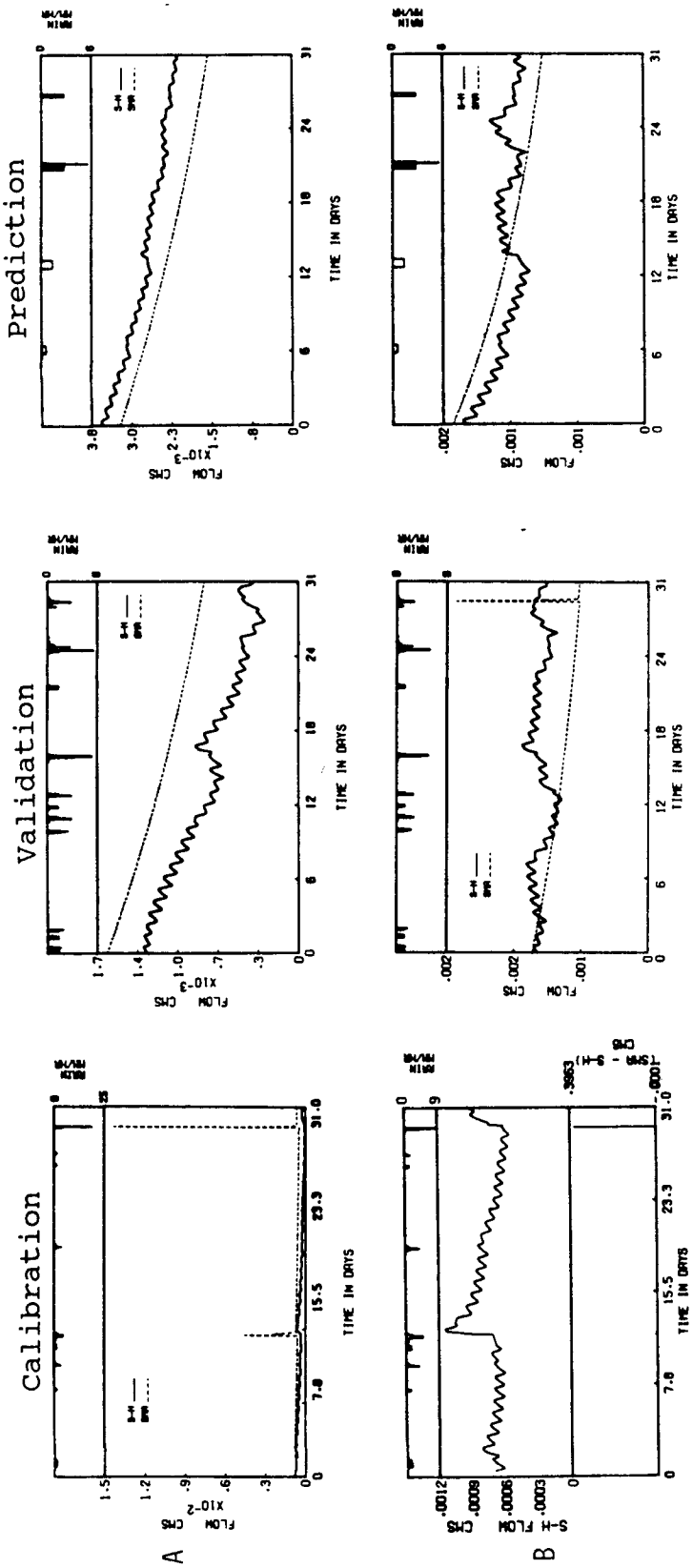

Figure A.19 6-minute hydrographs for HIL101 (A) and HIL105 (B) for dry months

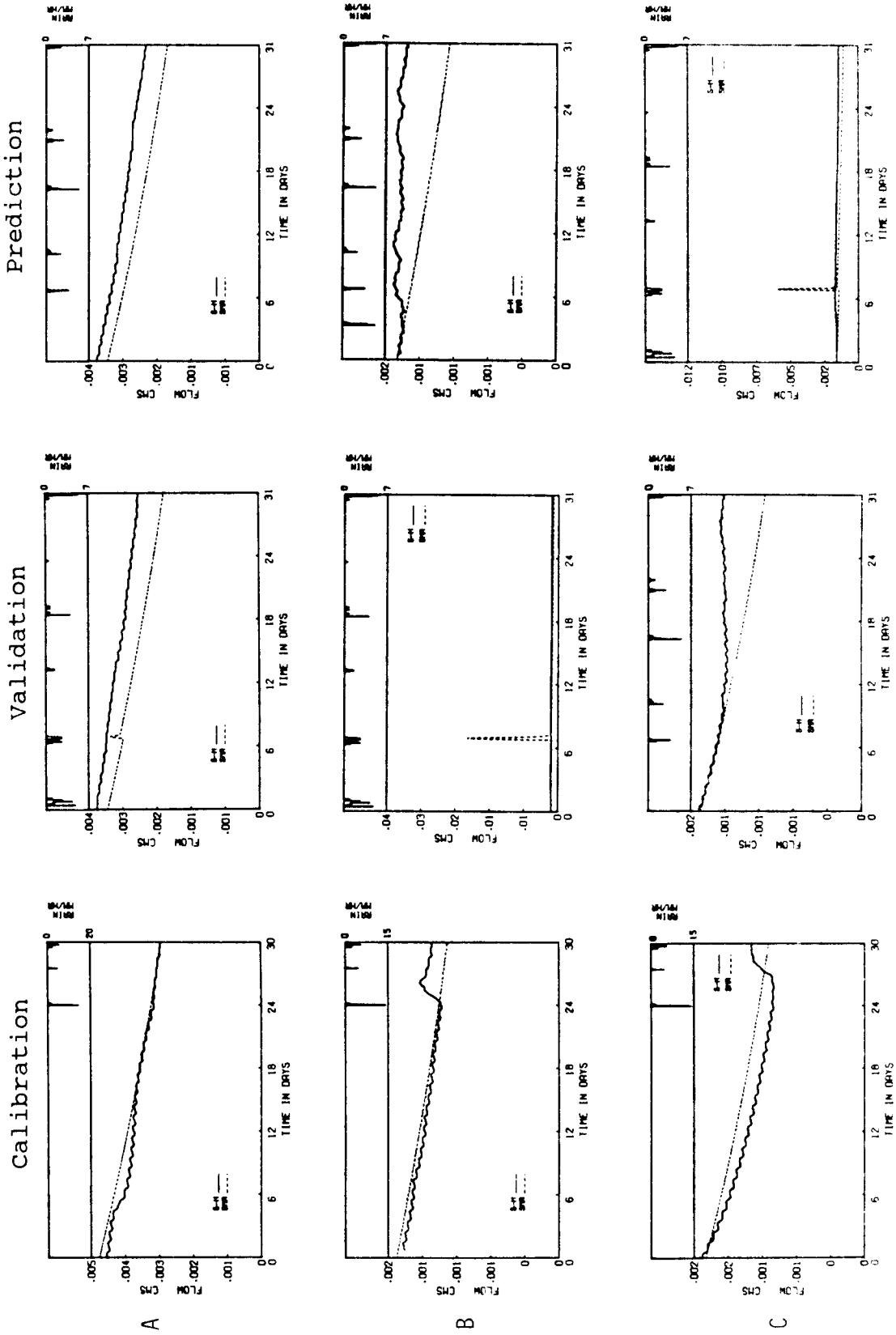

Figure A.20 6-minute hydrographs for HGL103 (A) and HGL104 (B) and HGL105 (C) for dry months

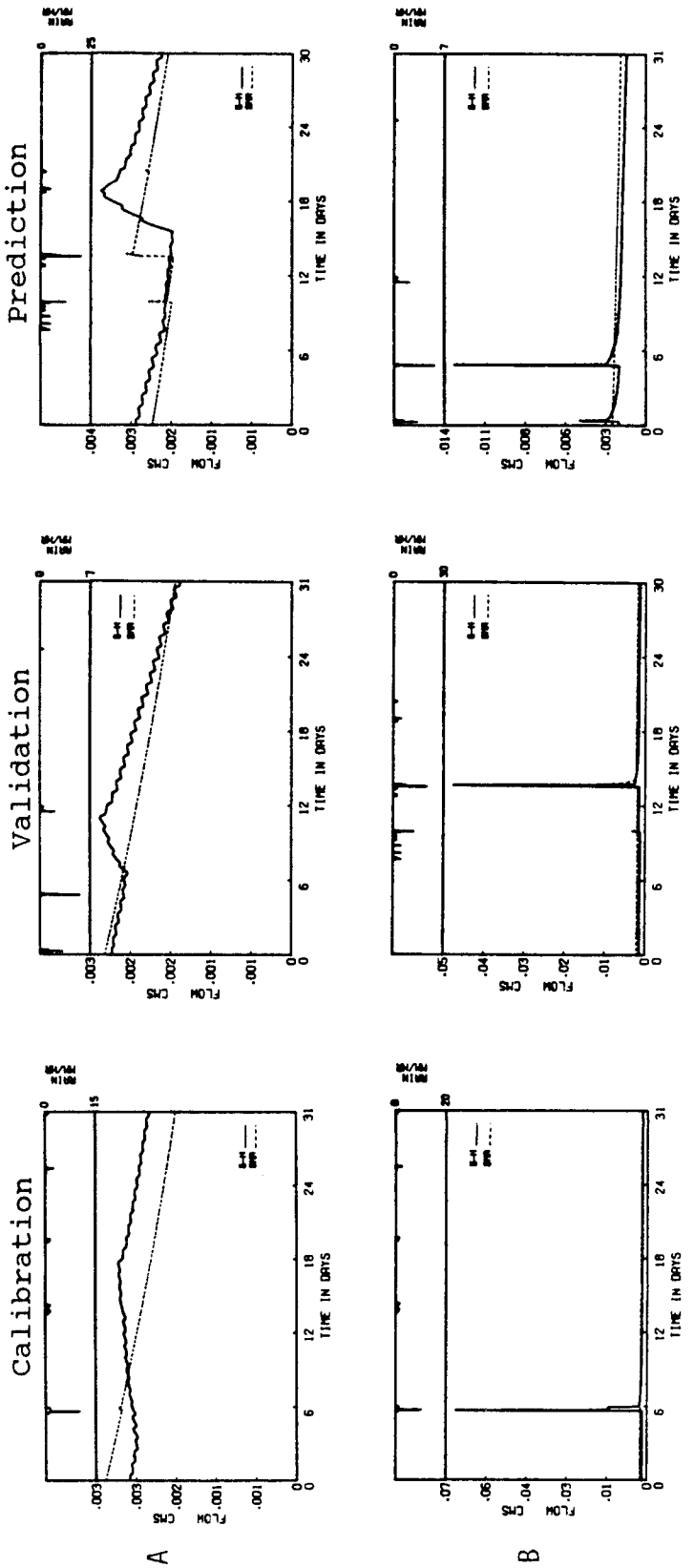

Figure A.21 6-minute hydrographs for HFL103 (A) and HFL104 (B) for dry months

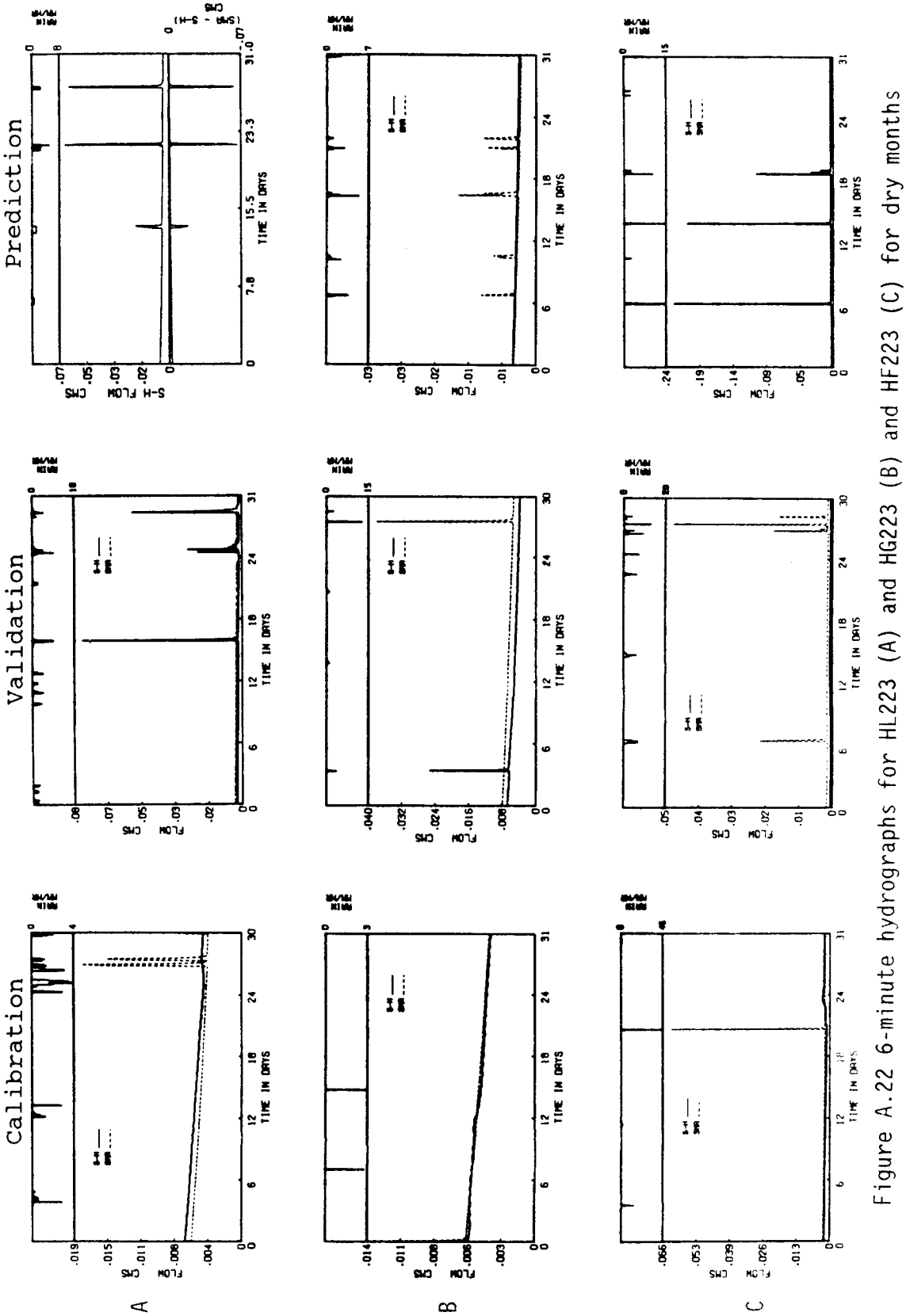

Figure A.22 6-minute hydrographs for HL223 (A) and HG223 (B) and HF223 (C) for dry months

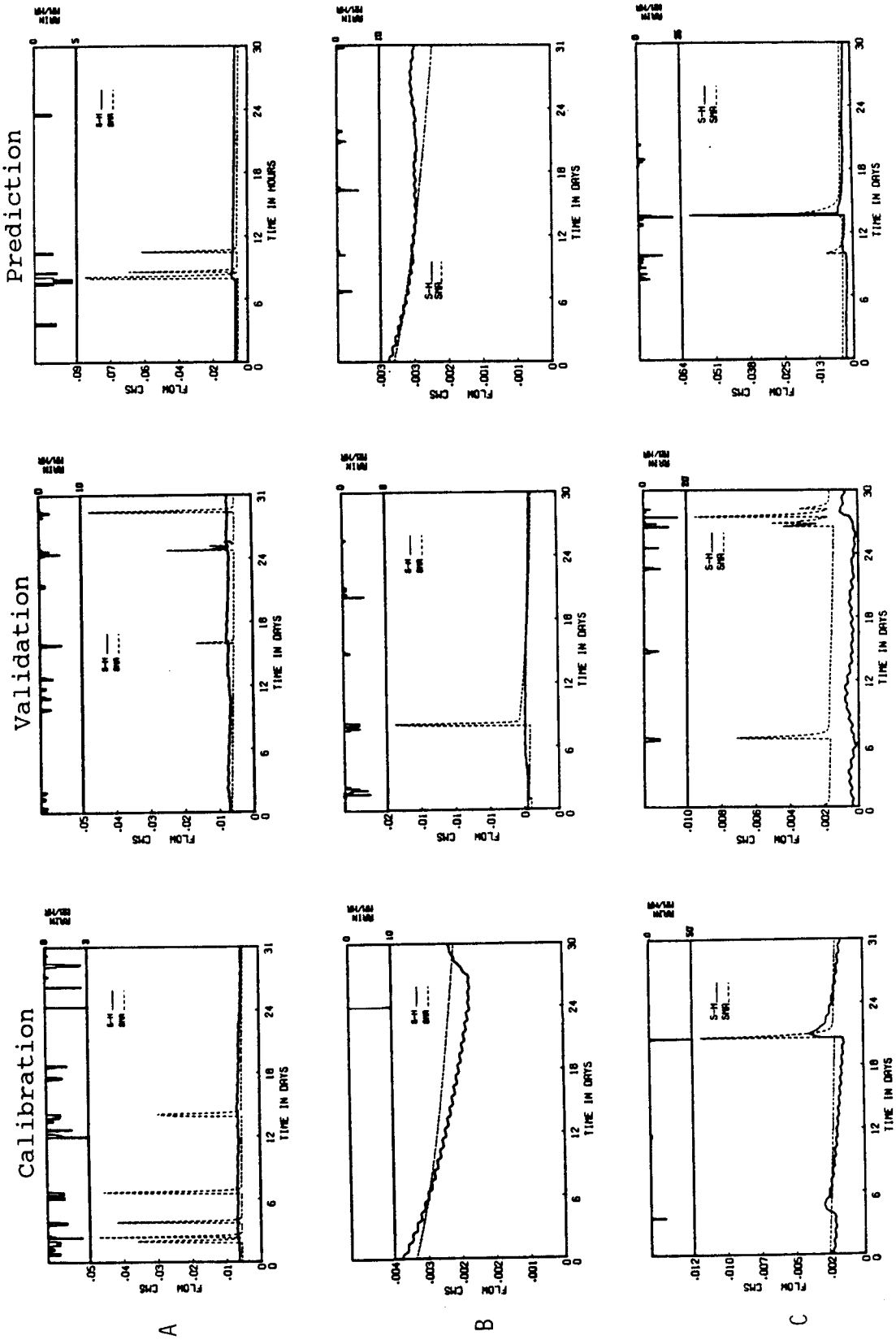

Figure A.23 6-minute hydrographs for HUL104 (A) and HUG105 (B) and HUF45 (C) for dry months

Appendix B

Optimized Parameters for the Sacramento Model (SMA)

The optimized parameters determined from calibration (Chapter 6) for the Sacramento model are reported in Table B.1. Each parameter is defined in Section 6.1.

Table B.1 Optimized parameters of the Sacramento model (SMA)

Parameter	Case					
	HIL101	HIL102	HIL103	HIL104	HUL104	HIL105
UZTWM[a]	154	9	187	207	189	140
UZFWM[a]	6	3	19	4	5	4
LZTWM[a]	80	56	84	49	153	56
LZFSM[a]	108	21	330	41	20	46
LZFPM[a]	272	51	465	200	232	176
ZPERC[b]	55	57	50	55	86.7	68.
REXP[b]	2.1	1.83	1.80	2.10	1.04	1.86
PBASE[b]	8.7	1.1	13.2	2.7	2.0	4.6
PEADJ[b]	.83	.76	.77	.76	.71	.78
UZK[b]	.66	.12	.17	.90	.98	.92
LZSK[b]	.028	.026	.018	.016	.03	.058
LZPK[b]	.021	.010	.017	.010	.006	.011
UZTWC[c]	148	0	71	48	56	48
UZFWC[c]	0	0	0	0	0	0
LZTWC[c]	77	0	61	15	95	15
LZFSC[c]	22	5	94	31	21	27
LZFPC[c]	60	15	184	102	180	100
ADIMC[c]	148	20	71	48	56	48

Table B.1(Contd) Optimized parameters of the Sacramento model (SMA)

Parameter	Case					
	HGL102	HGL103	HGL104	HGL105	HUG105	HUF45
UZTWM[a]	6.1	61	130	129	144	78
UZFWM[a]	3	43.9	10	5.4	5.4	34
LZTWM[a]	128	120	52	65	128	109
LZFSM[a]	74.6	14.5	46	47.5	20.4	72
LZFPM[a]	169	863	236	231	311	380
ZPERC[b]	95.2	88.1	67	84	90.2	78.7
REXP[b]	1.25	1.05	1.84	1.92	1.11	2.35
PBASE[b]	1.9	14.1	3.5	4.7	4.1	4.7
PEADJ[b]	.92	.93	.85	.91	.90	.96
UZK[b]	.98	.08	.98	.87	.88	.21
LZSK[b]	.009	.02	.015	.03	.096	.013
LZPK[b]	.007	.016	.012	.014	.007	.010
UZTWC[c]	0	60	48	48	40	40
UZFWC[c]	0	0	0	0	0	0
LZTWC[c]	1	99	25	15	90	90
LZFSC[c]	2	11	32	20	5	5
LZFPC[c]	100	399	100	80	166	130
ADIMC[c]	0	60	48	48	40	40

Table B.1(Contd) Optimized parameters of the Sacramento model (SMA)

Parameter	Case					
	HFL102	HFL103	HFL104	HL223	HG223	HF223
UZTWM[a]	167	51	141	84	8	74
UZFWM[a]	6.6	21	29	15.1	20	12.6
LZTWM[a]	111	110	142	77	107	38
LZFSM[a]	171	36	38	129	80	47
LZFPM[a]	341	809	517	250	300	434
ZPERC[b]	88.9	94	84.6	58.6	97	96
REXP[b]	2.6	1.03	1.04	1.14	1.03	1.85
PBASE[b]	5.6	12.8	4.9	5.4	5.0	6.3
PEADJ[b]	.98	.94	.95	.77	.94	1.0
UZK[b]	.94	.06	.44	.98	.97	.96
LZSK[b]	.015	.018	.02	.017	.014	.023
LZPK[b]	.009	.015	.008	.013	.013	.012
UZTWC[c]	100	50	48	50	1	9
UZFWC[c]	0	0	0	0	0	0
LZTWC[c]	111	78	25	60	10	10
LZFSC[c]	9	10	10	30	10	10
LZFPC[c]	130	420	260	120	244	275
ADIMC[c]	100	50	48	5	1	9

Legend

a Storages in mm
b Coefficients, dimensionless
c Initial storage contents in mm

Appendix C

Order of a Channel Network

Classification of a drainage basin is based on its size, a scale measurement that is usually specified by the order of the channel network in the basin. The method proposed by Horton (1945) was modified by Strahler (1952) and has remained the most widely used scheme for designating the order of a channel network. In Strahler's method, all the finger-tip channel segments, also known as sources, are designated first order, two first order channels join and form a second order channel, two second order channel form a third order channel and so on, as shown in Fig. C.1.

Since the order of Strahler's channels change only when two channels of the same order join, not all first order channels (also known as links) are accounted for. This inconsistency was overcome by Shreve (1967), who regarded channels within a basin as a link system, with the magnitude of each link representing the number of sources upstream from it. Shreve's theoretical prediction that magnitude gives a more precise description of networks was substantiated by observations on natural networks (Krumbein and Shreve, 1970). Shreve's system is used to designate catchment magnitude in the present work. The highest order catchment used has magnitude U = 2.

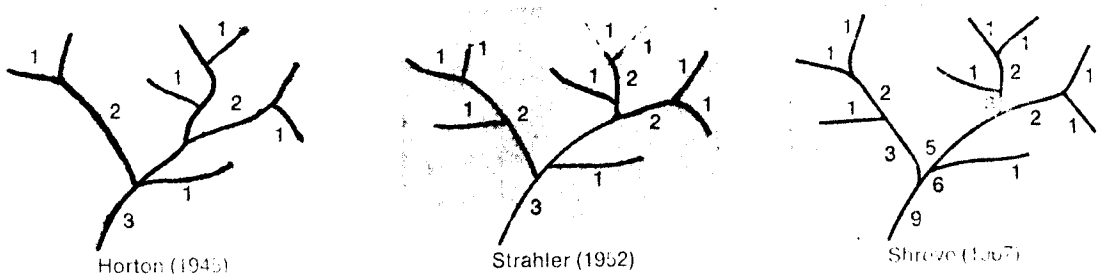

Figure C.1 Methods of ordering channels (from Ritter. 1984)

Appendix D

Estimation of Soil Sorptivity

By Parlange's (1972) approximation, with given initial and final soil moisture content θ_0 and θ_1, sorptivity S is

$$S^2 = 2\int_{\theta_0}^{\theta_1} (\theta - \theta_0)D(\theta)d\theta \qquad (D.1)$$

Assuming the relationship between $K(\theta)$ and θ is given by Brooks and Coreys'(1964) relation

$$K(\theta) = K_s\theta_e^{\epsilon} \qquad (D.2)$$

Where

$$\theta e = \left[\frac{\theta - \theta_r}{\theta_s - \theta_r}\right] \qquad (D.3)$$

$$= \text{Exp } (-\lambda F(Z,C))$$

ψ_b = Air entry pressure,

ψ = Soil capillary suction,

θ_r = Residual soil moisture (ψ --> $-\infty$),

θ_s = Saturated soil moisture (ψ = 0),

$Z = \ln (\psi / \psi_b)$,

$\epsilon = (2 + 3\lambda)\lambda^{-1}$

λ = parameter as shown in Fig. D.1.

From Smith(1982),

$$F(Z,C) = 0.5Z + (.25Z^2 + C) \qquad (D.4)$$

When C = 0, F(Z,C) = Z and so from Eq. D.3,

$$\theta e = \frac{\psi^{-\lambda}}{\psi_b} \quad (\mid \psi \mid > \mid \psi_b \mid) \tag{D.5}$$

But diffusivity $D(\theta) = K(\theta) d\psi / d\theta$ (D.6)

From Eqs. (D.2), (D.5) and (D.6),

$$D(\theta) = -K_s \frac{\psi_b \, \theta_e^{2/\lambda + 2 + \lambda^{-1}}}{(\theta_s - \theta_r)} \tag{D.7}$$

$$S^2 = \frac{2 K_s \psi_b}{(\theta_s - \theta_r)} \int_{\theta_o}^{\theta_1} \theta_e^{2/\lambda + 2 + \lambda} \, d\theta \tag{D.8}$$

$$S^2 = \frac{2\lambda K_s \psi_b}{2/\lambda + 4 + \lambda} \left[\left(\frac{\theta_1 - \theta_r}{\theta_s - \theta_r} \right)^{2/\lambda + 4 + \lambda} - \left(\frac{\theta_o - \theta_r}{\theta_s - \theta_r} \right)^{2/\lambda + 4 + \lambda} \right] +$$

$$\frac{\lambda K_s \psi_b (\theta_r - \theta_o)}{2/\lambda + 3 + \lambda} \left[\left(\frac{\theta_1 - \theta_r}{\theta_s - \theta_r} \right)^{2/\lambda + 3 + \lambda} - \left(\frac{\theta_o - \theta_r}{\theta_s - \theta_r} \right)^{2/\lambda + 3 + \lambda} \right] \tag{D.9}$$

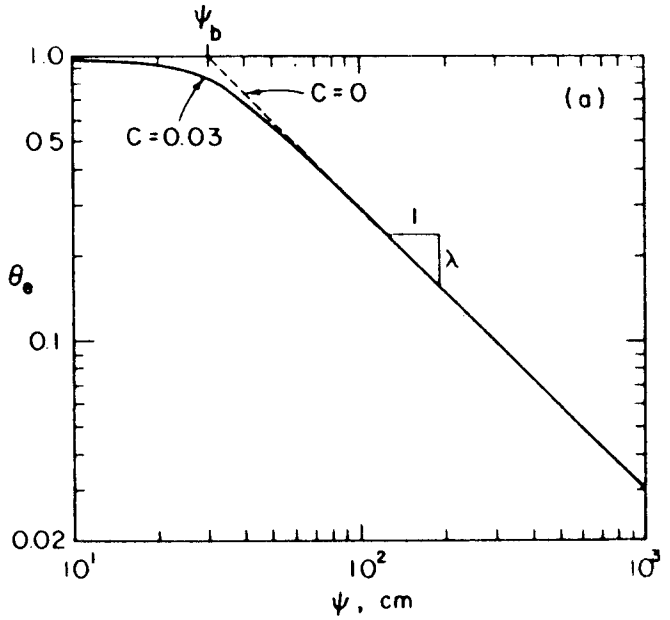

Figure D.1 θ_e, normalized water content as a function of capillary suction (from Smith, 1983)

APPENDIX E

Physical Considerations in Creating Hypothetical Hillslope Catchments

Channel networks, subsets of a network of indefinitely large extent which, in the absence of significant tectonic influence, are approximated as topologically random (Shreve, 1967, 1966). The size of one such channel subnetwork is described in terms of magnitude U (number of first order streams). Its mainstream length is defined as the length of the longest channel, measured as a sum of its link lengths, from a first-order stream to the outlet. The three methods available for computing the expected mainstream length $E_u(L)$ of a network of magnitude U are an analytical method by Shreve (1974), a least-squares fit, and a Monte Carlo method by Werner and Smart (1973); values of expected mainstream length are given in Table E.1. Values of relevant parameters for defining soil depths, hillslope dimensions and slopes, and channel roughness were taken from the literature. Values of parameters that were used to constrain the hypothetical catchments are within the ranges given in Table E.2. Typical hillslope soil hydraulic properties are shown in Table E.3.

Table E.1 Expected topological mainstream length Eu(L) of magnitude U

TDCN Magnitude U		from Shreve(1974) (Analytical Method) $E_u(L)$	from Werner and Smart(1973) Least-square Fit $1.98U^{.59}$	Monte Carlo Fit $1.4(2U-1)^{.58}$
1	1	1.00	1.98	1.40
1	2	2.00	2.98	2.65
2	3	3.00	3.78	3.56
5	4	3.80	4.48	4.32
14	5	4.57	5.12	5.01
42	6	5.24	5.69	5.62
132	7	5.88	6.24	6.19
429	8	6.47	6.75	6.73
1430	9	7.03	7.23	7.24
4862	10	7.56	7.70	7.72
16796	11	8.07	8.14	8.18

Note that mainstream length L is

$$L = l \times E_u(L) \qquad (E.1)$$

where l is the mean link length and TDCN denotes "topologically distinct channel network".

Table E.2 Range of parameter values for setting up hypothetical catchments

Input Parameters	Values (Range)	Symbol	Dimensions	Equations	Source
Basin Parameters					
Basin area	0.1 to 0.5 km^2	A	L^2		
Drainage density	1 - 5 km/km2	D	L^{-1}	(5.4)	Schumm(1956), Strahler(1968)
Basin shape				(5.2)	Hack(1957)
Mainstream length	0.3 - 1.5 km	L	L	(E.1)	
Magnitude	1 - 2	U	0		Shreve(1966)
Link length	0.2 - 0.5 km	l	L		Leopold et al(1964)
Valley slope	0.02 - 0.7	S_v	0		Strahler(1964), Carson & Kirkby(1972)
Channel slope	0.001 - .03	S_c	0		Leopold & Wolman(1957)
Manning's n(grass)	.053 - .20	n_m	0		Woolhiser(1974)
Darcy-Weisbach f	100 -1000	f_D	0		Dunne & Dietrich(1980)
Manning's n for channel	.02 - .03	n_c	0		Chow(1959)
Top soil thickness	.20 - 1.6 m	Y	L		Zazoski personal communication
Vegetation Cover					
Short grass root depth	.20 - 1.60 m	R_D	L		
Soil field capacity	-.33 bar	$ML^{-1}T^{-2}$			Hawks & Ashcroft(1980)
Plant wilting point	-15 bars	$ML^{-1}T^{-2}$			Denmead & Shaw(1962)

Table E.3 Hydrologic soil properties classified by soil texture (from Rawls et al., 1981)

Texture Class	Total porosity ϕ Cm^3/Cm^3	Residual saturation θ_r Cm^3/Cm^3	Bubbling pressure ψ_b[c] Cm	Pore size distribution λ[c]	Water[a] at -.33 bars Cm^3/Cm^3	Water[b] at -15 bars Cm^3/Cm^3	Saturated hydraulic conduct. K_s Cm/hr
Sand	.437	.02	15.98	.694	.091	.033	21.0
Loamy sand	.437	.031	20.58	.553	.125	.055	6.11
Sandy loam	.453	.041	30.20	.378	.207	.095	2.59
loam	.463	.027	40.12	.252	.270	.117	.68
Silt loam	.501	.015	50.87	.234	.330	.133	1.32
Sandy clay loam	.398	.068	59.41	.319	.255	.148	.43
Clay loam	.464	.075	56.43	.242	.318	.197	.23
Silty clay loam	.471	.040	70.33	.177	.366	.208	.15
Sandy clay	.43	.109	79.48	.223	.339	.239	.12
Silty clay	.479	.056	76.54	.150	.387	.250	.09
Clay	.475	.090	85.60	.165	.396	.272	.06

Legend

[a] Soil field capacity

[b] Plant wilting point

[c] Arithmetic mean

Appendix F

Properties of Rain Data

Summary statistics of rain data of the four rain stations used in the experiments under Tests I and II (Sections 5.3.1 and 5.3.2) are given in Tables F.1 to F.9. The rain stations are Quillayute and Aberdeen NNE (Washington), Tray Mountain (Georgia) and Niceville (Florida). The summary statistics reported include storm duration, volume, intensity, interarrival time and number of events. The summary statistics for the same sets of rain data, with storm depths "perturbed" by a uniformly distributed noise component for experiments under Test III (Section 5.3.3), are given in Tables F.10 to F.15. Only storm volume and intensity are reported since the time distributions of the rain data were not changed.

Table F.1 Summary statistics of rain data for Quillayute, Washington (calibration, two-year period)

Month	Duration (Hour)		Volume (mm)		Intensity (mm/hr)		Interarrival Time (Hour)		No of
	Mean	Std Dv	Mean	Std Dv	Mean	Std Dv	Mean	Std Dv	Events
Jan	9.80	9.93	11.8	22.4	0.763	0.624	17.0	25.7	51
Feb	15.1	13.5	23.7	41.8	1.12	0.888	23.8	49.5	36
Mar	10.6	10.1	16.7	24.1	1.20	1.00	32.7	40.7	33
Apr	10.4	10.0	10.2	15.8	0.717	0.539	29.4	46.2	36
May	6.87	5.36	4.28	5.54	0.549	0.408	35.0	55.9	38
Jun	8.81	7.87	8.43	9.94	0.899	0.706	32.0	56.4	36
Jul	5.16	4.02	4.53	3.67	0.985	0.828	35.5	39.2	37
Aug	8.21	5.91	10.2	8.84	1.07	0.658	68.9	55.2	19
Sep	9.33	9.22	10.5	13.0	0.995	0.765	39.3	53.1	27
Oct	11.0	13.3	16.5	26.9	1.25	0.858	35.0	47.8	34
Nov	13.2	12.8	19.2	28.1	1.11	0.861	16.6	23.8	47
Dec	10.9	9.94	15.4	20.1	1.13	0.828	18.0	25.4	55

Month	Duration (Hour)		Volume (mm)		Intensity (mm/hr)		Interarrival Time (Hour)	
	Min	Max	Min	Max	Min	Max	Min	Max
Jan	1.00	47.0	0.254	117.	0.169	2.69	4.0	182.
Feb	1.00	55.0	0.254	231.	0.212	4.19	4.0	228.
Mar	1.00	41.0	0.254	107.	0.198	3.36	4.0	147.
Apr	1.00	38.0	0.254	73.7	0.190	2.81	4.0	226.
May	1.00	21.0	0.254	22.1	0.169	1.60	4.0	327.
Jun	1.00	30.0	0.254	35.6	0.127	2.79	4.0	263.
Jul	1.00	18.0	0.254	13.7	0.226	3.39	4.0	144.
Aug	1.00	20.0	0.254	28.7	0.254	3.13	5.0	166.
Sep	1.00	37.0	0.254	53.3	0.254	3.64	4.0	200.
Oct	1.00	51.0	0.254	112.	0.102	3.33	4.0	155.
Nov	1.00	48.0	0.254	146.	0.169	4.41	4.0	96.0
Dec	1.00	41.0	0.254	97.3	0.231	4.29	4.0	144.

Annual	Mean	Std Dv	Min.	Max	No. of events
Duration (hr)	10.1	10.2	1.0	55.0	449
Volume (mm)	12.9	22.2	0.254	231.	
Intensity (mm/hr)	0.976	0.784	0.102	4.41	
Interarrival Time (hr)	28.9	43.6	4.0	327.	

Table F.2 Summary statistics of rain data for Quillayute, Washington (validation, one-year period)

Month	Duration (Hour)		Volume (mm)		Intensity (mm/hr)		Interarrival Time (Hour)		No of
	Mean	Std Dv	Mean	Std Dv	Mean	Std Dv	Mean	Std Dv	Events
Jan	10.9	11.6	9.65	13.7	0.693	0.542	32.0	43.8	17
Feb	12.5	12.0	18.1	29.2	1.32	1.73	27.7	51.1	17
Mar	10.4	10.1	10.7	14.4	0.805	0.548	21.4	30.3	25
Apr	10.2	9.43	10.8	13.1	0.933	0.716	26.9	28.9	18
May	7.84	9.20	4.29	8.15	0.458	0.292	35.5	31.1	19
Jun	4.68	5.18	4.32	4.67	0.810	0.534	30.1	39.6	19
Jul	6.00	7.65	7.94	19.4	0.604	0.816	41.0	57.9	15
Aug	6.73	6.06	7.23	5.54	1.02	0.652	42.8	54.3	15
Sep	7.41	6.71	11.6	19.4	0.957	1.20	35.6	43.7	17
Oct	15.6	15.0	18.9	22.3	1.36	0.818	24.1	24.6	12
Nov	13.1	11.7	13.0	14.3	0.947	0.329	33.5	61.9	15
Dec	16.5	14.8	28.6	45.5	1.28	1.04	14.2	12.3	25

Month	Duration (Hour)		Volume (mm)		Intensity (mm/hr)		Interarrival Time (Hour)	
	Min	Max	Min	Max	Min	Max	Min	Max
Jan	1.0	37.0	.508	42.9	0.102	1.86	4.0	164.
Feb	1.0	45.0	.508	114.	0.127	7.37	4.0	215.
Mar	1.0	38.0	.254	55.4	0.169	1.87	4.0	134.
Apr	1.0	33.0	.254	51.1	0.254	2.92	4.0	93.0
May	1.0	34.0	.254	36.1	0.127	1.29	4.0	98.0
Jun	1.0	20.0	.254	16.0	0.127	1.83	4.0	140.
Jul	1.0	30.0	.254	73.4	0.127	2.72	4.0	219.
Aug	1.0	23.0	.254	19.6	0.254	2.17	4.0	193.
Sep	1.0	23.0	.254	60.5	0.127	4.32	4.0	120.
Oct	1.0	53.0	1.27	81.0	0.317	3.30	4.0	70.0
Nov	2.0	48.0	2.03	59.4	0.339	1.65	4.0	241.
Dec	1.0	58.0	.508	172.	0.367	4.88	4.0	56.0

Annual	Mean	Std Dv	Min.	Max	No. of events
Duration (hr)	10.2	10.8	1.00	58.0	214
Volume (mm)	12.4	22.4	0.254	172.	
Intensity (mm/hr)	0.927	0.876	0.102	7.37	
Interarrival Time (hr)	29.4	40.6	4.00	241.	

Table F.3 Summary statistics of rain data for Aberdeen NNE, Washington (prediction, one-year period)

Month	Duration (Hour)		Volume (mm)		Intensity (mm/hr)		Interarrival Time (Hour)		No of
	Mean	Std Dv	Mean	Std Dv	Mean	Std Dv	Mean	Std Dv	Events
Jan	13.8	16.2	43.2	55.3	2.86	0.993	12.2	9.59	19
Feb	6.03	5.68	17.7	20.2	2.76	0.618	16.0	30.4	30
Mar	8.48	9.86	26.7	37.3	2.83	0.658	21.6	36.2	25
Apr	4.86	4.77	13.7	15.2	2.65	0.307	29.3	28.9	21
Mar	5.58	9.15	13.9	19.0	2.67	0.396	33.6	43.5	19
Jun	4.40	4.72	11.7	14.6	2.62	0.808	73.1	90.4	10
Jul	5.00	6.52	15.5	25.1	2.70	0.448	63.8	102.	12
Aug	9.60	6.27	12.7	7.41	1.73	0.869	127.	71.2	5
Sep	6.20	6.14	15.7	18.3	2.40	0.505	123.	121.	5
Oct	5.42	5.60	13.2	18.3	2.36	0.705	27.6	24.2	24
Nov	7.59	6.80	19.5	22.1	2.43	0.731	13.1	14.2	32
Dec	8.47	14.4	25.0	45.0	2.70	0.719	25.0	53.2	30

Month	Duration (Hour)		Volume (mm)		Intensity (mm/hr)		Interarrival Time (Hour)	
	Min	Max	Min	Max	Min	Max	Min	Max
Jan	1.0	73.0	2.54	239.	1.02	5.23	4.0	37.0
Feb	1.0	25.0	2.54	94.0	1.48	4.72	4.0	174.
Mar	1.0	41.0	2.54	165.	1.83	5.08	4.0	190.
Apr	1.0	18.0	2.54	63.5	2.12	3.53	5.0	115.
May	1.0	42.0	2.54	86.4	2.06	3.63	4.0	162.
Jun	1.0	14.0	2.54	45.7	1.45	4.16	9.0	237.
Jul	1.0	23.0	2.54	91.4	2.34	3.98	6.0	369.
Aug	1.0	16.0	2.54	20.3	0.508	2.54	4.0	181.
Sep	2.0	17.0	5.08	48.3	1.52	2.84	9.0	313.
Oct	1.0	26.0	2.54	88.9	1.27	3.81	4.0	89.0
Nov	1.0	26.0	2.54	88.9	0.953	4.13	4.0	74.0
Dec	1.0	72.0	2.54	198.	1.52	5.08	4.0	292.

Annual	Mean	Std Dv	Min.	Max	No. of events
Duration (hr)	7.22	9.41	1.00	73.0	232
Volume (mm)	20.3	30.8	2.54	239.	
Intensity (mm/hr)	2.63	0.688	0.508	5.23	
Interarrival Time (hr)	30.5	52.0	4.00	369.	

Table F.4 Summary statistics of rain data for Tray Mountain, Georgia (calibration, two-year period)

Month	Duration (Hour)		Volume (mm)		Intensity (mm/hr)		Interarrival Time (Hour)		No of
	Mean	Std Dv	Mean	Std Dv	Mean	Std Dv	Mean	Std Dv	Events
Jan	9.36	7.84	12.4	13.4	1.50	0.948	101.	90.0	14
Feb	13.1	9.55	34.7	37.5	2.29	1.65	70.1	50.2	17
Mar	6.25	4.73	16.9	24.7	3.53	6.30	62.8	54.3	20
Apr	7.45	6.23	18.4	21.7	2.85	4.26	77.8	103.	20
May	5.32	4.82	16.7	27.0	3.48	4.16	52.6	79.0	25
Jun	7.56	5.97	22.6	34.7	2.96	3.15	66.2	52.9	18
Jul	5.22	3.81	17.0	27.4	3.24	3.64	38.1	41.1	32
Aug	5.52	3.91	16.4	13.4	4.76	5.70	76.0	122.	25
Sep	4.90	3.67	10.5	9.30	3.25	3.85	91.4	93.6	10
Oct	7.06	4.25	16.0	11.7	2.26	1.24	87.3	68.2	16
Nov	5.60	4.16	9.14	11.5	1.51	1.55	77.3	85.6	20
Dec	8.28	6.36	20.2	28.0	1.80	1.57	55.6	65.9	18

Month	Duration (Hour)		Volume (mm)		Intensity (mm/hr)		Interarrival Time (Hour)	
	Min	Max	Min	Max	Min	Max	Min	Max
Jan	1.00	25.0	0.508	53.6	0.254	3.56	4.0	296.
Feb	3.00	29.0	0.762	115.	0.254	6.62	8.0	146.
Mar	1.00	18.0	0.762	84.8	0.254	28.3	5.0	176.
Apr	1.00	23.0	1.27	77.2	0.317	19.6	4.0	442.
May	1.00	17.0	0.762	104.	0.203	20.3	4.0	320.
Jun	1.00	25.0	0.508	153.	0.254	9.82	8.0	187.
Jul	1.00	13.0	0.254	141.	0.254	17.7	4.0	190.
Aug	1.00	13.0	1.02	53.3	0.508	20.3	4.0	594.
Sep	1.00	12.0	2.03	28.7	0.508	13.2	7.0	299.
Oct	1.00	17.0	0.508	48.3	0.508	4.64	4.0	188.
Nov	1.00	14.0	0.508	39.6	0.254	5.66	4.0	279.
Dec	1.00	21.0	0.508	113.	0.254	5.94	4.0	222.

Annual	Mean	Std Dv	Min.	Max	No. of events
Duration (hr)	6.91	5.80	1.00	29.0	235
Volume (mm)	17.7	24.2	0.254	153.	
Intensity (mm/hr)	2.90	3.80	0.203	28.3	
Interarrival Time (hr)	67.7	78.5	4.00	594.	

Table F.5 Summary statistics of rain data for Tray Mountain, Georgia (validation, one-year period)

Month	Duration (Hour)		Volume (mm)		Intensity (mm/hr)		Interarrival Time (Hour)		No of
	Mean	Std Dv	Mean	Std Dv	Mean	Std Dv	Mean	Std Dv	Events
Jan	11.0	6.32	21.1	15.0	2.34	1.78	96.3	31.6	6
Feb	13.6	9.13	19.8	13.5	1.51	0.935	120.	68.9	5
Mar	11.3	8.98	15.6	15.3	1.20	0.803	55.5	51.5	11
Apr	4.90	2.60	13.7	10.2	2.62	1.79	70.4	61.0	10
May	7.20	7.50	20.0	19.5	5.19	6.81	63.3	90.8	10
Jun	8.50	10.6	27.0	44.1	3.72	4.35	79.4	78.0	10
Jul	5.17	7.46	17.5	39.7	2.87	3.40	48.8	55.5	12
Aug	8.00	10.3	16.2	23.4	2.19	1.99	82.0	47.0	8
Sep	4.44	3.28	14.6	17.2	2.71	1.89	73.1	74.0	9
Oct	12.4	11.6	32.7	65.0	1.42	1.57	112.	75.3	8
Nov	8.60	3.51	18.1	31.2	1.48	2.14	110.	56.9	5
Dec	10.4	9.29	21.9	23.7	1.77	1.46	70.8	55.3	9

Month	Duration (Hour)		Volume (mm)		Intensity (mm/hr)		Interarrival Time (Hour)	
	Min	Max	Min	Max	Min	Max	Min	Max
Jan	3.00	22.0	5.33	47.8	0.667	5.31	54.	131.
Feb	4.00	28.0	3.05	33.5	0.664	2.86	14.	196.
Mar	3.00	31.0	1.02	48.0	0.339	2.54	14.	180.
Apr	2.00	10.0	1.52	30.7	0.762	6.86	7.0	179.
May	1.00	24.0	1.52	61.2	0.699	23.1	8.0	285.
Jun	1.00	33.0	2.54	144.	0.593	15.7	4.0	248.
Jul	1.00	28.0	1.52	142.	0.508	12.7	4.0	159.
Aug	1.00	33.0	2.03	70.6	0.677	6.10	8.0	142.
Sep	1.00	11.0	1.02	52.3	0.813	6.30	8.0	255.
Oct	2.00	37.0	1.02	192.	0.339	5.18	5.0	230.
Nov	5.00	14.0	1.27	73.7	0.254	5.26	45.	182.
Dec	1.00	27.0	0.508	71.6	0.508	4.93	4.0	177.

Annual	Mean	Std Dv	Min.	Max	No. of events
Duration (hr)	8.41	8.21	1.00	37.0	103
Volume (mm)	19.6	29.8	0.508	192.	
Intensity (mm/hr)	2.54	3.15	0.254	23.1	
Interarrival Time (hr)	76.7	64.7	4.00	285.	

Table F.6 Summary statistics of rain data for Tray Mountain, Georgia (prediction, one-year period)

Month	Duration (Hour)		Volume (mm)		Intensity (mm/hr)		Interarrival Time (Hour)		No of
	Mean	Std Dv	Mean	Std Dv	Mean	Std Dv	Mean	Std Dv	Events
Jan	10.2	11.0	26.9	51.6	2.37	3.41	57.2	46.2	11
Feb	11.0	7.96	19.8	18.7	1.54	1.00	89.9	85.0	8
Mar	7.78	5.36	19.8	17.9	2.68	1.75	63.3	59.4	9
Apr	15.1	9.34	29.3	22.9	2.01	0.983	75.7	80.6	7
May	4.00	2.54	21.9	20.5	6.00	5.67	87.3	99.0	10
Jun	13.8	20.4	56.5	84.8	4.38	3.07	109.	118.	5
Jul	5.80	4.11	19.7	20.0	3.63	3.46	40.6	77.2	15
Aug	6.27	4.42	14.8	14.2	2.37	1.54	44.7	53.1	15
Sep	10.2	10.1	38.5	60.2	2.69	1.62	126.	109.	5
Oct	8.83	2.48	8.93	3.16	1.05	0.387	93.5	65.6	6
Nov	11.6	6.55	44.9	45.2	3.30	2.14	54.6	43.2	11
Dec	9.27	6.44	14.9	13.4	1.43	0.679	61.3	49.9	11

Month	Duration (Hour)		Volume (mm)		Intensity (mm/hr)		Interarrival Time (Hour)	
	Min	Max	Min	Max	Min	Max	Min	Max
Jan	3.00	41.0	1.52	178.	0.381	12.0	5.0	153.
Feb	3.00	27.0	1.27	52.6	0.423	3.51	4.0	227.
Mar	1.00	16.0	1.52	60.5	0.635	5.04	6.0	184.
Apr	5.00	34.0	11.9	70.6	1.09	3.52	5.0	198.
May	1.00	10.0	3.30	57.9	0.686	19.3	8.0	266.
Jun	1.00	50.0	4.57	205.	1.06	9.30	6.0	300.
Jul	2.00	14.0	1.27	56.1	0.444	12.3	5.0	305.
Aug	2.00	15.0	1.78	51.8	0.508	5.23	4.0	165.
Sep	3.00	28.0	4.57	146.	1.49	5.21	5.0	269.
Oct	6.00	11.0	4.32	13.5	0.540	1.61	17.0	190.
Nov	4.00	22.0	1.78	152.	0.444	6.93	4.0	152.
Dec	2.00	20.0	1.78	42.2	0.762	2.64	5.0	187.

Annual	Mean	Std Dv	Min.	Max	No. of events
Duration (hr)	8.85	7.88	1.00	50.0	113
Volume (mm)	24.4	33.8	1.27	205.	
Intensity (mm/hr)	2.83	2.89	0.381	19.3	
Interarrival Time (hr)	67.4	71.9	4.00	305.	

Table F.7 Summary statistics of rain data for Niceville, Florida (calibration, two-year period)

Month	Duration (Hour)		Volume (mm)		Intensity (mm/hr)		Interarrival Time (Hour)		No of
	Mean	Std Dv	Mean	Std Dv	Mean	Std Dv	Mean	Std Dv	Events
Jan	6.75	3.65	11.6	9.78	2.10	2.19	111.	95.0	12
Feb	7.94	5.78	16.9	28.8	2.84	4.98	74.9	93.7	17
Mar	7.06	5.36	11.7	9.58	2.04	1.51	84.1	61.4	17
Apr	8.75	4.67	16.8	18.8	1.64	1.09	103.	64.3	12
May	5.45	2.58	19.1	17.5	4.34	5.54	132.	109.	11
Jun	6.33	7.51	17.1	24.4	3.37	4.05	49.0	54.3	27
Jul	4.52	2.79	10.6	10.3	3.28	3.28	63.7	71.4	21
Aug	5.41	5.30	20.0	23.7	4.65	5.33	43.1	42.8	29
Sep	4.36	4.58	15.6	21.3	3.73	3.07	97.9	97.3	14
Oct	5.00	3.18	13.5	16.8	2.51	2.41	95.2	132.	17
Nov	4.23	3.37	9.34	13.0	5.03	13.2	119.	115.	13
Dec	5.64	4.55	10.8	11.2	3.99	8.40	84.1	57.0	14

Month	Duration (Hour)		Volume (mm)		Intensity (mm/hr)		Interarrival Time (Hour)	
	Min	Max	Min	Max	Min	Max	Min	Max
Jan	1.00	13.0	1.02	33.0	0.508	6.60	5.00	288.
Feb	1.00	26.0	1.27	126.	0.317	21.6	6.00	381.
Mar	1.00	19.0	1.78	40.6	0.617	5.81	8.00	189.
Apr	4.00	17.0	3.81	58.2	0.762	4.47	7.00	227.
May	2.00	10.0	2.54	58.4	0.988	19.5	10.00	325.
Jun	1.00	40.0	0.762	120.	0.381	17.8	4.00	211.
Jul	1.00	9.0	1.27	32.8	0.282	11.4	5.00	239.
Aug	1.00	26.0	1.27	92.5	0.317	19.1	9.00	170.
Sep	1.00	18.0	0.762	78.7	0.381	9.78	8.00	356.
Oct	1.00	10.0	0.508	57.4	0.339	8.38	4.00	498.
Nov	1.00	12.0	0.508	48.8	0.254	48.8	5.00	329.
Dec	1.00	13.0	1.02	32.8	0.254	32.8	5.00	186.

Annual	Mean	Std Dv	Min.	Max	No. of events
Duration (hr)	5.90	4.98	1.00	40.0	204
Volume (mm)	14.8	18.9	0.508	126.	
Intensity (mm/hr)	3.36	5.28	0.254	48.8	
Interarrival Time (hr)	80.0	84.4	4.00	498.	

Table F.8 Summary statistics of rain data for Niceville, Florida (validation, one-year period)

Month	Duration (Hour)		Volume (mm)		Intensity (mm/hr)		Interarrival Time (Hour)		No of
	Mean	Std Dv	Mean	Std Dv	Mean	Std Dv	Mean	Std Dv	Events
Jan	8.20	5.16	16.0	15.0	1.91	1.24	60.2	53.4	10
Feb	8.00	5.76	19.9	25.1	1.80	1.38	97.0	69.8	6
Mar	4.00	1.41	4.37	3.70	1.00	0.78	171.	124.	5
Apr	2.00	1.41	20.1	19.0	17.9	22.2	357.	291.	2
May	7.20	1.64	25.0	5.79	3.60	1.19	144.	47.9	5
Jun	9.00	8.29	19.0	14.6	2.39	1.58	98.4	94.3	7
Jul	5.08	3.29	16.2	11.4	3.56	3.14	56.9	88.6	12
Aug	4.25	2.12	14.3	16.8	2.86	2.71	102.	155.	8
Sep	8.17	14.2	29.6	67.9	1.60	1.53	64.7	76.9	6
Oct	4.60	3.58	6.76	5.21	1.47	0.849	153.	153.	5
Nov	5.83	6.24	18.1	18.4	3.69	2.12	104.	74.0	6
Dec	6.43	5.35	16.6	27.6	2.32	2.63	115.	116.	7

Month	Duration (Hour)		Volume (mm)		Intensity (mm/hr)		Interarrival Time (Hour)	
	Min	Max	Min	Max	Min	Max	Min	Max
Jan	2.00	17.0	0.762	46.7	0.381	4.32	4.00	148.
Feb	3.00	19.0	1.27	67.1	0.423	3.53	6.00	187.
Mar	2.00	6.0	0.762	8.89	0.317	2.22	4.00	312.
Apr	1.00	3.0	6.60	33.5	2.20	33.5	151.0	563.
May	5.00	9.0	16.5	31.0	2.73	5.64	68.0	200.
Jun	1.00	26.0	0.508	37.3	0.508	4.57	9.00	222.
Jul	1.00	12.0	0.762	38.4	0.762	12.8	4.00	314.
Aug	1.00	7.0	0.762	48.5	0.254	8.09	22.0	483.
Sep	1.00	37.0	1.02	168.	0.203	4.54	4.00	197.
Oct	1.00	10.0	0.762	11.9	0.381	2.54	8.00	321.
Nov	1.00	18.0	2.54	52.1	0.508	6.94	22.0	223.
Dec	1.00	14.0	0.762	76.2	0.254	6.93	7.00	267.

Annual	Mean	Std Dv	Min.	Max	No. of events
Duration (hr)	6.33	5.85	1.00	37.0	79
Volume (mm)	17.0	23.4	0.508	168.	
Intensity (mm/hr)	2.86	4.07	0.203	33.5	
Interarrival Time (hr)	104.	112.	4.00	563.	

Table F.9 Summary statistics of rain for Niceville, Florida (prediction, one-year period).

Month	Duration (Hour)		Volume (mm)		Intensity (mm/hr)		Interarrival Time (Hour)		No of
	Mean	Std Dv	Mean	Std Dv	Mean	Std Dv	Mean	Std Dv	Events
Jan	3.27	3.15	11.5	13.4	3.12	1.09	48.2	70.1	15
Feb	2.30	1.64	10.2	9.27	4.74	3.90	63.7	60.9	10
Mar	3.75	4.13	14.3	16.3	3.56	1.51	79.4	101.	8
Apr	2.38	1.33	10.6	12.2	4.10	2.21	61.1	98.7	13
May	2.93	2.23	16.0	24.8	4.45	2.68	52.7	66.1	14
Jun	1.94	0.827	14.3	15.7	7.84	8.96	35.9	35.6	17
Jul	6.21	9.38	42.5	79.8	5.97	3.18	49.4	42.7	14
Aug	2.30	1.77	9.65	6.96	4.58	3.09	66.8	57.3	10
Sep	5.30	6.93	43.9	75.1	6.22	4.03	64.3	48.7	10
Oct	8.00	7.00	29.0	42.2	4.24	4.86	324.	308.	3
Nov	3.20	1.64	17.3	16.6	4.74	2.21	120.	89.6	5
Dec	2.25	1.49	10.9	13.5	4.22	4.00	79.8	56.9	8

Month	Duration (Hour)		Volume (mm)		Intensity (mm/hr)		Interarrival Time (Hour)	
	Min	Max	Min	Max	Min	Max	Min	Max
Jan	1.00	10.0	2.54	48.3	2.54	5.93	5.00	250.
Feb	1.00	6.0	2.54	27.9	1.27	14.0	7.00	203.
Mar	1.00	11.0	2.54	43.2	2.31	6.10	8.00	305.
Apr	1.00	5.0	2.54	48.3	1.91	9.65	4.00	334.
May	1.00	9.0	2.54	99.1	2.03	11.0	4.00	221.
Jun	1.00	3.0	2.54	61.0	2.54	35.6	4.00	144.
Jul	1.00	37.0	2.54	312.	2.54	11.7	7.00	112.
Aug	1.00	7.0	2.54	20.3	2.18	10.2	21.0	206.
Sep	1.00	22.0	2.54	236.	2.54	14.0	5.00	151.
Oct	1.00	15.0	2.54	77.7	0.457	9.72	11.0	626.
Nov	2.00	6.0	5.08	45.7	2.54	7.62	14.0	233.
Dec	1.00	5.0	0.762	38.1	0.254	12.7	4.00	178.

Annual	Mean	Std Dv	Min.	Max	No. of events
Duration (hr)	3.37	4.37	1.00	37.0	127
Volume (mm)	18.8	37.5	0.762	312.	
Intensity (mm/hr)	4.99	4.37	0.254	35.6	
Interarrival Time (hr)	65.8	85.9	4.00	626.	

Table F.10 Summary statistics of rain data "perturbed" by random noise, for Quillayute, Washington (Calibration and Validtion)

(Calibration, 2-year period)

Month	Volume (mm)				Intensity (mm/hr)			
	Mean	Std Dv	Minimum	Maximum	Mean	Std Dv	Minimum	Maximum
Jan	12.2	23.7	0.216	127.	0.775	0.647	0.149	2.70
Feb	23.9	47.1	0.207	268.	1.09	0.936	0.207	4.88
Mar	16.9	24.3	0.240	108.	1.24	1.03	0.185	3.39
Apr	10.6	16.4	0.243	73.2	0.744	0.565	0.202	2.94
May	4.01	5.12	0.207	20.1	0.519	0.363	0.173	1.47
Jun	8.17	9.31	0.209	34.5	0.899	0.750	0.144	3.26
Jul	4.54	3.67	0.217	13.3	0.992	0.850	0.217	3.21
Aug	9.91	7.92	0.211	24.5	1.05	0.620	0.211	2.72
Sep	10.0	12.4	0.250	47.8	0.975	0.772	0.205	3.49
Oct	17.2	28.2	0.230	117.	1.30	0.897	0.104	3.19
Nov	19.1	28.3	0.210	154.	1.09	0.859	0.188	4.68
Dec	14.5	17.8	0.279	82.7	1.10	0.775	0.227	4.06
Annual	12.9	23.1	0.207	268.	0.974	0.795	0.104	4.88

Validation (1-year period)

Month	Volume (mm)				Intensity (mm/hr)			
	Mean	Std Dv	Minimum	Maximum	Mean	Std Dv	Minimum	Maximum
Jan	10.4	15.1	0.425	48.5	0.738	0.628	0.085	2.23
Feb	18.6	30.5	0.486	117.0	1.39	1.96	0.121	8.26
Mar	10.8	15.3	0.219	59.4	0.803	0.575	0.153	2.05
Apr	10.6	12.8	0.232	50.8	0.913	0.686	0.232	2.89
May	3.95	6.86	0.205	30.4	0.449	0.270	0.131	1.09
Jun	4.35	4.94	0.217	17.3	0.793	0.521	0.133	1.94
Jul	8.31	20.2	0.237	76.8	0.627	0.840	0.150	2.74
Aug	7.30	5.70	0.251	20.3	1.03	0.679	0.251	2.25
Sep	11.3	19.0	0.215	55.7	0.918	1.14	0.105	3.98
Oct	17.7	18.8	1.37	65.6	1.38	0.904	0.342	3.52
Nov	12.4	12.1	1.83	50.1	0.940	0.346	0.317	1.69
Dec	27.4	41.0	0.584	158.0	1.28	0.910	0.348	4.29
Annual	12.2	21.3	0.205	158.0	0.931	0.903	0.085	8.26

Table F.11 Summary statistics of rain data "perturbed" by random noise, for Quillayute, Washington (Prediction)

Month	(Prediction, 1-year period) Volume (mm)				Intensity (mm/hr)			
	Mean	Std Dv	Minimum	Maximum	Mean	Std Dv	Minimum	Maximum
Jan	43.0	56.2	2.35	240.	2.81	1.13	0.884	4.86
Feb	18.2	21.0	2.22	95.5	2.83	0.783	1.33	5.40
Mar	26.1	34.8	2.16	147.	2.83	0.752	1.65	5.73
Apr	14.6	17.4	2.12	74.9	2.68	0.482	2.12	4.16
May	13.8	20.4	2.04	92.1	2.55	0.493	2.04	4.10
Jun	11.5	13.7	2.23	42.0	2.68	0.817	1.30	4.02
Jul	16.7	29.8	2.07	109.	2.71	0.745	2.07	4.73
Aug	12.3	7.56	2.38	21.2	1.67	0.912	0.459	2.76
Sep	13.9	15.8	5.32	42.1	2.17	0.449	1.49	2.66
Oct	13.4	19.2	2.08	93.3	2.40	0.807	1.16	4.40
Nov	19.1	20.6	2.19	78.3	2.45	0.717	0.919	3.89
Dec	25.7	46.4	2.18	216.	2.75	0.725	1.39	4.72
Annual	20.4	31.2	2.04	240.	2.63	0.771	0.459	5.73

Table F.12 Summary statistics of rain data "perturbed" by random noise, for Tray Mountain, Georgia (Calibration and Validtion)

(Calibration, 2-year period)

Month	Volume (mm)				Intensity (mm/hr)			
	Mean	Std Dv	Minimum	Maximum	Mean	Std Dv	Minimum	Maximum
Jan	10.9	10.4	0.655	40.5	1.36	0.930	0.328	3.62
Feb	36.5	39.9	0.611	133.	2.33	1.52	0.204	4.93
Mar	18.9	28.2	0.777	103.	3.86	6.73	0.243	29.6
Apr	17.3	19.5	1.08	70.0	2.92	4.70	0.270	21.9
May	17.0	28.7	0.718	125.	3.44	4.47	0.144	22.4
Jun	18.9	25.5	0.495	111.	2.55	2.56	0.247	9.30
Jul	15.7	21.0	0.276	102.	3.14	3.33	0.276	15.3
Aug	14.8	11.1	1.17	41.1	4.28	4.91	0.378	19.9
Sep	11.0	9.38	1.82	25.8	3.14	2.87	0.455	9.89
Oct	16.0	10.6	0.642	39.8	2.35	1.48	0.642	5.34
Nov	8.02	10.3	0.356	33.9	1.32	1.35	0.281	4.84
Dec	21.6	29.7	0.569	119.	1.91	1.67	0.320	6.26
Annual	17.2	23.2	0.276	133.	2.82	3.71	0.144	29.6

Validation (1-year period)

Month	Volume (mm)				Intensity (mm/hr)			
	Mean	Std Dv	Minimum	Maximum	Mean	Std Dv	Minimum	Maximum
Jan	20.5	17.0	6.10	53.2	2.23	1.95	0.762	5.92
Feb	17.2	11.5	2.23	28.4	1.29	0.752	0.557	2.27
Mar	16.6	16.5	1.32	48.1	1.25	0.901	0.381	2.90
Apr	13.2	9.96	1.35	27.8	2.45	1.46	0.673	5.10
May	20.7	21.7	1.90	69.4	5.31	7.13	0.823	24.3
Jun	22.6	34.3	2.44	111.	3.33	3.54	0.560	13.0
Jul	16.5	36.5	1.13	131.	2.70	2.93	0.375	11.0
Aug	19.3	28.8	1.90	86.0	2.28	1.75	0.635	5.32
Sep	16.2	18.3	1.25	53.1	3.12	2.28	0.751	7.94
Oct	38.1	78.2	1.15	230.	1.58	1.93	0.414	6.20
Nov	19.8	35.3	1.26	82.8	1.59	2.43	0.252	5.91
Dec	20.0	22.8	0.376	70.9	1.54	1.05	0.376	3.54
Annual	19.8	31.2	0.376	230.0	2.50	3.08	0.252	24.3

Table F.13 Summary statistics of rain data "perturbed" by random noise, for Tray Mountain, Georgia (Prediction)

Month	(Prediction, 1-year period) Volume (mm)				Intensity (mm/hr)			
	Mean	Std Dv	Minimum	Maximum	Mean	Std Dv	Minimum	Maximum
Jan	31.8	67.1	1.31	230.	2.50	3.66	0.326	12.5
Feb	17.9	16.2	1.39	40.8	1.43	0.989	0.463	3.49
Mar	18.9	15.2	1.21	46.7	2.58	1.76	0.627	5.97
Apr	30.2	25.9	13.0	85.6	1.97	0.755	1.18	3.11
May	20.1	19.2	2.54	57.7	5.28	4.31	0.671	13.6
Jun	53.0	75.9	4.53	186.	4.31	2.72	1.35	8.70
Jul	20.0	22.0	1.40	67.0	3.68	3.48	0.494	11.2
Aug	14.3	14.5	1.69	51.5	2.31	1.62	0.422	5.33
Sep	31.4	46.7	5.31	115.	2.32	1.05	1.52	4.10
Oct	7.99	2.66	5.14	10.9	0.94	0.348	0.559	1.55
Nov	40.7	39.3	2.08	134.	3.00	1.79	0.519	6.09
Dec	17.1	16.8	2.28	52.1	1.59	0.853	0.606	3.25
Annual	23.9	33.9	1.21	230.	2.73	2.61	0.326	13.6

Table F.14 Summary statistics of rain data "perturbed" by random noise, for Niceville, Florida (Calibration and Validtion)

(Calibration, 2-year period)

Month	Volume (mm)				Intensity (mm/hr)			
	Mean	Std Dv	Minimum	Maximum	Mean	Std Dv	Minimum	Maximum
Jan	12.3	10.4	0.822	31.7	2.17	2.15	0.411	6.34
Feb	18.7	36.4	1.50	158.	2.80	4.41	0.374	18.9
Mar	11.2	9.04	1.88	39.0	2.05	1.57	0.631	5.57
Apr	16.3	18.2	3.58	56.6	1.57	1.00	0.809	3.90
May	20.1	20.0	1.88	64.2	4.63	6.22	0.731	21.4
Jun	17.0	20.7	0.689	87.5	3.56	4.39	0.345	18.7
Jul	10.3	9.89	1.48	33.5	3.25	3.25	0.341	11.2
Aug	21.1	27.9	0.918	115.	4.70	5.29	0.306	17.0
Sep	13.0	16.1	0.853	57.5	3.37	2.75	0.427	8.49
Oct	12.6	16.6	0.536	64.9	2.27	2.19	0.351	7.45
Nov	9.80	13.6	0.584	50.5	5.24	13.6	0.259	50.5
Dec	10.9	11.9	1.29	39.2	4.10	8.43	0.231	32.9
Annual	14.9	20.0	0.536	158.0	3.38	5.37	0.231	50.5

(Validation, 1-year period)

Month	Volume (mm)				Intensity (mm/hr)			
	Mean	Std Dv	Minimum	Maximum	Mean	Std Dv	Minimum	Maximum
Jan	16.4	15.8	0.688	47.2	2.00	1.47	0.344	5.42
Feb	18.0	21.4	1.29	56.6	1.68	1.33	0.340	2.98
Mar	3.59	2.58	0.963	6.71	0.848	0.515	0.405	1.68
Apr	20.1	18.3	7.13	33.1	17.7	21.7	2.38	33.1
May	26.6	9.60	15.8	38.8	3.77	1.23	1.97	5.18
Jun	20.9	17.2	0.512	45.6	2.49	1.58	0.512	4.38
Jul	16.7	12.7	0.552	41.9	3.67	3.51	0.552	14.0
Aug	12.6	13.4	0.934	36.9	2.64	2.19	0.311	6.15
Sep	27.8	63.5	0.717	157.	1.54	1.46	0.143	4.25
Oct	6.79	5.22	0.711	11.6	1.47	0.714	0.356	2.06
Nov	17.3	15.6	1.98	43.3	3.78	2.44	0.395	7.72
Dec	12.7	19.8	0.858	54.9	1.85	1.95	0.286	4.99
Annual	16.5	21.7	0.512	157.	2.83	4.05	0.143	33.1

Table F.15 Summary statistics of rain data "perturbed" by random noise, for Niceville, Florida (Prediction)

Month	(Prediction, 1-year period) Volume (mm)				Intensity (mm/hr)			
	Mean	Std Dv	Minimum	Maximum	Mean	Std Dv	Minimum	Maximum
Jan	12.5	15.9	1.78	59.7	3.23	1.57	1.78	7.36
Feb	10.1	9.92	1.78	30.3	4.74	4.60	1.24	15.1
Mar	14.4	17.5	2.34	48.8	3.38	1.14	2.34	5.43
Apr	10.6	12.5	2.76	48.2	4.04	2.30	1.85	9.64
May	14.7	20.3	1.88	80.8	4.09	2.19	1.88	8.98
Jun	13.2	13.0	2.12	42.8	7.70	9.97	2.12	41.6
Jul	39.2	72.1	1.79	282.	5.44	2.62	1.79	9.82
Aug	8.69	6.68	2.04	21.4	4.10	3.03	2.04	10.7
Sep	41.7	68.8	2.59	196.	6.28	4.81	1.99	17.8
Oct	40.5	52.8	3.10	77.8	6.41	4.68	3.10	9.72
Nov	18.1	19.6	4.25	52.1	4.70	2.65	2.13	8.68
Dec	9.28	11.0	0.559	29.8	3.61	3.20	0.186	9.95
Annual	18.0	34.5	0.559	282.	4.83	4.66	0.186	41.6